DOI: 10.31577/ahs-2021-0022.01.0001

ACTA HYDROLOGICA SLOVACA

Volume 22, No. 1, 2021, 3 – 14

CLIMATE CHANGE IN THE UKRAINIAN CARPATHIANS AND ITS POSSIBLE IMPACT ON RIVER RUNOFF

Viktor I. Vyshnevskyi*, Olena A. Donich

Based on the results of regular monitoring at 11 meteorological stations in the Ukrainian Carpathians, it was discovered a vivid tendency of air temperature increase. It was defined that thermal gradient in the mountains is much less than it is in the free troposphere; at the small altitude it is larger than it is on the tops of mountains. The largest gradient it is observed in period from March till July, the lowest one in period from November till January. It was revealed the cyclical fluctuations of precipitation, in particular the existence of a modern dry phase. There is a tendency of decrease in wind speed during all seasons, which is more evident in the second part of year. There is also the increase in snow cover depth at high altitude. In spite of climate change the river runoff has not changed essentially for the last decades. Like the precipitation the river runoff is of a cyclic nature too. During the last four decades the increase in evaporation, calculated on the base of water balance, has been observed. There is the tendency of runoff increase in a cold period at the large altitude. In turn the water runoff of rivers, located on low-mountain terrain, decreases in the summer period.

KEY WORDS: air temperature, precipitation, snow cover, river runoff, the Ukrainian Carpathians

Introduction

The impact of climate change on the river runoff is a very popular issue of scientific studies, which is considered in many scientific papers (Blöschl at al., 2017; Didovets et al., 2019; Duethmann and Blösch, 2018; Gorbachova et al., 2018; Halmová and Pekarová, 2020; Holko et al., 2020; Loboda and Kozlov, 2020; Kubiak-Wojcicka, 2020; Mostowik et al., 2019; Spinoni et al., 2015; Stagl and Hattermann, 2015; Szolgay et al., 2020). The changes of runoff are caused by many factors, i.e. air temperature, the amount of precipitation, evaporation, etc. The essential problem is to clarify the role of different factors, which impact is simultaneous and different by consequences. This problem is more difficult when it comes to the conditions in mountain areas due to the lack of observation at high altitudes. Under these conditions the obtained results are not often very clear and certain. In many cases the changes in meteorological and hydrological parameters are not statistically proved. Some authors consider (Gorbachova, 2015; Obodovskyi and Lukianets, 2017; Zabolotnia at al., 2019) that even having essential increase in air temperature the time series of annual runoff are stationary with long-term cyclical fluctuations. There is a point of view that the cyclical fluctuations are caused by solar activity and other factors, which refer the Earth in a whole (Fendekova et al., 2018).

So, the main goal of this study is to specify the changes in river runoff in the Ukrainian Carpathians and the role of different factors influencing these changes.

The study area

The study area covers the territory of the Ukrainian Carpathians, which is the central part of the Carpathian Mountains. The total length of these mountains is about 240 km, the width is 50 km, the largest altitude is 2061 m a.s.l. (Hoverla Mountain). The characteristic feature of these mountains is the presence of ridges, which go almost parallel to each other. The highest ridge, where Hoverla Mountain is located, has the name of Chornohora or Chornohirskyi Ridge. The volumetric image of the Ukrainian Carpathians, created on the base of Shuttle Radar Topography Mission (SRTM) digital elevation model, is shown in Fig. 1.

Methodology and data

There is about a dozen meteorological stations in the Ukrainian Carpathians, located at the different altitudes. Among these stations only two ones are located at the rather high altitude. The first station Plai is located on the southwestern macroslope of the mountains; its altitude is 1331.5 m. The second station Pozhezhevska with the altitude of 1451 m is located on the northeastern macroslope. The other stations are located at low-mountain terrain; their altitudes range 432.1–762.5 m

(Table 1).
Among many variables measured at these stations, the main ones are air temperature, precipitation, wind speed and snow cover depth. The period of 1961–2019 was taken for the study. In many cases the data for the periods of 1961–1990 and 1991–2019 were analyzed separately. The same approach was carried out in the study (Rožnovský et al., 2020).
The factor that can impact on air temperature and other parameters, is the difference in geographical latitude and longitude of the meteorological stations. In both cases it exceeds 1°. Thus, the meteorological station Turka has the coordinates as N49°09'01" and E23°01'47", while the meteorological station Seliatyn – N47°52'36" and E25°12'59". The significance of geographical latitude was studied on the base of regression analyze. It was found out that the impact of latitude on air temperature is very small. In most cases the correction is less than 0.1 °C, i.e. it is equal to the measurement accuracy. That is why the actual data were operated without any correction. In our opinion such small impact of geographical latitude on air temperature can be explained the mountains extend from northwest to southeast. In case of their extend from southwest to northeast the impact of latitude would be obvious. It is well known that in a whole air temperature in Europe decreases when moving from southwest towards northeast.
The data on river runoff at the hydrological network were

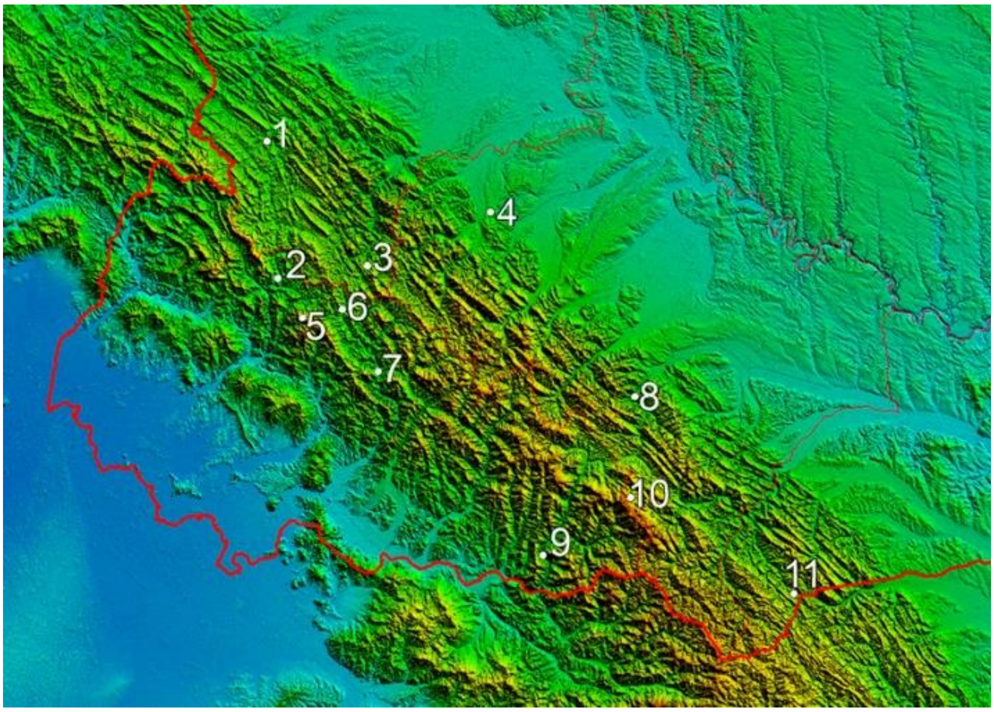

Fig. 1. Volumetric image of the Ukrainian Carpathians with the location of meteorological stations: 1 – Turka, 2 – Nyzhni Vorota, 3 – Slavske, 4 – Dolyna, 5 – Plai, 6 – Nyzhnii Studenyi, 7 – Mezhihiria, 8 – Yaremche, 9 – Rakhiv, 10 – Pozhezhevska, 11 – Seliatyn.

Table 1. Meteorological stations in the Ukrainian Carpathians and their altitudes

№	Name	Altitude [m a.s.l.]
1	Turka	592.4
2	Nyzhni Vorota	488.7
3	Slavske	593.6
4	Dolyna	467.6
5	Plai	1331.5
6	Nyzhnii Studenyi	611.4
7	Mezhihiria	455.4
8	Yaremche	531.3
9	Rakhiv	432.1
10	Pozhezhevska	1451
11	Seliatyn	762.5

analyzed as well. The hydrological parameters of rivers, which neither small no large, were processed. The features of water runoff of the rivers, located on the different macroslopes in the Ukrainian Carpathians were studied. An important issue, which was considered, is the differences in river basin altitude. The annual and monthly data were processed. The annual data was studied for the whole observation period, the monthly ones – for 1961–2019. In many cases the data for the periods of 1961–1990 and 1991–2019 were analyzed separately. Correlation and regression analysis were used in the study. To determine the spatio-temporal fluctuations of the precipitation and river runoff the residual mass curves were drawn.

Results and discussion

Air temperature

Air temperature is the main climatic parameter, which is paid the largest attention of scientists. Similar to many places in the world, in the Ukrainian Carpathians there is a tendency to increase in air temperature. That refers to both low and high altitude stations (Fig. 2).

As can be seen on Fig. 2, the lowest temperature was observed in 1980, the highest one in 2019 (for most stations) and in 2014 for the two ones, located at the largest altitude. During the observed period, starting since 1961, the increase in mean air temperature is about 2 °C. The mean air temperature at all 11 meteorological stations during 1961–1990 was 5.6 °C, and during 1991–2019 it was 6.6 °C.

It is important to note that the increase in air temperature is registered in all seasons. The largest increase is observed in January and in August. In the last decades the mean air temperature in August has become almost the same as it is in July. The smallest increase is observed in autumn period (Fig. 3).

The similar results as to the seasonal features were described in many other papers (Grebin, 2010; Rangwalla and Miller, 2012; Spinoni et al., 2015). The study (Rangwalla and Miller, 2012) showed that in the Swiss Alps the rate of temperature rise in autumn period is less, than it is in other seasons. Possible

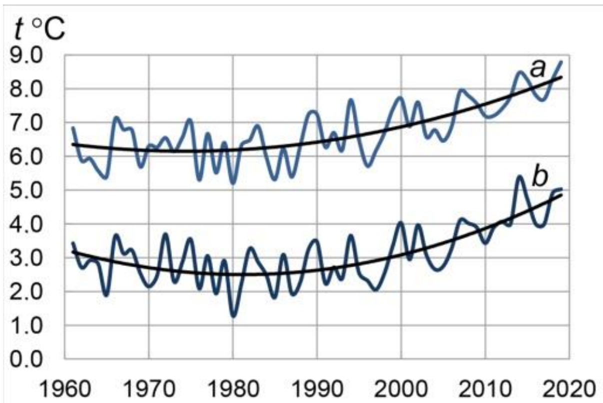

Fig. 2. The increase in mean annual air temperature in the Ukrainian Carpathians during 1961–2019: a) – at 9 meteorological stations, located at the low attitude, b) – at two ones, located at the high attitude.

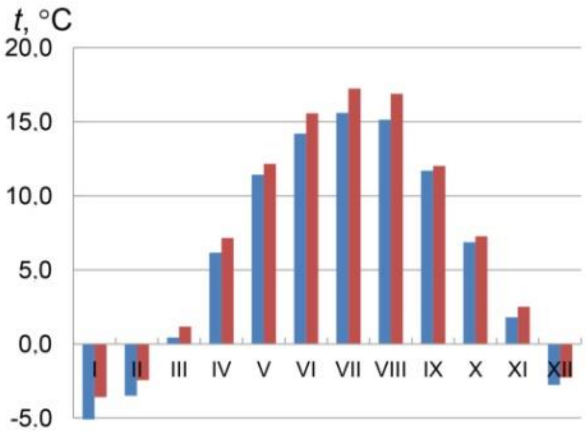

Fig. 3. The mean monthly temperature at 11 meteorological stations in the Ukrainian Carpathians: left columns – during 1961–1990, right columns – during 1991–2019.

differences in our and others' findings can be explained by the different observation periods taken for the studies. The last years in Europe were much warmer than there were at the beginning of observations.

The seasonal increase in air temperature depends on altitude of the meteorological stations. The increase in temperature in January (the coldest month of the year) at the stations, located at a rather small altitude, in most cases was in the range of 0.5–0.6°C per decade. In turn at the highest stations Plai and Pozhezhevska the increase is much less – 0.15–0.2°C per decade. Taking into account the essential variability of air temperature in January it is possible to say, that at high altitude the temperature has not changed. The increase in air temperature in August at the studied meteorological stations has a range of 0.5–0.6°C per decade.

The changes in mean temperature by altitude are uneven as well. At low altitude the decrease is more essential, than at a higher one (Fig. 4).

During the period 1961–1990 the mean air temperature at the altitudes 500, 1000 and 1500 and 2000 m was the following: 6.4, 3.8, 2.4 and 1.4°C. During 1991–2019 the mean air temperature became higher. At the above mentioned altitudes it was 7.5, 4.7, 3.3 and 2.2°C.

The gradient of mean air temperature at the altitudes 500–1000 m, 1000–1500 and 1500–2000 m during the first period was 0.52, 0.28, and 0.20°C per 100 m, during the second one it was 0.56, 0.28 and 0.22°C per 100 m. The obtained result essentially differs from those ones, which are based on the aerological study. It is well known that a thermal gradient in the troposphere is about 0.6°C per 100 m and it is almost stable along the first kilometers from the earth surface. In particular, such results of the aerological study were obtained in the Western Ukraine (Kablak, 2007). In the mentioned study it was also clarified that thermal gradient in winter is slightly smaller than it is in summer time.

Based on the available data the mean air temperature during 1991–2019 was calculated for each month and at different altitude (Fig. 5).

Fig. 5 indicates that at high altitude, i.e. on the tops of the mountains, the warmest month is August. During the year, the gradient of air temperature by altitude is uneven. The largest thermal gradient is observed in period of March–July, when the difference in air temperature at the altitudes 1000 and 2000 m is equal to 0.33–0.36°C per 100 m. The lowest gradient (0.15–0.18°C per 100 m) is observed in the period of November–January.

It is worth noting that, according to the obtained data,

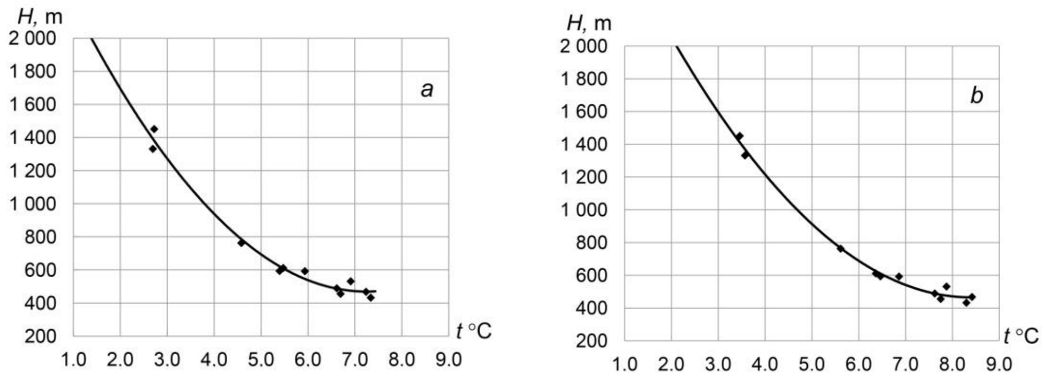

Fig. 4. The dependence of mean air temperature in the Ukrainian Carpathians on altitude: a) – during 1961–1990, b) – during 1991–2019.

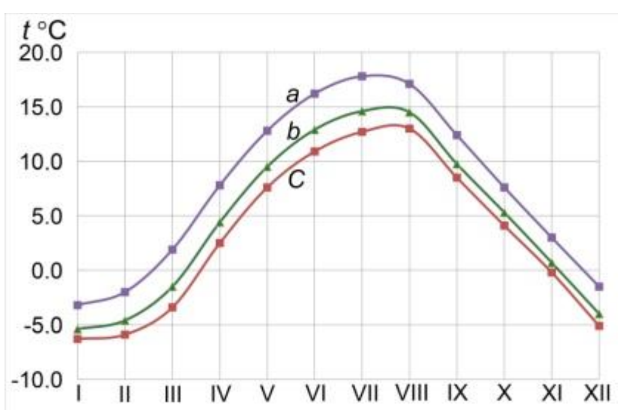

Fig. 5. The monthly mean air temperature in the Ukrainian Carpathians during 1991–2019 at different altitudes: a) – 500 m, b) – 1000 m, c) – 1500 m.

the gradient of air temperature by altitude in the Ukrainian Carpathians is smaller than it is in many studies in other regions (Rangwala and Miller, 2012; Rolland, 2003; Wang et al., 2017). To some extent it can be explained by the relief of the studied region, characterized by rather gentle slopes.

Precipitation

The precipitation in the Ukrainian Carpathians is uneven in space and in time. It depends on altitude and location of the meteorological stations as to the mountains ridges. The largest precipitation is observed at meteorological stations Plai and Pozhezhevska, which altitudes are the highest. The mean precipitation during the period of 1991–2019 at Plai station was 1456 mm, at Pozhezhevska one – 1525 mm. At the same time the lowest precipitation is observed at the meteorological stations Dolyna (901 mm) and Seliatyn (853 mm) located on the northeastern macroslope of the mountains. There is a dependency of precipitation on altitude, but not very close – the precipitation increases by about 1 mm per meter of altitude.

The lowest precipitation (the mean value is 828 mm) at all 11 meteorological stations was observed in 1961, the highest one (1579 mm) was in 1998.

During 1961–2019 the amount of precipitation did not change significantly. In our view, these changes are in the form of two cyclic fluctuations with the period of about 30 years having wet and dry phases. The last cycle started in the beginning of the 1990s and it is likely will finish in 2022–2025. Nowadays it is observed the dry phase, which started in 2011 (Fig. 6).

The mean annual precipitation at all 11 meteorological stations in 1961–1990 was 1101 mm, and in 1991–2019 it was 1124 mm. It can be assumed that when the dry phase will finish, the amount of precipitation in both periods will be the same. The comparison of data for 1961–1990 and 1991–2019 shows a small tendency in increasing the precipitation in the cold period from September till March. During the last three decades it is observed the decrease in precipitation in summer time, primarily in June. This feature refers both low-mountain terrain and a rather large altitude where the meteorological stations Plai and Pozhezhevska are located (Fig. 7).

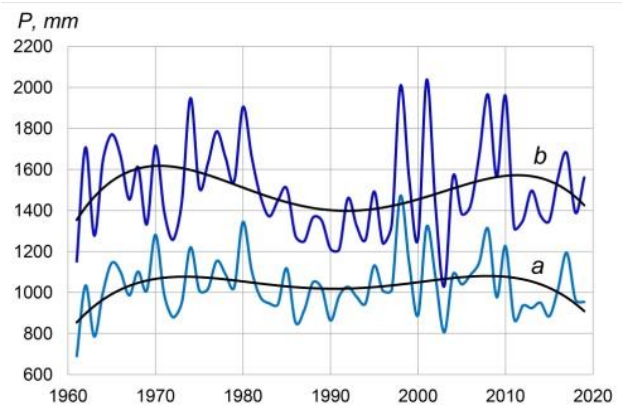

Fig. 6. The changes in mean annual precipitation in the Ukrainian Carpathians: a) – at 9 meteorological stations, located at low attitude, b) – at two ones, located at high attitude.

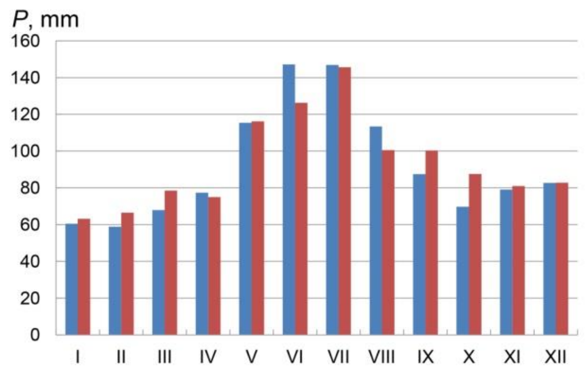

Fig. 7. The intra-annual distribution of precipitation at 11 meteorological stations in the Ukrainian Carpathians: left columns – during 1961–1990, right columns – during 1991–2019.

The similar results for the studied region and the periods from the beginning of observation till 1988 and for the period of 1989–2008 were obtained in the paper (Grebin 2010). The tendency of increasing winter precipitation is observed in the Bieszczady Mountains, located to the northwest from the Ukrainian Carpathians (Mostowik et al., 2019).

Relative humidity

The mean relative humidity at the meteorological stations, located in the Ukrainian Carpathians, is about 80 %. The largest value is observed in December, the lowest one in April and May. The similar results were obtained for the adjacent areas of the Carpathian Mountains (Marin et al 2014, Spinoni et al 2015). During the observation period there is a small tendency of decreasing relative humidity at about 0.15 % per decade. This decrease can be considered as a consequence of air temperature increasing.

Wind speed (WS)

During the observation period there was a tendency of decreasing wind speed. In 1961–1990 its mean value at 11 meteorological stations was 2.5 m/sec, in 1961–2019 it was 2.1 m/sec. The mean annual decrease in wind speed is about 0.14 m/sec per decade. It means that during the analyzed period the mean wind speed decreased in a whole at about 0.8 m/sec (Fig. 8).
The similar results as to the decrease in wind speed were obtained in many other regions of the world including the Carpathian Mountains (Guo et al., 2011; Marin et al., 2014; Spinoni et al., 2015). It is likely this decrease is considered to be a global tendency.
This decrease is observed throughout the year, but in the second part of the year it is the most essential (Fig. 9).
The data referring air temperature, precipitation and wind speed show that the most suitable month for tourism activities in the Ukrainian Carpathians is August. In this time the air temperature is the highest and the wind speed is the lowest. August is also characterized by a relatively small amount of precipitation.

Snow depth

This parameter, like precipitation, has the essential impact on the river runoff. Snow depth depends on altitude of the meteorological stations, their location as to the mountain ridges, precipitation in cold period and to some extent on geographical latitude and longitude.
The largest snow depth is observed at the meteorological stations Plai and Pozhezhevska, which altitudes are the highest. During 1991–2019 the mean snow depth at the meteorological station Plai in the third decade of February, when it is the largest, is 46 cm. In turn the mean snow depth at the meteorological station Pozhezhevska in the third decade of March, when it is the largest, reaches 42 cm. The mean snow depth among the largest measured values at these meteorological stations is 73 and 78 cm respectively.
During 1991–2019 the largest snow depth was registered at the end of the cold and snowy winter of 1998/1999. That winter the mean snow depth among the largest measured ones at 11 stations was 106 cm. The lowest value was observed in winter 2015/2016, when it was 20 cm.
The available data show that despite the increase in air temperature (primarily at small altitudes), the snow depth increases as well. The most essential increase is observed in February, March and the first half of April. During 1961–1990 the mean snow depth at 9 meteorological stations in low-mountain terrain, when it is the largest, was 17 cm, during 1991–2019 it was 18 cm. The more essential changes are observed at the meteorological stations Plai and Pozhezhevska, located at the highest altitudes, – correspondingly 33 and 42 cm (Fig. 10).
Nowadays the largest snow cover is observed some later, than it was before. In our view the increase in snow depth at two meteorological stations, located at the highest

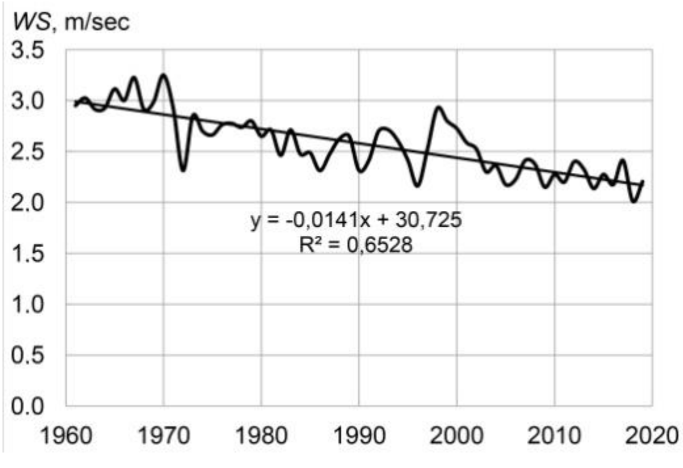

Fig. 8. The changes in mean wind speed at 11 meteorological stations in the Ukrainian Carpathians.

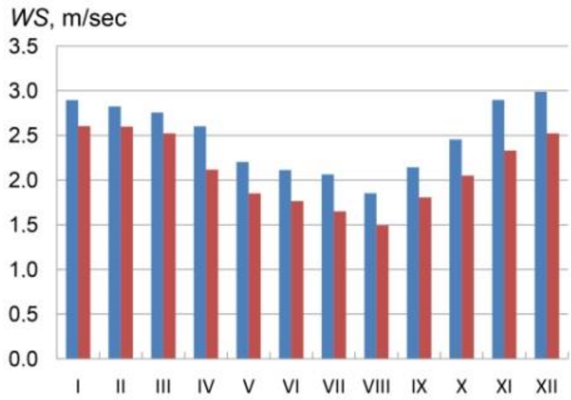

Fig. 9. Wind speed at 11 meteorological stations in the Ukrainian Carpathians: left columns – during 1961–1990, right columns – during 1991–2019.

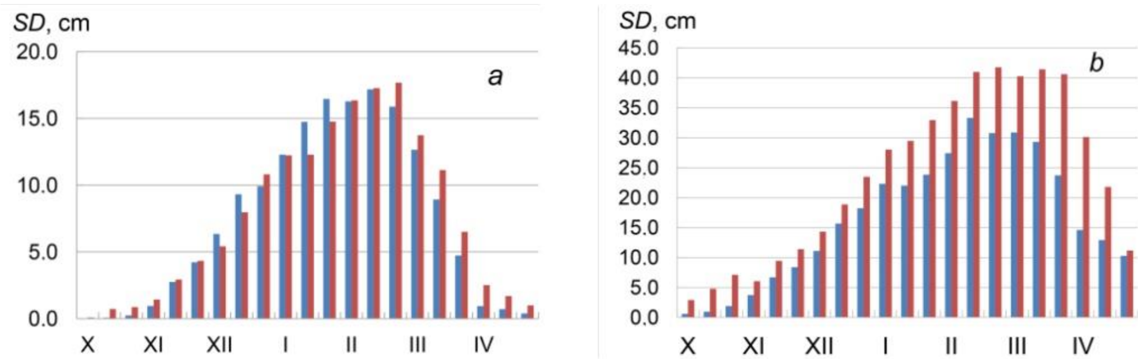

Fig. 10. The mean snow depth in the Ukrainian Carpathians: a) – at 9 meteorological stations in low-mountain terrain, b) – at highest Plai and Pozhezhevska stations; left columns – during 1961–1990, right columns – during 1991–2019.

altitudes, is caused by the precipitation increase in cold period. It should be noted that at these meteorological stations the changes in air temperature in winter are not significant and are statistically unreliable.

Another reason for the increase in snow depth at the Plai and Pozhezhevska meteorological stations, located on the mountain tops, may be the decrease in wind speed. At high wind speeds snow mainly accumulates in the lower parts of the area. Now that the wind speed has decreased, its depth has become more uniform.

The meteorological stations Plai and Pozhezhevskaya are characterized not only by the largest snow cover, but also by its longest duration. For example, in the first decade of October, the presence of snow has a probability of 28–30%.

River runoff

There are some dozens of gauging stations on the rivers of the Ukrainian Carpathians. In most cases the observation of river runoff was started in the middle of 20th century. For analyzing of water runoff the data of 8 rivers, which are not small and not large, were analyzed. The studied rivers are located evenly by territory. Four rivers basins are located on the southeastern macroslope of the mountains (Bila Tysa – Luhi, Teresva – Ust-Chorna, Rika – Mezhihiria, Latoritsa – Pidpolozzia) and four ones (Stryi – Matkiv, Limnitsa – Osmoloda, Prut – Yaremche, Chorna Tysa – Verkhovyna) – on the northeastern macroslope. It is important that the data of all selected rivers practically do not have the observation gaps. The catchment areas of the selected rivers range from 106 km^2 (Stryi – Matkiv) to 657 km^2 (Chorna Tysa – Verkhovyna). The range of altitudes of the river basins is 720–1200 m with a mean value of 1009 m. The range of runoff depth is 666–1050 mm with a mean value of 842 mm (Table 2).

The river runoff at all studied gauging stations is characterized with the essential variability, both annual and seasonal. There is no tendency in increasing or decreasing in annual values of water discharge or runoff depth during the observation period. At the same time it can be observed two cycles similar to precipitation (Fig. 11).

As it can be seen, the Fig. 6 and Fig. 11 are rather similar. It means that precipitation plays an essential role in river runoff formation. The correlation coefficient between the mean annual runoff depth (RD) of 8 studied rivers and the mean annual precipitation reaches 0.90 (Fig. 12). This result was confirmed by the use of correlation and regression analyses. The effect of air temperature on river runoff is reverse and rather small. Nevertheless taking into consideration this factor this dependence becomes closer with a correlation coefficient of 0.95.

Comparing the available precipitation and runoff depth data, one should take into account the essential differences in mean altitude of meteorological stations (702 m) and studied river basins (1009 m). It means that actual precipitation in the studied river basins is larger, than average values of measured data. Based on the dependence of precipitation on altitude, it can be considered that it is 1.1–1.2 times larger than the mean values at the studied meteorological stations.

Many authors (Gorbachova, 2015; Obodovskyi and

Table 2. The main hydrological parameters of the selected rivers in the Ukrainian Carpathians

River	Gauging station	Area of river basin [km^2]	Average altitude of river basin [m a.s.l.]	Average discharge 1961–2019 [m^3·s^{-1}]	Runoff depth [mm]
Bila Tysa	Luhi	189	1200	5.09	849
Teresva	Ust-Chorna	572	1100	18.3	1009
Rika	Mezhihiria	550	800	13.6	780
Latoritsa	Pidpolozzia	324	720	9.25	900
Stryi	Matkiv	106	860	2.69	800
Limnitsa	Osmoloda	203	1200	6.76	1050
Prut	Yaremche	597	990	12.6	666
Chorna Tysa	Verkhovyna	657	1200	14.2	682

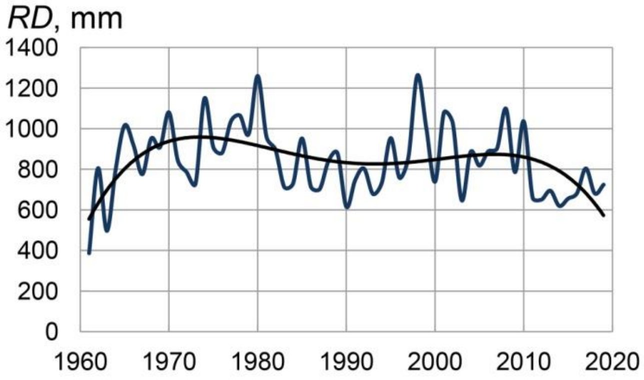

Fig. 11. The changes in annual runoff depth at 11 gauging stations.

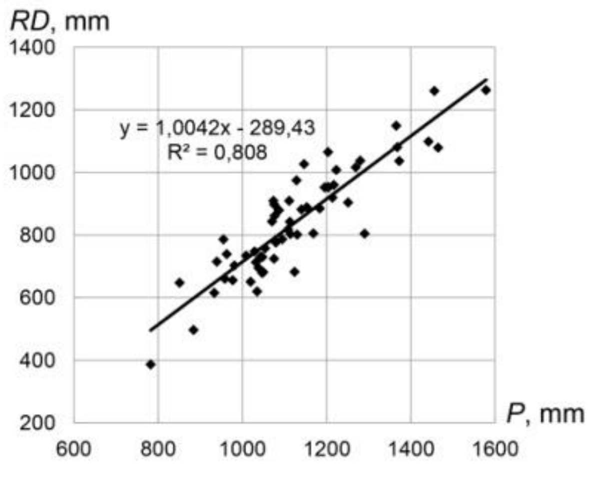

Fig. 12. The dependence of mean runoff depth of 8 studied rivers (Bila Tysa – Luhi, Rika – Mezhihiria, Teresva – Ust-Chorna, Latoritsa – Pidpolozzia, Stryi – Matkiv, Limnitsa – Osmoloda, Prut – Yaremche, Chorna Tysa – Verkhovyna) in the Ukrainian Carpathians on mean annual precipitation at 11 meteorological stations.

Lukianets, 2017) found out that the river runoff in this region is of a cycle nature. The duration of the cycles determined in the paper (Obodovskyi and Lukianets, 2017) is 29 years, which is practically equal to our findings.

There is a point of view (Duethmann and Blösch, 2018) that during four last decades the tendency of evaporation increase is observed. This result is based on the calculation of water balance made for the territory of Austria, mainly covered by mountains. The available data, collected for the Ukrainian Carpathians, enable to evaluate these changes as well. The calculations were carried out in two ways. The first one was based on precipitation data at 11 studied meteorological stations and water discharge of 8 studied rivers. It was found out that the calculated evaporation at the beginning of the observation had the tendency to decrease and during the last decades – to increase.

The more reliable result was obtained with the use of the data from the Prut River basin within which two meteorological stations Pozhezhevska and Yaremche are located. It is important that average altitude of this river basin (990 m) coincides with the mean altitude of these stations (991 m). During 1961–2019 the actual precipitation at these stations was 1473 and 968 mm respectively. The mean precipitation value for these two stations was 1220 mm, the mean runoff depth was 666 mm. It means that mean evaporation in this river basin was 554 mm and runoff coefficient was 0.55.

During the observation period the calculated evaporation in the Prut River basin was characterized with essential fluctuations. The first reason of these fluctuations is insufficient data on the precipitation within the river basin. Another important factor is the use of the data of a calendar year, but not of the hydrological one. For example, the essential precipitation in the end of 2001 had an effect on the water storage and river runoff formed next year. In any cases the calculated evaporation at the beginning of the observation period in a whole had the tendency to decrease and during the last four decades – to increase. This result is similar to the one obtained for the territory of Austria (Duethmann and Blösch, 2018), (Fig. 13).

The important issue is the seasonal changes in river runoff. These changes were analyzed by division of available runoff data on two periods: 1961–1990 and 1991–2019, as it was carried out in other cases. It turned out that these changes are not very essential. With a certain level of probability, we can state that these changes only in separate months.

The common feature of the rivers, located at high altitude, is the increase in water runoff in cold period from September till April. This feature can be explained by the increase in precipitation during this period of year and melting of snow cover in March and April. The common feature of the rivers, primarily located in low-mountain terrain, is the decrease in water runoff from May till August. In our view it is caused by the decrease in precipitation during this period along with the simultaneous increase in air temperature and evaporation (Fig. 14).

The differences in seasonal distribution of river runoff become more evident for high-water and low-water phases of the obtained cycles. The common feature of the seasonal distribution during the last wet (1998–2010) and dry (2011–2019) phases is the similar runoff in January–February. In contrast to that in the rest months the water runoff in low-water phase is much less than in high-water one. It means that the main role in the river runoff formation in the mountains plays the precipitation in warm period.

In our view the result of study referring to the changes in precipitation, river runoff and evaporation, essentially depends on the observation period. If we operate with the data during a high-water phase, the findings are essentially different than in case of low-water phase or the whole cycle of river runoff.

Our results and the results of many other scientists (Duethmann and Blösch, 2018; Lukianets et al., 2019; Obodovskyi and Lukianets, 2017; Zabolotnia et al., 2019) show that nowadays the period of lower than usual water runoff is observed. The presence of the strong correlation between river runoff and precipitation proves that last one is the main influencing factor in the observed changes. Air temperature increase, which intensifies evaporation, causes the additional effect.

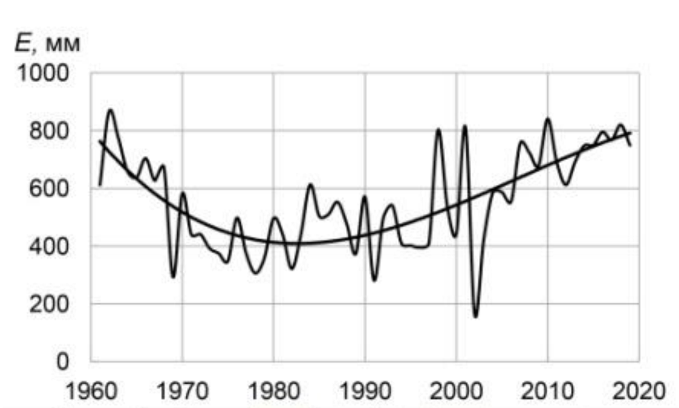

Fig. 13. The changes in calculated evaporation in the Prut River basin upstream Yaremche gauging station.

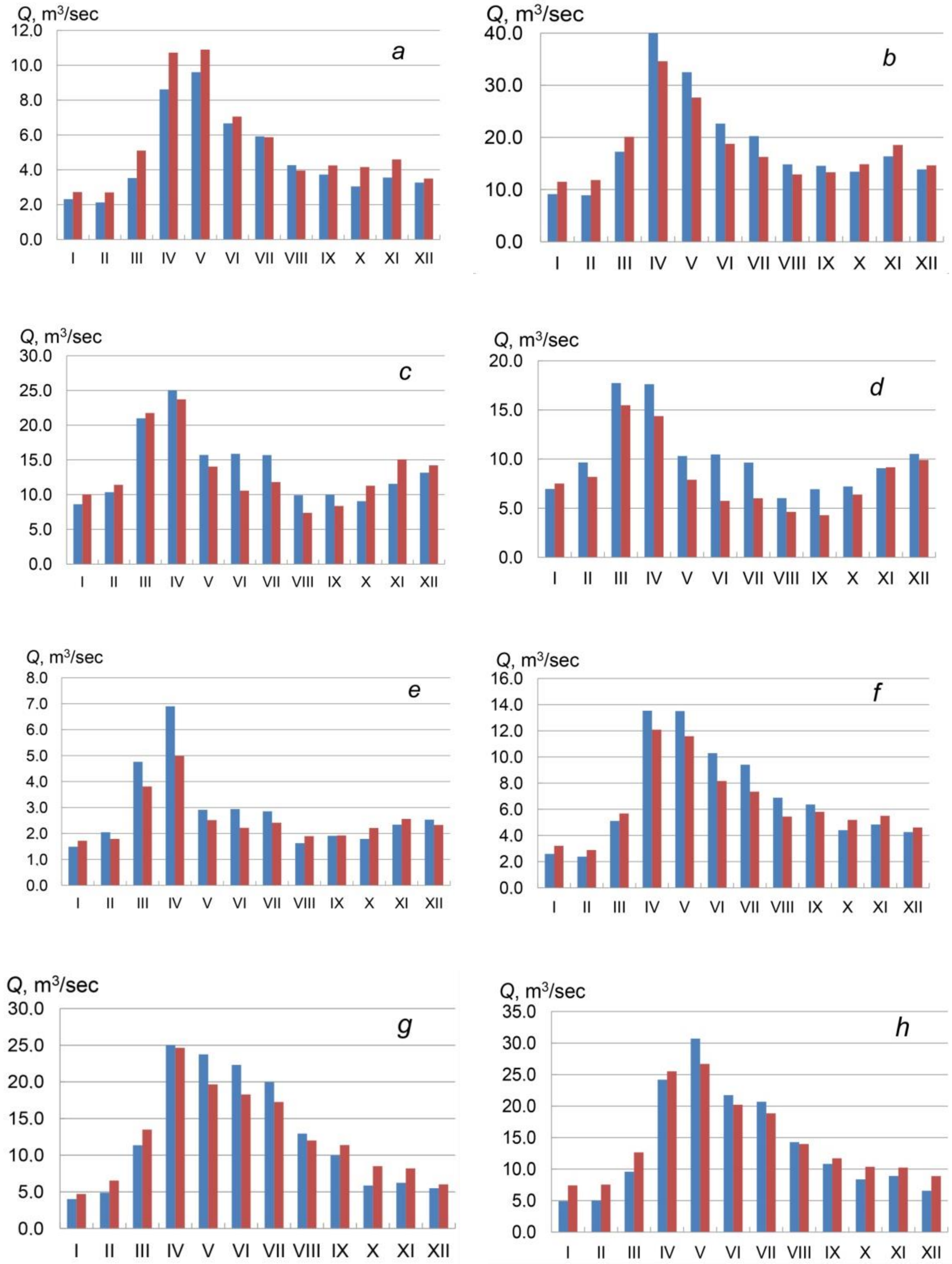

Fig. 14. The intra-annual distribution of water discharge in the Ukrainian Carpathians rivers: a) – Bila Tysa – Luhy, b) – Teresva – Ust-Chorna, c) – Rika – Mezhihiria, d) – Latoritsa – Pidpolozzia, e) – Stryi – Matkiv, f) – Limnitsa – Osmoloda, g) – Prut – Yaremche, h) – Chornyi Cheremosh – Verkhovyna (left columns – during 1961–1990, right columns – during 1991–2019), (a) – d) – south-western macroslope, e) – h) – north-eastern macroslope).

Conclusions

The available data obtained from 11 meteorological stations in the Ukrainian Carpathians show the presence of vivid tendency of air temperature increase. During 1961–2019 the increase in air temperature is about 2°C. The thermal gradient in the mountains is much less than it is in free troposphere. At the low altitude it is larger than on the tops of the mountains. The largest gradient is observed in the period from March till July, when the difference in air temperature at the altitude of 1000 and 2000 m is equal to 0.33–0.36°C per 100 m. The lowest gradient (0.15–0.18°C per 100 m) is observed at these altitudes in the period from November till January. The changes in annual precipitation in the Ukrainian Carpathians are not essential. These changes are of a cycle nature with the period of about 30 years. It is likely that modern dry phase will continues till the mid-2020s. The seasonal changes in the precipitation are rather small. Probably there is a small increase in cold period from September till March. In turn the precipitation in summer time is characterized with a tendency to decrease, primarily in June. Nowadays it is observed the increase of snow cover depth on the tops of the mountains. There is a vivid tendency of wind speed decrease, which is the most obvious in the second part of a year.

In spite of some changes in the climatic parameters the annual river runoff has not changed essentially for some last decades. Similar to the changes in precipitation, it is of a cyclic nature. Nowadays the phase of relative small water runoff, which started in 2011, is observed.

The calculated evaporation, based on the water balance, shows up the cyclic nature of this phenomenon, but the duration of the cycles is larger, than for precipitation and river runoff. The available data indicate that the increase in evaporation has been lasting for about 40 years.

The warer runoff of the rivers, located at high altitudes, has the tendency to increase in cold period. In turn the common feature of the rivers, primarily located in low-mountain terrain, is the decrease in water discharge in the period from May till August.

References

Bednorz, E. (2004): Snow cover in Eastern Europe in relation to temperature, precipitation and circulation. Int. J. Climatol. 24: 591–601. DOI: 10.1002/joc.1014.

Blöschl, G., Hall, J., Parajka, J. et al. (2017): Changing climate shifts timing of European floods. Science 357, 588–590. DOI: 10.1126/science.aan2506.

Didovets, L., Krysanova, V., Bürgera, G. et al. (2019): Climate change impact on regional floods in the Carpathian region. Journal of Hydrology: Regional Studies, 22, 1–14. DOI.org/10.1016/j.ejrh.2019.01.002.

Duethmann, D., Blösch, G. (2018): Why has catchment evaporation increased in the past 40 years? A data-based study in Austria. Hydrol. Earth Syst. Sci., 22, 5143–5158. DOI.org/10.5194/hess-22-5143-2018.

Fendekova, M., Gauster, T., Labudova, L. et al. (2018): Analysing 21st century meteorological and hydrological drought events in Slovakia. J. Hydrol. Hydromech., 66, 2018, 4, 393–403. DOI: 10.2478/johh-2018-0026.

Gorbachova, L. (2015): The intra-annual streamflow distribution of Ukrainian rivers in different phases of long-term cyclical fluctuations. ENERGETIKA. 61, 2, 71–80.

Gorbachova, L., Zabolotnia, T., Khrystyuk, B. (2018): Homogeneity and stationarity analysis of the snow-rain floods in the Danube Basin within Ukraine. Acta Hydrologica Slowaca. 19, 1, 35–41.

Grebin, V. V. (2010): The modern water regime of the Ukrainian rivers (landscape-hydrological analyses). Kyiv, 316. (in Ukrainian).

Guo, H., Xu, M., Hu, Q. (2011): Changes in near-surface wind speed in China: 1969–2005. Int. J. Climatol. 31: 349–358. DOI/epdf/10.1002/joc.2091.

Halmová, D., Pekárová, P. (2020): Runoff regime changes in the Slovak Danube River tributaries. Acta Hydrologica Slovaca. 21, 1, 2020, 9–18. DOI: 10.31577/ahs-2020-0021.01.0002.

Holko, L., Sleziak, P., Danko, M., Bičárová, S., Pociask-Karteczka, J. (2020): Analysis of changes in hydrological cycle of a pristine mountain catchment. 1. Water balance components and snow cover. J. Hydrol. Hydromech., 68, 2, 180–191. DOI: 10.2478/johh-2020-0010.

Kablak, N. I. (2007): Modeling changes of physical parameters of the atmosphere with a height. Kinematics and physics of sky. 23, 1, 18–24 (in Ukrainian).

Kubiak-Wojcicka, K. (2020): Variability of air temperature, precipitation and outflows in the Vistula Basin (Poland). Resources 9, 103, 1–26. DOI.org/10.3390/resources 9090103.

Loboda, N. S., Kozlov, M. O. (2020): Assessment of water resources of the Ukrainian rivers according to the average statistical models of climate change trajectories RCP4.5 and RCP8.5 over period of 2021 to 2050. Ukrainian Hydrometeorological Journal, 25, 93–104. DOI: 10.31481/uhmj.25.2020.09 (in Ukrainian).

Lukianets, O., Obodovskyi, O., Grebin, V., Pochaievets, O. (2019): Time series analysis and forecast estimates of the mean annual water runoff of rivers in of the Prut and Siret basins (within Ukraine). Electronic book with full papers from XXVIII Conference of the Danubian Countries on Hydrological Forecasting and Hydrological Bases of Water Management, Kyiv, 133–139.

Marin, L., Birsan, M.-V., Bojaru, R., Dumitrescu, A. et al. (2014): An overview of annual climatic changes in Romania: trends in air temperature, precipitation, sunshine hours, cloud cover, relative humidity and wind speed during the 1961–2013 period. Carpathian Journal of Earth and Environmental Sciences, November, 9, 4, 253–258.

Mostowik, K., Siwek, J., Kisiel, M. et al. (2019): Runoff trends in a changing climate in the Eastern Carpathians (Bieszczady Mountains, Poland). Catena, 182. DOI.org/ 10.1016/j.catena.2019.10417.

Obodovskyi, O., Lukianets, O. (2017): Patterns and forecast of long-term cyclical fluctuations of the water runoff of Ukrainian Carpathians rivers. Research, Engineering & Management. 73, 1, 33–47.

Rangwala, I., Miller, J. R. (2012): Climate change in mountains: a review of elevation-dependent warming and its possible causes. Climatic Change. DOI 10.1007/ s10584-012-0419-3.

Rolland, C. (2003): Spatial and seasonal variations of air temperature lapse rates in Alpine regions. J. Climate 16 (7): 1032–1046. DOI.org/10.1175/1520-0442(2003)016< 1032:SASVOA>2.0.CO;2.

Rožnovský, J., Střeštík, J., Štěpánek, P., Zahradníček, P.

(2020): The dynamics of annual and seasonal precipitation totals in the Czech Republic during 1961–2019. Acta Hydrologica Slovaca. 21, No. 2, 197–204. DOI: 10.31577/ahs-2020-0021.02.0024.
Spinoni, J., Szalai, S., Szentimrey, T. et al. (2015). Climate of the Carpathian Region in the period 1961–2010: climatologies and trends of 10 variables. Int. J. Climatol. 35: 1322–1341. DOI: 10.1002/joc.4059.
Stagl, J. C., Hattermann, F. F. et al. (2015): Impacts of climate change on the hydrological regime of the Danube River and its tributaries using an ensemble of climate scenarios. Water 7(11), 6139-6172. DOI.org/10.3390/w7116139.
Szolgay, J., Blöschl, G., Gribovszk, Z., Parajka, J. et al. (2020): Hydrology of the Carpathian Basin: interactions of climatic drivers and hydrological processes on local and regional scales – HydroCarpath Research. J. Hydrol. Hydromech., 68, 2020, 2, 128–133. DOI: 10.2478/johh-2020-0017.
Wang, G., Zhao, M., Kang, M. et al. (2017): Diurnal and seasonal variation of the elevation gradient of air temperature in the northern flank of the western Qinling Mountain range, China. J. Mt. Sci. 14, 94–105. DOI.org/10.1007/s11629-016-4107-z.
Zabolotnia, T., Gorbachova, L., Khrystiuk, B. (2019): Estimation of the long-term cyclical fluctuations of snow-rain floods in the Danube basin within Ukraine. Meteorology, Hydrology and Water Management. 7, 2. 3–9. DOI: https://doi.org/10.26491/mhwm/99752.

Prof. Viktor I. Vyshnevskyi (*corresponding author e-mail: vishnev.v@gmail.com)
National Aviation University,
Liubomyra Huzara Ave, 1,
03058, Kyiv,
Ukraine,

Ing. Olena A. Donich
Central Geophysical Observatory,
Nauka Ave, 39,
03028, Kyiv,
Ukraine

DOI: 10.31577/ahs-2021-0022.01.0002

ACTA HYDROLOGICA SLOVACA

Volume 22, No. 1, 2021, 15 – 21

WATER MANAGEMENT SYSTEM LIPTOVSKÁ MARA – BEŠEŇOVÁ IN THE CONTEXT OF CLIMATE CHANGE

Emília Bednárová*, Juraj Škvarka, Patrik Václavík, Jana Poórová

The presented article briefly presents the impact of the Liptovská Mara – Bešeňová water management system operation on the runoff conditions downstream the dam. The analysis showed that its benefit is evident, especially in the period of extreme hydrological phenomena, with the occurrence of long-lasting low flows or in the event of short-term flood flows. In the area of Liptovská Mara and Bešeňová, this is evident mainly in winter and spring, because of a small amount of liquid precipitation in winter and melting snow in the surrounding mountain massifs in spring. Other hydraulic structures' actual experiences also convince us that Slovakia's variability of natural conditions requires artificial water sources. In the interest of raising living standards, protecting the environment, and sustainable development, their role is irreplaceable. In recent decades, there has been an increasing debate about the growing demands on water caused by registered climate change and its effects on weather extremes, as well as human demographic change. History confirms that water reservoirs can reduce negative impacts caused by extreme hydrological phenomena – floods and droughts. In line with the need for adaptation to climate change and sustainable development, in addition to measures close to nature, technical measures, reservoirs, and dams are also necessary.

KEY WORDS: reservoir, dam, climate change, floods, drought, minimum flow

Introduction

The Liptovská Mara – Bešeňová water management system is located in the northern part of central Slovakia, in the upper section of the Váh River. It was built between 1967 and 1975, and it is one of the crucial hydraulic structures of the Slovak Republic. Its purpose is to produce electricity for peak hours, flood control, and improve the flows of the Váh for industry and agriculture. The Liptovská Mara reservoir, together with the second largest Orava reservoir on the Orava River, which is the right-side stream of the Váh, as top reservoirs control flows in the Váh, starting from the riverbed downstream Bešeňová reservoir to the estuary to the Danube (Fig. 1). Both hydraulic structures use the rivers' energy potential, significantly reducing flood flows and reducing possible flood damage.

Through coordinated action in the system, they improve the river's flow rates in favor of domestic water and industrial or irrigation. They also enable the dilution of wastewater and improve the self-purification of the river. They also play a significant role in ensuring a sufficient flow in the Váh and its derivation channels when using the hydropower potential at the Vážská cascade. Both reservoirs simultaneously compose the scenery of the landscape. These reservoirs are an integral part of the country, and they enable sports activities and createcenters of tourism.

Recurring hydrological extremes are also an accompanying feature of registered climate change and global warming. Short-term flood flows vary with long periods of drought. Thus, the question of the large water reservoirs' influence on the hydrological regime of streams under dams comes to the forefront. In this article, we present the impact of the Liptovská Mara – Bešeňová water management system operation on the runoff conditions in the Váh River.

Basic parameters and a brief description of objects

The objects of the Liptovská Mara are the dam and the reservoir, appurtenant structures as intakes and outlets of the hydroelectric power plant, spillways, and bottom outlets, a channel downstream of the dam. The objects of the Bešeňová are the dam with a compensating reservoir, an associated appurtenant structure, and a channel downstream of the dam. The essential data of both structures are given in Table 1. Other objects of the water management system are dikes for the protection of adjacent municipalities, dikes of the canal between the Liptovská Mara power plant and the Bešeňová reservoir, and pumping stations (Bednárová et al., 2010).

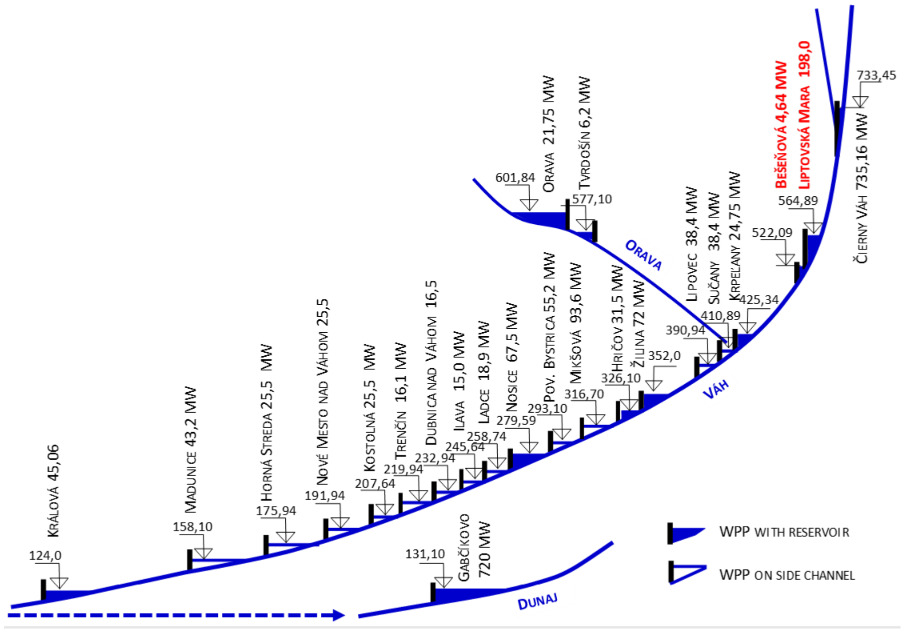

Fig. 1. Longitudinal elevation section of the Váh with plotted WPP in operation.

Table 1. Basic parameters of hydraulic structures

Basic information	Liptovská Mara	Bešeňová
construction	1967–1975	1967–1975
nearest municipality/stream	Vlachy and Vlašky / Váh	Bešeňová / Váh
height of the dam above the terrain / above the foundation joint	45 m / 52.5 m	12.5 m / 12.9 m
length of the dam's crest	1225 m	1109.4 m
volume of reservoir	361.9 mil m^3	10.73 mil m^3
purpose	electricity production, flood protection, flow improvement, recreation, fish farming	electricity production, compensating reservoir for Liptovská Mara, railway on the dam's crest

Description of the Liptovská Mara dam

The Liptovská Mara dam is located on the Váh River. The dam is an earth-fill heterogeneous dam with silty sealing (Fig. 2). A double-layer filter protects the silty sealing.
Stabilizing prisms are made of gravelly and sandy soils, excavated in the alluvium of Váh. The subsoil of the dam was sealed from the grouting gallery by a grout curtain. The dam's upstream slope has slopes of 1:2.25 to 1:3, in the lower part 1:5. The downstream slope inclines 1:1.8; for every 10 m, there are 4 m wide berms. There is a drain on the downstream toe of the dam. A riprap protects the upstream slope; the downstream slope is humidified and grassed.
Appurtenant structures consist of a spillway in the area of the left valley slope. These are two fields, 11.0 m wide with a height of 3.6 m and a total capacity of 268.50 $m^3\ s^{-1}$. The left tunnel and the right tunnel used as bottom outlets with a total capacity of 80–280 $m^3\ s^{-1}$. The capacity depends on the water level in the Liptovská Mara and Bešeňová reservoirs. The hydraulic structure's integral part is a pumped-storage hydroelectric power plant with an installed capacity of 198 MW (2 x Kaplan + 2 x Dériaz, flow $2{\cdot}140\ m^3\ s^{-1} + 2{\cdot}130\ m^3\ s^{-1}$).
The geological composition of the Liptovská Mara and Bešeňová consists of a Paleogene and a Quaternary. Slope sediments were formed mainly by weathering of the Paleogene. The Paleogene is formed mainly by flysch layers of claystone and various types of sandstones.
Quaternary sediments form slope debris with a low content of silty components. Fluvial sediments occur in two terraces, covered with a thick layer of sloping silt or clay. Eolithic sediments form a thick cover of terraces. In many cases, they are moved by deluvial material (mainly deluvial clays).

Description of the Bešeňová dam

The Bešeňová dam is situated at the river kilometer of 335.22 (Fig. 3). The backwater level is at an elevation of 522.09 m a.s.l. and creates a reservoir that serves as a compensating reservoir for the peak load hydropower plant of the Liptovská Mara. It is an earth-fill heterogeneous dam with silty sealing. The sealing of the dam protected by a double-layer filter on both sides is embedded to the subsoil by a silty-concrete cutoff wall and grouting curtain. There is a railway at the crest of the dam. The hydroelectric power plant has two direct flow Kaplan turbines with a capacity of $2 \cdot 20\ m^3\ s^{-1}$ and with a maximum output of 2·2.4 MW with bypassed alternators.

Hydrological parameters

Liptovská Mara and Bešeňová are in the Liptovská basin, in the valley of the upper section of the Váh River. They are surrounded on the northeast by the Western Tatras, on the south by the Low Tatras, west by the Great and Little Fatra, and the northwest by the Choč Hills. The catchment area of the Liptovská Mara dam profile is 1,481.90 km^2, and the Bešeňová dam profile 1,612.23 km^2. The average annual rainfall is about 710 mm. There are 11 tributaries to the reservoirs, but Váh, Demenovka, Palúdžanka, Lupčianka, Jalovský, and Kvačianka have a significant influence (Fig. 4).

The measurement results for the period 1978–2019 (Fig. 5) show that the average monthly inflow into the reservoirs is 27.988 $m^3\ s^{-1}$ and the average monthly outflow from the Bešeňová reservoir is 26.184 $m^3\ s^{-1}$. The difference between inflow and outflow can be attributed to vapor losses and seepage.

The system of Liptovská Mara – Bešeňová, besides its activities (usage of hydropower potential, reduction of flood flows, flows improvement for the industry, agriculture, improving water quality, recreation, and sports, navigation, and fishing), has to provide a minimum flow of 15 $m^3\ s^{-1}$ year-round in the river Váh downstream the compensating reservoir Bešeňová. Exceptionally, the outflow can be reduced to 10 $m^3\ s^{-1}$ if the flow of the left-side tributary Váh – Revúca downstream the Bešeňová exceeds 5.0 $m^3\ s^{-1}$, or if the level in Liptovská Mara falls below the level of 562.00 a.s.l. in the period from July to December (due to reserving a sufficient volume of water in the reservoir for safe winter operation) (Lukáč et al., 1996).

Influence of hydraulic structure on outflow downstream the dam

The operation's influence on the outflow conditions downstream of the dam can be presented by the probability curve of the inflow into the reservoirs (Q_p) and the outflow into the riverbed downstream the dam (Q_o) (Lukáč et al., 1991, Votruba and Patera, 1997). Fig. 6 shows the average monthly flows in the winter months (January February), in the spring months (April and May), in the summer months (July, August), and in the autumn months (November December).

The presented graphs show the minimum flow of 15 $m^3\ s^{-1}$ and its reduced value of 10 $m^3\ s^{-1}$. The average monthly flow analysis shows that the water management system's operation redistributes them during the year. While in the winter months, the flows under the dam are significantly improved, in the spring months, the higher

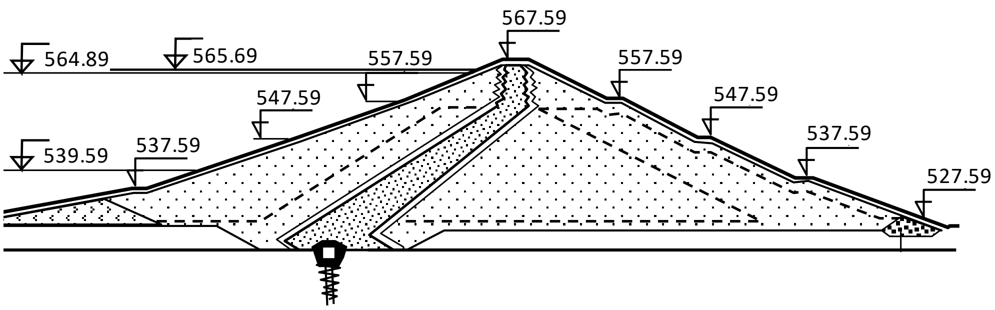

Fig. 2. Cross-section profile of the Liptovská Mara dam.

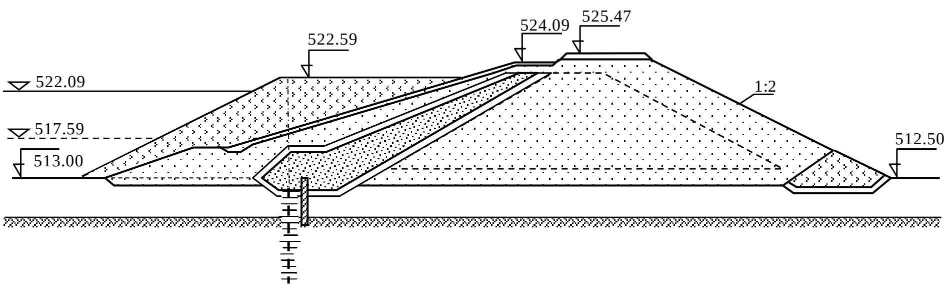

Fig. 3. Cross-section profile of the Bešeňová dam.

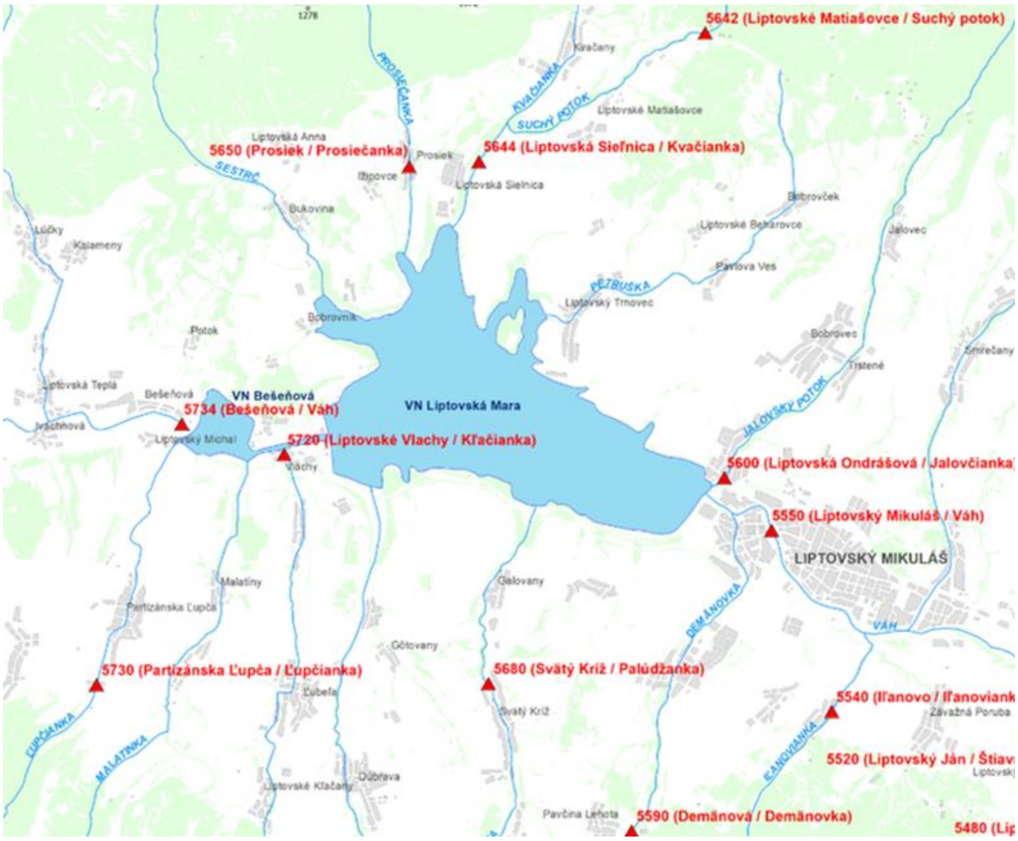

Fig. 4. The situation of water reservoirs de Liptovská Mara and Bešeňová with gauging stations of Slovak Hydrometeorological Institute.

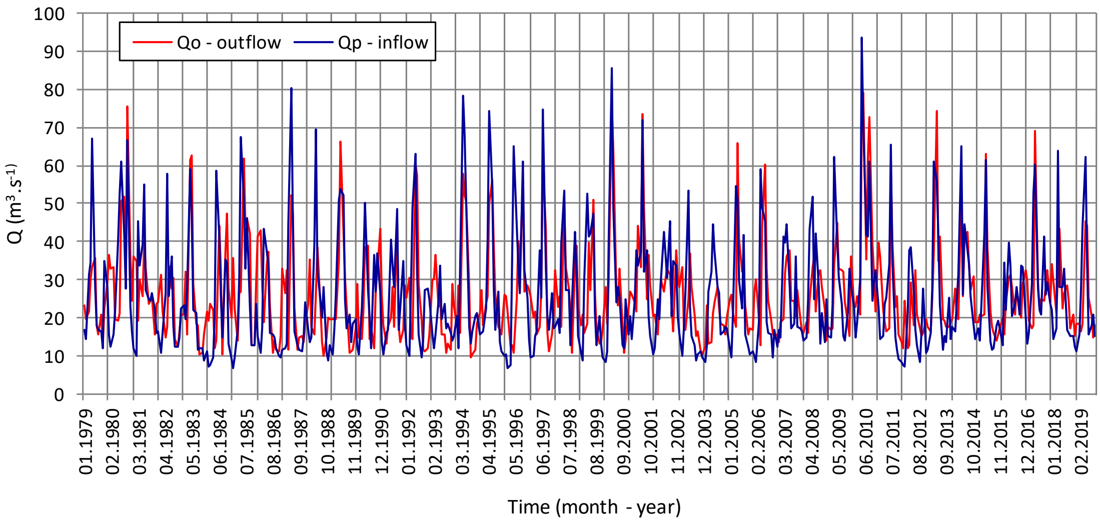

Fig. 5. Development of the average monthly inflow to the Liptovská Mara reservoir and outflow to the riverbed downstream the Bešeňová dam.

flows are reduced. In the summer and autumn months, the reservoir's impact on the runoff conditions downstream of the dam is less significant. The water management system's positive function on the outflow ratios in the Váh can also be registered in Fig. 7. There are presented inflows and outflows with a probability of 5% (increased flows), 50% (average flow values), and 90% and 95% (low flow values). We can register the positive impact of the reservoir's operation on the hydrological regime of the Váh downstream the Bešeňová dam profile. The positive effect of the Liptovská Mara operation on the redistribution of flows is evident from the fluctuating annual cycle of inflows – the accumulation of water in the spring months and increasing outflows in the winter months. This is also confirmed by the decrease in the coefficients of the variation value of the analyzed average monthly inflows and outflows with a presented probability of occurrence of 5% to 95% (Table 2).

The documented results (Fig. 8) show that the most vulnerable is the winter period. Then the natural reliability *Pα* reaches the specified minimum flow of 15 $m^3 \cdot s^{-1}$ with a probability of only 30 to 40%. Without

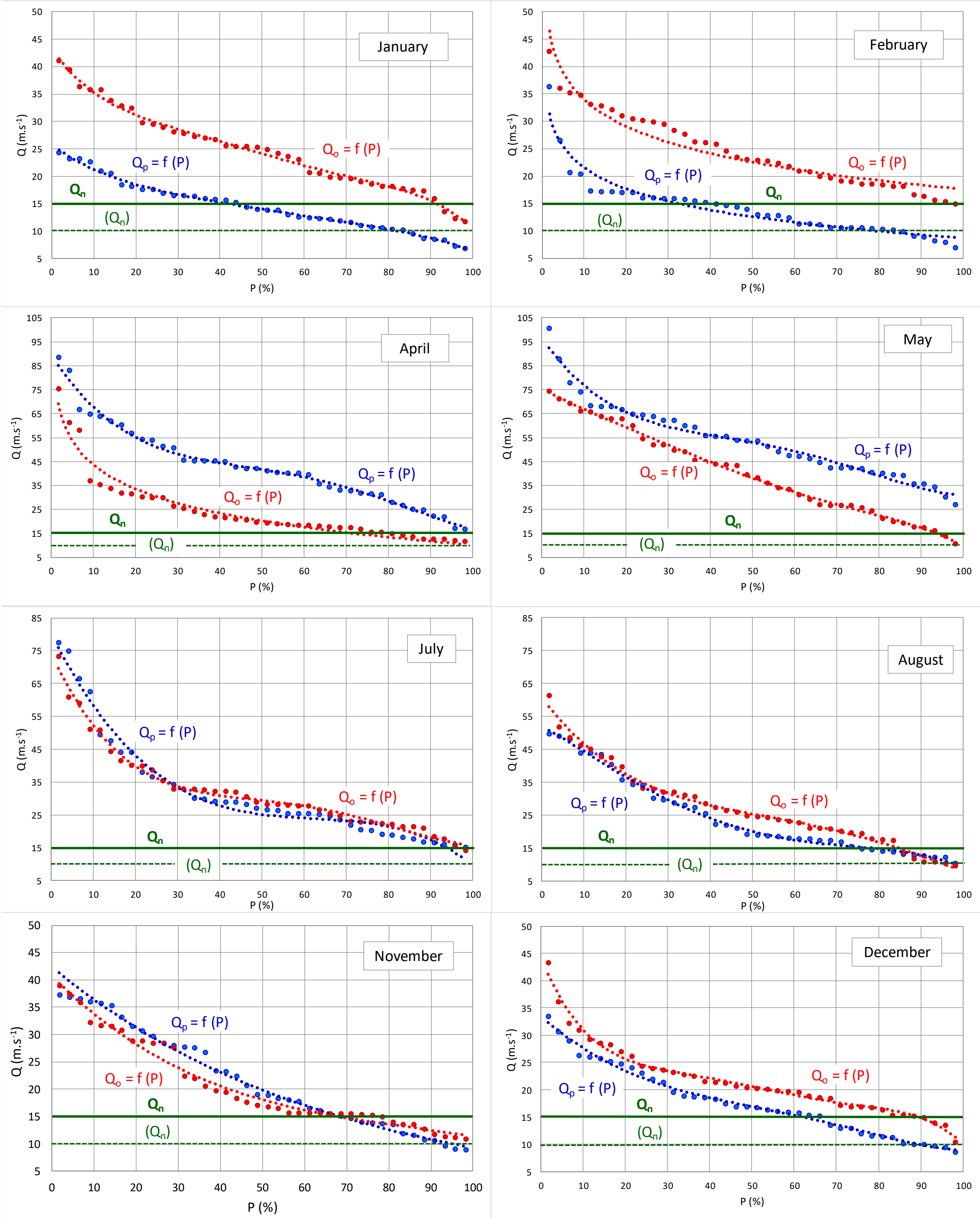

Fig. 6. Probability curves of inflow and outflow in winter, spring, summer, and autumn months.

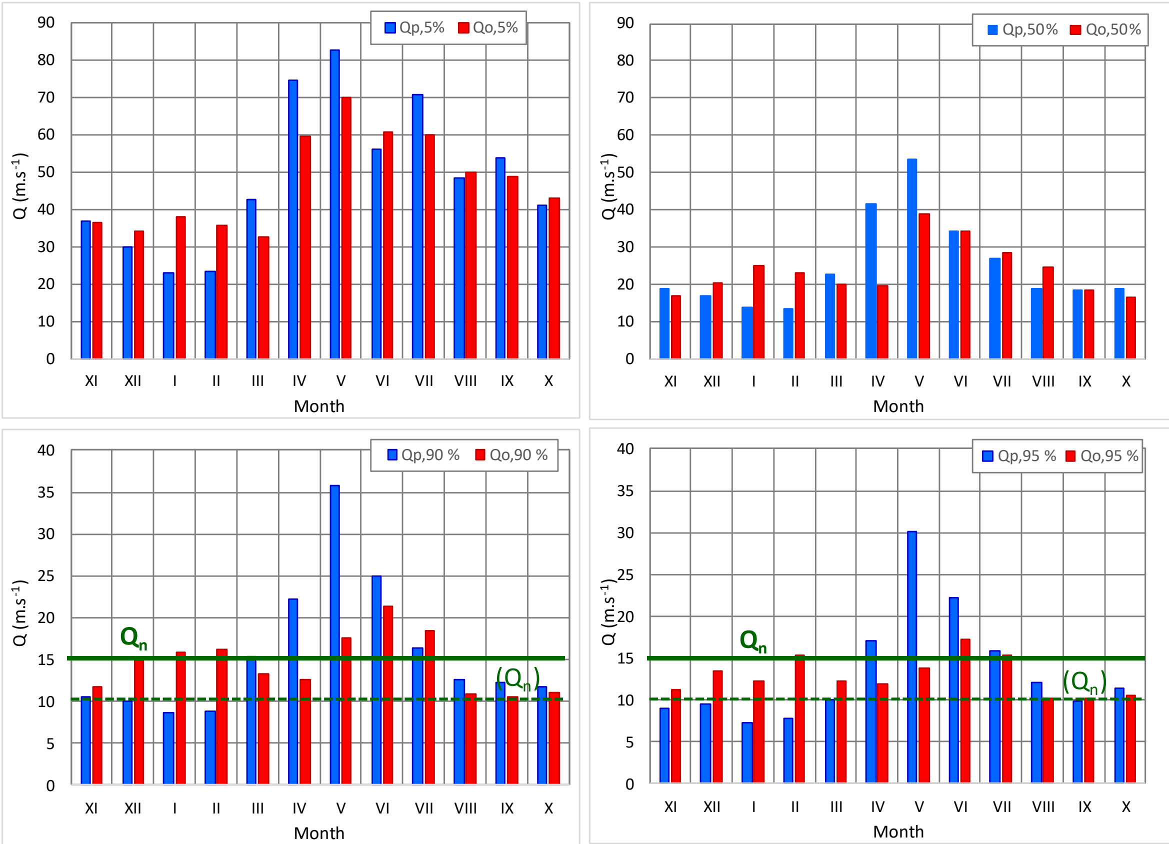

Fig. 7. *Development of average monthly inflows and outflows with probabilities of occurrence of 5%, 50%, 90%, and 95%.*

Table 2. Coefficients of variation of inflows (Q_p) and outflows (Q_o)

Q	$Q_{p,5\,\%}$	$Q_{o5\%}$	$Q_{p,50\%}$	$Q_{o,50\%}$	$Q_{p90\%}$	$Q_{o,90\,\%}$	$Q_{p,95\,\%}$	$Q_{o,95\,\%}$
C_v	1.666	1.451	0.619	0.361	0.466	0.360	0.493	0.420

Fig. 8. *View of the Liptovská Mara dam with the High Tatras in the background.*

improving the flows in the Váh through the Liptovská Mara reservoir, with a probability of more than about 65% (almost two months from the three-month winter period), a minimum flow of 15 $m^3 s^{-1}$ would not be ensured in the Váh riverbed.

The flood control function cannot be neglected either when evaluating the impact of reservoirs on the outflow regime downstream of the dam. Data shows that there were often recurring major floods in the period before 1950 when there were no reservoirs and dams in Slovakia. On the Orava River we can mention floods in the years 1725, 1748, 1749, 1750 ... 1813, 1830, 1870 ... 1848, on the Váh River in the years 1557, 1593, 1594 ..., 1602, 1622, 1625 ... 1710, 1714 ... 1813, 1880 ... 1950 ... 1960. The construction of the Orava and Liptovská Mara reservoirs (Fig. 8) significantly eliminated their occurrence.

The production of green electricity must be added to the positives of the Liptovská Mara – Bešeňová water management system to ensure minimum flows under the dam. The Liptovská Mara and Bešeňová hydro-electric power plants have produced more than 6,500 GWh of green electricity from a renewable source – water, with an average annual production of 152.8 GWh (134.5 GWh + 18.3 GWh). An essential function of the water management system is also to improve the flow for hydropower plants throughout the Vážská cascade.

Conclusion

The Liptovská Mara – Bešeňová water management system, which has been in operation for 45 years, reliably fulfills all planned purposes. These hydraulic structures have significantly reduced floods in the Váh basin since 1975. Using the energy potential of Váh, the water management system contributed to the energy network by producing more than 6,500 GWh of green electricity. There is enough water for industry and agriculture by improving the Váh River flows through the Liptovská Mara reservoir. Within the framework of registered climate change and global warming, with recurring hydrological extremes, the function of this water management system is increasing 10 $m^3 s^{-1}$ under the Bešeňová dam. The analysis showed that the winter season is the most vulnerable. Without the accumulation storage of the Liptovská Mara reservoir, approx. 362 million m^3, for almost two months a year, the minimum flow of 15 $m^3 s^{-1}$ would not be ensured in the Váh River. The added value of the Liptovská Mara and Bešeňová reservoirs is also the completion of the landscape character, the development of tourism, the possibility of recreational and sports use of this area.

Acknowledgement

We would like to express our gratitude to the Slovak Hydrometeorological Institute for providing data and information.

References

Bednárová, E. et al.: Dam construction in Slovakia. Originalities - Milestones - Noteworthy facts. Bratislava, Kuskus 2010, 207. ISBN 978-80-970428-0-6

Lukáč, M. et al. (1996): Evaluation of selected water reservoirs' real operation impacts on the flow regime. Stage 2, SvF STU, 1996, 258.

Lukáč, M., Bednárová, E., Štefanek, J. (1991): Reservoirs and water management systems. ES STU, Bratislava 1991, 277.

Votruba, L., Patera, A. (1997): Reservoirs and water management systems. ES ČVUT Praha, 1997, 191. Hydrological data from the data SHMÚ set time.

Prof. Ing. Emília Bednárová, PhD. (*corresponding author, email: emilia.bednarova@stuba.sk)
Ing. Juraj Škvarka, PhD.
Ing. Patrik Václavik
Slovak University of Technology in Bratislava
Radlinského 11
810 05 Bratislava
Slovak Republic

Ing. Jana Poórová, PhD.
Slovak Hydrometeorological Institute
Jeséniova 17
833 15 Bratislava
Slovak Republic

DOI: 10.31577/ahs-2021-0022.01.0003

ACTA HYDROLOGICA
SLOVACA

Volume 22, No. 1, 2021, 22 – 29

THE IMPACT OF CLIMATE CHANGE ON THE HYDROPOWER POTENTIAL: A CASE STUDY FROM TOPĽA RIVER BASIN

Peter Rončák*, Peter Šurda, Justína Vitková

The contribution presents the impact of climate change on the hydropower potential in the Topľa River basin. There are various methodological approaches for determining the impact of climate change on the hydrological regime. One of them is the assessment of the impact of climate change on the hydropower potential. Changed climatic conditions, characterized mainly by changes in precipitation, potential evapotranspiration, and air temperature in future decades were predicted by recent outputs of the KNMI and MPI regional climate change models and the A1B emission scenario. To specify changes in long-term mean monthly runoff in comparison with the reference period 1981-2010 and future time horizons, the physically based WetSpa rainfall-runoff model was used. As a basic indicator of the potential for water energy utilization, hydropower potential (HPP) was calculated. An assessment of possible adaptation strategies for water management with respect to the hydropower potential and its utilization for energy production in Slovakia was attempted. The hydropower potential of small, run-of-river and storage hydropower plants is strongly related to the distribution of runoff over the year and can therefore affect not only the total change in runoff but also changes in its distribution in the future.

KEY WORDS: hydropower potential, the WetSpa model, climate change

Introduction

The utilization of water flows is an indispensable source of energy. Hydropower plants were also one of the first power plants to produce electricity in Slovakia. The hydropower potential used in hydropower plants is one of the natural resources of every country. Particularly, they determine in particular the natural conditions and the degree of economic, technical and social development of the country concerned. Hydropower is a dominant renewable source of energy production and has received significant worldwide attention for further development (Resch et al., 2008; Liu et al., 2011; Stickler et al., 2013).
Climate change caused by rising concentrations of greenhouse gases in the atmosphere may affect the hydrological cycle and the availability of water to humans, there-by affecting agriculture, forestry and other industries.
Reduced hydropower generation has been reported to be associated with climate change (Qiu, 2010; Bahadori et al., 2013), and significant progress has been made in assessing the impacts of climate change on hydropower elsewhere in the world. For example, it was reported that a future decrease in climate-change-induced runoff would reduce energy generation and revenues of hydropower plants under current regulations in the Columbia River and California hydropower systems in the United States (Hamlet et al., 2010; Vicuña et al., 2011). Considerable impact of climate change on hydropower was reported in the Swiss and Italian Alps regions, but the impacts varied for different locations, hydropower systems, and projections of climate change (Maran et al., 2014). Most studies suggested that new adaptive management may mitigate projected losses of hydropower in the Alps regions (Majone et al., 2016).
Few studies perform a broad analysis of climate change impacts on the energy system, from the effects on climate parameters (e.g. temperature and precipitation) to the resulting technological structure, inherent financial costs and GHG emissions. Climate change impacts on natural resources, and also on hydropower, are often analysed through climate and hydrological models (whose character is eminently biophysical) and/or electrical grid models (Tarroja et al., 2016; Van Vliet et al., 2016. Economic impacts of climate change on the energy sector are mainly assessed through bottom-up technological models that rely on techno-economic data, but disregard the biophysical component. An exception is the study from Seljom et al. (2011) that use ten climate experiments and a bottom-up energy model to analyse the impacts of climate change on energy demand and supply, considering the effects on hydro- and wind power potential for Norway by 2050. They find that climate

change will increase precipitation and hydropower potential.
In Slovakia, few researches deal with different hydrologically - distributed models, which have been used to simulate runoff processes under climate change conditions. Good examples of such models include: WetSpa (Valent et al. 2016; Rončák et al., 2016; 2017). This article builds on previously published papers and uses several older outputs of global and regional models, climate change scenarios, and various conceptual or distributed hydrological models in Slovakia (see, e.g., Štefunková et al. 2013; Hlavčová et al., 2015).
This study presents a model-based approach for analysing the possible effects of climate change on hydropower potential at a basin scale. By comparing current conditions of climate and water use with future scenarios, an overview is provided of today's potential for hydropower potential and its and long-term prospects.

Material and methods

Study area

The Topľa is a river in eastern Slovakia which is the right tributary of the Ondava River. It rises in the Čergov mountain under Minčol peak. The Topľa catchment (1062.24 km^2) is situated in eastern Slovakia (Fig. 1). The catchment is in a flysch mountain area of Nízke Beskydy on Slovakia's border with Poland; it is characterised by numerous springs, bogs and streams. Prolonged rainfall has a great influence on the runoff regime, especially during the growing season and periods of melting snow. The climate is warm and moderately humid with cool winters. The potential natural vegetation is characterized by submontane beech forests in the north, while the lowlands are covered by Carpathian oak-hornbeam forests (Maglocký, 2002).

The climate change scenarios

The KNMI and MPI regional climate change models (with A1B emission scenario) were used for this research. They were downscaled for the territory of Slovakia in a daily time step. These regional circulation models (RCMs) belong to newest category of so-called coupled atmosphere-ocean models with more than 10 atmospheric levels and 20 oceanic depths of model equations and the integration of variables in a network of grid points. The KNMI and MPI models represent a more detailed integration of the atmospheric and oceanic dynamic equations with a grid point resolution of about 25x25 km, while the boundary conditions are taken from the outputs of ECHAM5 global model. The KNMI and MPI RCMs have 19x10 grid points (190) in Slovakia and its surroundings with a detailed topography and an appropriate expression of all topographic elements larger than 25 km. Scenarios for the variables have mainly been prepared: the daily means, maximum and minimum of the air temperature, the daily means of the relative air humidity, daily precipitation total, daily means of the wind speed, and daily totals of the global radiation. (Hlavčová et al., 2016).
The latest climate change scenarios for the territory of Slovakia were processed on the basis of outputs from climatic atmospheric models at the Department of Astronomy, Earth Physics and Meteorology at the Faculty of Mathematics, Physics and Informatics of Comenius University (Lapin et al., 2012).

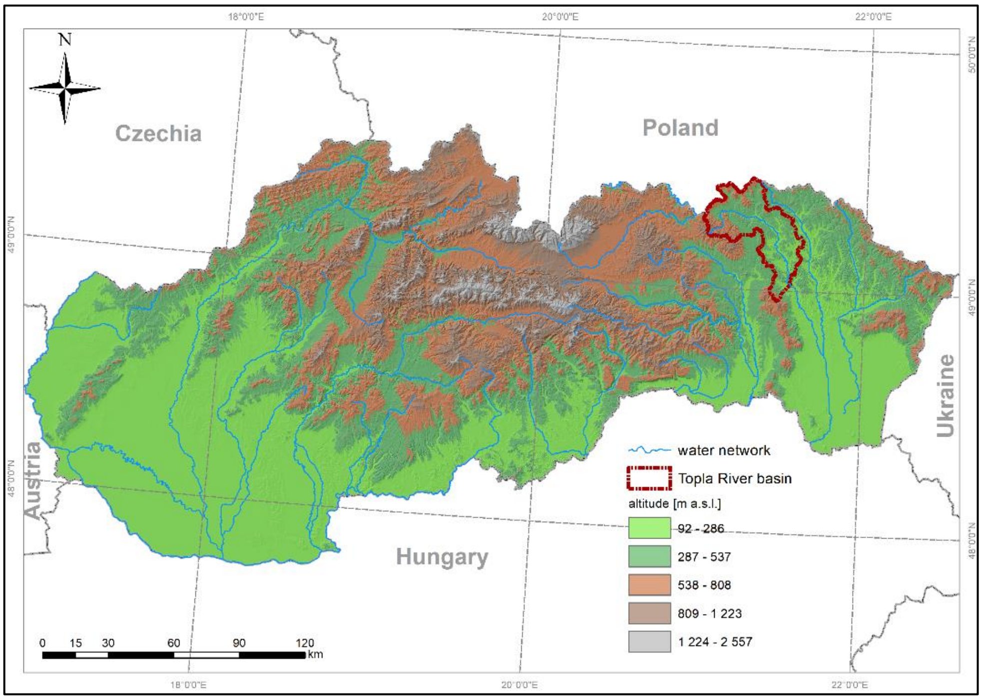

Fig. 1. Location of the Topľa River basin.

Table 1 shows a comparison of the long-term mean monthly air temperature in °C between the period 1951–1980 and the climate change scenarios (KNMI and MPI) in the period 2071–2100 for all of Slovakia. We can observe an increase in the average air temperature in the winter months by 3°C and in the summer season by 4°C in the future horizon.

Figure 2 shows the differences in the long-term mean monthly air temperature in the Topľa River basin in the 2071–2100 horizon. The air temperature has a rising trend. The mean monthly air temperature will rise, without any exception, in the river basin at about the same rate.

Table 2 presents the long-term mean monthly values of the precipitation for the 1981–2010 reference period in the selected river basins and the changes in their values for three future time horizons till 2100 according to the KNMI and MPI regional climate change scenarios.

Table 1. Long-term mean monthly values of the air temperature [°C] during the period 1951–1980 and for the future time horizon of 2071–2100 in Slovakia

Scenario	horizon	I	II	III	IV	V	VI	VII	VIII	IX	X	XI	XII
	1951–1980	-3.8	-1.8	2.2	7.7	12.5	16.1	17.5	16.8	13	8	3	-1.5
KNMI [°C]	2071–2100	-0.6	1.6	4.9	9.8	15.6	20	21.7	20.6	15.9	11.4	6.4	2.3
MPI [°C]		-0.1	2.2	4.6	9.5	15	19.5	20.8	20.8	16.6	11.6	6.7	2.4

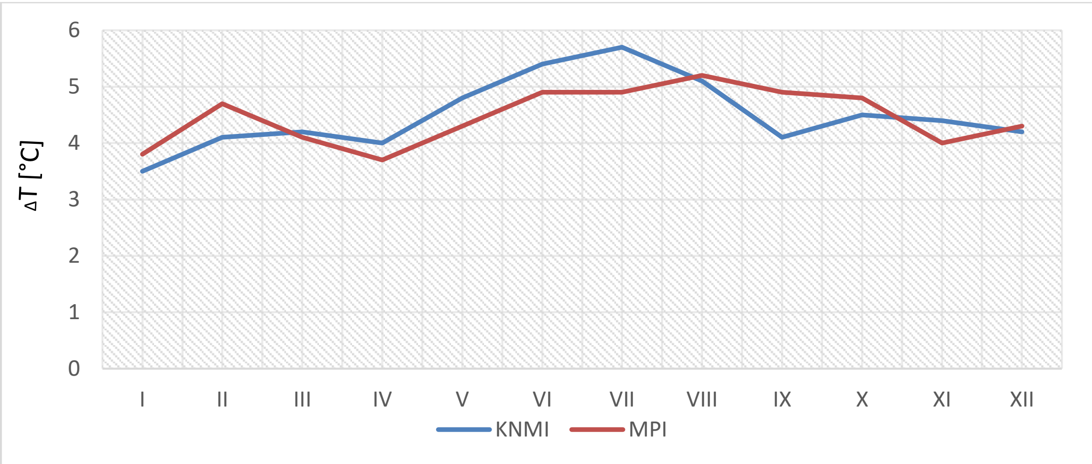

Fig. 2. Differences in the long-term mean monthly values of the air temperature in the Topľa River basin in the 2071–2100 horizon.

Table 2. Long-term mean monthly values of the areal mean monthly precipitation of the reference period (1981–2010) and the changes in their values in [%] for the future time horizons of 30 years from 2010–2100 in the Topľa River basin

	precipitation [mm]		I	II	III	IV	V	VI	VII	VIII	IX	X	XI	XII
Topľa	1981–2010		35.8	33.8	33.5	51.7	84.1	96.4	96.1	74.9	64.1	44.1	38.1	43
	KNMI [%]	2010–2040	-8.4	-0.7	-4.4	-7.8	-6	6.1	-3.5	-0.5	27.9	1.7	2.4	3.1
		2041–2070	-1	-0.2	4.6	12.4	-6	2.5	-9	-6.1	14.7	10.4	-2	15.3
		2071–2100	7.3	11.5	11.4	7.9	-13.4	-25.6	-19.6	0.9	50.8	10.9	4.6	17.8
	MPI [%]	2010–2040	-1.3	9.2	-2.1	-5.6	-1.2	12.7	-4.9	12.9	6.9	1.4	1.3	1.3
		2041–2070	4.7	0.2	11.4	12.9	-8.6	10.3	-0.3	10.7	16.1	13.1	-2.1	10.2
		2071–2100	13.3	10.2	12.6	10.8	-2.1	-15.9	-19.7	5.6	12.5	9.5	4.9	8.2

According to the individual climatic models as seen in Table 2 and Fig. 3, a decrease in the mean monthly precipitation in the summer period can be expected. On the other hand, the winter period should be more humid in comparison with the current conditions.

Both the KNMI and MPI scenarios gave similar seasonality change prognoses. They predict a general increase in precipitation amounts, with the highest precipitation amounts from September to winter period and less precipitation from May to July. The air temperature should increase, mainly during the winter period, and this could result in less snow accumulation and increased winter snow-melt runoff. While the onset or dry periods should be more frequent, with low precipitation, low runoff and less water storage, the most pronounced seasonality change is expected to be evapotranspiration.

The rainfall-runoff model

The WetSpa model simulates runoff and river flow in a watershed on a daily time step (Wang et al., 1996; Bahremand and De Smedt, 2006). Availability of spatially distributed data sets (digital elevation model, landuse, soil and radar-based precipitation data) coupled with GIS technology enables the WetSpa to perform spatially distributed calculations. The hydrological processes considered in the model are precipitation, interception, depression storage, surface runoff, infiltration, evapotranspiration, percolation, interflow and ground water drainage. The total water balance for each raster cell is composed of a separate water balance for the vegetated, bare-soil, open water, and impervious part of each cell. The model predicts discharges in any location of the channel network and the spatial distribution of hydrological characteristics (Safari et al., 2012).

Input data in a daily step in the period between January 1981 and December 2010 was used in this study. The following hydro-meteorological data were used in the model: daily precipitation totals from spot measurements at 15 stations and the average daily values for the air temperature at 4 climatological stations. The flow data consisted of the average daily flows at the Topľa – Hanušovce nad Topľou profile.

'Gross' hydropower potential calculation

The 'gross' hydropower potential is analysed, in order to outline the general distribution and trends in hydropower capabilities. According to Eurelectric (1997), the 'gross' hydropower potential is defined as the annual energy that is potentially available if all natural runoff at all locations were to be harnessed down to the sea level (or to the border line of a country) without any energy losses. The share of this highly theoretical value that has been or could be developed under current technology, regardless of economic and other restrictions, forms the 'technical' hydropower potential.

The gross hydropower potential can be directly calculated from water availability and elevation data. The analysis of climate and global change impacts on the gross hydropower potential can provide an overall indication of regional trends, but does not allow for immediate conclusions on changes in the actual hydroelectricity production of a country. For example, a decrease of discharges in a region where only few hydropower plants exist may not significantly alter the overall hydroelectricity supply. A more realistic interpretation of changes in future hydropower production within the existing hydropower park is provided by the developed hydropower potential, i.e. the part of the gross potential which is or will be utilized through power plants. However, the latter approach

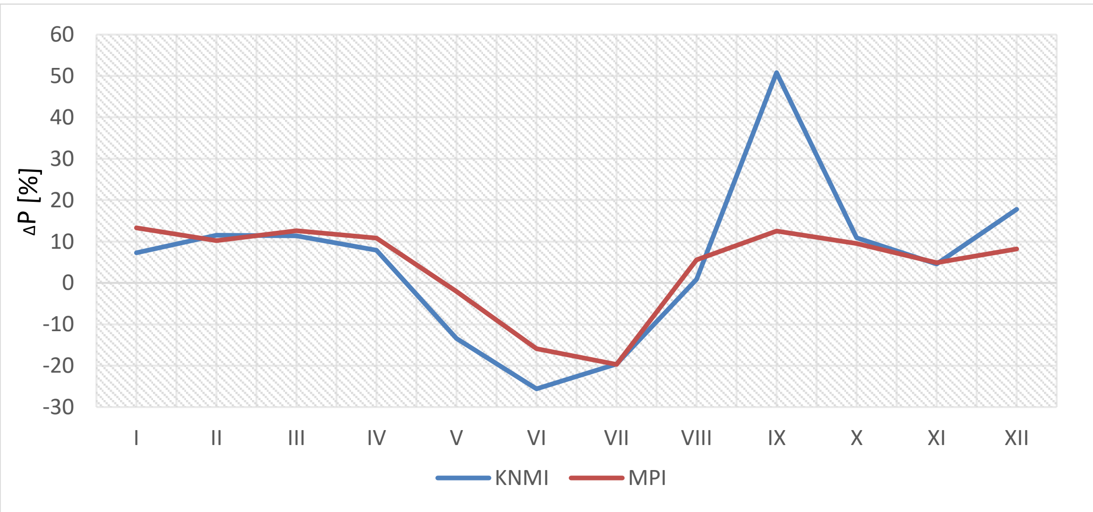

Fig. 3. Differences in the long-term mean monthly values of the precipitation in the Topľa River basin in the 2071–2100 horizon.

requires the reliable identification of plant locations and their installed capacities (Lehner et al., 2005).
For purposes of this study, the 'gross' hydropower potential of selected river basis has been calculated based on the relation for theoretical hydraulic power P_i of a river reach (between two profiles)

$$P_i = P_{1-2} = 9{,}81.\frac{(Q_1+Q_2)}{2}.(H_1 - H_2).\eta \quad \text{[kW]} \qquad (1)$$

where
Q_1 – discharge in the upstream profile [m^3 s^{-1}],
Q_2 – discharge in the downstream profile [m^3 s^{-1}],
H_1 – altitude of the upstream profile [m a.s.l.],
H_2 – altitude of the downstream profile [m a.s.l.],
η – overall efficiency of energy transformation, $\eta = 1$ for 'gross' hydropower.

The 'gross' hydropower potential HP_i was then calculated as a theoretical value of energy in river per year

$$HP_i = \sum_{i=1}^{n} Pi\,.8760.\,10^{-6} \quad \text{[GWh]} \qquad (2)$$

Calculations were made for:
Q_{50} = medial discharge with 50% probability of exceedance,
Q_{95} = minimal discharge with 95% probability of exceedance.

Results and discussion

Using the parameters of the calibrated WetSpa model and the outputs from the KNMI and MPI climate scenarios, the simulation of flows in the final profile for the future time periods until the year 2100 was made. The 30-year period from 1981 to 2010 was chosen as the reference period.
Based on simulated long-term mean daily discharges, we calculated gross hydropower potential. Then, the comparison between the reference period and the climate change scenarios was made. The outputs from the WetSpa distributed hydrological model were divided to five 15-years periods.
The future changes in runoff due to climate change were evaluated by comparing the simulated average daily flows and their statistical characteristics for the current state and the modelled scenarios; they are presented in Table 3.
From the results of the scenarios of the long-term mean monthly flows presented in the future horizons and comparing them to the reference period 1981–2010, we can state that change in the monthly discharge regime in Topľa River basin analysed could be expected. Also, the evidence of an increase in the long-term runoff can be seen; it has a linear relationship with the increase in mean precipitation in the future in this catchment.
In the Topľa River basin similar changes in future runoff can be observed, i.e., in the winter period up to a 90% increase according to the KNMI scenario, and in the summer months, e.g., August, up to a 38% decrease according to the MPI scenario in comparison to the reference period.
Changing climatic conditions may also present themselves as a persistent reduction in the potential of surface and water resources, which should also be taken into account in the planning and management of water resources in the future.
It can be seen on the Fig. 4, that the hydropower potential for medial discharge with 50% probability of exceedance slight increase. This phenomenon may be related to increase in the long-term runoff; it has a linear relationship with the increase in mean precipitation.
The opposite situation may occur at the comparison of the theoretical hydropower potential (Q_{95} minimal discharge with 95% probability of exceedance) between the reference period and the climate change scenarios (Fig. 5). The decrease of the hydropower potential can move between 25–70%. At minimum flows, climate change is likely to have negative effects.

Table 3. Simulated long-term mean monthly discharge in [m^3 s^{-1}] using the parameters from the 1981–1995 calibration period and their changes in [%] for the three future time horizons of 30 years from 2010–2100 in the Topľa River basin

River basin	Scenario	Horizon	I	II	III	IV	V	VI	VII	VIII	IX	X	XI	XII	*Q* annual [m^3 s^{-1}]
Topľa	1981–2010 [mm]		196	259	477	413	307.3	258.1	204	151.2	138.9	129.1	147.5	177	2851.5
	KNMI [%]	2010–2040	8	16	-19	-26	-20	-13	35	21	104	79	20	13	3011.2
		2041–2070	41	46	-18	0	-5	1	-6	-9	29	82	9	23	3134.1
		2071–2100	102	69	4	1	-18	-33	-19	-31	68	93	41	82	3453.7
	MPI [%]	2010–2040	-22	17	-6	19	-7	4	12	35	36	48	14	-11	3085
		2041–2070	32	59	-6	19	9	6	-13	9	64	85	21	28	3429.1
		2071–2100	54	51	4	11	7	-32	-38	-15	-8	41	10	31	3109.6

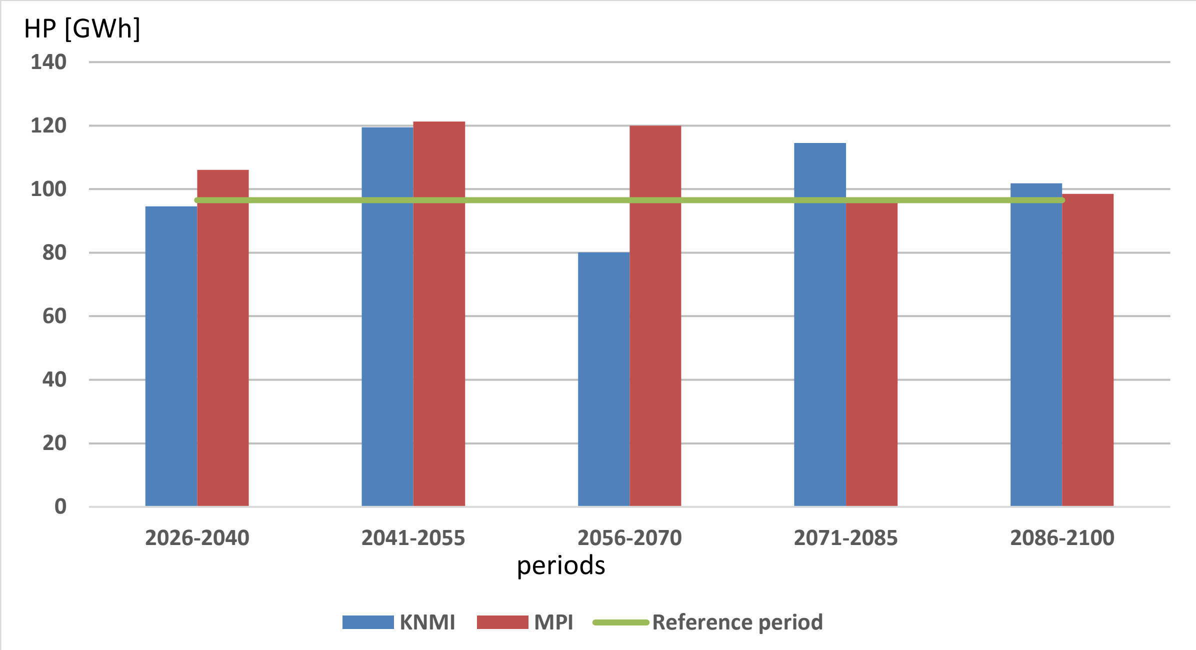

Fig. 4. Comparison of the theoretical hydropower potential (Q_{50} medial discharge with 50% probability of exceedance) between the reference period and the climate change scenarios.

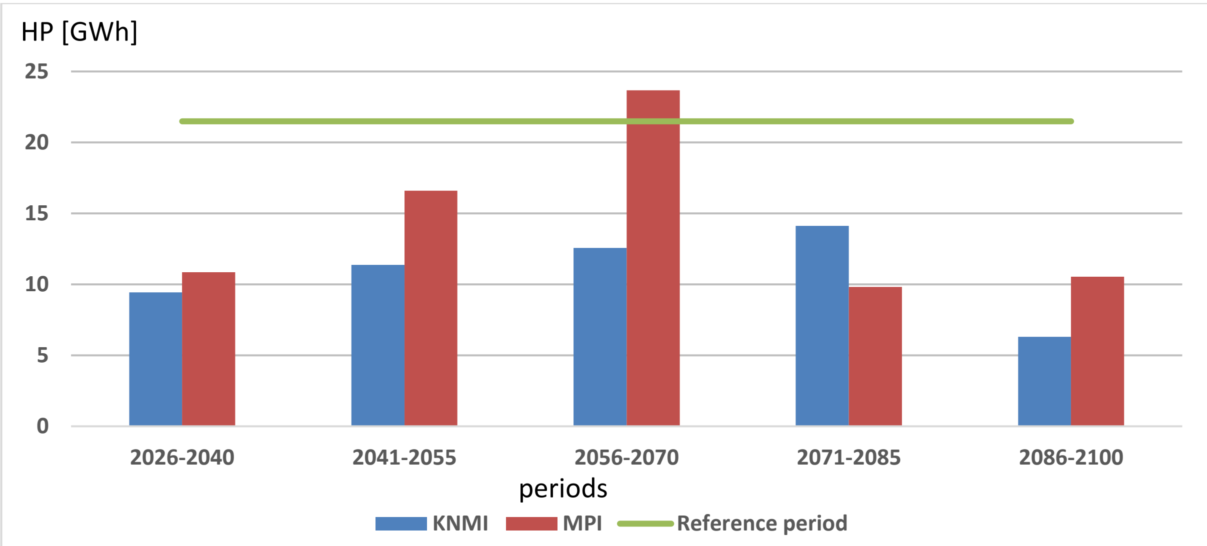

Fig. 5. Comparison of the theoretical hydropower potential (Q_{95} minimal discharge with 95% probability of exceedance) between the reference period and the climate change scenarios.

Conclusion

This paper described a concept of analysing the impacts of climate and global change on future hydropower potentials on a catchment scale. Based on the research results, changes in precipitation and discharges can be expected. The change in these characteristics is related to the development of hydropower potential. The hydropower potential of the Topľa River basin should not be significantly affected by the impact of climate change. It needs to be mentioned that the KNMI and MPI climate change scenarios represent less extreme changes (the A1B emission scenario). The scenarios considered suggest that practically all the basins analysed could be at risk from summer or early autumn droughts. Prolonged droughts can cause significant water shortages. These dry periods may be interrupted by short episodes of extreme rainfall or severe storm activity with rainfall inducing the formation of flash floods. According to current developments, it is likely that climate change can have a significant negative impact on local water resources with low water yields, especially in the sub-mountainous regions of the Slovak Republic. On the other hand, it is possible that the long-term mean monthly runoff will increase in the winter. This could be due to higher temperatures and earlier snowmelt in these regions. The lack of water stored as snowpack in the winter could affect the availability of water for the rest of the year. It could also cause earlier snowmelt floods. Based on the results for the five basins from the north, central and eastern parts of Slovakia, it is likely that this effect will apply to the whole territory of Slovakia.

It is generally expected that increased temperature causes stronger water evaporation from the continents and from all water surfaces, also rivers and lakes. The evaporation reduces available river water, but at the same time more evaporated water origins in more precipitation. Therefore, this effect must be investigated in particular for each water basin. Climate change will cause increased variability of precipitation events and will pose significant problems for hydroelectric generation. The increased variability of precipitation will result in more severe and frequent floods and droughts, seasonal offsets, or the altering timing and magnitude of precipitation for traditional rainy and dry seasons and peak snowmelt. Droughts reduce water availability and therefore the amount of the produced energy, but in case of a longer lasting drought (several years) not only the discharge, but also the available head for energy production could be reduced. Seasonal offset will additionally sharpen the situation, especially in case of shorter and more intense precipitation periods and longer lasting and dryer periods.

The Topľa River basin represents the north-eastern part of Slovakia. Climate change will affect hydropower potential in a more significant way in the lowland part of eastern Slovakia. The hydropower potential in this basin may not be dramatically affected by climate change.

The results of the simulation are highly dependent on the availability of the input data. The outputs of the study could be used in an adaptation strategy for integrated river basin management and especially in the organization of the river basin management process and the assessment of the impacts of changes the use of river basin on runoff.

Acknowledgement

This work was supported by Scientific Grant Agency No. Vega 2/0155/21.

References

Bahadori, A., Zahedi, G., Zendehboudi, S. (2013): An overview of Australia's hydropower energy: Status and future prospects, Renew. Sust. Energ. Rev., 20, 565—569.

Bahremand, A., De Smedt, F. (2006): Sensitivity and uncertainty analysis of a GIS-based flood simulation model using PEST. WSEAS Transactions on environment and development, 2(1), 29–37.

Eurelectric. (1997): Study on the importance of harnessing the hydropower resources of the world, Union of the Electric Industry (Eurelectric), Hydro Power and other Renewable Energies Study Committee, Brussels.

Hamlet, A., Lee, S.-Y., Mickelson, K. B., Elsner, M. (2010): Effects of projected climate change on energy supply and demand in the Pacific Northwest and Washington State, Clim. Change, 102, 103– 128.

Hlavčová, K., Štefunková, Z., Valent, P., Kohnová, S., Výleta, R., Szolgay, J. (2016): Modelling the Climate Change Impact On Monthly Runoff in Central Slovakia. Procedia engineering, 161, 2127–2132.

Hlavčová, K., Lapin, M., Valent, P., Szolgay, J., Kohnová, S., Rončák, P. (2015): Estimation of the impact of climate change-induced extreme precipitation events on floods. In: Contributions to Geophysics and Geodesy 45 (3), 173–192.

Lapin, M., Bašták, I., Gera, M., Hrvoľ, J., Kremler, M., Melo, M. (2012): New climate change scenarios for Slovakia based on global and regional general circulation models. Acta Meteorologica Universitatis Comenianae, 37, 25–73.

Lehner, B., Czisch, G., Vassolo, S. (2005): The impact of global change on the hydropower potential of Europe: a model-based analysis. Energy Policy, 33(7), 839–855.

Liu, W., Lund, H., Mathiesen, B. V., and Zhang, X. (2011): Potential of renewable energy systems in China, Appl. Energy, 88, 518–525.

Maglocký, Š. (2002): Potenciálna prirodzená vegetácia (Potential natural vegetation). In: Zaťko, M. (Ed.), Atlas krajiny Slovenskej republiky, IV. Prvotná krajinná štruktúra (Primary landscape structure). MŽP SR a SAŽP, 114–115.

Majone, B., Villa, F., Deidda, R., Bellin, A. (2016): Impact of climate change and water use policies on hydropower potential in the south-eastern Alpine region, Sci. Total Environ., 543, 965–980.

Maran, S., Volonterio, M., Gaudard, L. (2014): Climate change impacts on hydropower in an alpine catchment, Environ. Sci. Policy, 43, 15–25.

Qiu, J. (2010): China drought highlights future climate threats, Nature News, 465, 142–143.

Resch, G., Held, A., Faber, T., Panzer, C., Toro, F., Haas, R. (2008): Potentials and prospects for renewable energies at global scale, Energ. Policy, 36.

Rončák, P., Hlavčová, K., Látková, T. (2016): Estimation of the effect of changes in forest associations on runoff processes in basins: case study in the Hron and Topla river basins. Slovak Journal of Civil Engineering 24(3), 1–7.

Rončák, P., Lisovszki, E., Szolgay, J., Hlavčová, K., Kohnová, S., Csoma, R., Poórová, J. (2017): The potential for land use change to reduce flood risk in mid-sized catchments in the Myjava region of Slovakia. Contributions to Geophysics and Geodesy, 47(2), 95–112.

Safari, A., De Smedt, F., Moreda, F. (2012): WetSpa model application in the distributed model intercomparison project (DMIP2). Journal of Hydrology, 418, 78–89.

Seljom, P., Rosenberg, E., Fidje, A., Haugen, J. E., Meir, M., Rekstad, J., Jarlset, T. (2011): Modelling the effects of climate change on the energy system – a case study of Norway. Energy policy, 39(11), 7310–7321.

Stickler, C. M., Coe, M. T., Costa, M. H., Nepstad, D. C., McGrath, D. G., Dias, L. C. P., Rodrigues, H. O., Soares-Filho, B. S. (2013): Dependence of hydropower energy generation on forests in the Amazon Basin at local and regional scales, P. Natl. Acad. Sci., 110, 9601–9606.

Štefunková, Z., Hlavčová, K., Lapin, M. (2013): Runoff change scenarios based on regional climate change projections in mountainous basins in Slovakia. In: Contributions to Geophysics and Geodesy 43(4):327-350.

Tarroja, B., AghaKouchak, A., Samuelsen, S. (2016): Quantifying climate change impacts on hydropower generation and implications on electric grid greenhouse gas emissions and operation. Energy, 111, 295–305.

Valent, P., Rončák, P., Maliariková, M., Behan, Š. (2016): Utilization of historical maps in the land use change impacts studies: a case study from Myjava River basin.Slovak Journal of Civil Engineering, 24(4), 15–26.

Van Vliet, M. T., Wiberg, D., Leduc, S., Riahi, K. (2016): Power-generation system vulnerability and adaptation to changes in climate and water resources. Nature Climate Change, 6(4), 375–380.

Vicuña, S., Dracup, J., Dale, L. (2011): Climate change impacts on two high-elevation hydropower systems in California, Clim. Change, 109, 151–169.

Wang, Z., Batelaan, O., de Smedt, F. (1996): A Distributed Model for Water and Energy Transfer between Soil, Plants and the Atmosphere (WetSpa). Phys. Chem. Earth, 21(3): 189–193.

Mgr. Peter Rončák, PhD. (*corresponding author, e-mail: roncak@uh.savba.sk)
Ing. Peter Šurda, PhD.
Ing. Justína Vitková, PhD.
Institute of Hydrology SAS
Dúbravská cesta 9
84104 Bratislava
Slovak Republic

DOI: 10.31577/ahs-2021-0022.01.0004

ACTA HYDROLOGICA
SLOVACA

Volume 22, No. 1, 2021, 30 – 39

TESTING OF WATER EVALUATION AND PLANNING (WEAP) MODEL FOR WATER RESOURCES MANAGEMENT IN THE HRON RIVER BASIN

Miroslav Kandera*, Roman Výleta, Anna Liová, Zuzana Danáčová, Ľubica Lovasová

The assessment of water resources and the availability of water in river basins is one of the main tasks enabling efficient water management. One of the bases for the Water Plan of the Slovak Republic is a retrospective water management balance of the amount of surface water in Slovakia, which compares the requirements for water with the usable amount of water. As part of the efforts to improve the plan, the possibility of modelling the water management balance of surface waters using appropriate software for the integrated planning of water resources was outlined. The Water Evaluation and Planning (WEAP) software was selected to test this modelling according to the current methodology. In the Hron river basin, a time series in a monthly time step of data input in the period 2000–2019 was selected. The focus was on the compatibility of the current methodology of the water management balance and methods of modelling it in the WEAP software. The output is a river basin model capable of producing outputs above the level of the original processing of the water management balance, while the compilation of the graphic and data structure of the modelled river basin is fully automated, mainly by using command lines. This modelling approach has shown that, thanks to the possibility of creating new variables within the data structure, it is possible to achieve the required level of compatibility with the set methodology for water management balances. The results demonstrate that the WEAP could be an easy-to-use model building tool for the optimal and successful development, planning and forecasting of water management in space and over time in Slovakia.

KEY WORDS: WEAP, Water Resources Management, Water Supply and Demand, Hron River Basin

Introduction

In Slovakia, there has recently been increasing interest in reassessing the structure and valid methodology of the water management balance of the amount and regime of surface waters in previous year. It is important to realize that it is no longer nowadays possible to think exclusively about water use in addressing this issue, but the balances should also include the needs of ecosystems (not just respecting the ecological limits of water use) and ongoing global changes. With regard to the goals of sustainable development in water management, the balances are based not only on the knowledge and definition of water resources, but also on the impact on water resources over time and in space. The chief requirement for the correct evaluation of the balance status of water bodies within water management is the achievement of a sufficient level of the quality and quantity of the method used for processing information based on the natural regime of water in nature and the individual impacts of water use.

A considerable amount of simulation software integrated into interactive graphic interfaces is currently available around the world for research and the solutions to water management and water redistribution in river basins, all of which create simplified representations of real-world systems. They serve both to plan and manage the use of water in river basins but are also suitable to facilitate the involvement of stakeholders in the planning and decision-making process at various levels (Assaf et al., 2008). They have also been used and proved successful in countries that have already established a quality monitoring network and methodology for obtaining data on water use, e.g., the Slovak Republic, other countries in Western Europe, North America, etc. Although each model has its own special features, they are all designed to facilitate the input and storage of data, the retrieval and display of the geographical, hydrological and, depending on the type of model and application, socio-economic data associated with specific river basins or regions. Over the years, they developed their so-called genericity, i.e., a set of features that programs of this kind have in common, whether they include the method of simulation or the creation of the data or schematic structure of a river basin and a river network. However, each software has its own special features and user interface that was specified for each software when it was created and which is then supplemented over the years with features that are primarily helpful to the user, thereby reinforcing this common genericity. Their advantage is in their ability to solve variations with the help of computers, both in the sources and in the water requirements. Due to the mentioned genericity of the software developed to solve water balance issues, the selection of a specific software without testing it and its properties is a complex question. The best-known balance simulation models include AQUATOOL (Andreu et al., 1996), MIKE HYDRO BASIN (DHI, 2003), MODSIM (Labadie, 2005), RIBASIM (WL/Delft Hydraulics, 2007), WARGI (Sechi and Sulis, 2009), WBalMo (Kaden et al., 2006), and WEAP (Yates et al., 2005).

The paper deals with testing a balance simulation model for modeling the quantitative water management balance of surface waters, taking into account the valid methodology of the Slovak Republic. In Slovakia, simulation balance models have not yet been fully applied in water management; therefore, research in this area could be helpful not only for planning and solving problem areas (detailed balances) but also to facilitate the involvement of stakeholders in the planning and decision-making process at various levels. In this paper, the selection of the software was carried out based on the available information and considering the predetermined criteria, such as the purpose of its use, availability, requirements for the preparation and compatibility of input data, software updates, clarity of the user environment, software limits, etc. In this study, the Water Evaluation and Planning (WEAP) software was selected for the specific resolution and analysis of the water management balance of Slovakia according to the valid methodology in the pilot river basin (Hron river basin). The authors aim to evaluate its possibilities for application in our geographical conditions.

Material and methods

Actual methodology of the water management balance of surface waters

The water management balance has been used in Slovakia to frame water planning since 1973 (European Union, 2015). According to the decree on the Water Act No. 418/2010 Coll., as later amended, the water management balance compares the requirements for water with the usable amount of water and its quality. The water requirements stand for abstractions of the surface water, groundwater, water discharges, and special water. The water management balance is prepared for the purposes of the Water Plan of Slovakia according to an approved time plan using approved data acquisition procedures, processing methodologies and forms of outputs. It is processed separately for surface waters and for groundwater, as well as for the quantity and quality of the water.

This paper focuses only on the quantitative water management balance of surface water. In term of the quantity of surface water, the universal relationship of water management considers all the most impactful types of the elements of this inequality between sources and needs, i.e., natural water resources, water abstractions, water discharges, the impact of reservoirs, water transfers, and the minimum required flow (Poórová, 2007). The positive or negative impact of manipulation on reservoirs and water transfers is determined by whether they improve or reduce the streamflow. The relationship is given by:

$$\begin{gathered} RESOURCES <=> NEEDS \\ C \pm N \pm P <=> O - V + MQ \end{gathered} \tag{1}$$

where:
C – natural water resources,
N – activity of reservoirs,
P – water transfers,
V – water discharges,
O – water abstractions,
MQ – minimum required flows.

The water management balance of surface water is evaluated in balance profiles that cover important locations for water use, the effect of water reservoirs, and water transfers, thereby focusing on the availability of the hydrological information with the maximum connection to the existing network of water gauging stations. The characteristics in every balance profile are evaluated for the 12 months of the calendar year and the annual streamflow average value (Danáčová et al., 2011). The main characteristic describing a balance profile's condition is the balance status. It is a dimensionless characteristic evaluated as two alternatives:

i) As BSC, i.e., evaluating what would be the balance situation under natural flows when considering the realized abstractions as well as water discharges, while the developed form of the relationship appears as:

$$BSC = \frac{E - X \pm N \pm P}{MQ - X} \tag{2}$$

ii) BSENP (equals BSC) is the balance status that is focused on an assessment of a stream affected by a reservoir or water transfer. In its developed form, it is given by the following equation:

$$BSENP = \frac{E - X}{MQ - X} \tag{3}$$

where:
BSC, BSENP – value of balance status [-],
E – affected streamflow [$m^3 s^{-1}$],
N – changes in the volume of water in the reservoir [$m^3 s^{-1}$],
P – water transfer values [$m^3 s^{-1}$],
MQ – minimum balance streamflow [$m^3 s^{-1}$],
X – impact on the flow of water users [$m^3 s^{-1}$].

Based on the calculated BSC or BSENP values, the balance condition in Slovakia is determined in a monthly time step in categories A, B, and C as seen in Table 1.

The balance status, which is evaluated as passive or tense, is the signal to review the original measures or to develop new ones. Where there are problems, the input data are determined again, especially the data on the monitored abstractions and water utilization, as well as the streamflow data from the water gauging stations. These tasks, along with a requirement for a new course in evaluating and representing the results of the water management balance, are reasons for the testing and application of the simulation model. As an initial test of compatibility with the water management balance, all the characteristics evaluated in the balance profiles could be transformed into the outputs of the WEAP model described in Fig. 1, thus outlining its probable success.

Study area

As the second longest river flowing through the territory of Slovakia, the Hron River has a length of 298 km, a total catchment area of 5463.5 km^2, and an average altitude of 550.4 m a.s.l.; its most important tributary is the Slatina, with its outfall at river kilometer 153 of the Hron river (see Fig. 2). It has a length of 55.2 km and a total catchment area of 792.56 km^2. There is a dense water gauging network of 55 stations in the whole river basin.

In terms of surface water management, 4 streams are balanced in the Hron river basin, while there are 11 balance profiles on the Hron river, 3 balance profiles on the Slatina river, one on the Zolná river, and one on the Bystrica river (a total of 16 balance profiles, 8 of which are out of the position of water gauging stations at a distance greater than 200 m). The time series of the input data in the period 2000–2019 was selected for modelling the quantitative water management balance of the surface waters according to the valid methodology in the Hron river basin in a monthly time step. In the given period, 122 abstractions of surface water, 772 abstractions of groundwater, 319 water discharges, 4 reservoirs, and 2 water transfers were active.

Table 1. The classes according to the water balance condition (BSC or BSENP) of the river

Class	Threshold [-]	Tension level of a river
A	> 1.1	Active state – Good: appropriate use of resources (blue)
B	0.9 to 1.1	Tense state – Acceptable: need to define the causes (yellow)
C	≤ 0.9	Passive state – Unacceptable: inappropriate and excessive use of resources (red)

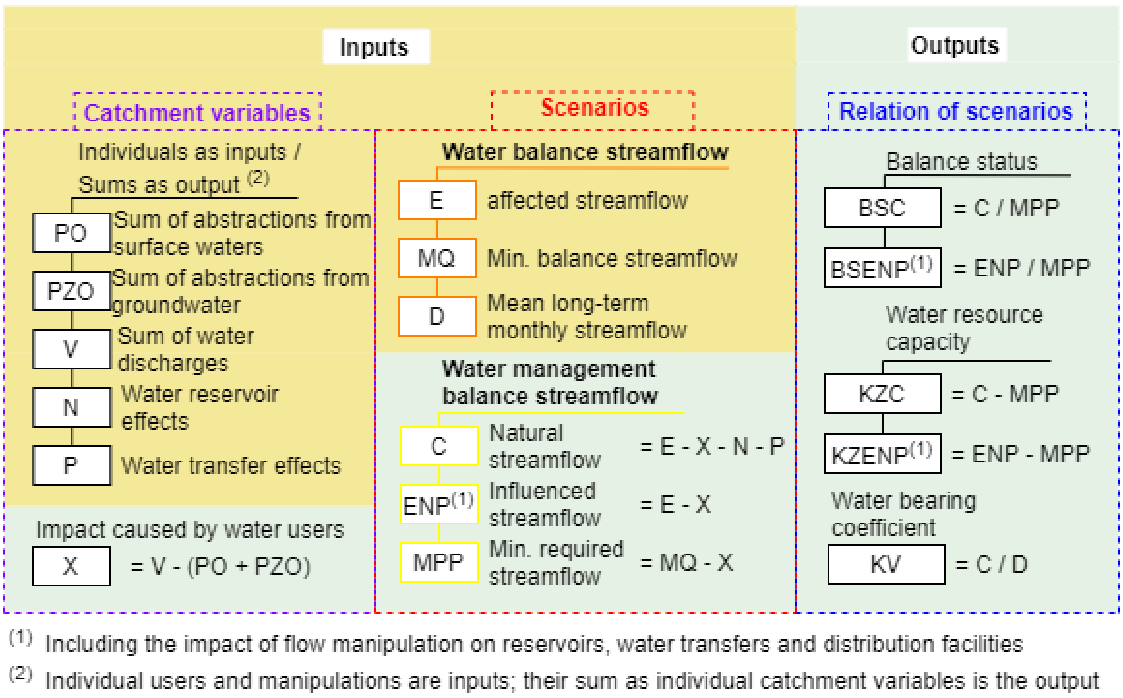

Fig. 1. Initial implementation of water management balance characteristics into the WEAP model.

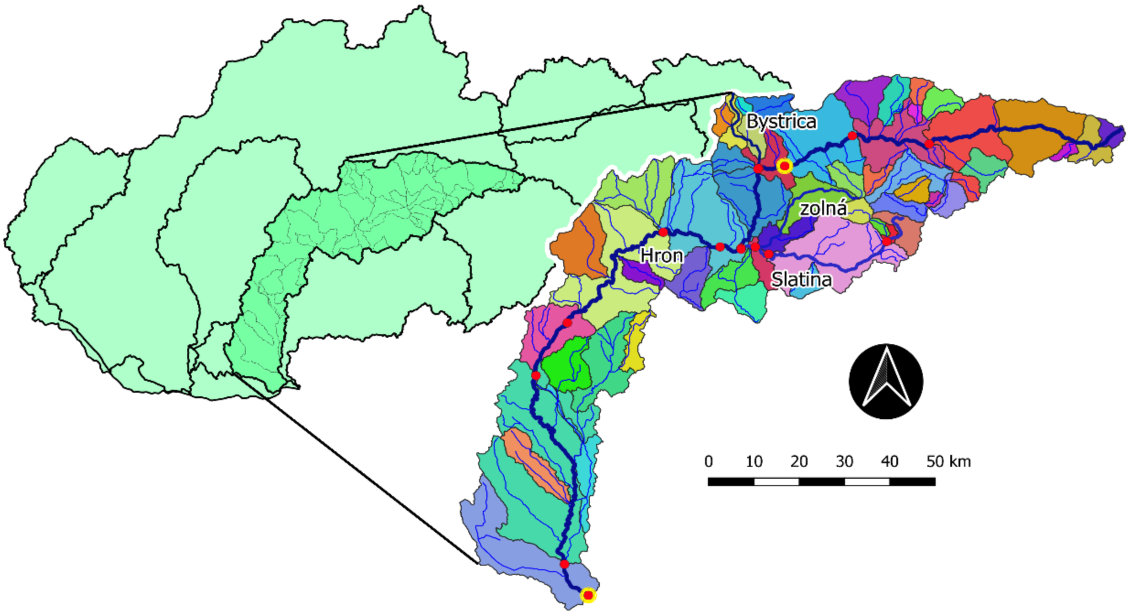

Fig. 2. Location of the Hron river basin, including balanced rivers (blue lines) and balance profiles (red points).

Modelling approach and data structure

The element that participates in the data structure for the calculation of the outflow in the "Data" part and the creation of the outflow in the scheme is the element representing the sub-basin, i.e., the "Catchment". From this element, the outflow can be distributed to the streams in several ways, which can be applied in individual scenarios. The "Runoff / Infiltration" element is used to distribute the outflow from the "Catchment" sub-basin element. With this element, it is possible to distribute a set percentage of the runoff from a given sub-basin to selected points in the streams in each sub-basin. In the scheme, the closure profiles of the sub-basins are water gauging stations with exceptional balance profiles. The outflow in the model is created by setting up the value of the precipitation variable of the catchment element. This precipitation value is calculated so that the modelled streamflow matches the streamflow data in the water gauging stations. Since the created model is purely retrospective, the streamflow data from the water gauging stations representing the affected streamflow E (which is the main model scenario) in the water management balance are available for the whole time period. The exceptions are water gauging stations with incomplete time series, as well as balance profiles, that are too far from nearby water gauging stations and are therefore required to have their own "Catchment" element. The total number of catchments was 55 (distinguished by the color scale on Fig. 2), i.e., 53 for the water gauging stations and 2 for the balance profiles (marked by the yellow circle on Fig. 2).

As the manipulation and users of the water are part of the model, they have to be the part of the equation calculating the precipitation value that forms the outflow from the sub-basin to the streams located in it. The simplified version of the equation is:

$$P_{precip.} = \frac{\Delta Q + PO + PZO - V \pm N \pm P}{A} \tag{4}$$

where:

- $P_{precip.}$ – value of the part of the precipitation representing the outflow from the sub-basin [m converted to mm],
- ΔQ – difference between the inflow into and the outflow from the sub-basin based on the streamflow data [m^3],
- PO – summary of abstractions of surface water located in sub-basin [m^3],
- PZO – summary of abstractions of groundwater located in sub-basin [m^3],
- V – summary of water discharges located in sub-basin [m^3],
- N – summary of flow manipulations on reservoirs located in sub-basin [m^3],
- P – summary of water transfers located in sub-basin [m^3],
- A – area of sub-basin [m^2].

In the case of balance profiles with their own modelled sub-basins as well as incomplete time periods of the water gauging stations concerned, the value of $P_{precip.}$ was taken from the nearby sub-basin of a water gauging station with similar morphology, as well as similar values of the average monthly precipitation.

All the individual inputs of the equation are computed as variables of the "Catchment" elements of the data structure. Fig. 3 displays the data structure of the model created including the links of the data inputs from their source to the variables of the individual elements of the water management balance (names of the variables above the arrows).

To calculate the balance status at the balance profiles, scenarios with the long-term values of the minimum balance streamflow (MQ) and minimum required streamflow (MPP) had to be created (see Blaškovičová, et al., 2015) for a thorough description of the method of MQ determination used). As the streamflow is based on data from the water gauging stations, but the water gauging stations did not yet have an MQ set, it was replaced with the long-term values of the 355-day streamflow Q_{355}. For BP2640 – Šálková and BP9800 – the Hron estuary, which does not have same location as water gauging stations, MQ was calculated by same method as the affected streamflow, E.

Results and discussion

The precision of the streamflow calculations highly depends on the correct construction of the scheme and the data structure of the model. The profiles of the water

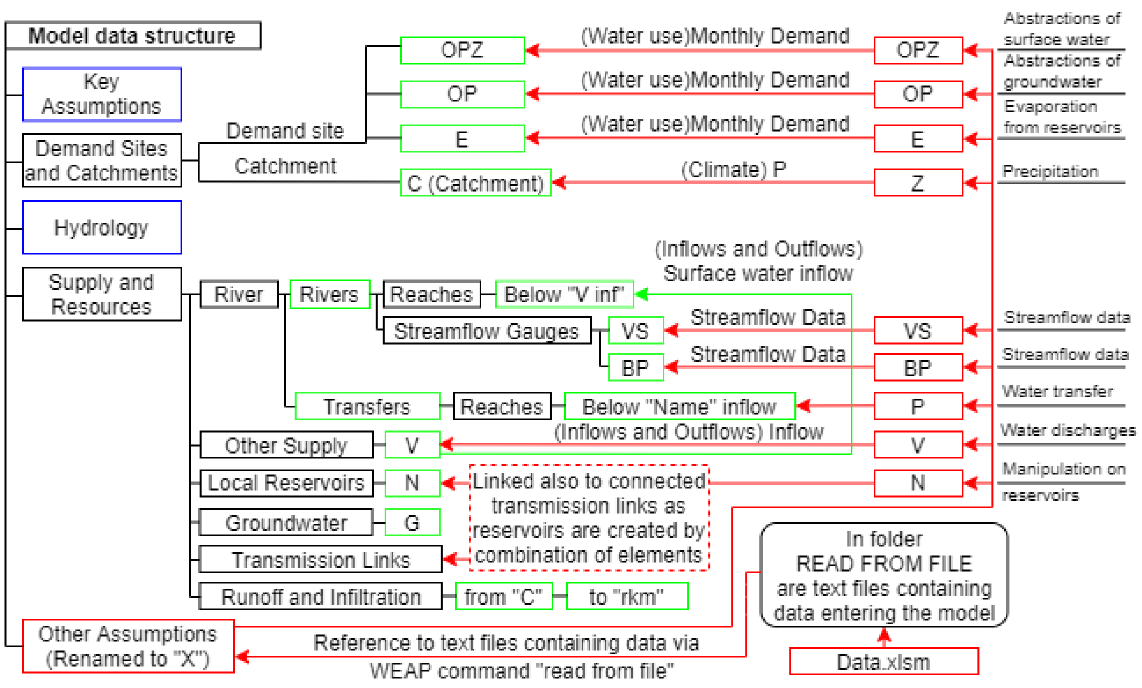

Fig. 3. The basic scheme of the data structure: Parts of the data structure without the inputs and the necessary adjustments (blue), parts of the individual elements of the scheme (green), edited and command lines used to form part of the data structure – "X" (red), links to the input data in the "X "(red arrow)..

Table 2. Comparison of MQ and Q_{355} values in the balance profiles (BP) with the same locations as the water gauging stations (WGS) on the Hron River

Registration number	Type of profile	Profile name	River km [rkm]	Area [km^2]	Q_{355} [m^3 s^{-1}]	MQ [m^3 s^{-1}]	Ratio [%]
1480R0 7015	BP WGS	Brezno	223.3	582.08	- 1.773	1.085 -	61.2
2360R0 7081	BP WGS	Nemecká Dubová	202.2 203.1	1249.8 1244.1	- 4.642	2.700 -	58.2
3240R0 7160	BP WGS	Hron under Bystrica Banská Bystrica	175.2	1766.48	- 7.549	4.755 -	63.00
5600R0 7260	BP WGS	Žiar nad Hronom	131.5	3310.62	- 10.427	7.025 -	67.4
6950R0 7298	BP WGS	Kozmálovce below water reservoir	73.4 73.1	4015.67 4015.73	- 11.690	7.905 -	67.6
8880R0 7335	BP WGS	Kamenín	10.7 10.9	5149.8	- 12.300	8.470 -	68.9

gauging stations serve as a control of this assembly, so that, when the model is correctly assembled, the modelled streamflow should be equal to the measured one. In the first step, the flows were ordered chronologically and used to calculate the differences between $Q_{modelled}$ and $Q_{measured}$. Fig. 4 shows that most of the differences are minimal, which means that, in general, the model is setting correctly. On these profiles, the percentual differences only range from -0.39 to 1.39 percent, which could be caused in part by partial errors in the model construction or incomplete input data.

The streamflow at the balance profiles without the streamflow measured from the nearby water gauging station was simulated in two ways: i) distributing the outflow to each river kilometer according to its share of the sub-basin area (BP5080, BP3920 and BP6425), or ii) by creating an individual catchment element for the sub-basin area of the balance profile (BP2640 and BP9800). A comparison of the modelled $Q_{modelled}$ and calculated streamflow $Q_{calculated}$ for the water management balance at the BP2640, balance profile of Šálková, and the BP9800, balance profile of the Hron estuary, shows that the differences are not significant, despite the simple methods used to calculate the streamflow (see Fig. 5a, b), while the balance profiles with the streamflow simulated by the distributed outflow had annual mean difference values between -0.78 to -1.36 percent, i.e., differences that are assumed to be negligible.

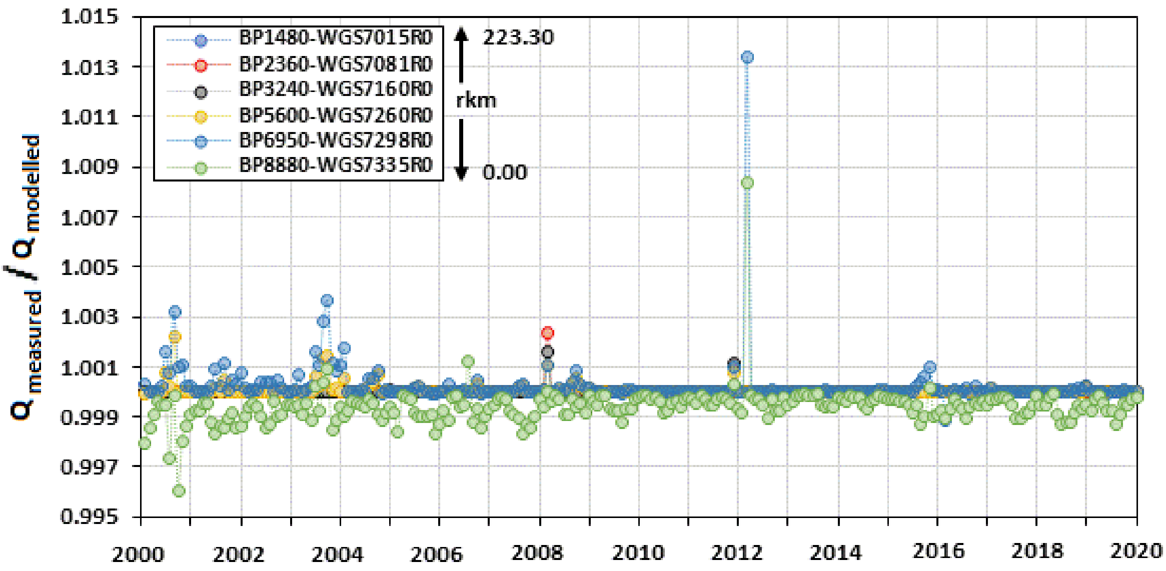

Fig. 4. Comparison of the modelled streamflow and measured streamflow at the water gauging stations which share a position with the balance profiles on the Hron river for the period 2000–2019.

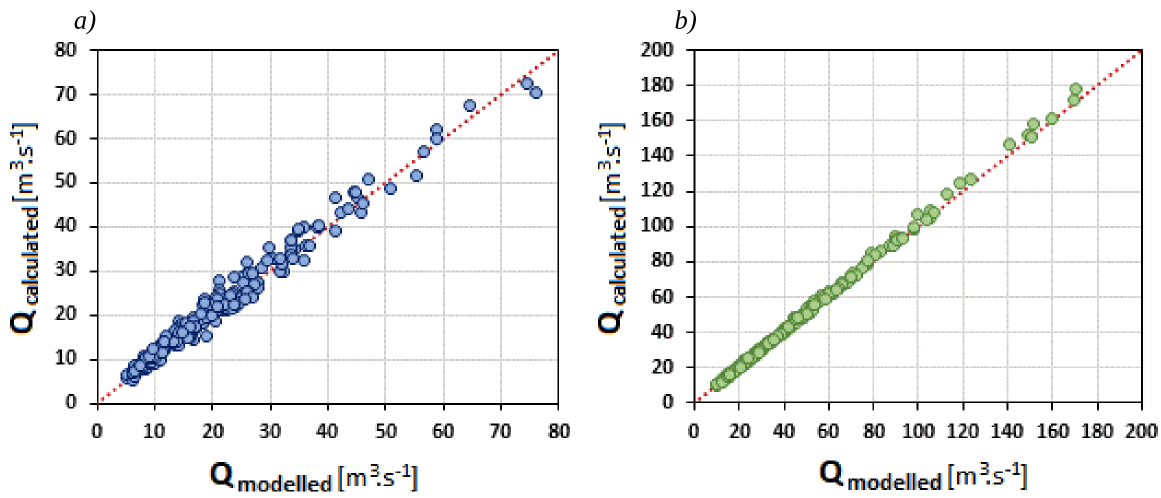

Fig. 5. Comparison of the streamflow modelled and streamflow calculated by the Slovak Hydrometeorological Institute for the water management balance in monthly time steps at the balance profiles: a) BP2640 – Šálková; b) BP9800 – the Hron estuary.

Fig. 6 shows the color-coded states for a balanced period of 20 years in the profiles located on the river Hron, using Q_{355} as MQ in BSC calculation. The active balance status (blue) was reached in 2341 months in this period on the stream, while the tension status (yellow) occurred 195 times and the passive (red) status 104 times. for comparison, using the original MQ values, the BSC values were not in the passive or tense state once throughout the 20 years period, outlining not negligible impact of using Q_{355} as MQ in BSC calculation. It is clear from the figure that the tense and passive balance statuses occur with a certain periodicity, while it can be assumed that this could be related to the year-on-year flow regime in the given years, as well as the occurrence of normal and dry years occurring in the river basin. This assumption is confirmed by a spectral map of the water flow in space and over time made as a ratio between the average monthly streamflow and long-term average monthly streamflow over the balance period (Q_m/Q_{ma}), see Fig. 7. More problematic places regarding the tension

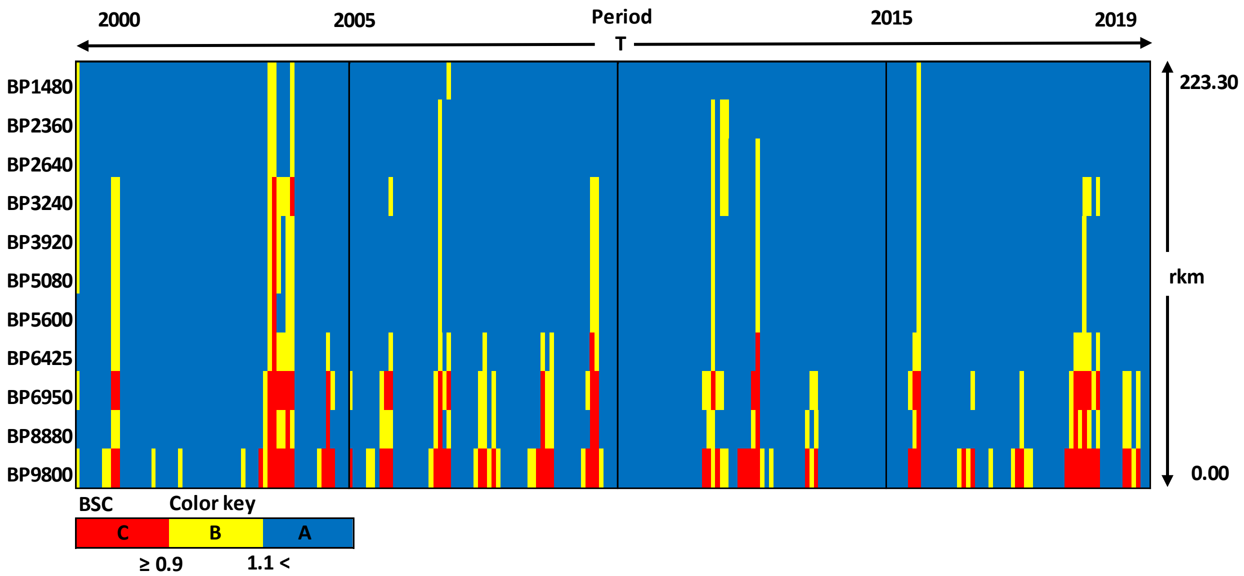

Fig. 6. Condition of balance status areas at balance profiles on the Hron river for the period 2000–2019, marked passive (red), tense (yellow) and active (blue).

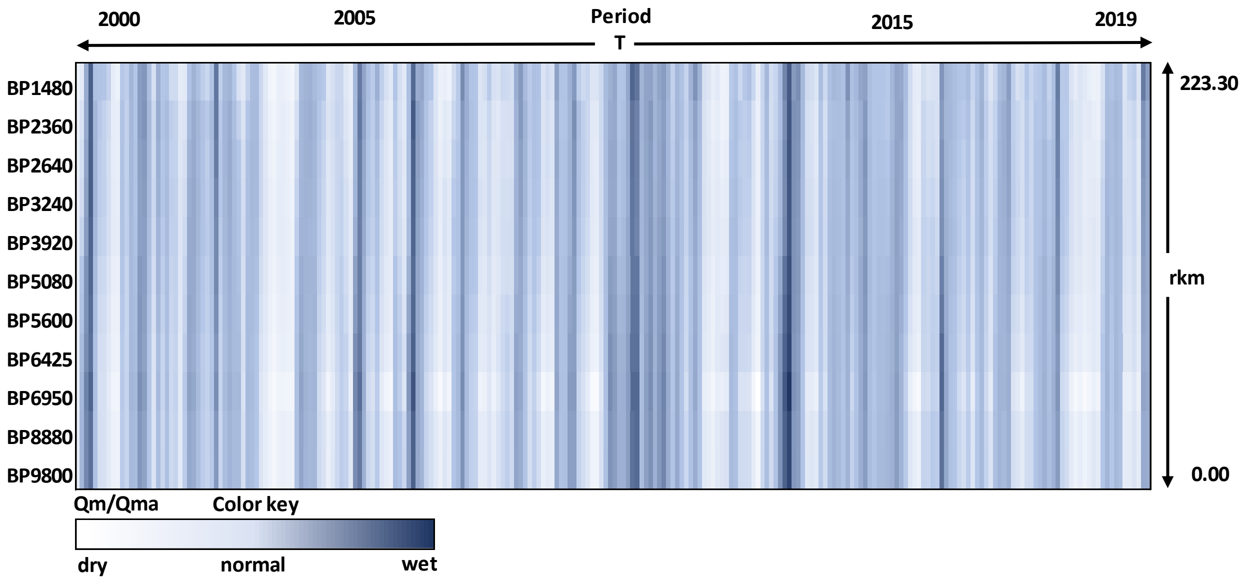

Fig. 7. Colormap of the Hron river's water content in space and over time (color spectrum from white to dark blue, or from dry to wet periods).

of the stream are situated from the source to the outfall (from BP6425 after BP9800), which certainly affects the increasing demand for water in the southern regions of Slovakia multiplied by the occurrence of a lower water period (pale spectrum in Fig. 7).

In comparison, the long-term average monthly BSC values at the balance profiles on the Hron river very rarely get below a value of 1.1 as a tense balance status. As the monthly average BSC is lowest in September and October (see Fig. 8), while highest in March and April, it appears that that is mainly due to the hydrological regime of the streams in Slovakia.

To partially verify this statement, Fig. 9 shows the average long-term monthly effect of water use and manipulation in the years 2000–2019, as summaries for the whole catchment of the Hron river. While the abstractions have the most negative impact in June and the least negative in October, the water discharges do have higher (because they include retained rainwater), yet contrary effect, as there is a connection between them. Compared to these effects, the summaries of the water transfers and impacts of the reservoirs do not show a significant impact. The difference between the impacts shows that while it is positive the whole year, except the most negative impact in July, it does not agree with the passive BSC in September and October.

However, these statements apply only in the case of the average long-term monthly values, while the use of

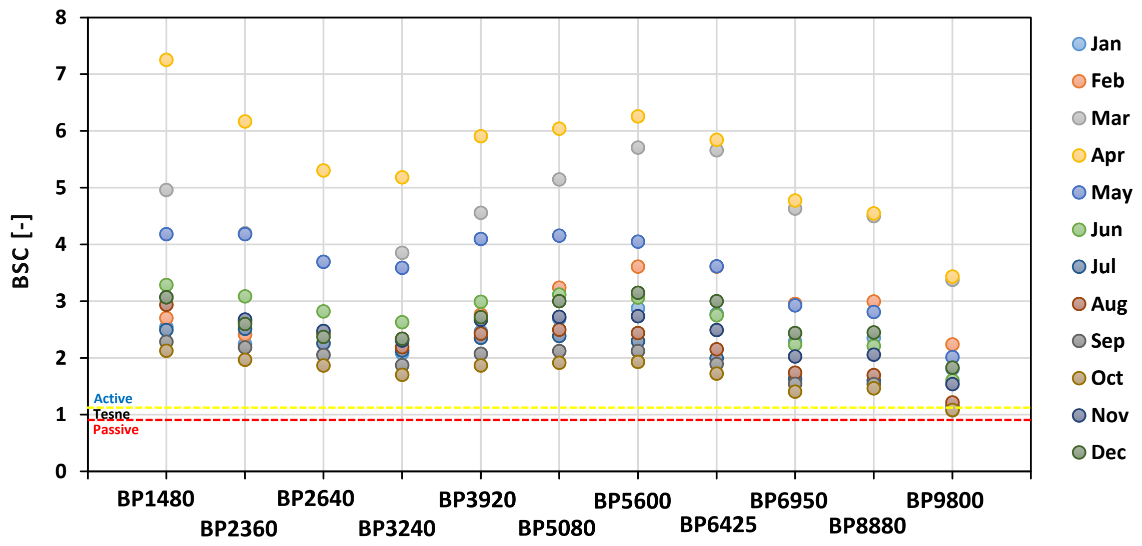

Fig. 8. Long-term average monthly BSC at the balance profiles on the Hron river for the period 2000–2019.

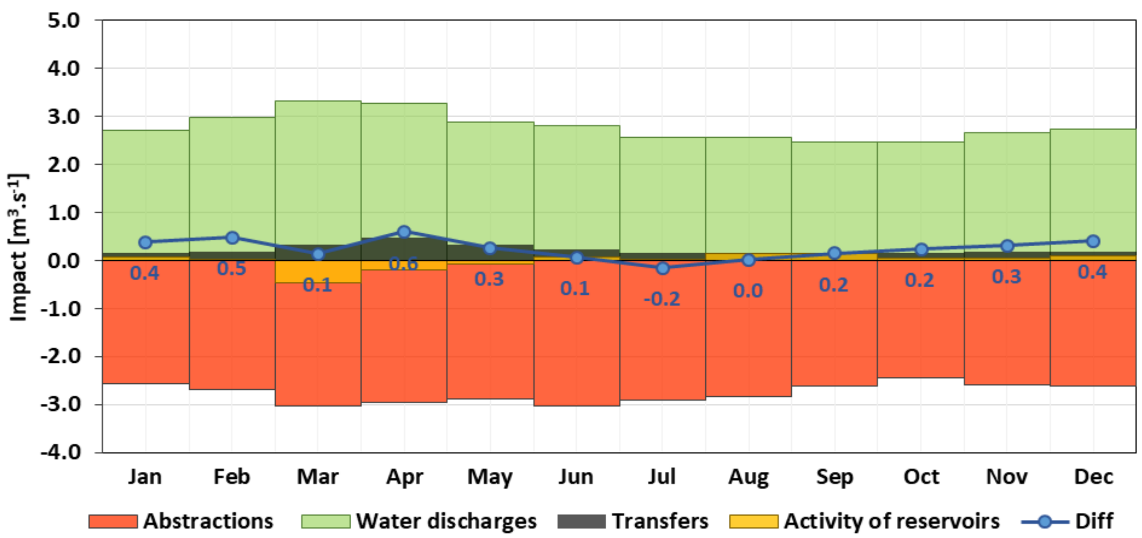

Fig. 9. Long-term average monthly summarized impact of water use and manipulation at the final profile (BP9800 – Hron estuary) for the period 2000–2019.

water and manipulation with water can have a much greater impact in the case of the evaluation of individual years. From the perspective of the long-term trends, according to Melová et.al. (2016), the development of water use in Slovakia in the period of years 2002–2014 was declining.

Conclusion

Water management balances are one of the main activities of water management in securing water requirements and their redistribution in space and over time. The resolution of the water balance has a non-uniform form in the global understanding, not only in terms of the time step in which it is addressed in various countries, or in its methodology or method of solution, but also in the very principles that individual countries apply in water management.

This paper describes the testing and application of integrated software (Water Evaluation and Planning) designed to address the issue of the redistribution of available water resources in space and over time in our physical and geographical conditions. A balance simulation model was created in the WEAP software by working in a monthly time step for the period 2000–2019, when all the elements of the water management balance of the surface waters were modelled, and the balance status was evaluated. In addition to the distribution of runoff from the river basin, an internal model was created in the data structure, which can be used to define the modelled runoff with respect to the impact of the manipulation by the water users, i.e., a flow rate identical to the flow rate observed in the water gauging stations. Due to the methodological procedure compiled in this way, it was possible to subsequently distribute the runoff along the length of the streams, depending on the share of the area and the slope of the terrain (see Kandera and Výleta, 2020) for more about runoff distribution along a stream in WEAP). Thus, it is possible to better analyze the current methodology of the water management balance of the surface waters in the Slovak Republic and consider its modifications.

The approach applied to modelling the water balance shows its potential, especially in terms of control over the model itself. It provides an ability to model the streamflow with a full degree of accuracy if the streamflow data are available, as well as calculate it if it is not available. It is not only a hydrological model, but it can also include complex elements of water management. Along with this potential, it also requires the user to fully understand the defined properties of the model, as well as the interconnection of the individual elements of the scheme and data structure. In the case of a relatively large model such as the Hron river basin, working with the model could be challenging for the unskilled user.

The model was used in a simple analysis of the effects from the change in the minimum balance flow on the value of Q_{355}, and although there were no visible significant differences between the modelled and calculated flows in the balance profiles outside the water gauging stations, the simplicity of the flow calculation method in these profiles must be considered when looking at the results. A more important result is the sheer number of outputs that the model brings. In addition to its potential for supplementing the current production of water management balance outputs with a long-term time series of data, it shows its potential capability as an analytical tool, which in principle the WEAP software itself is. Consequently, its primary usefulness will be focused on the direction in which the development of the established methodology for modelling the water management balance of the amount of surface water will go.

One of the future research goals is to implement the usual method of calculating runoff from a river basin at a smaller catchment into the created methodology and to compare the results. That approach could serve subsequent goals to deal with the problems which occurred during the modelling, along with efforts to connect the water management of the amount of surface water and groundwater through modelling in the WEAP software.

Models like WEAP are based on a mathematical description of all the dependencies between the resources and requirements and permit solving them by computer technology, a number of variant changes in the resources, as well as the water requirements. Due to the mentioned fact that in Slovakia, balance simulation models have never been fully applied in practice, the outputs of this paper are assessed as necessary and considered an effort to move forward in this area within Slovakia.

Acknowledgement

This work has been funded by the Slovak Research and Development Agency under Contract No. APVV-19-0340, and the VEGA grant agency under Contract No. VEGA 1/0632/19. The authors are grateful for their financial support.

References

Andreu, J., Capilla, J., Sanchìs, E. (1996): AQUATOOL, a generalised decision-support system for water-resources planning and operational management. Journal of Hydrology, 177, (3–4), 269–291.

Assaf, H., van Beek, E., Borden, C., Gijsbers, P., Jolma, A., Kaden, S., Kaltofen, M., Labadie, J. W., Loucks, D. P., Quinn, N. W. T., Sieber, J., Sulis, A., Werick, W. J., Wood, D. M. (2008): Chapter thirteen: generic simulation models for facilitating stakeholder involvement in water resources planning and management: a comparison, evaluation, and identification of future needs. Developments in Integrated Environmental Assessment, 3, 229–246.

Blaškovičová, L., Melová, K., Danáčová, Z., Lovásová, Ľ., Šimor, V., Poórová, J. (2015): Minimum balance streamflow in relation to ecological flows. Acta Hydrologica Slovaca, 16, 23–30.

Danáčová, Z., Gápelová, V., Lovásová, Ľ., Ľupták, Ľ., Melová, K., Podolinská, J., Rischáneková, M., Síčová, B., Staňová, J. (2011): Water resource balance of surface water quantity for 2010, SHMÚ Bratislava, 328.

DHI (2003): MIKE BASIN: A Versatile Decision Support

Tool for Water Resources Management Planning, Guide to Getting Started Tutorial. Danish Hydraulic Institute, Denmark.

European Union (2015): Guidance document on the application of water balances for supporting the implementation of the WFD. ISBN 978-92-79-52021-1

Kaden, S., Kaltofen, M., Koch, H. (2006): Water resources management and water availability in the Elbe River Basin under conditions of global change. In: Voinov, A., Jakeman, A. J., Rizzoli, A. E. (Eds.), Proceedings of the iEMSs Third Biennial Meeting: "Summit on Environmental Modelling" and Software. International Environmental Modelling and Software Society, Burlington, VT, USA.

Kandera, M., Výleta, R. (2020): Application of the Water Evaluation And Planning (WEAP) Model to Quantitative Water Balance Modelling in the Upper Hron River Basin (Slovakia). In: IOP Conference Series: Earth and Environmental Science, Vol. 609, No. 1, p. 012055. IOP Publishing.

Labadie, J. (2005): MODSIM: River basin management decision support system. Watershed Models. CRC Press, Boca Raton, FL, USA.

Melová, K., Lovásová, Ľ., Blaškovičová, L., Danáčová, Z. (2016): Evaluation of water use in comparison with water resources in surface waters in the period 2002–2014 based on the results of the water management balance, Presentation at international conference on the “Effective use of water resources in the conditions of the ongoing climate change (dry and water deficiencies)”, under the auspices of Priority Area 4, Water Quality of the Danube Strategy and the Minister of the Environment of the Slovak Republic.

Poorová, J. (2007): Methods of water management balance. Dissertation work, STU Bratislava.

Sechi, G. M., Sulis, A. (2009): Water system management through a mixed optimization-simulation approach. Journal of Water Resources Planning and Management, 135 (3), 160–170.

WL/Delft Hydraulics, (2007): RIBASIM. http://www.wldelft.nl/soft/ribasimlint/. Last accessed on June 23, 2007.

Yates, D., Sieber, J., Purkey, D., Huber-Lee, A. (2005): WEAP21: a demand, priority, and preference driven water planning model. Part 1. Model characteristics. Water International, 30 (4), 487–500.

Ing. Miroslav Kandera (*corresponding author, e-mail: miroslav.kandera@stuba.sk)
Ing. Roman Výleta, PhD.
Bc. Anna Liová
Department of Land and Water Resources Management
Faculty of Civil Engineering
Slovak University of Technology in Bratislava
Radlinského 11
810 05 Bratislava
Slovak Republic

Ing. Miroslav Kandera
Ing. Zuzana Danáčová, PhD.
Ing. Ľubica Lovásová
Slovak hydrometeorological institute
Jeséniova 17
833 15 Bratislava
Slovak Republic

DOI: 10.31577/ahs-2021-0022.01.0005

ACTA HYDROLOGICA SLOVACA

Volume 22, No. 1, 2021, 40 – 49

COMPARISON OF THE VARIABILITY OF SNOW COVER PARAMETERS OF THE HBV MODEL USING LUMPED AND DISTRIBUTED PRECIPITATION INPUTS AND MULTI-BASIN CALIBRATION

Adam Brziak*, Martin Kubáň, Silvia Kohnová, Ján Szolgay

Snow cover is a significant source of water supply, mainly in mountainous regions, as snow precipitation fundamentally affects a catchment´s water balance. The correct simulation of the water balance with rainfall-runoff models is therefore important for the effective management of water resources. Three basic factors may affect the efficiency of hydrological models and the quality of the modelled outputs: The spatial representativeness of the input data, the model´s structure, and the uncertainties of the model parameters. A comparison of the variability of snow cover parameters and model efficiency of two versions of the HBV model using spatially lumped and distributed precipitation inputs by a multi-basin calibration exercise was performed in this study. Both the lumped and semi-distributed versions of the HBV model were calibrated for discharges, precipitation, and the air temperature on 180 catchments located all over the territory of Austria using data from the period 1991–2000. The analysis focused on the variability of the parameters controlling the snowmelt and the accumulation of the snow components of the two models. The efficiency of the models based on lumped and spatially distributed inputs was compared. The question as to how the catchment´s mean elevation, and the number of days with an air temperature below zero affects the model´s performance was targeted, too.

KEY WORDS: HBV model, Austria, snow cover parameters, multi- basin calibration

Introduction

Rainfall-runoff models are often applied when solving various water resource problems, e.g., forecasting flood events, estimation of the effects of climate change, simulating extreme discharges, etc. Snow accumulation and snow-melt fundamentally affect the water balance and runoff in river basins. Therefore, the correct modeling of the duration of the snow cover and its properties is an important factor in improving the efficiency of similations of rainfall-runoff models.

Three basic factors may affect the efficiency of hydrological models and the quality of the outputs modeled: the spatial representativeness of the input data, the structure of the model, and the uncertainties of the parameters. Model-based approaches are imperfect due to model biases and uncertainties about the input data, too (O'Connell, 1991). In this respect, and based on a review of several studies, Finger et al. (2015), pointed out that analyses of rainfall-runoff model performances in various environments indicated the fact that focusing on a model´s complexity may be less important than the use of proper calibration methods. Kirchner (2006) recommended that in addition to developing better models and better analytic tools, the quality of the data input to models should also get attention. Instead of fitting a pre-defined model and data structure to a catchment via the calibration of parameters, different sources of additional field data could improve the adequacy of representing the dominant hydrological processes in the modelled catchments (McMillan et al., 2011). Respecting the spatial variability of precipitation and snowcover and accounting for other spatially nonhomogeneous basin properties (e.g. soil moisture) could significantly improve the quality of modelled hydrological responses. Khakbaz et al. (2012) discussed issues relating to characterizing the impact of the spatial distribution of rainfall and basin characteristics on runoff generation and the structure of a model. They investigated lumped and distributed calibration strategies and suggested that the performance of a model at an outlet can be improved by using a semi-distributed structure and spatially distributed inputs.

A particular problem in the estimation of hydrological model parameters is equifinality, which has been discussed in-depth in a large number of studies (e.g., Freer et al., 1996). As a consequence, many authors have also attempted to constrain such uncertainties in model parameters by using additional data sets for multi-site model calibrations (e.g. Perrin et al., 2001; Hailegeorgis and Alfredsen, 2016; Finger et al., 2015; Knoben et al., 2019).

Research on enhancing the reliability of estimations of snowpack parameters and their contributions to discharges in mountainous regions has also made use of multi-basin data sets. The inclusion of the remote sensing of satellite snow cover images during calibrations has led to the improvement of both snow cover and discharge simulations and the reduction of parameter uncertainties (e.g., Jiang and Wang, 2019; Lopez et al., 2020; Ruelland, 2020).

We may account for different climatic conditions in catchments with larger elevation ranges. Various authors have pointed out that not respecting the different climatic conditions in the use of models may lead to uncertainties that could affect the quality of the outputs (e.g., Vaze, 2010; Merz, 2011; Coron, 2012; Saft, 2016; Ceola et al. 2015). Differentiating model inputs by elevation zones may contribute to resolving such problems.

One challenge in correctly estimating the properties of snow processes for modelling is the sparse observational network of climatic and hydrological variables in many regions. The preparation of representative model inputs and the resulting model simulations are affected by the uncertainties of the measurements, their spatial representativeness, and the spatial interpolation of the point precipitation measurements. The impact of the spatial representation of the variability of snow cover properties on model simulations therefore continues to receive interest (Finger et al., 2015; Lopez et al., 2020; Ruelland, 2020).

Since the snow routine parameters of the conceptual rainfall-runoff models usually cannot be obtained or derived directly from field measurements of the snowpack properties in the climatic stations, they have mainly been estimated by the calibration of the mathematical models. Recently, the streamflow-based model calibrations were extended by remotely sensed snow observations in snow-dominated areas by making use of their increasing spatial resolution and reasonable spatio-temporal coverage. Several studies have shown that incorporating snow observations into the multivariable calibration of a hydrological model could improve streamflow estimates (see Jiang and Wang, 2019).

The main objective of this paper is to observe how the lumped and semi-distributed versions of the HBV type TUW conceptual rainfall-runoff model compare when using lumped and spatially distributed climatic inputs in a multi-basin calibration in 180 Austrian catchments. The study closely focuses on a comparison of the parameters of the snow component modeling part of both model versions. The model versions differ mainly in the spatial resolution of the inputs; the semi-distributed version divides each catchment into elevation zones of 200 m, while the lumped model takes every input and output component as a mean value for the whole catchment. The catchments were divided into three groups based on their mean elevation. The model efficiency and snow-related parameters were analyzed separately in catchments with different hypsometric characteristics in flat, hilly, and mountainous catchments. It was attempted to verify if improvement of the model efficiency could be achieved by only using spatially interpolated distributed inputs in a semi-distributed version of a lumped conceptual model (without using distributed parameter calibrations and remotely-sensed snow observations). The analysis also focused on a comparison of the variability of snow cover parameters of two versions of the HBV model using a multi-basin calibration exercise. We hypothesized that the different spatial resolutions of the lumped and semi-distributed models with regard to their input values may lead to observable differences, both in the variability of their performance and parameters, especially in catchments with higher mean elevations in mountainous or alpine regions.

Methods

In this study, the TUW rainfall-runoff model TUW was used in its lumped and semi-distributed versions (Parajka et al., 2007; 2009). The model is based on the philosophy of the Swedish HBV model (Bergström, 1995).

The lumped version of the TUW model uses the averaged values of the air temperature, precipitation, and potential evapotranspiration as inputs over the whole catchment. The semi-distributed version of the TUW model considers spatially variable inputs over the catchments in 200 m elevation zones. The parameters of the semi-distributed model were considered as lumped in this study. Both versions have extensively been used for solving various hydrological problems (see e.g., Sleziak et al., 2016; Parajka et al., 2007; Viglione et al., 2013).

The TUW model consists of three sub-models: the snow sub-model, the soil sub-model, and the runoff formation sub-model. Fig. 1 represents the structure of the lumped version of the TUW model.

The model has 15 parameters, which are listed in Table 1 together with the recommended ranges of their respective values according to Merz et al., (2011); the same ranges were used in this study.

The snow submodel simulates the accumulation of water in a snowpack and inputs water from the melted snow to the catchment. At the centre of interest of this study was the behaviour and variability of the 5 snow routine parameters of both versions of the TUW model.

Snow accumulation and snowmelt are controlled by the following parameters:

- the snow correction factor (SCF), which represents the uncertainty in the precipitation measurements input in the winter and the large spatial variability of the snow cover; the snowfall is corrected by this corrective snow factor;
- the degree-day factor (DDF); a factor influencing the melting of snow;
- threshold air temperature (Tr); precipitation above this is considered as rain;
- threshold air temperature (Ts); below which, precipitation is considered as snow;
- threshold air temperature (Tm); above which, melting in the snowpack takes place.

For calibrating the model in this study, the DEoptim differential evolution algorithm was used (Sleziak et. al., 2017), and the warm-up period was set at one year.

The objective function, which is described in Eq. 1, combined the well-established Nash-Sutcliffe efficiency and the logarithmic Nash-Sutcliffe efficiency (log NSE). The NSE and log NSE coefficients range from -∞ to 1, where 1 indicates a perfect simulation, i.e., an absolute equality between the observed and simulated flows. While the NSE is considered more appropriate for high flows, the log NSE is more appropriate for low flows (Merz et al., 2011).
The following NSE and log NSE formulas were used:

$$\mathrm{NSE} = 1 - \frac{\sum_{i=1}^{1}\left(Q_{sim,i} - Q_{obs,i}\right)^2}{\sum_{i=1}^{1}\left(Q_{obs,i} - \overline{Q}_{obs}\right)^2} \qquad (1)$$

$$\mathrm{logNSE} = 1 - \frac{\sum_{i=1}^{1}\left(\log(Q_{sim,i}) - \log(Q_{obs,i})\right)^2}{\sum_{i=1}^{1}\left(\log(Q_{obs,i}) - \log(\overline{Q}_{obs})\right)^2} \qquad (2)$$

where
Q_{sim} – are the simulated mean daily flows,
Q_{obs} – are the observed mean daily flows,
$\overline{Q}_{obs}$ – is the average of the observed flows.

The objective function (RME) was defined as:

$$RME = \frac{NSE}{2} + \frac{logNSE}{2} \qquad (3)$$

Input data

The calibration of the model was performed on data from 180 catchments, which are distributed over the whole territory of Austria. These data have also been extensively used in previous modeling studies, e.g., by Viglione et al. (2013) and Sleziak et al. (2016). The catchment areas varied from 14.2 km^2 to 6214 km^2. Before processing the data, quality flags, missing data, etc., were visually inspected. Catchments that were selected which were not affected by an anthropogenic influence, e.g., by dams, canals, or any other artificial runoff regime transformations.
The input data (rainfall, runoff, potential evaporation, air temperature) in daily time steps from the period 1.1.1991 to 31.12.2000 were interpolated for the lumped TUW model version from point measurements taken across Austria from 1091 stations by the external drift kriging method (Sleziak et al., 2017). The runoff data were from 180 gauging stations of the Austrian Hydrographical Service. The potential evaporation data were calculated with the Blaney-Criddle method (Parajka et al., 2003). The rainfall and air temperature input data for the semi-distributed version of the TUW model were taken from the Spartacus database (Hiebl et al., 2016) and were interpolated into the hypsometric zones by 200 vertical meters. The potential evaporation was calculated with the Blaney-Criddle method in the same hypsometric zones.
In order to separate the effect of the prevailing climatic conditions and the respective runoff regimes in the analysis of the variability of the snow parameters on the results, we clustered the catchments into three groups based on their respective mean elevations:

- the first group (86 catchments) with mean elevations between 0–1000 m.a.s.l;
- the second group (80 catchments) with elevations between 1000–2000 m.a.s.l;
- the third group (14 catchments) with elevations above 2000 m.a.s.l..

The first group includes catchments where the major

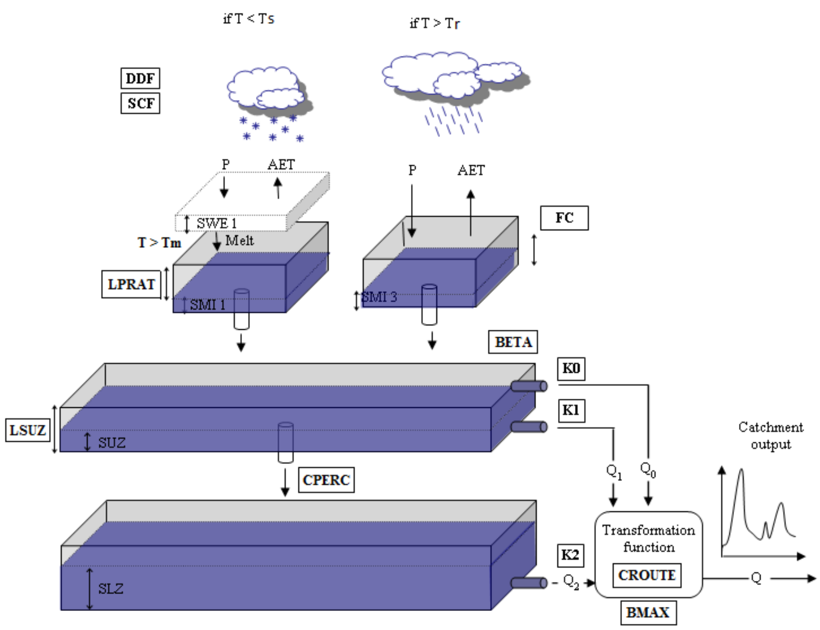

Fig. 1. Schematic structure of the lumped version of the TUW model (Sleziak, 2017).

contributor to the runoff is liquid precipitation; this group is labeled the "Lowland" type. The second group includes catchments where a significant part of the runoff is also contributed to by meltwater and is referred to as the "Hilly" type; and the third group represents the "Alpine" type of catchments, where snow and glaciers largely impact the runoff from the catchments. In Fig. 2 we can see the location of the selected catchments, which are clustered into three groups and color-coded as green – Lowland, orange – Hilly, red – Alpine.

The left graph in Fig. 3a shows the median of the number of days with a temperature below zero in the three groups of catchments. The right graph, Fig. 3b, represents the mean elevation of the catchments (726.2 m.a.s.l in the lowland catchments, 1385.7 m.a.s.l in the hilly catchments, and 2212.1 m.a.s.l in the alpine catchments). We can observe that the triangles indicate that a portion of the days with a temperature below zero is directly related to the mean elevation of the catchments; therefore, the separation of the catchments into groups also reflects the differences in the snow regimes.

Table 1. The TUW model parameters and their recommended range (Merz et al., 2011)

Abbreviations	Description of the model parameters	Range
1. SCF	snow correction factor	0.9–1.5 [-]
2. DDF	degree day factor	0.0–5.0 [mm/degC/day]
3. Tr	threshold temperature above which precipitation is rain	1.0–3.0 [degC]
4. Ts	threshold temperature below which precipitation is snow	-3.0–1.0 [degC]
5. Tm	threshold temperature above which melting starts	-2.0–2.0 [degC]
6. LPRAT	parameter related to the limit for potential evaporation	0.0–1.0 [-]
7. FC	field capacity, i.e., max soil moisture storage	0–600 [mm]
8. BETA	the non-linear parameter for runoff production	0.0–20.0 [-]
9. K0	storage coefficient for a very fast response	0.0–2.0 [days]
10. K1	storage coefficient for a fast response	2.0–30.0 [days]
11. K2	storage coefficient for a slow response	30.0–250 [days]
12. LSUZ	threshold storage state, i.e., start of the very fast response if exceeded	1.0–100 [mm]
13. CPERC	constant percolation rate	0.0–8.0 [mm/day]
14. BMAX	maximum base at low flows	0.0–30.0 [days]
15. CROUTE	free scaling parameter	0.0–50.0 [$days^2$ /mm]

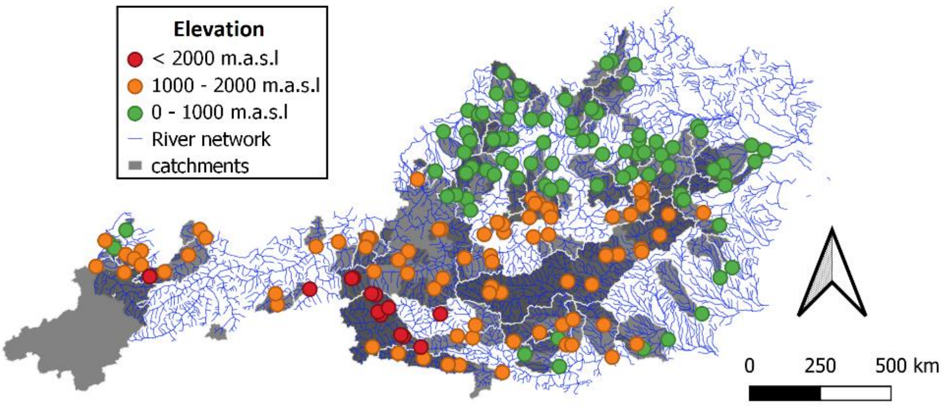

Fig. 2. Location of the selected 180 Austrian catchments clustered into elevation zones and color-coded as green – Lowland, orange – Hilly, and red – Alpine.

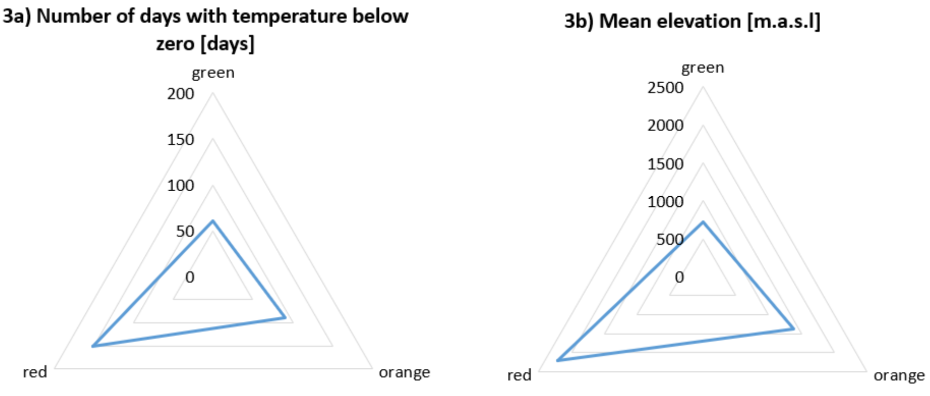

Fig. 3. Illustration of the interdependence between the mean number of days with a temperature below zero and the mean elevation of the catchments divided into the three groups, green – Lowland, orange – Hilly, and red – Alpine catchments.

Results and discussion

Comparing the distribution of the RME efficiency measure of the calibration of both model versions in the groups of catchments (Figs. 4 and 5) shows notable differences in all three groups. The boxplots shown the minimum and maximum value of RME, first and third quartile and mean value represented by black cross. We assessed the model efficiency over three different groups of catchments (i.e., green – Lowland, orange – Hilly, red – Alpine).

In the lowland catchments, where the soil-moisture regime is the more dominant runoff generation mechanism, we did not expect a significant contribution of the snow precipitation to the runoff. The RME values were 0.64 in the lumped version of the TUW model and 0.76 in the semi-distributed version (Figs. 4 and 5) in these catchments. A lumped version of the model shows a slightly lower performance in comparison with the semi-distributed version. This means that the semi-distributed model also performs better in the lowland catchments, which could be caused by the lower spatial variability of the input data.

The Hilly type of catchments with a mean elevation between 1000–2000 m.a.s.l, have seasonal precipitation regime characteristics with the main proportion of liquid precipitation in the summer season and solid precipitation in the winter season. This means that the snow routine of the rainfall runoff model has a stronger influence on the final efficiency of the model´s performance more than in the lowland group of catchments. The median RME values were 0.67 for the lumped version and 0.81 for the semi-distributed version of the TUW model (Figs. 4 and 5). Again, we can observe that the semi-distributed model outperformed the lumped version, probably due to the different spatial resolutions of the inputs into both versions of the model.

The third group of catchments with alpine characteristics is the group with snow-dominated catchments, where the melting of accumulated snow precipitation mainly contributes to the catchment´s runoff. In part of the catchments in the alpine group catchments, we may also consider a significant contribution to runoff from glaciers, which represent an important storage of water in high elevation zones. In the alpine group of catchments, the median RME values were 0.51 for the lumped version and 0.88 for the semi-distributed version of the TUW model. Here, we can observe a great difference in the performance between both model versions. The lumped version of the TUW model showed poor performance. The spatial differentiation of the model inputs in the semi-distributed version of the model, which divides catchments into elevation zones, can better reflect the snow regime influenced by the climatic differences between the lowest and highest parts of the catchments.

In general, by also comparing Figs. 4 and 5, we can see that the semi-distributed version outperformed the lumped model. We observed that the results of the lumped version of the TUW model showed a poorer performance in catchments with a mean catchment elevation above 2000 m.a.s.l and with alpine climate characteristics (Fig. 4). The semi-distributed version of the TUW model performed better in catchments in the Alpine group compared to those in the Lowland or Hilly groups of catchments (Fig. 5). The main reason for the differences in the quality of the calibration results of both versions of the TUW model may be attributed to the effects of the spatial distribution of the input of the climatic values. Since these values were more pronounced in the Alpine group, it could be expected that the spatially distributed inputs of the winter precipitation improved the model´s performance.

In the next step the median values of the snow sub-model parameters were compared in the three groups of catchments (Fig. 6), and the parameter variances in the boxplot charts were compared. The boxplots show the minimum and maximum value of each parameter, first and third quartile and mean value represented by black cross (Fig. 7–11).

We can observe differences in the general behavior of the variability of the snow routine parameter among the catchment groups. Fig. 6a shows that the snow

Fig. 4. Runoff model efficiency boxplot of the lumped model version in all the catchments divided into three groups: Green –Lowland, orange – Hilly, and red – Alpine catchments.

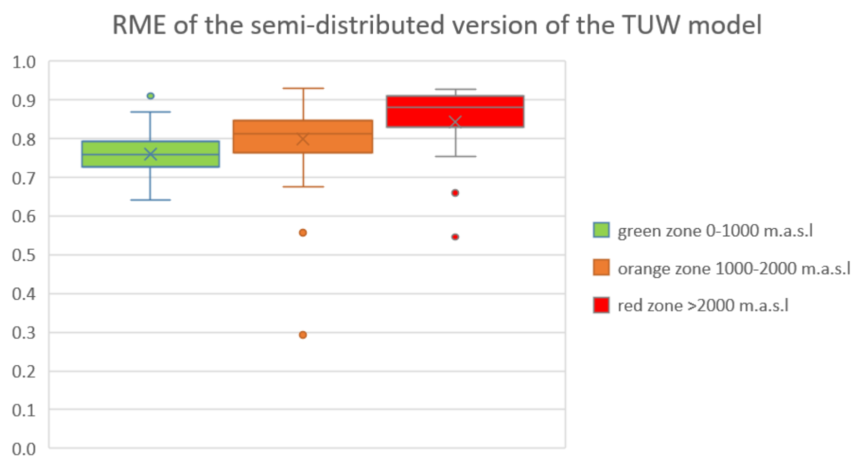

Fig. 5. Runoff model efficiency boxplot of the semi-distributed model version in all the catchments divided into three groups: Green – Lowland, orange – Hilly, and red – Alpine catchments.

correction factor (SCF) is the highest for both models in the Alpine group; on average, it practically does not strongly correct the winter precipitation amounts in the other two clusters as the boxplot chart (Fig. 7) indicates.

This could be expected, and it also shows that the multi-site calibration was able to capture this behaviour across all the catchments.

The distribution of the values of the degree-day factor (DDF) in Figs. 6b and 8 shows a different pattern: the highest values can be observed for the semi-distributed model in the red group, followed by the orange and green catchments. This is consistent with the idea that snowmelt (and snow accumulation, too) has to be most pronounced in an Alpine region, followed by the hilly and lowland catchments. It can be expected in the behaviour of the lumped model that the snow cover may have a greater temporal and spatial variability in the Lowland group. Consequently, the snowmelt can have a shorter duration and be more intensive in some of the lowland catchments, which can explain the distribution and peaking of the median of the DDF parameter there.

In the threshold temperature above which precipitation is considered to be liquid (Tr), (Figs. 6c and 9), we can observe consistency in the values for both the semi-distributed and lumped versions in the Alpine and Lowland groups, which is to be expected and acceptable. In the Alpine group of catchments the Tr parameter reached almost the same value of +3°C for all the catchments analysed in this group. The lower median value for the lumped model in the Hilly group of catchments could be connected to the larger variability of the duration and extent of the snowpack at these altitudes, but that would need a detailed catchment-based analysis, which was not performed here.

In Figs. 6d and 10, the threshold temperature below which precipitation is snow (Ts) gave similar calibration values for all three groups of catchments and both versions of the TUW model. It is physically acceptable that at lower elevations, the snow accumulation is connected with air temperatures below zero (for majority of chatchments Ts is about -2.5ºC), whereas in high elevations, this temperature can be higher. This could be observed especially in the Alpine group of catchments, where the median value of this parameter reaches a value of about +1ºC.

The threshold temperature above which melting starts (Tm) (Figs. 6e and 11), is an important parameter that indicates the start of snow melting and thereby runoff generation. Whereas its similar values in the lumped model´s representation of the spatial variability of the inputs in all three groups are to be expected, the patterns and significant changes in the parameter values in the semi-distributed version of the TUW model are difficult to explain and could be connected to the larger variability of the duration and altitudinal variability of the extent of the snowpack in the orange altitudes (and maybe by the selection of the altitudinal thresholds, too). This would need a detailed catchment-based analysis and maybe a more differentiated subdivision of this group of catchments, which was not performed here.

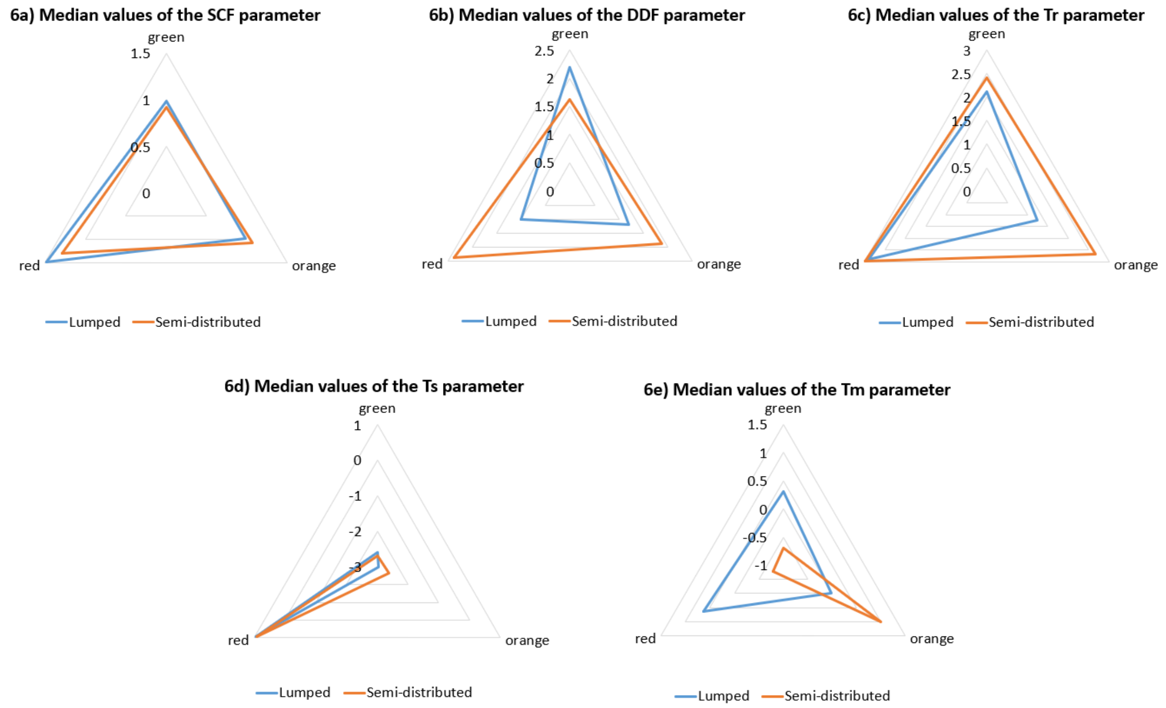

Fig. 6. Comparison of the median values of the snow submodel parameters for both model versions.

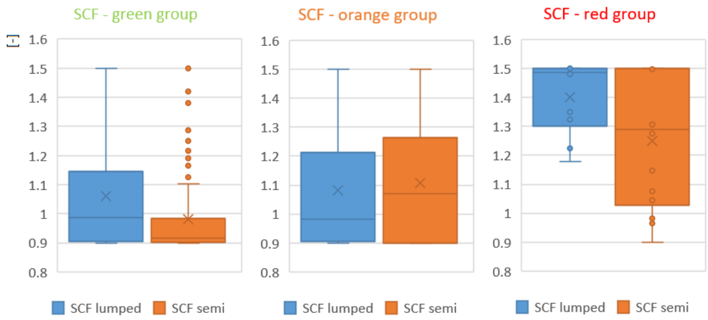

Fig. 7. Boxplots of the distribution of the SCF parameter in all the catchments divided into the three groups. Green – Lowland, orange – Hilly, and red – Alpine catchments.

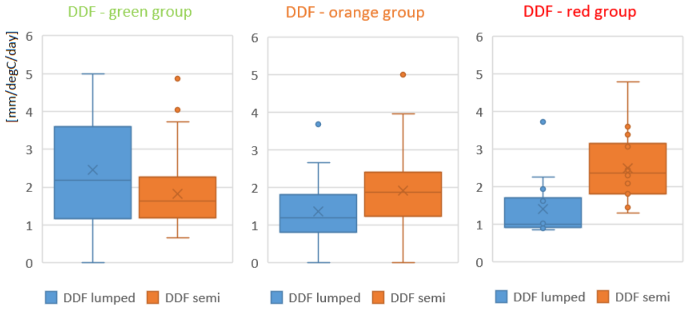

Fig. 8. *Boxplots of the distribution of the DDF parameter in all the catchments divided into the three groups. Green –Lowland, orange – Hilly, and red – Alpine catchments.*

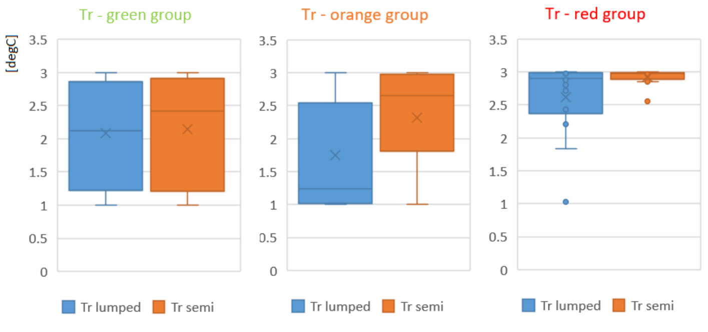

Fig. 9. *Boxplots of the distribution of the Tr parameter in all the catchments divided into the three groups. Green – Lowland, orange – Hilly, and red – Alpine catchments.*

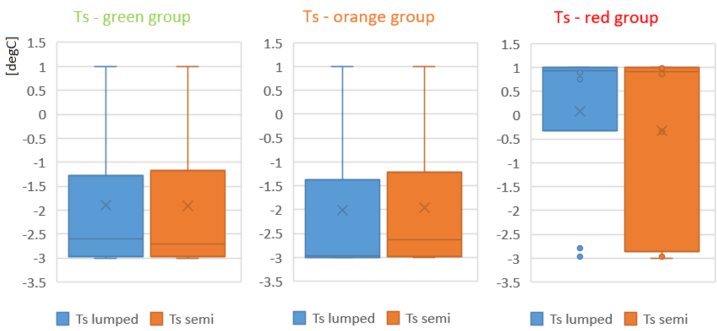

Fig. 10. *Boxplots of the distribution of the Ts parameter in all the catchments divided into the three groups. Green – Lowland, orange – Hilly, and red – Alpine catchments.*

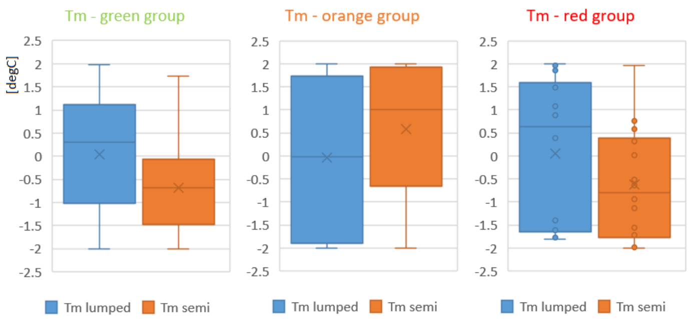

Fig. 11. *Boxplots of the distribution of the Tm parameter in all the catchments divided into the three groups. Green – Lowland, orange – Hilly, and red – Alpine catchments.*

Conclusion

Snow cover is a significant factor for the supply of water for diverse uses and is an important part of runoff processes, especially in mountainous regions. It is necessary to observe and evaluate how rainfall-runoff models simulate each runoff component in order to ensure reliable simulations that can improve decisions in solving water resources management problems. In this study, we compared the model efficiency of the HBV type TUW rainfall-runoff model in its lumped version and semi-distributed versions. We performed multi-site calibrations of both models for 180 catchments across Austria, which were divided into three groups, according to their respective mean elevation. For the lumped TUW model version, the input data (rainfall, runoff, potential evaporation, air temperature) in daily time steps from the period 1.1.1991 to 31.12.2000 were interpolated from point measurements across Austria (Sleziak et al., 2017) from 1091 stations by the external drift kriging method. The rainfall and air temperature input data for the semi-distributed version of the TUW model were taken from the Spartacus database (Hiebl et al., 2016) and were interpolated into the hypsometric zones by 200 vertical meters.

We analyzed if and how the mean elevation of the catchments and the spatial variability of the input values can affect both the calibration efficiency and the values of the snow sub-model parameters. The results of the runoff model efficiency showed that the semi-distributed version of the model performed better in all the catchments. The efficiency of the lumped version mainly struggled in the group of high altitude catchments. With the variations of the snow sub-model parameters, we can conclude that the overall behavior of the parameter values was physically consistent with the expectations for all the parameters, except for the threshold temperature above which melting starts. Since this can play a huge role in the estimation of the amount of water melted from snow, its behavior in the multi-site calibration requires further analysis, which could improve runoff model efficiency in the semi-distributed model version. The spatial differentiation of the model inputs proved to be beneficial and the multi-site calibration in the attitudinally grouped catchment clusters led to better insights into the physical consistency and reliability of the snow parameters in the case of the TUW model.

Acknowledgment

This work was supported by the Slovak Research and Development Agency under Contract No. APVV-19-0340 and the VEGA Grant Agency No. 1/0632/19.

This work has also been supported within the frame of the AlpCarp Project No. 2019-10-15-002 under the bilateral program "Action Austria – Slovakia, Cooperation in Science and Education".

The authors thank the agencies for their research support.

References

Bergström, S. (1995): The HBV model. Computers models of watershed hydrology, edited by V.P. Sing. Water. Resour. Publ, pp. 443–476.

Ceola, S. et al. (2015): Virtual laboratories: new opportunities for collaborative water science, Supplement of Hydrol. Earth Syst. Sci., 19, 2101–2117, doi:10.5194/hess-19-2101–2015-supplement

Coron, L., Andréassian, V., Perrin, C., Lerat, J., Vaze, J., Bourqui, M., Hendrickx, F. (2012): Crash testing hydrological models in contrasted climate conditions: An experiment on 216 Australian catchments, Water Resour. Res., 48, W05552, doi:10.1029/2011WR011721.

Jiang D., Wang, K. (2019): The Role of Satellite-Based Remote Sensing in Improving Simulated Streamflow: A Review. In Water 11 (8), 1615. DOI: 10.3390/ w11081615.

Finger, D., Vis, M., Huss, M., Seibert, J. (2015): The value of multiple data set calibration versus model complexity for improving the performance of hydrological models in mountain catchments. In Water Resources Research. 51 (4), 1939–1958. DOI: 10.1002/2014WR015712.

Freer, J., Beven, K., Ambroise, B. (1996): Bayesian Estimation of Uncertainty in Runoff Prediction and the Value of Data: An Application of the GLUE Approach. In Water Resources Research 32 (7), 2161–2173.

Lopez, G. M., Vis, M. J. P., Jenicek, M., Griessinger, N., Seibert, J. (2020): Complexity and performance of temperature-based snow routines for runoff modelling in mountainous areas in Central Europe. In: Hydrol. Earth Syst. Sci. Discussions (13 February 2020), 1–31. DOI: 10.5194/hess-2020-57.

Hailegeorgis, T. T., Alfredsen, K. (2016): Multi-basin and regional calibration based identification of distributed precipitation–runoff models for hourly runoff simulation: calibration and transfer of full and partial parameters. In: Hydrology Research 47 (2), 239–259. DOI: 10.2166/ nh.2015.174.

Hiebl, J., Frei, C. (2016): Daily precipitation grids for Austria since 1961, development and evaluation of spatial dataset for hydroclimatic monitoring and modeling. Theoretical and Applied Climatology 124, 161–178, doi:10.1007/ s00704-015-1411-4

Khakbaz, B., Imam, B., Hsu, K., Sorooshian, S. (2012): From lumped to distributed via semi-distributed: Calibration strategies for semi-distributed hydrologic models. In Journal of Hydrology 418–419, 61–77. DOI: 10.1016/ j.jhydrol.2009.02.021.

Kirchner, J. W. (2006): Getting the right answers for the right reasons: Linking measurements, analyses, and models to advance the science of hydrology. In: Water Resour. Res. 42 (3). DOI: 10.1029/2005WR004362.

Knoben, W. J. M., Freer, J. E., Fowler, K. J. A., Peel, M. C., Woods, R. A. (2019): Modular Assessment of Rainfall–Runoff Models Toolbox (MARRMoT) v1.2: an open-source, extendable framework providing implementations of 46 conceptual hydrologic models as continuous state-space formulations. In Geosci. Model Dev. 12 (6), 2463–2480. DOI: 10.5194/gmd-12-2463-2019.

Merz, R., Parajka, J., Blöschl, G. (2011): Time stability of catchment model parameters: Implications for climate impact analyses, Water Resour. Res., 47, W02531, doi: 10.1029/2010WR009505.

McMillan, H. K., Clark, M. P., Bowden, W. B., Duncan, M., Woods, R. A. (2011): Hydrological field data from a modeller's perspective: Part 1. Diagnostic tests for model structure. In Hydrol. Process. 25 (4), 511–522. DOI: 10.1002/hyp.7841.

O'Connell, P. E. (1991): A historical perspective. In Bowles D. S. and O'Connell, P. E., editors, Recent Advances in the Modeling of Hydrologic System, 3–30. Kluwer, Dordrecht.

Parajka, J., Merz, R., Blöschl, G. (2003): Estimation of daily potential evapotranspiration for regional water balance modeling in Austria. In 11th International Poster Day and Institute of Hydrology Open Day "Transport of Water, Chemicals and Energy in the Soil – Crop Canopy – Atmosphere System". Slovak Academy of Sciences: Bratislava; 299–306.

Parajka, J., Merz, R., Blöschl, G. (2007): Uncertainty and multiple calibration in regional water balance modelling case study in 320 Austrian catchments, Hydrol. Process., 21, 423–446. Doi: 10.1002/hyp.6253.

Parajka, J., Naiemi, V., Blöschl, G., Komma, J., (2009): Matching ERS scatterometer based soil moisture patterns with simulation of a conceptual dual layer hydrologic model over Austria Hydrol. Earth Syst. Sci. 13, 259–271.

Perrin, C., Michel, C., Andréassian, V. (2001): Does a large number of parameters enhance model performance? Comparative assessment of common catchment model structures on 429 catchments. In Journal of Hydrology 242 (3–4), 275–301. DOI: 10.1016/S0022-1694(00)00393-0

Ruelland, D. (2020): Should altitudinal gradients of temperature and precipitation inputs be inferred from key parameters in snow-hydrological models? In Hydrol. Earth Syst. Sci. 24 (5), 2609–2632. DOI: 10.5194/hess-24-2609-2020.

Saft, M., Peel, M. C., Wewtern, A. V., Perraud, J. M., Zhang, L. (2016): Bias in streamflow projections due to climate induced shifts in catchment response. Geophys. Res. Lett., 43, 1574 – 1581, doi:10.1002/2015GL067326.

Sleziak, P., Szolgay, J., Hlavčová, K., Parajka, J. (2016): The impact of the variability of precipitation and temperatures on the efficiency of a conceptual rainfall-runoff model. Slovak Journal of Civil Engineering, 24, 4, 1–7. DOI: 10.1515/sjce-2016-0016.

Sleziak, P., Hlavčová, K., Szolgay, J., Parajka, J. (2017): Dependence of the quality of runoff-simulation by a rainfall-runoff model on the differences in hydroclimatic conditions of calibration and validation period. Acta Hydrologica Slovaca. 18, 1, 23–30.

Vaze, J., Post, D. A., Chiew, F. H. S., Perraud, J. M., Viney, N. R., Teng, J. (2010): Climate nonstationarity – Validity of calibrated rainfall-runoff models for use in climatic changes studies. J. Hydrology, 394 (3–4), 447–457, doi:10.1016/j.jhydrol.2010.09.018.

Viglione, A., Parajka, J., Rogger, M., Salinas, J. L., Laaha, G., Sivapalan, M., Blöschl, G., (2013): Comparative assessment of predictions in ungauged basins – Part 3: Runoff signatures in Austria. Hydrol. Earth Syst. Sci., 17, 2263–2279. doi:10.5194/hess-17-2263-2013.

Ing. Adam Brziak (* corresponding author, e-mail: adam.brziak@stuba.sk)
Ing. Martin Kubáň
Prof. Ing. Silvia Kohnová, PhD.
Prof. Ing. Ján Szolgay PhD.
Department of Land and Water Resources Management
Faculty of Civil Engineering
Slovak University of Technology
Radlinského 11
810 05 Bratislava
Slovak Republic

DOI: 10.31577/ahs-2021-0022.01.0006

ACTA HYDROLOGICA SLOVACA

Volume 22, No. 1, 2021, 50 – 60

ANALYZING CHANGES AND FREQUENCY DISTRIBUTION IN MAXIMUM RUNOFF VOLUMES WITH DIFFERENT DURATION OF THE DANUBE RIVER AT BRATISLAVA

Veronika Bačová Mitková*, Dana Halmová

The volume of the flood waves and its importance is evaluated rarely. But, without these data, it would not be possible to imagine the extreme nature of the distribution system. Several hypotheses claim that more extremes in climatic and hydrologic phenomena are anticipated. In the present study, the annual maximum runoff volumes with *t*-day durations were calculated for a 144-year series of mean daily discharge of the Danube River at Bratislava gauge (Slovakia). The statistical methods were used to estimate *T*-year annual maximum runoff volumes and clarify how the annual maximum runoff volumes of the Danube River at Bratislava changed over period 1876–2019 and over dry and wet periods. The conclusion is that the runoff volume regime during floods has not changed significantly during the last 144 years. The annual maximum runoff volumes of the wet period have a greater impact on changes in LPIII exceedance curves at volumes with a time duration more than 20-days.

KEY WORDS: The Danube River, wave volume, Log-Pearson III probability distribution, *T*-year volume

Introduction

In studying the flood wave parameters, the attention is often focused on the culmination or maximum water level. However, these basic data on extreme floods are not enough for modern water management needs. Apart from the peak runoff another very important streamflow characteristic of a river is its runoff volume. Some issues in water management and engineering hydrology require that peak discharge (Q_{max}) and the shape of a flood wave or a flood runoff volume (V_{max}) are known. In applied hydrology, it is often difficult to assign exact values of a flood wave volume to a particular probability of exceedance and hence to its corresponding *T*-year discharges. Such relationships are very irregular in nature, so a flood wave hydrograph of a given exceedance probability must be a priory known. Pekárová and Miklánek (2019) described statistical processing of the maximum discharges and flood volumes based on a set of distribution function. The team of authors Hladný et al. (1970) dealt with the processing of volumes of flood waves from stations throughout the territory of the Czechoslovakia. To define the volumes of individual waves, the authors introduced the parameter *t* – the duration of the flood wave in days. In this way, they determined maximum runoff volumes lasting 2, 5, 10 and 30 days. Čermak (1956) studied the flood wave volumes of flood events with peaking above the long-term annual mean discharge Q_a, on the regional scale. The determination of maximum volumes was, for example, addressed by Beard (1956). Beard (1956) also used theoretical exceedance probability curves and the parameter *t* – for flood wave duration, to determine the annual extreme runoff volumes. The values of *t* – parameter depend on the catchment characteristics of the river being studied. However, the author selected only one value for the extreme runoff volumes in every year of the data sets. Knowledge of flood-wave volumes – as an important hydrological characteristic – was apparent during a flood on the Danube in 1965 (Zatkalik, 1970; Hladný et al., 1970). During this flood event, the river dikes broke under the pressure exerted by the long duration of high water stages, but not because of the extremely high water stages themselves. Recently in Slovakia a few studies, analyses and estimations of flood wave volumes corresponding to the maximum design discharge with a return period of *T*-year on the River Danube at Bratislava have been carried out by e.g. Mitková et al. (2002) and Halmova et al. (2008), but more studies have focused on the joint probability of total volume and peak discharges, e.g. Bačová Mitková and Halmová (2014), Gaal et al. (2010), Szolgay et al. (2012), Szolgay et al. (2016), and Pekárová et al. (2018). The influence of human activity occurs in the Danube River to change the transformation properties of the channel, to change the travel time of the waves as well as to a different outflow behaviour at the passage of the flow wave through the riverbed compared to the past. Case study of large flood events and hydrological simulation of flood transformations in the upper Danube River were investigated in Bačová Mitková et al. (2016). Authors concluded that the travel times of high floods have not significantly changed at the Kienstock–Devín section. On the other hand, the peak water levels for recent river conditions are higher at the same discharges.

In assessment of the climate change impacts on the river discharge regime (extremes, flood hydrographs and drought periods), it is expected that an increase in air temperature may cause (or already has caused) an increase in extreme discharges and flood volumes (Blöschl et al., 2017; 2019).

Since a 143-year series of the mean daily discharge of the Danube at Bratislava gauging station is available. Therefore, we could calculate the 144-year series of the highest (annually) 2-, 5-, 10-, 20-, 30- and 60-consecutive days' wave volumes. Than their probability distribution functions and trends were analysed. These series were subsequently divided into dry and wet periods and changes in their probability distribution functions and trends were analysed.

The aim of this study is:

- assess the maximum annual runoff volumes V_{tmax} lasting 2-, 5-, 10-, 20-, 30- and 60-days of the wave belongs to annual maximum discharges of the Danube River at Bratislava (1876–2019);
- determine the theoretical exceedance probability curves;
- estimate the *T*-year annual maximum runoff volumes with *t*-day durations belongs to annual maximum discharges;
- analyze changes in the maximum annual runoff volumes V_{tmax} of the Danube River at Bratislava during the period (1876–2019);
- analyze the changes in the maximum annual runoff volumes V_{tmax} in wet and dry periods during the period 1876–2019.

Methodology

In Czechoslovakia, Bratránek (1937) was the first who investigated the issue of runoff volumes. He used direct and indirect methods of peak vs. flood volume assessment.

The direct method was based on compiling runoff volumes higher than a chosen discharge threshold with assistance of the probability of exceedance (related to the *T*-year return period). The *T*-year discharges were then determined by extrapolating probability curves to the domain of low exceedance probability. In the latter method the author used generalized results of empirical relationships among several flood hydrograph characteristics.

In order to determine the runoff volume $W_{20,Q1}$ (Equation 1), the author used not only the highest discharge *Q* reduced to (Q_{20} –Q_1), but also values of the flood wave duration t_{20}, related to the catchment area.

$$W_{20,Q_1} = \frac{3600\,.t_{20}.Q}{2.10^6} = \frac{t_{20}.Q}{556} \qquad (1)$$

where:

$W_{20,Q1}$ – runoff wave volume with the extreme discharge Q_{20} above the selected threshold Q_1 [mil m^3];

Q – reduced extreme cumulative discharge (Q_{20}–Q_1) [m^3 s^{-1}];

Q_{20} – extreme 20-year discharge;

Q_1 – extreme 1-year discharge;

t_{20} – the average flood wave duration of the reduced discharge (Q_{20}–Q_1) [hrs].

The main disadvantage of this method is that it is not applicable for flood-wave volumes with smaller exceedance probabilities than once in 20 years.

The treatment of the calculation of the maximum volumes of the Danube was dealt with by Zatkalík (1970). When calculating the maximum volumes of flood waves, he chose as a basis a procedure taking into account the duration of the flood wave in days – *t*.

The introduction of this parameter allows:

- a clear assessment of the probability of exceeding the volume of a given flood wave,
- creation of a basis for solving the problem of design flood, which would consist in allocating such a flood wave volume that would be maximum for a given *T*-year peak flow.

Log-Pearson III distribution

For the estimation of the maximum annual runoff volume V_{tmax} series distribution function we used Log-Pearson type III distribution. The Log-Pearson distribution type III. is used to estimate extremes in many natural processes and it is one of the most commonly used probability distribution in hydrology (Bobee, 1975; Pilon and Adamowski, 1993; Griffis and Stedinger, 2007; Pawar and Hire, 2018). In some previous works (Pekárová et al., 2018; Pekárová and Miklánek, 2019) we compared LPIII distribution with theoretical probability distributions, which were and still are also among the most used in Slovak hydrological practice. The Log-Pearson Type III distribution is a three-parameter gamma distribution with a logarithmic transformation of the variable. The cumulative distribution function and probability distribution function according Hosking and Wallis (1997) are defined as:

If $\gamma \neq 0$ let $\alpha=4/\gamma^2$ and $\xi=\mu-2\sigma/\gamma$

If $\gamma > 0$ then:

$$F(x) = G(\alpha, \frac{x-\xi}{\beta})/\Gamma(\alpha) \qquad (2)$$

$$f(x) = \frac{(x-\xi)^{\alpha-1}e^{-(x-\xi)/\beta}}{\beta^{\alpha}\Gamma(\alpha)}, \qquad (3)$$

where:

ξ – location parameter;

α – shape parameter;

β – scale parameter
Γ – Gamma function.

If γ <0 then

$$F(x) = 1 - \frac{G\left(\alpha, \frac{x-\xi}{\beta}\right)}{\Gamma(\alpha)}, \qquad (4)$$

$$f(x) = \frac{(\xi - x)^{\alpha-1} e^{-(\xi-x)/\beta}}{\beta^{\alpha}\Gamma(\alpha)}. \qquad (5)$$

The Kolmogorov-Smirnov test was performed to test the assumption that the discharge magnitudes follow the theoretical distributions. The p-value ($p \geq 0.05$) was used as a criterion for rejection of the proposed distribution hypothesis.

Mann-Kendal nonparametric test

The Mann-Kendall nonparametric test (M-K test) was used for determining the significant trends detection in time series. The nonparametric tests are more suitable for the detection of trends in hydrological time series, which are usually irregular, with many extremes (Hamed, 2008; Yue, et al. 2002; Gilbert, 1987). By M-K test, we want to test the null hypothesis H0 of no trend, i.e. the observations x_i is randomly ordered in time, against the alternative hypothesis *H1*, where there is an increasing or decreasing monotonic trend.
For n (number of tested values) ≥ 10, the statistic S is approximately normally distributed with the mean and variance as follows

$$E(S) = 0 \qquad (6)$$

$$VAR(S) = \frac{1}{18}\left[n(n-1)(n-2) - \sum_{p=1}^{q} t_p\left(t_p - 1\right)\left(2t_p + 5\right)\right] \qquad (7)$$

where:
q – is the number of tied groups,
t_p – the number of data values in the p group.

The standard test statistic Z is computed as follows

$$Z = \begin{cases} \dfrac{S-1}{\sqrt{VAR(S)}} & if \quad S \rangle 0 \\ 0 & if \quad S = 0 \\ \dfrac{S+1}{\sqrt{VAR(S)}} & if \quad S \langle 0 \end{cases} \qquad (8)$$

The presence of a statistically significant trend is evaluated using Z value. A positive (negative) value of Z indicates an upward (downward) trend. The statistic Z has a normal distribution. To test for either an upward or downward monotone trend (a two-tailed test) at α level of significance, hypothesis *H0* (no trend) is rejected if the absolute value of $|Z|$ is greater than Z_1-$\alpha/2$, where Z_1-$\alpha/2$ is obtained from the standard normal cumulative distribution tables. The M-K test detects trends at four levels of significance: α=0.001, 0.01, 0.05 and α=0.1. Significance level of 0.001 means that there is a 0.1% probability that the value of x_i is from a random distribution and are likely to make a mistake if we reject the hypothesis *H0*; Significance level of 0.1 means that there is a 10% probability that we make a mistake if we reject the hypothesis *H0*. If the absolute value of Z is less than the level of significance, there is no trend.
For the four tested significance levels the following symbols are used in the template:
*** if trend at α=0.001 level of significance – *H0* seems to be impossible,
** if trend at α=0.01 level of significance,
* if trend at α=0.05 level of significance – 5%, mistake if we reject the *H0*,
+ if trend at α=0.1 level of significance.

Blank: the significance level is greater than 0.1, cannot be excluded that the *H0* is true.
The most significant trend is assigned three stars (***), with a gradual decrease in importance, the number of stars also decreases.

Case study area

The Danube River and Input data

The Danube River is the second greatest river in Europe, after the Volga. The basin covers an area of 817 000 km^2. The river originates from the Black Forest in Germany at the confluence of the Briga and the Breg streams. The Danube then discharges southeast for 2 872 km (1 785 mi), passing through four Central European capitals before emptying into the Black Sea via the Danube Delta in Romania and Ukraine. The Danube River Basin landscape geomorphology is characterized by a diversity of morphological patterns. The territory of the Danube River Basin is also one of the most flood-endangered regions in Europe.
The mean daily discharges (Fig. 1) and maximum annual discharges of the Danube River at Bratislava from the period 1876–2019 were used as input data. The course of annual peak discharges, long-term linear trend and 5-year moving trend are illustrated on the Fig. 2a. The annual peak discharges of the Danube River at Bratislava show increasing long-term linear trend during the selected period of 1876–2019. There were also occurred some extreme floods in 1899, 1954, 2002 or 2013 (Fig. 2a). The Fig. 2b shows the alternation of dry and wet years at intervals of approximately every three to four years. The minimum annual discharge was occurred in 1934 (3000 m^3 s^{-1}). Since year 2014 to year 2019 we also record dry years.
The maximum number of the events with annual maximum flows occurs in month of July it can be cause by summer rainfall especially in upper part of the Danube basin. The second peak of the number in occurrence of the annual maximum flows is in month of March when snow melts in higher parts of the basin and rainfall occur in lower part of the basin. The Fig. 3a illustrates the distribution of the annual maximum flows occurrence in individual months during the period of 1876–2019 and in dry and wet years. The Fig. 3a shows, that distribution

of the annual maximum occurrence during the period 1876–2019 has maximum in the month of July. The dry and wet years has annual maximum flows occurrence in July. The annual maximum flows occurrence during the last nineteen years (2001–2019) was in January (Fig. 3b).

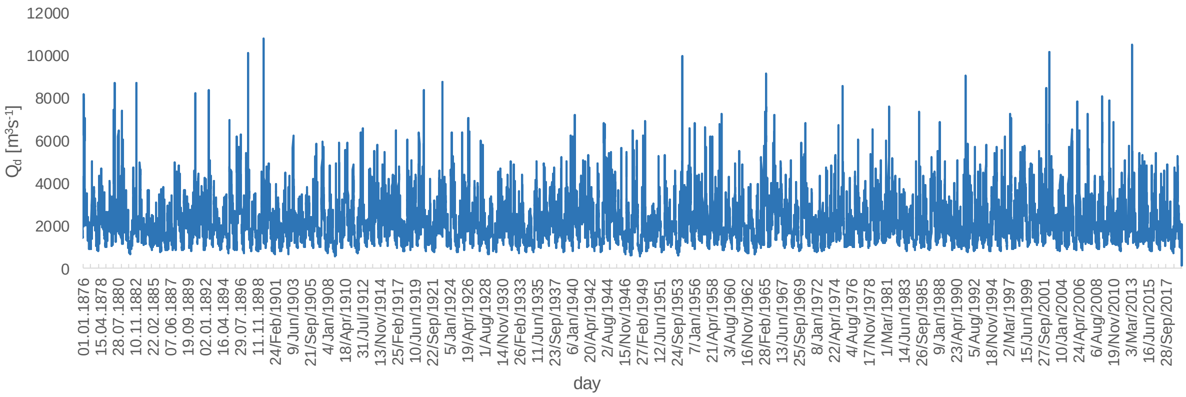

Fig. 1. The mean daily discharges of the Danube river at Bratislava (1876–2019).

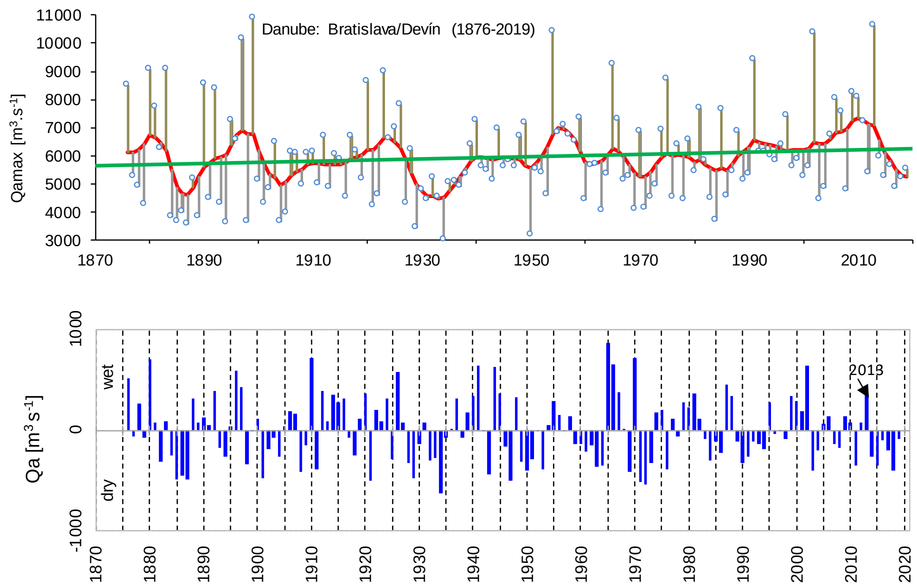

a)

b)

Fig. 2. a) the maximum annual discharges of the Danube River at Bratislava (1876–2019), their linear trend and 5-year moving trend, b) the deviation from long-term annual discharge during the period of 1876–2019.

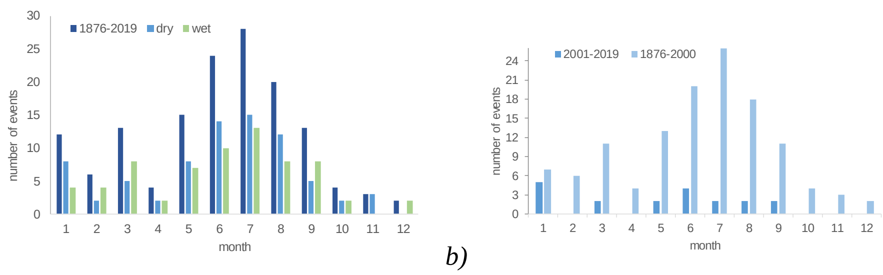

a) *b)*

Fig. 3. Monthly distribution of the annual maximum flows of the Danube river at Bratislava a) for period 1876–2019 and in dry and in wet years and b) for periods of 1876–2000 and 2001–2019.

Results

Determination of maximum volumes of Danube flow waves for the period 1876–2019

In the present paper for determining the maximum annual runoff volumes V_{tmax}, we used the procedure published in Zatkalík (1970). The mean daily discharges and maximum annual discharges of the Danube River at Bratislava from the period 1876–2019 were used as input data. We introduced the parameter *t* – runoff duration in days to define the *t*-days maximum volumes of individual waves. In this way, we determined the maximum runoff volumes of *t*=2-, 5-, 10-, 20-, 30- and 60-days. The series of mean daily discharges were used to determine the annual maximum runoff volume V_{tmax} lasting 2-, 5-, 10-, 20-, 30- and 60-days. In each year separately, a flood event with an annual maximum flow was selected for the set of volumes. Than the 2-, 5-, 10-, 20-, 30- and 60-days moving averages of the volume around the peak flow were calculated and the maximum volume for each *t*-days were selected. Fig. 4 presents an example of the determination of maximum volumes with a given runoff duration.

The runoff volume series are shown in Fig. 5. Considering the 2-day and 5-day maximum runoff volumes, the flood of 1899 was the highest one and the lowest one was in 1934, within the period 1876–2019. But considering the 10- to 60-day runoff volumes, the highest flood was that of 1965.

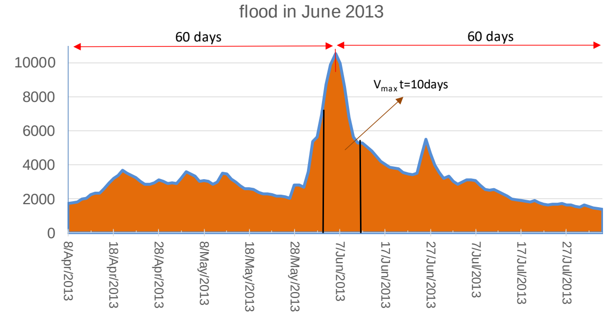

Fig. 4. Example of the determination of the maximum volume with a given runoff duration t=10 days on The Danube River at Bratislava (flood occurred in 2013).

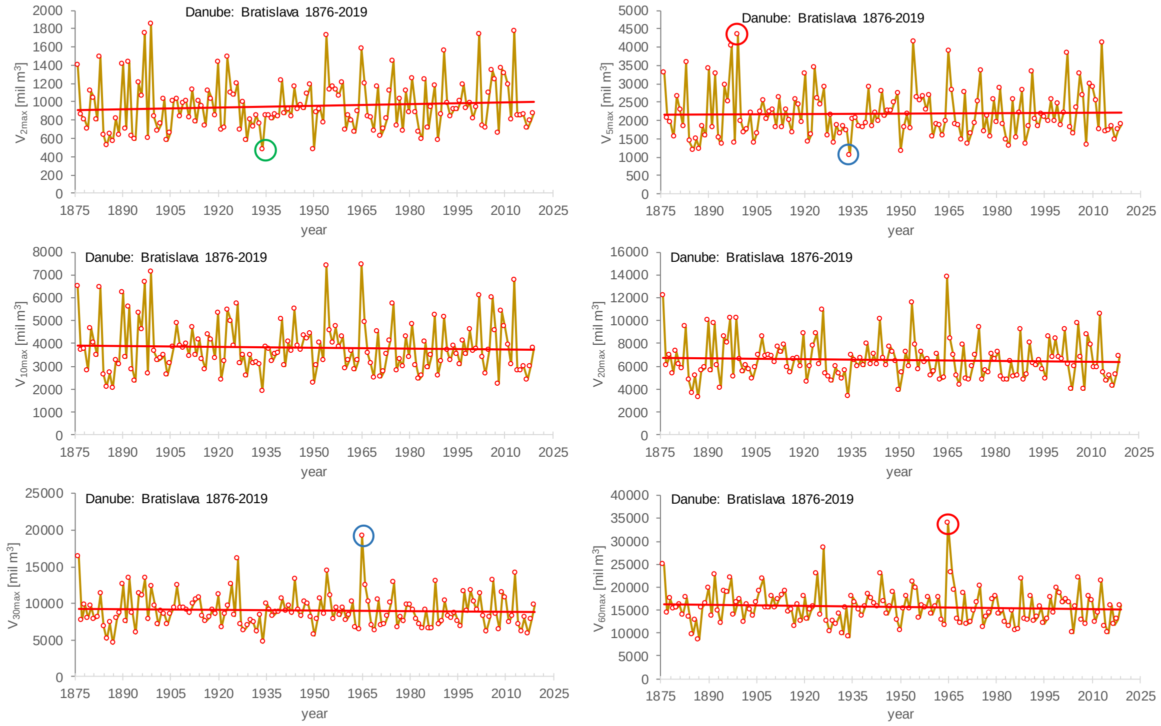

Fig. 5. Flood wave volume series of the Danube for various flood durations t (e.g. V_{20}max means maximal annual runoff volume in 20 days).

Calculation of the theoretical probability curves of the maximum annual runoff volumes V_{tmax} for various flood durations t

A Log-Pearson III distribution was selected to calculate the *T*-year maximum runoff volume with the given runoff time duration (*t*). The examples of the theoretical (LPIII) exceedance probability curves of the maximum annual runoff volumes with durations *t* equal to 2-, 5-, 10-, and 60- days are demonstrated in Fig. 6. The results suggest (Table 1) that the 100-year maximum of 2-day runoff volume (V_{2max}) is 1896 mil m^3, 4398 mil. m^3 for 5-day (V_{5max}), and 7470 mil. m^3 for 10-day (V_{10max}) runoff volumes.

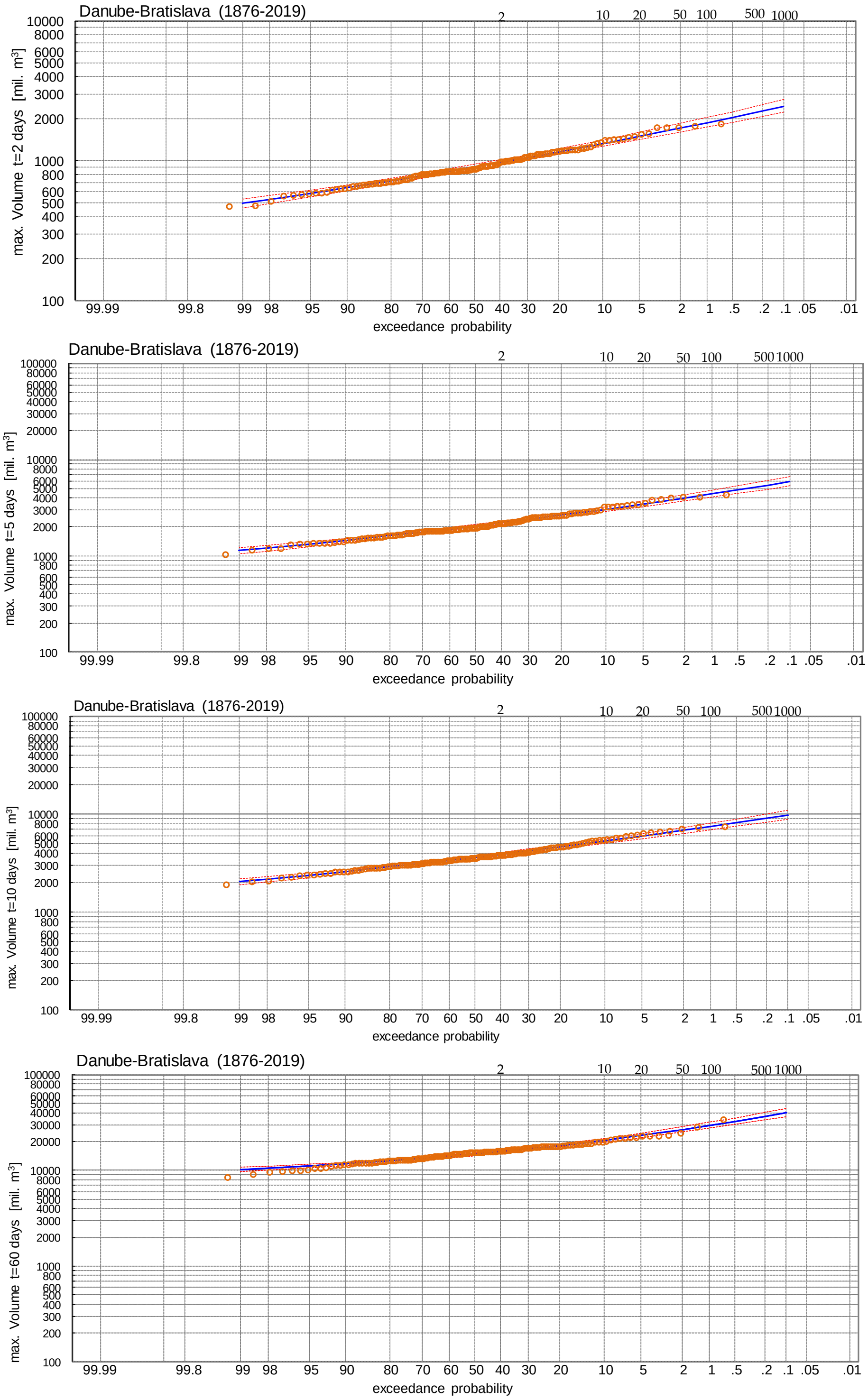

Fig. 6. Examples of the theoretical LPIII exceedance probability curves of the Danube maximum annual runoff volumes V_{2max}, V_{5max}, V_{10max} and V_{60max} for Danube: Bratislava (1876–2019).

Trend analysis of annual maximum runoff volumes V_{tmax} on the Danube River at Bratislava (1876–2019)

The Mann-Kendall nonparametric test (M-K test) was used for detection of the significance in long-term trends of annual maximum runoff belong to annual maximum flows of the Danube River at Bratislava for period 1876–2019. The M-K trend test did not show significant long-term trends in annual maximum runoff volumes with duration *t* belong to annual maximum flows of the Danube River at Bratislava for selected period.
After dividing the whole time series1876–2019 into shorter periods, about 40 years the M-K trend analysis indicates an increasing long-term trends in annual maximum runoff volumes V_{tmax} with t=2 days and t=5 days and we can reject the hypothesis *H0* at significance level α=0.05 and α=0.1, for period 1921–1960 (Table 3). The long-term trend of the M-K test for annual maximum runoff volumes with duration t=2 days and t=5 day of the Danube River at Bratislava (1921–1960) are illustrated in Fig. 7.

Analysis of annual maximum runoff volumes V_{tmax} on the Danube River at Bratislava (1876–2019) in dry and wet periods

In this part of the work, we divided the sets of volumes with *t*-day into two sub-sets based on dry and wet multiannual periods. The dry and wet periods we determined on the basis of double 5-year moving averages of the Danube River flows at Bratislava for the period 1876–2019 (Fig. 8a).
The wetness of individual years is different and more or less independent of each other. It is to be understood that the various physical causes also distort the action of the decisive factors to such an extent that we can speak of randomness. According to this, but also from experience, we can say that years of a similar nature usually group together, (Dub, 1957). The limit value for determining the dry and wet periods was the value of the long-term average annual flow Q_a=2049 m^3 s^{-1}. Due to the fact that we took the period as a result of the moving average, dry and wet years can also occur in it.

Table 1. ***T*-year maximum discharges Q_{max} and *T*-year annual maximum runoff volumes V_{tmax} of the Danube River at Bratislava (1876–2019) (Log-Pearson III) (P=p*100%, p=1-e$^{-1/T}$)**

River: Gauging station	*P*	Q_T [m^{3}s^{-1}]	*t*=2 days	*t*=5 days	*t*=10 days	*t*=20 days	*t*=30 days	*t*=60 days
Danube: Bratislava	2	Q_{50}			V_{50tmax} [mil. m^3]			
		10159	1706	3985	6814	11292	15777	26666
	1	Q_{100}			$V_{100tmax}$ [mil. m^3]			
		11060	1869	4398	7470	12329	17513	29464
	0.2	Q_{500}			$V_{500tmax}$ [mil. m^3]			
		13193	2262	5410	9056	14830	21989	36654
	0.1	Q_{1000}			$V_{1000tmax}$ [mil. m^3]			
		14140	2439	5875	9773	15961	24141	40100

Table 2. **Conclusions of Mann-Kendall trend test for annual maximum runoff volumes V_{tmax} with time duration *t* for waves belong to annual maximum flows of the Danube River at Bratislava (1876–2019)**

				Mann-Kendall trend		Sen's slope estimate	
V_{tmax} [mil m^3]	First year	Last Year	*n*	Test Z	Signific.	A	B
V_{2max}	1876	2019	144	0.91	No	0.84	864
V_{5max}	1876	2019	144	0.02	No	0.06	1975
V_{10max}	1876	2019	144	-0.43	No	-1.76	3682
V_{20max}	1876	2019	144	-0.77	No	-4.67	6450
V_{30max}	1876	2019	144	-1.10	No	-8.83	8791
V_{60max}	1876	2019	144	-1.53	No	-23.40	15935

The number of 71 years were included in the dry period and number of 73 years in the wet period (Fig. 8b). Fig. 8b also shows that since 2005 to 2019 the dry period is recorded. The M-K trend analysis indicates an increasing long-term trend in annual maximum runoff volumes V_{tmax} with t=2-days and we can reject the hypothesis $H0$ at significance level α=0.05 for dry period (Fig. 9). A Log-Pearson III distribution was used to calculate the T-year maximum runoff volume with the given runoff time duration (t) for dry and wet periods. The T-year maximum annual runoff volumes of duration t=2-days, 5-days and 10-days has no significant changes in estimation. In the wet period (except for volumes with t=2- and 5-days), with the same probabilities of exceeding, higher values of maximum volumes may occur compared to the dry period. Dividing of the period 1876–2019 into dry and wet periods had a greater impact on changes in LPIII exceedance curves of the maximum runoff at higher values of volumes with time duration t=20-, 30-, and 60-days. The examples of differences between estimated T-year maximum annual runoff volumes for dry and wet period are illustrated in Fig. 10.

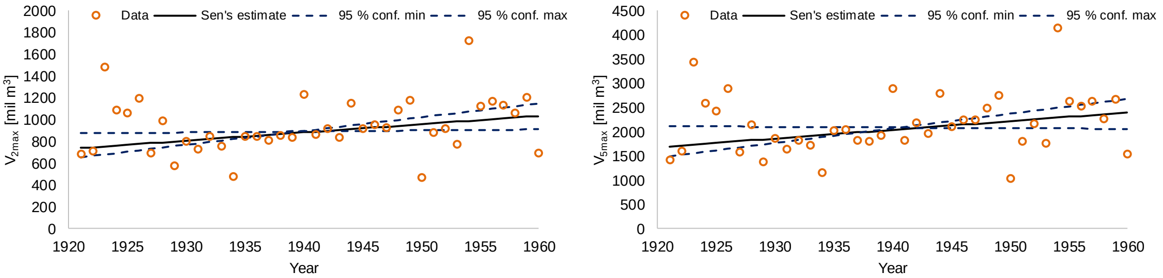

Fig. 7. The Mann-Kendall trend test for annual maximum runoff volumes V_{tmax} with time durations t=2 days and t=5 days for waves belong to annual maximum flows of the Danube River at Bratislava (1921–1960).

Table 3. Conclusions of Mann-Kendall trend test for annual maximum runoff volumes V_{tmax} with time durations t=2 days and t=5 days for waves belong to annual maximum flows of the Danube River at Bratislava (1921–1960)

				Mann-Kendall trend		Sen's slope estimate	
V_{tmax} [mil m^3]	First year	Last Year	n	Test Z	Signific.	A	B
V_{2max}	1921	1960	40	2.20	*	7.572	735.74
V_{5max}	1921	1960	40	1.83	+	17.970	1690.04

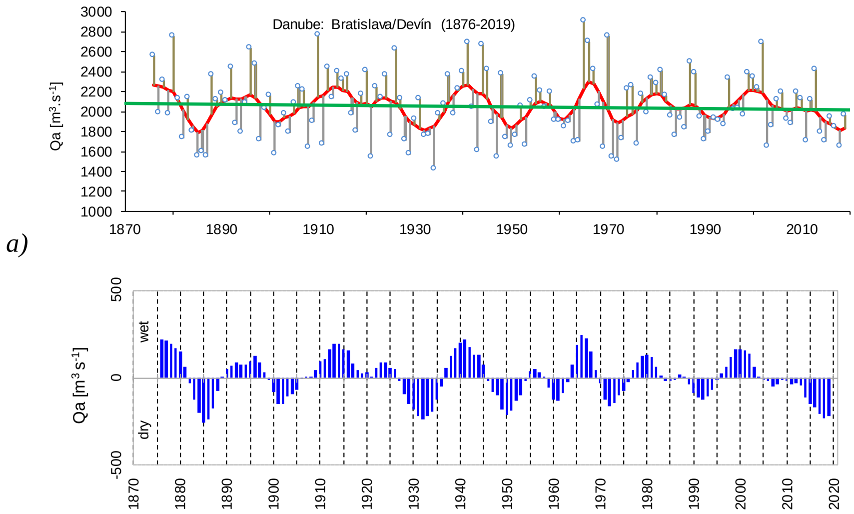

Fig. 8. Course of the a) mean discharges, their linear trend and b) dry and wet periods based on double 5-year moving averages of Danube flows of the Danube River at Bratislava for the period 1876–2019.

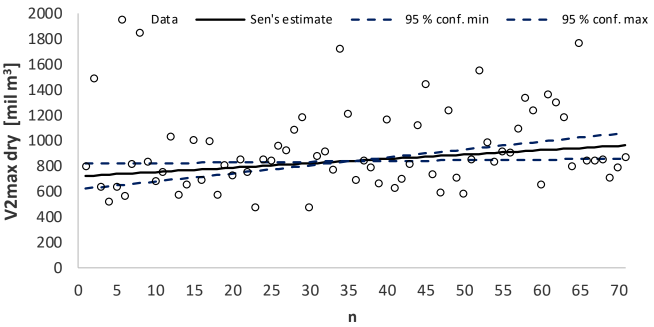

Fig. 9. The Mann-Kendall trend test for annual maximum runoff volumes V_{tmax} with time durations t=2-days for waves belong to annual maximum flows of the Danube River at Bratislava (dry period).

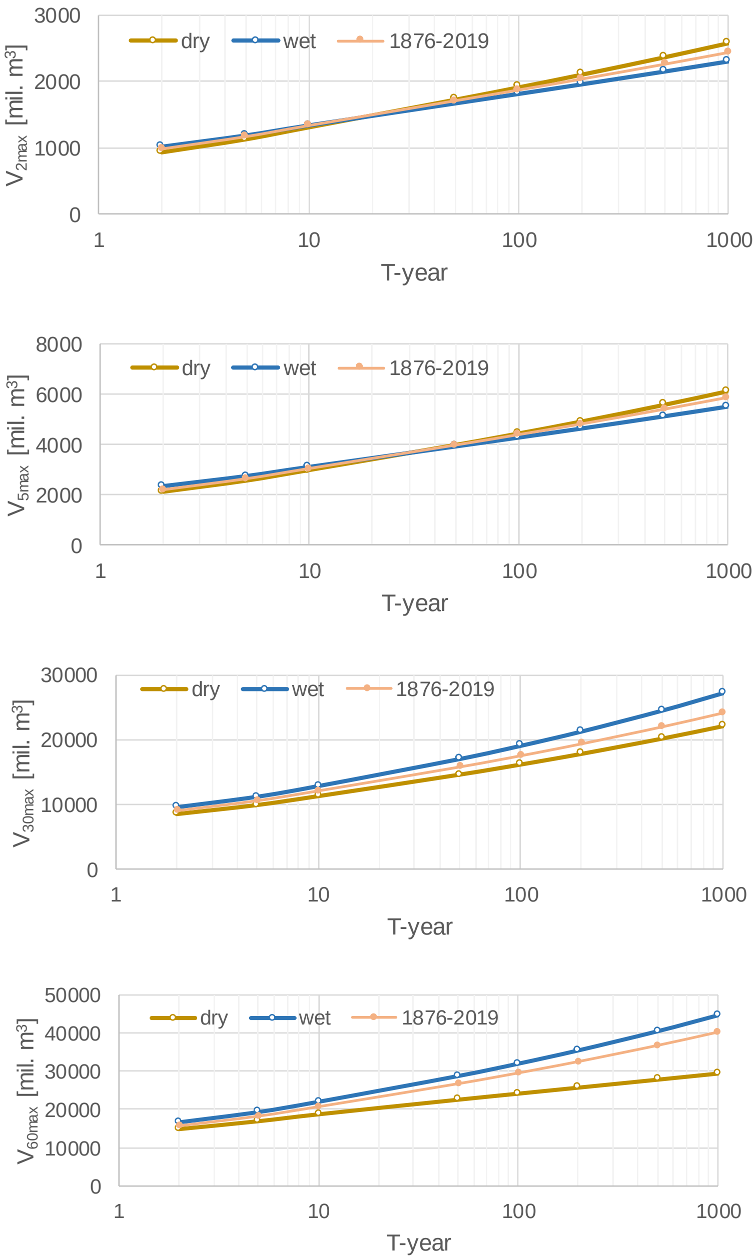

Fig. 10. Example of the differences in estimated T-year maximum annual runoff volumes with time duration t=2-, 5-, 30- and 60 - days for dry and wet periods of the Danube River at Bratislava (1876–2019).

Conclusion

In the present paper we analyzed, the occurrence of annual maximum runoff volumes with *t*-day durations for a 144-year series of mean daily discharge of the Danube River at Bratislava gauge (Slovakia). The statistical methods were used to clarify how the maximum runoff volumes of the Danube River at Bratislava changed over period 1876–2019 and over dry and wet periods. On the Danube River is usually the maximum annual flow occur simultaneously with the annual maximum runoff volume of waves with a given time duration *t*. However, the corresponding values in terms of significance are not equivalent. Based on the exceeding probability curves of the annual maximum runoff volumes, it is possible to determine to the selected volume *V* for different *t* the probability of its exceeding and return period.

The M-K tests showed increasing trend of the annual maximum runoff volume at significance level α=0.05 and α=0.1, for period 1921–1960. Based on M-K test we can conclude that the runoff volume regime during floods has not changed substantially during the last 144 years, which is of importance to water management. This conclusion pertains not only to the short-term flood runoff episodes (V_{2max}), but also the long-term ones (V_{60max}).

Based on the division of the given interest period 1876–2019 into dry and wet ones, we also plotted and compared the probabilities of exceedance the annual maximum runoff volumes on the Danube at Bratislava for selected runoff durations t = 2, 5, 10, 30, 60 days in given periods. The M-K trend analysis indicates an increasing long-term trend in annual maximum runoff volumes V_{tmax} with t=2 days and we can reject the hypothesis *H0* at significance level α=0.05 for dry period. The results suggest that the *T*-year maximum annual runoff volumes of duration t=2- days, 5-days and 10-days has no significant changes in estimation. In the wet period (except for volumes with t=2- and 5-days), with the same probabilities of exceeding, higher values of maximum volumes may occur compared to the dry period. Dividing the period 1876–2019 into dry and wet periods had a greater impact on changes in LPIII exceedance curves of the maximum runoff at higher values of volumes with time duration t=20-, 30-, and 60-days.

The results are useful in the water planning and flood protection and can help mapping flood risk areas and developing river management plans in Danube River basin. In the future, it would be desirable to confirm the conclusions also on other rivers in Slovakia with satisfactory long runoff data series, or on the basis of reconstructed discharge values by indirect methods (analogy, mathematical runoff modeling etc.).

Acknowledges

This work was supported by the project VEGA No. 2/0004/19 "Analysis of changes in surface water balance and harmonization of design discharge calculations for estimation of flood and drought risks in the Carpathian region".

References

Bačová Mitková, V., Pekárová, P., Miklánek, P., Pekár, J. (2016): Hydrological simulation of flood transformations in the upper DanubeRiver: Case study of large flood events. In Journal of Hydrology and Hydromechanics, Vol. 64, No. 4, p. 337–348. https://doi.org/10.1515/johh-2016-0050

Bačová Mitková, V., Halmová, D. (2014): Joint modeling of flood peak discharges, volume and duration: a case study of the Danube River in Bratislava. In Journal of Hydrology and Hydromechanics, Vol. 62, no. 3, p. 186–196. https://doi.org/10.2478/johh-2014-0026

Beard, L. R. (1956): Statistical Evaluation of Runoff Volume Frequencies. Symposium Dorcy, IASA, Dijon.

Blöschl, G. et al. (2017): Changing climate shifts timing of European floods. Science 357, 588–590. DOI: 10.1126/science.ann2506

Blöschl, G., Hall, J., Viglione, A. et al. (2019): Changing climate both increases and decreases European river floods. Nature 573, 108–111. https://doi.org/10.1038/s41586-019-1495-6

Bobee, B. (1975): The Log Pearson Type 3 Distribution and Its Application in Hydrology. Water Resources Research, Vol. 11, No. 5, 681–689.

Bratránek, A. (1937): Determination of protective areas of the dams. Work and Studies, Workbook 20, State Institute of Hydrology and Hydrotechnics, Prague. (In Czech)

Čermak, M. (1956): Flood wave volumes. J. Hydrol. Hydromech. 4.

Dub, O. (1957): Hydrológia, Hydrografia, Hydrometria. Slovenské vydavateľstvo technickej literatúry. Bratislava, 266.

Gaal, L., et al. (2010): Copula-based assessment of the relationship between food peaks and flood volumes using information on historical floods by Bayesian Monte Carlo Markov Chain simulations. Geophysical Research Abstracts, Vol. 12, EGU2010-13534-3.

Gilbert, R. O. (1987): Statistical Methods for Environmental Pollution Monitoring. John Wiley & Sons, Inc., New York.

Griffis, V. W.; Stedinger, J. R. (2007): The Log-Pearson type III distribution and its application in flood frequency analysis. I: Distribution characteristics. J. of Hydrologic Engineering, 12, 5, 482–491.

Halmova, D., Pekarova, P., Pekar, J., Onderka, M. (2008): Analyzing temporal changes in maximum runoff volume series of the Danube River. IOP Conf. Series: Earth and Environmental Science 4, IOP Publishing. 1–8. doi:10.1088/1755-1307/4/1/012007.

Hamed, K. H. (2008): Trend detection in hydrologic data: The Mann-Kendall trend test under the scaling hypothesis. Journal of Hydrology, 349(3-4), 350–363.

Hladný, J., Doležal, F., Makeľ, M., Sacherová, D. (1970): Peak runoff volumes of a given duration (in Czech) Hydrological conditions of the CSSR Volume III.

Hosking, J. R. M., Wallis, J. R. (1997): Regional Frequency Analysis. Cambridge University Press. Cambridge.

Mitková, V., Pekárová, P., Babiaková, G. (2002): Maximálne objemy odtoku Dunaja daného trvania v suchých a vodných obdobiach (Maximum runoff volumes of the Danube of a given duration in dry and water periods). In Acta Hydrologica Slovaca, Vol. 3, No. 2, 185–191. ISSN 1335-6291. (In Slovak)

Pawar, U., Hire, P. (2018): Flood Frequency Analysis of the Mahi Basin by Using Log Pearson Type III Probability Distribution. Hydrospatial Analysis 2(2), 102–112. Dx.doi. org/10.21523/gcj3.

Pekárová, P., Bačová Mitková, V. Pekár J., Miklánek P., Halmová D., Liova, S. (2018): Historical food on the territory of Slovakia and their importance in hydrology. (In Slovak: Historické povodne na území Slovenska a ich význam v hydrológii. Bratislava: Veda, SAS, 135. ISBN 978 -80-224-1684-9.

Pekárová, P., Miklánek, P. (eds.) (2019): Flood regime of rivers in the Danube River basin. Follow-up volume IX of the Regional Co-operation of the Danube Countries in IHP UNESCO. IH SAS, Bratislava, 215 p. + 527 p. app., DOI: 10.31577/2019.9788089139460.

Pilon, P. J., Adamowski, K. (1993): Asymptotic variance of flood quantile in log Pearson type III distribution with historical information, J. of Hydrol., 143, 3–4, 481–503.

Szolgay, J., et al. (2016): A regional comparative analysis of empirical and theoretical flood peak-volume relationships. J. Hydrol. Hydromech. Vol. 64(4), 367–381. doi: 10.1515/johh-2016-0042.

Szolgay, J., Kohnová, S., Bacigál, T., Hlavčová, K. (2012): Proposed flood: Joint probability analysis of maximum discharges and their pertaining volumes. Acta Hydrologica Slovaca. Vol. 13(2), 289–296.

Zatkalík, G. (1970): Calculation of the basic parameters of the flow waves. PhD. thesis. 71 p. (In Slovak)

Yue, S., Pilon, P., Cavadias, G. (2002): Power of Mann-Kendall and Spearman's rho tests for detecting monotonic trends in hydrological series. Journal of Hydrology, 259, 254–271.

Ing. Veronika Bačová Mitková, PhD. (*corresponding author, e-mail: mitkova@uh.savba.sk)
Ing. Dana Halmová, PhD
Institute of Hydrology SAS
Dúbravská cesta 9
84104 Bratislava
Slovak Republic

DOI: 10.31577/ahs-2021-0022.01.0007

ACTA HYDROLOGICA SLOVACA

Volume 22, No. 1, 2021, 61 – 69

INFLUENCE OF SUBMERGED VEGETATION ON THE MANNING´S ROUGHNESS COEFFICIENT FOR GABČÍKOVO – TOPOĽNÍKY CHANNEL

Radoslav Schügerl*, Yvetta Velísková, Renáta Dulovičová, Valentín Sočuvka

The aim of this study was to investigate the variation of flow conditions along the Gabčíkovo – Topoľníky channel (Žitný Island) on the base of Manning´s roughness coefficient value. This coefficient is not easy to determine and its value is varying constantly during the growing season, especially in a lowland stream with aquatic vegetation occurrence. Vegetation impedes the water flow and may increase flood risks. Thus, determining the effect of aquatic vegetation on flow conditions in streams is very important for estimation of hydrodynamics in natural streams. Measurements performed during growing season at the Gabčíkovo – Topoľníky channel stream were used for an evaluation of vegetation impact on flow conditions. The variations of roughness coefficients of Gabčíkovo – Topoľníky channel are presented in Manning's equation, and the results reveal that the *n* value increases with the decreasing of flow depth. Manning's coefficient value found in this study is in the range of 0.020 to 0.079. The outcomes of this study can be concluded that the variation of Manning's coefficient value is influenced by the cross-section profile characteristic, flow depth, slope of channel, and especially quantity of submerged vegetations in the channel.

KEY WORDS: Manning´s roughness coefficient, flow conditions, submerged vegetation, River Surveyor

Introduction

The channel roughness is affected by a lot of factors which are difficult to translate into a single value. More authors (Green, 2006; Nikora et al., 2008) stated that aquatic macrophytes are often the dominant factor influencing flow conditions within the channels they occupy. Furthermore, it is more difficult to determine the Manning coefficient for vegetated streams than for open channel flow (Green, 2005). Also Vereecken et al. (2006) showed that seasonal variations in the aquatic vegetation have an important influence on the flow resistance. It is possible to estimate the value, but the deviation from reality may be large.

The flow regime in channels or in surface water at lowland territories during the growing season is often very strongly influenced by the occurrence of aquatic vegetation. From a hydrodynamic point of view, water plants alter the size and distribution of flow velocities at a large rate; they increase the stream bed roughness and decrease the discharge capacity of a stream. As the progress of water plants runs, the coefficient of roughness value is changed. In general, this parameter determines the extent of flow resistence and impacts the flow capacity of channels or watercourses. For correct design or computation of flow in an open channel, it is necessary to evaluate the flow resistance to a stream, which is typically represented by a roughness parameter, such as Manning's (Carollo et al., 2002; Cassan et al., 2015). Its determination is not easy for natural streams, because the characteristics of channels and the factors that affect channel capacity can vary greatly; furthermore, the combinations of these factors are numerous. Therefore, the selection of roughness for natural and constructed channels is often based on field judgment and personal skill, which are acquired mainly through experience (De Doncker et al., 2009; Velísková et al., 2017).

The aim of this contribution is to demonstrate, on the basis of results from experimental field measurements on the Gabčíkovo – Topoľníky channel (Žitný Island – Slovakia), how the sprouting of vegetation in a stream bed influences channel's flow conditions and its capacity.

Theoretical background

The measured discharges and water levels are used for the calculation of the roughness coefficient of the stretch, making use of the Bresse equation and the Manning equation (Chow, 1959). Manning's equation uses a single parameter, *n*, to represent the frictional nature of a given channel cross section, and hydraulic reference manuals provide roughness guides for channels based on their composition and morphology. A channel's reference roughness is meant to be constant for all withinbank flows; however, studies of flow in natural rivers have frequently found variability in Manning's coefficient value n, often in the form of a nonlinear, inverse relationship between n and stage or discharge. In general, hydraulic models for open channel flow are based on the Saint-Venant equations. These equations (continuity equation and momentum equation) are the one dimensional simplification of the Navier Stokes equations, which describe fluid flow in three dimensions. By calculation of the discharge and the water levels, the Saint-Venant equations allow for the calibration of the roughness of the channel (expressed by the roughness coefficient or friction factor) by comparing with field data. Here, this roughness is represented by the Manning coefficient n and it is calculated from the energy slope (Boscolo, 2014; Tuozzolo et al., 2019).

Hydraulic data as water levels and discharges are necessary, but also topographical data of the river bed and banks have to be collected. While carrying out velocity measurements in the river, the water depth and consequently, the bottom profile is registered.

There are various approaches how the roughness can be expressed, for example description with constant roughness coefficient through the Chézy formula, the Dardy-Weisbach equation, the Manning´s equation or roughness coefficient dependent on flow characteristics, for example the Strickler and Keulegan approach. In addition, there is known a new approach for determination of aquatic vegetation resistence, mainly for flexible submerged vegetation (Kutija and Hong, 1996; Stone and Shen, 2002; Wilson et al., 2007).

Most often description of hydraulic resistance can be found in literature as:

– *Manning´s equation:* $v = \frac{1}{n} R^{2/3}\, i_o^{1/2}$ (1)

– *Darcy-Weisbach equation:* $v = \sqrt{\frac{8g}{f}} \sqrt{R i_o}$ (2)

– *Chézy´s equation:* $v = C \sqrt{R i_o}$ (3)

where

v – mean flow velocity [m s^{-1}],
R – hydraulic radius [m],
i_o – water level slope,
n – Manning´s roughness coefficient [s m$^{-1/3}$],
g – gravity acceleration [m s^{-2}],
C – Chézy´s coefficient [m$^{1/2}$ s^{-1}].

The Manning´s formula is most used for expressing flow resistance (Chow, 1959). It might be determined for more complex part of a stream by empirical formula, e.g. by (Coon, 1998) who splitted channel resistance into several parts, including the bed material, presence of vegetation in the river, meandering

- $n = (n_0 + n_1 + n_2 + n_3 + n_4).m$ (4)

where

n_0 – basic value, for a straight, uniform channel,
n_1 – irregularities of the bottom,
n_2 – variations in the geometry of the channel,
n_3 – obstacles,
n_4 – vegetation,
m – correction factor for meandering.

To apply this approach, it is important that conditions already included in another parameter or element of this equation are not doubled. The equation requires an estimation of separate n factors for different channel conditions. However, the great variability of the used factors causes large degree of freedom for the precise roughness coefficient determination. Another methodology is to use a set of pictures from literature which represent a comparable situation orto make use of graphs and tables (Dyhouse et al., 2003). Photographs and descriptive data of typical type of river parts, for which the Manning coefficient is determined, can be found in (Barnes, 1967).

Channel roughness is influenced by grain size of the bedmaterial, the surface irregularities of the channel, the channel bed forms (such as ripples and dunes), erosion and deposition characteristics, meandering tendencies, channel obstructions (downed trees, exposed root wads, debris, etc.), geometry changes between channel sections, vegetation along the bankline and in the channel, etc. One single value of the roughness coefficient has to include all these parameters. Furthermore, as vegetation is strongly dependent on the season, the roughness coefficient can be fairly different for summer and winter conditions.

There are many vegetation characteristics that affect the hydraulic resistance in vegetated channels. The first important vegetation characteristic that affects the flow resistance is the geometry of the vegetation itself, concerning the taxonomy of the species as the branching index, the density of the shoots, the maximum level of growth that each species can reach in a cross section, the seasonal presence of the plant. In addition to this, there is a hydraulic parameter which considers the characteristic dimension of the vegetation in relation to flow conditions. One of the main problems in vegetated channel is the determination of the vegetation height. This can be solved if the flexural and drag properties of the vegetation are known. Flow over flexible vegetation induces bends and reduces the height of the vegetation stems. As a result, the flow-vegetation interactions are reduced. The vegetation configuration depends on flexural rigidity and density of the vegetation itself. These characteristics depend essentially on the species. The blockage factor B is the parameter that measures the portion of the channel blocked by vegetation, or equivalently the proportion of the channel containing vegetation. Several types of blockage factors have been proposed in the literature (Boscolo, 2014).

Evaluation of the impact of aquatic plants on flow conditions in a lowland stream is complicated. Nevertheless, it is possible to determine the value of the roughness coefficient n for a stream reach by using the Chézy – Manning equation for steady uniform flow condition (Eq. 5):

$$n_m = \frac{A_m R_m^{2/3} i_{om}^{1/2}}{Q_m} \qquad (5)$$

where
i_o – water level slope,
A – discharge area [m^2],
R – hydraulic radius [m],
Q – discharge [m^3 s^{-1}],
m – means a measured value.

This approach is used also in this study.

Material and methods

Field measurements, related to the investigation of submerged vegetation impact on flow in a lowland stream, were performed along the Gabčíkovo – Topoľníky channel (Žitný Island – ŽI). It is flat area and one of the most productive agricultural region of Slovakia.

Žitný Island lies between two branches of the Danube River, on which this river is divided just below the Slovak capital Bratislava: the Danube and the Small Danube (Fig. 1). The area of the Žitný Island is approximately 2000 km^2 and represents about 4% of the Slovak territory. Its average slope is only about 2.5x10^{-4} and this was one of the reasons for building the channel network within this area. The channel network was built up for drainage and also to safeguard irrigation water. The water level in the whole channel network system has affect to groundwater level on the Žitný Island and in reverse (Dulovičová, 2019).

The Gabčíkovo – Topoľníky channel is the biggest one from three main channels of the channel network at Žitný Island (besides Chotárny and Komárňanský channel). The Gabčíkovo – Topoľníky channel was built primary for drainage, later it was used also for irrigation. The length of the Gabčíkovo – Topoľníky channel is about 30 km. Its width oscillated between 11.50–17.5 m along the channel, its depth registered maximal values up to 2.6 m (according to located cross-section profiles). Sixteen observing cross-section profiles were selected along the Gabčíkovo – Topoľníky channel, their locations are shown in Fig. 2. Measurements were carried out from rkm 1 to rkm 17 (in each kilometre, except rkm 14).

Cross-section profiles parameters – channel width, distribution of water depth along the cross-section profile width, water levels (by levelling device), discharges and velocity distribution in the cross-section profile (by ADV method – Acoustic Doppler Velocimeter – River Surveyor device) were measured (Fig. 3). This device is suitable for measurements of deeper streams. Example of record of measurement by River Surveyor device is shown on the Fig. 4 (for cross-section profile without submerged vegetation) and on the Fig. 5 (cross-section profile with submerged vegetation). All field measurements were done during one week in the begining of summer. Data used for roughness coefficient determination are from the channel segments with steady uniform flow conditions.

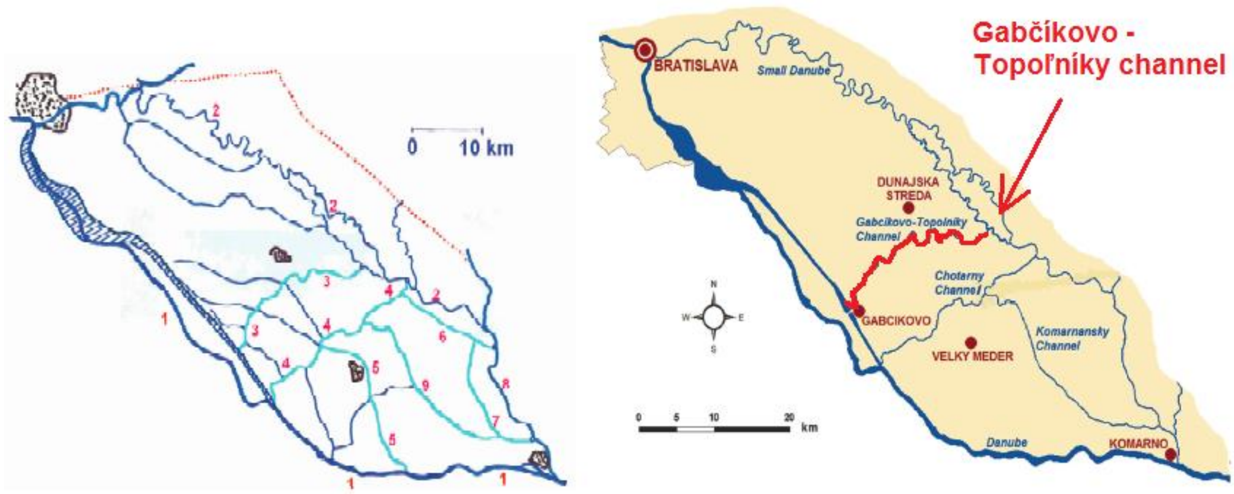

Fig. 1. Schematic map of channel network at Žitný Island (left) and three main channels of channel network at Žitný Island (right).

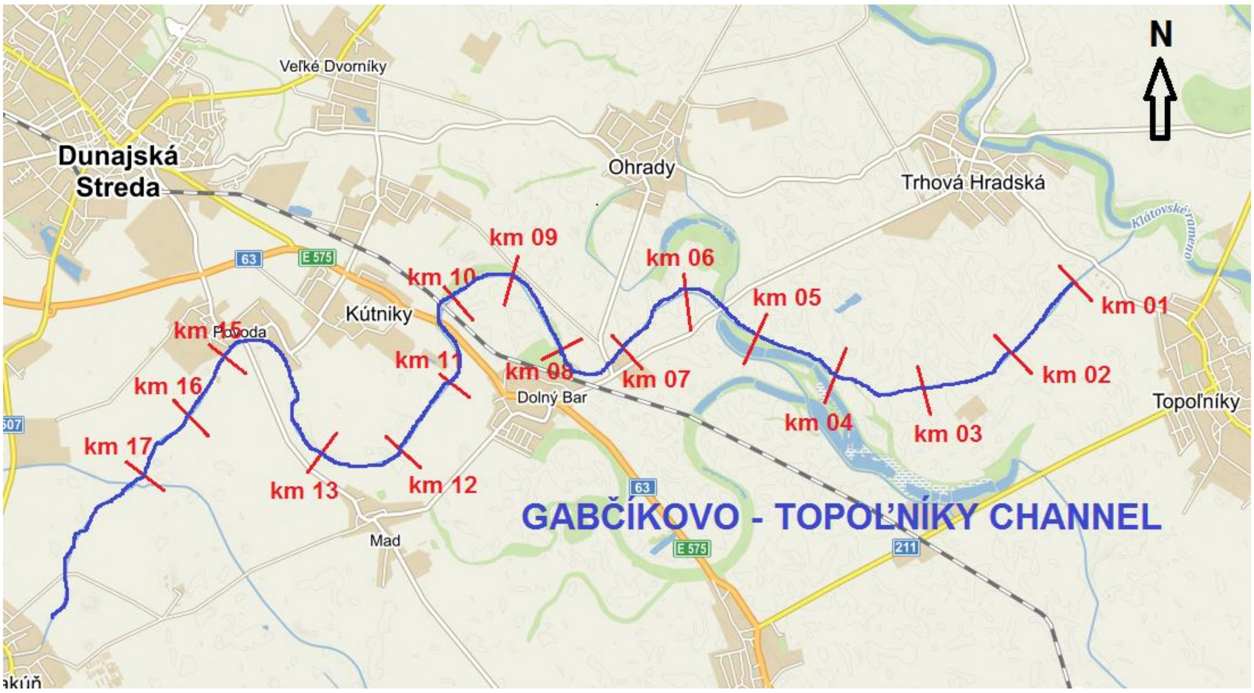

Fig. 2. Map of the Gabčíkovo – Topoľníky channel (measurements cross-section profiles in particular kilometers).

Fig. 3. Acoustic Doppler Velocimeter – River Surveyor device for measurement velocity profile and discharge.

Results and discussion

As it was mentioned, there exists a number of ways how to evaluate the influence of aquatic vegetation on flow in lowland streams. Quantification of the impact of aquatic vegetation through the roughness coefficient is one of the practically suitable methods. This roughness coefficient represents a parameter influencing discharge capacity of streams. Ranges of measured data are condensed in Table 1 (for each measured kilometer, except rkm 14). Table 1 contain number of measured cross-section profile (rkm), width (w), average depth (d), cross-section profile area (A), wetted perimeter (P), hydraulic radius (R), mean flow velocity (v) and meters above sea level (m.a.s.l.).

Table 2 contains measured data of elevation above sea and calculated data of water level change (Δd), water level slope (i_o) and Manning´s roughness coefficient (n). The roughness coefficient value in the sprouted stream bed is changing during the growing season depending on aquatic vegetation growth. In consequence of raised roughness, the velocity profile is changing and thereafter the discharge capacities are also changed. Value of the Manning´s roughness coefficient by Chow (1959) for channels not maintained (dense uncut weeds, the high equals flow depth) is from 0.050 to 0.120 or channels

with dense brush is from 0.080 to 0.140.
Distribution of submerged vegetation along Gabčíkovo – Topoľníky channel is different. However, because the measurements were carried out in the beginning of summer, there are a lot of reaches with large amount of submerged vegetation in cross-section profiles. In this case, the Manning´s coefficient increases rapidly with the amount of submerged vegetation.

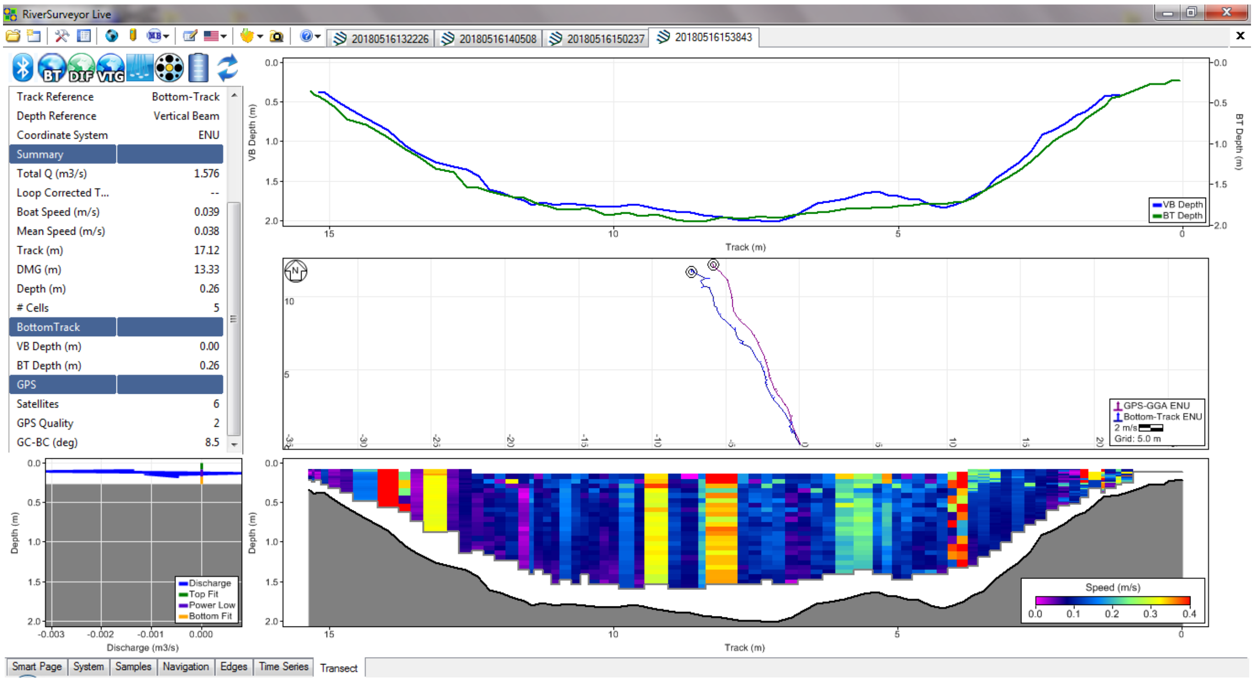

Fig. 4. Record of measurement by River Surveyor device (cross-section profile without vegetation).

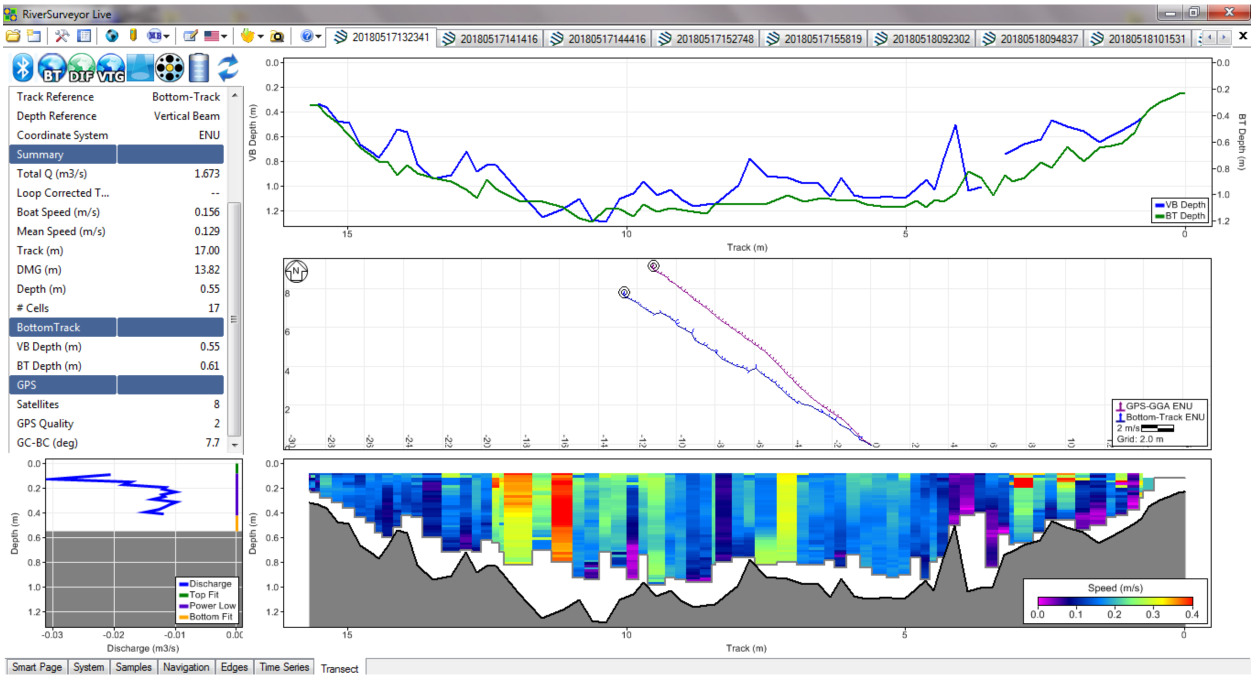

Fig. 5. Record of measurement by River Surveyor device (cross-section profile with submerged vegetation – peaks on the bed- stream indicated growing up vegetation).

Table 1. Summary of measured and calculated data for Gabčíkovo – Topoľníky channel (for measured rkm)

rkm	width [m]	average depth [m]	area [m^2]	wetted perimeter [m]	hydraulic radius [m]	flow velocity [$m\ s^{-1}$]	meters above sea level [m.a.s.l.]
01	15.5	0.72	24.49	20.25	1.210	0.084	110.632
02	14.5	0.41	19.88	18.25	1.089	0.097	110.671
03	16.5	0.39	17.11	16.50	1.037	0.118	110.685
04	16.0	0.68	19.22	18.31	1.050	0.100	110.689
05	13.5	0.67	15.50	15.65	0.990	0.112	110.732
06	16.0	0.32	10.70	17.87	0.599	0.170	110.776
07	17.5	0.21	15.17	18.34	0.827	0.118	110.808
08	17.0	0.48	11.52	18.15	0.635	0.165	110.905
09	15.0	0.46	10.10	14.50	0.697	0.128	110.935
10	14.5	0.33	11.75	15.91	0.739	0.155	111.060
11	16.5	0.55	12.21	17.82	0.685	0.137	111.168
12	15.5	0.36	11.51	17.18	0.670	0.126	111.214
13	16.0	0.43	11.96	16.59	0.721	0.132	111.305
15	11.5	0.38	9.51	8.87	1.072	0.139	111.462
16	14.5	0.40	6.98	13.24	0.527	0.128	111.612
17	16.0	0.26	19.76	17.32	1.141	0.080	111.670
Average	**15.375**	**0.44**	**14.21**	**16.54**	**0.856**	**0.124**	**111.020**

Table 2. Summary of calculated data for Gabčíkovo – Topoľníky channel (between cross-section profiles – rkm)

rkm	Δ water level [cm]	water surface slope	**Manning´s coefficient [$m^{-1/3}\ s$]**
01–02	3.9	0.000039	**0.075**
02–03	1.4	0.000014	**0.036**
03–04	0.4	0.000004	**0.018**
04–05	4.3	0.000043	**0.063**
05–06	4.4	0.000044	**0.037**
06–07	3.2	0.000032	**0.031**
07–08	9.7	0.000097	**0.051**
08–09	3.0	0.000030	**0.028**
09–10	12.5	0.000125	**0.056**
10–11	10.8	0.000108	**0.050**
11–12	4.6	0.000046	**0.039**
12–13	9.1	0.000091	**0.058**
13–15	15.7	0.000157	**0.058**
15–16	15.0	0.000150	**0.079**
16–17	5.8	0.000058	**0.065**
Average	**6.92**	**0.000069**	**0.049**

Variation of Manning´s coefficient along the Gabčíkovo – Topoľníky channel is summarized in Table 2. The highest value is in between river kilometers 15–16 (0.079), the lowest value is in rkm 03–04 (0.018). Average value for all cross-section profile is 0.049. Diaz (2005) claimed that the variations in the *n* values diminish when the slope increases. For intermediate flows in which the flow depth is greater than the height of vegetation (the grasses submerged), the *n* values decrease as average velocity increases. The decrease of *n* is regarded as a result of the increase of plant bending and submergence when velocity increases. For unsubmerged vegetation, Ding et al. (2004) hypothesized that an increase in flow depth less than that required to top the vegetation causes little change in the mean velocity. Therefore, flow resistance tends to increase with the depth. The roughness coefficients *n*, varies with the type of vegetative cover, longitudinal slope, and average flow depth. Fig. 6 shows the variation of the Manning´s coefficient and slope values along the evaluated channel reach. Fig. 7 shows growth of the slope value with value of the Manning´s coefficient at all evaluated cross-section profiles along Gabčíkovo – Topoľníky channel. Trend is relatively steep, when we compared this trend with other interdependences between Manning´s coefficient and flow velocity (Fig. 8) or average depths (Fig. 9). At the same time, there is the opposite course of the trend.

When it comes to flow velocity values (from 0.080 $m.s^{-1}$ for rkm 17 to 0.170 $m.s^{-1}$ for rkm 06), we observe a relatively small decline in the trend of the measured data (Fig. 8). We can state, that with decreasing values of the flow velocities are higher values of the Manning´s coefficient. On the Fig. 4 and 5 we see the course of velocity in cross-section profile (biggest value of flow velocity is recorded by red colour, smallest value of flow velocity is recorded by purple colour).

As regards average depth (Fig. 9), these values are from 0.21 to 0.72 m (maximum depth is 2.2 m for rkm 02). Average depths were obtained by River Surveyor device. We observe minimum decline of trend for values of the average depth. This trend is very similar with trend of the interdependence between values of flow velocity and Manning´s coefficient. Of course, depth in the measured cross-section profiles can be influenced by aquatic vegetation (Fig. 5. – peaks on the bed-stream), and for this reason, the depth recorded by the River Surveyor device can be a little bit different from the actual depth.

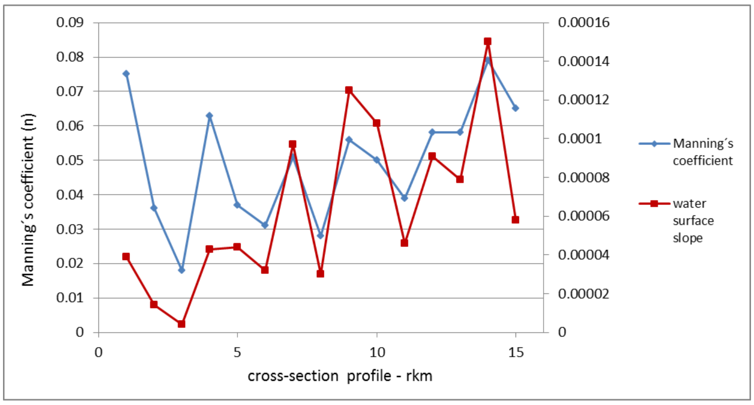

Fig. 6. Variation of Manning´s coefficient and slope along evaluated reach of the Gabčíkovo – Topoľníky channel.

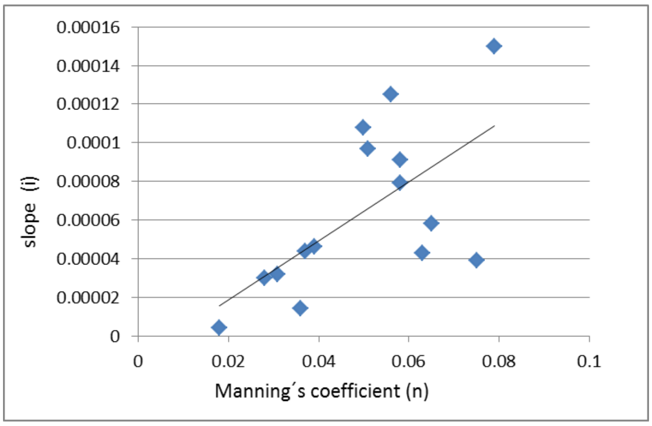

Fig. 7. Interdependence between values of slope and Manning´s coefficient at all evaluated cross-section profiles along Gabčíkovo – Topoľníky channel.

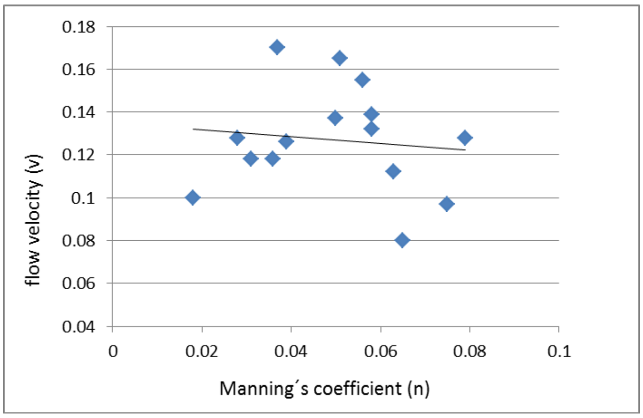

Fig. 8. Interdependence between values of flow velocity and Manning´s coefficient at all evaluated cross-section profiles along Gabčíkovo – Topoľníky channel.

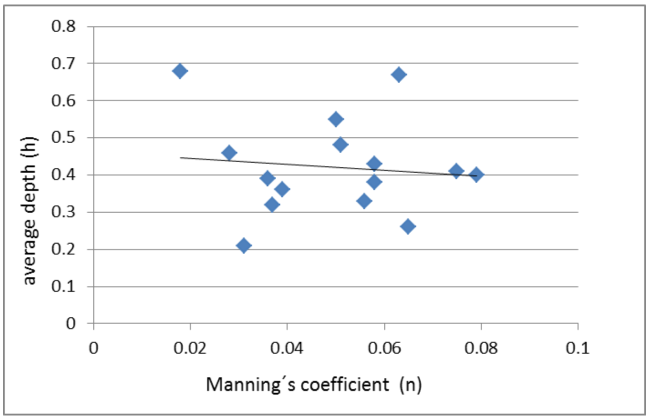

Fig. 9. Interdependence between values of average depth and Manning´s coefficient at all evaluated cross-section profiles along the Gabčíkovo – Topoľníky channel.

Conclusion

Vegetation in natural streams influences the flow and related characteristics and phenomena, such as roughness, discharge capacity, velocity profile, but also erosion and sedimentation, pollutant transport and water biota. The aim of this paper was to investigate and determine the impact rate of aquatic vegetation on flow conditions, based on field measurements along the Gabčíkovo – Topoľníky channel. The roughness coefficient n was used as a way of quantifying the impact. An analysis of the obtained data revealed that the roughness coefficient value changes along the channel, ant that the *n* value increases with the decreasing of flow depth. There were determined ranges of Mannings´s roughness coefficient values for relevant period of year with aquatic vegeration occurrence. Manning's coefficient value found in this study is in the range of 0.020 to 0.079. The analyses of measured data showed and confirmed the complexity of the impact of in-channel vegetation on stream flow, and the necessity to continue investigation of this problem.

Acknowledgement

This paper was prepared with the support of the project No. VEGA 2/0025/19.

References

Barnes, H. (1967): Roughness characteristics of natural channels. Technical report, USGS, Water-Supply Paper 1849, Denver, 1967, 213.

Boscolo, V. (2014): Effect of in-stream vegetation on hydraulic resistance in regulated rivers. Master thesis, Universita degli Studi di Padova, Aberdeen, 2014, 117.

Carollo, F. G., Ferro, V., Termini, D. (2002): Flow velocity measurements in vegetated channels. In: Journal of Hydraulic Engineering, vol. 128, no. 7, 2002, 664–673. ISSN 0733-9429

Cassan, L., Belaud, G., Baume, J. P., Dejean, C., Moulin, F. (2015): Velocity profiles in a real vegetated channel. In: Environmental Fluid Mechanics, vol. 15, no. 6, 1263– 1279. DOI: 10.1007/s10652-015-9417-0

Chow, V. T. (1959): Open channel hydraulics. McGraw-Hill, 1959.

Coon, W. (1998): Estimating of Roughness Coefficients for

Natural Stream Channels with Vegetated Banks. USGS, Water-Supply Paper 2441, Denver, 1998, 135. ISBN 0-607-88701-X.

De Doncker, L., Verhoeven, R., Bal, K., Meire, P., Quintelier, J. (2009): Determination of the Manning roughness coefficient influenced by vegetation in the river Aa and Biebrza river. Environmental Fluid Mechanics, vol. 9, no. 5, 2009, 549–567. https://doi.org/10.1007/s10652-009-9149-0

Diaz, R. G. (2005): Analysis of Manning Coefficient for Small-Depth Flows on Vegetated Beds. Hydrological Processes, Vol. 19, No. 16, 2005, 3221–3233. DOI: 10.1002/hyp.5820

Ding, Y., Jia, Y., Wang, S. S. Y. (2004): Identification of Manning's Roughness Coefficient in Shallow Water Flows. Journal of Hydraulic Engineering, Vol. 130, No. 6, 2004, 501–510. ISSN 0733-9429

Dulovičová, R. (2019): Transformation of bed silts along lowland channel Gabčíkovo – Topoľníky and comparison of their saturated hydraulic conductivity values. Acta Hydrologica Slovaca, vol. 20, no. 2, 151–159. DOI: 10.31577/ahs-2019-0020.02.0018

Dyhouse, G., Hatchett, J., Benn, J. (2003): Floodplain modeling using HEC-RAS. Haestad Method, USA, 2003, 744. ISBN 0-9714141-0-6.

Green, J. C. (2005): Modeling flow resistance in vegetated streams: review and development of new theory. Hydrological processes, vol. 19, no. 6, 2005, 1245– 259. https://doi.org/10.1002/hyp.5564

Green, J. C. (2006): Effect of macrophyte spatial variability on channel resistance. In: Advances in Water Resources, vol. 29, no. 3, 426–438. ISSN: 0309-1708. DOI:10.1016/j.advwatres.2005.05.010

Kutija, V., Hong, H. T. M. (1996): A numerical model for assessing the additional resistance to flow introduced by flexible vegetation. Journal of Hydraulic Research, vol. 34, no. 1, 1996, 99–114.

Nikora, V., Larned, S., Nikora, N., Debnath, K., Cooper, G., Reid, M. (2008): Hydraulic resistance due to aquatic vegetation in small streams: Field study. Journal of Hydraulic Engineering, vol. 134, no. 9, 2008, 1326–1332. ISSN 0733-9429.

Stone, M. B., Shen, H. T. (2002): Hydraulic resistance of flow in channels with cylindrical roughness. Journal of Hydraulic Engineering, vol. 128, no. 5, 2002, 500–506.

Tuozzolo, S., Langhorst, T., Moraes Frasson, R. P., Pavelski, T., Durand, M., Schobelock, J. J. (2019): The impact of reach averaging Manning´s equation for an in-situ dataset of water surface elevation, width and slope. Journal of Hydrology, vol. 578, 2019, ISSN 0022-1694. https://doi.org/10.1016/j.hydrol.2019.06.038

Velísková, Y., Dulovičová, R., Schügerl, R. (2017): Impact of vegetation on flow in a lowland stream during the growing season. Biologia, vol. 72, no. 8, 2017, 840–846. DOI: 10.1515/biolog-2017-0095

Vereecken, H., Baetens, J., Viaene, P., Mostaert, F., Meire, P. (2006): Ecological manegement of aquatic plants: effect in lowland streams. In: Hydrobiologia, vol. 570, 2006, 205–210. DOI 10.1007/s10750-006-0181-5

Wilson, C. A., Hoyt, J., Schnauder, I. (2007): Flow resistance models for flexible submerged vegetation. Journal of Hydrology, vol. 134, no. 7, 2007, 213–222.

Mgr. Radoslav Schügerl, PhD. (*corresponding author, e-mail: schugerl@uh.savba.sk)
Ing. Yvetta Velísková, PhD.
Ing. Valentín Sočuvka, PhD.
Ing. Renáta Dulovičová
Institute of Hydrology SAS
Dúbravská cesta 9
84104 Bratislava
Slovak Republic

DOI: 10.31577/ahs-2021-0022.01.0008

ACTA HYDROLOGICA
SLOVACA

Volume 22, No. 1, 2021, 70 – 77

ANALYSIS OF FACTORS INFLUENCING THE INTENSITY OF SOIL WATER EROSION

Matúš Tomaščík, Zuzana Németová, Michaela Danáčová*

Soil water erosion is one of the most widespread and most damaging processes of degradation in the world. Despite the fact that extensive research on it is carried out by a large number of scientists all around the world, it still occupies a leading position among global threats. Because soil erosion is a complex and quite complicated process, small steps have to be undertaken in order to reach any relevant conclusions. In most cases, in order to simulate soil erosion processes, mathematical models are widely used that are considered useful and helpful tools since the measurement of the erosion of terrain consumes time and space and is impossible in many parts of the world. The aim of the study presented lies in an analysis of elements input into a physically-based erosion model. Those input factors directly influence the model's end results, i.e., the soil erosion processes. The article attempts to define to what extent they affect the model results and soil erosion processes as well. The specific parameters of the soil erosion model, i.e., resistance to erosion and hydraulic roughness, were determined by simulated rainfall experiments. The results identify changes in the parameters input to the final model results together with different initial conditions.

KEY WORDS: surface roughness, erosion resistance, soil water erosion, rainfall intensity, surface runoff

Introduction

Soil erosion is a very popular and well-known research topic; nevertheless, it poses some unanswered and scientifically unexplored questions. The reason is that soil erosion is a natural and complex process ongoing in nature; it is quite variable in space and over time and is strongly dependent on many factors. Some of the most significant elements in soil erosion research are soil roughness and the state of the vegetation cover to protect the surface of soil against external factors. Soil roughness characterizes micro-variations in surface elevations that have especially occurred due to management practices and tillage systems (Vázquez et al., 2005). Soil roughness also indicates irregularities of soil surfaces resulting from the soil's texture and type, the sizes of aggregates and rock fragments, the surface cover, land use, and management practices used (Thomsen et al., 2015). According to (Michael et al., 1996), the roughness of surface soil represents a hydraulic parameter (roughness coefficient) and means a reduction in the flow velocity of the surface runoff, thanks to microrelief irregularities (soil aggregates, plant residues). Increasing the values of this coefficient leads to a reduction in the flow velocity and other related soil processes. Because soil roughness increases water retention and infiltration, it is considered a principal element influencing wind and water erosion (through the reduction of runoff volume and speed). Soil roughness represents one of the factors controlling surface runoff and soil loss, but it is also a main indicator of the degradation of a soil's microstructure. However, few studies have been conducted on this parameter. The roughness of the soil surface is directly connected with land use management practices in several ways. The preparation of the soil can influence the soil roughness, depending on the soil type and mineralogy and the management techniques used (Bramoski et al., 2012). The roughness of the soil surface influences the speed and accumulation capacity of the surface runoff, the infiltration rate, and the related soil erosion processes (Römkens et al., 2002). Two components are used to define soil roughness, i.e., random roughness (RR) (Currence and Lovely, 1970) and the tortuosity index *T* (Boiffin, 1984). Both components mentioned describe the relationships of the surface water storage in the soil (Govers et al., 2000; Kamphorst et al., 2000).

In order to reduce potential soil loss and decrease the intensity of soil erosion processes or the volume of surface runoff, one of the first measures taken should be to analyse the agricultural practices in the area under consideration. As mentioned above, the roughness of the soil surface directly influences soil erosion processes and is affected by management practices; therefore, a small change in the agricultural practices used can lead to increasing the roughness of the soil surface (Honek at al., 2020).

Another parameter strongly impacted by the loss of soil is represented by soil erosion resistance, which represents the total of various forces. This parameter is influenced by different physical and chemical soil attributes such as aggregate stability, organic matter content, rooting, soil cover, surface structure, and tillage practices, and is variable over time and in space within the same soil texture group.

Because soil erosion is a complicated process influenced by many changeable factors, in most cases the models developed to simulate the soil erosion contain some parameters that are used to modify the unstable condition and the prediction errors. In the model used in this study, this parameter is called the "skin factor"; it not only allows eliminating the errors resulting from the simplified assumptions of the model, but also evaluates the impact of agricultural management practices on the soil (Michael et al., 1996).

The aim of the study lies in an analysis of the soil input parameters used in the physically-based Erosion-2D model, which are considered the most important parameters not only in the model analysed (Erosion-2D model) but also in many other soil erosion and erosion prediction models as well. The rainfall simulator is an indispensable device used for parametrization of the soil input parameters and on which basis the laboratory measurements were performed. The rainfall simulator is a tool with which it is possible to simulate the characteristics of natural rainfall events as closely as possible (Clarke and Walsh, 2007). These types of devices are widely used in laboratory and field experiments in order to imitate and analyse the effects of alterations in vegetation cover, management practices or changes in soil.

Laboratory conditions eliminate the external factors such as wind, soil moisture, or the antecedent soil conditions that are considered the main advantages of laboratory experiments (Aksoy et al., 2012). Therefore, this study can also be used for informational purposes of a general character without considering a specific model.

Material and methods

The water erosion of soil is commonly studied in laboratories, and experiments are based on artificially generated precipitation using rainfall simulators. Typically, the influence of various factors, such as the intensity or total amount of rainfall, soil characteristics, or the influence of the slope and length of the eroded area on soil erosion, is evaluated. The results of these experiments are used for a better understanding of erosion processes, estimations of sediment transported on the ground, or the calibration of mathematical simulation models. In this paper, we will focus on the possibility of the parameterization of the Erosion-2D model. The model parameters will be calibrated according to the measurement results and compared with the values in the literature.

EROSION-2D MODEL

The Erosion-2D model is a physically-based and single event erosion model with a focus on simulating soil water erosion on a slope profile. The model can be used for slopes of different lengths with a spatial resolution of 1 m. Because all the calculations are performed for single rainfall events, the erosive impact of a rainfall event is expressed by two major elements (Werner, 2006):

- The intensity and duration of the rainfall,
- The management practices (the type and development stage of the cultivated crop, the type of tillage, etc.).

The Erosion-2D model describes the erosion processes in a complex way and is therefore constructed based on the following components (Werner, 2006):

1. *The digital elevation model,* which includes interpolation of a 1 m grid from the input data, calculation of the topographic parameters from the slope profile, calculation of the individual catchment area and length of the flow path for each cell (runoff concentration),
2. *The Infiltration model which includes* rainfall infiltration (Green-Ampt approach) (Green and Ampt, 2011),
3. *The runoff and erosion sub model* performs the simulation calculations.

The surface roughness in the model is calculated based on the equation given by Manning:

$$v_q = \frac{1}{n} \cdot \delta^{\frac{2}{3}} \cdot S^{\frac{1}{2}} \tag{1}$$

where
v_q flow velocity of surface runoff [m/s],
n roughness coefficient according to Manning-Strickler [s/m$^{1/3}$],
S slope [m/m],
δ flow depth of surface runoff [m].

$$\delta = \left[\frac{q * n}{S^{\frac{1}{2}}}\right]^{\frac{3}{5}} \tag{2}$$

where
q runoff rate [m^3/(s m)],
S slope gradient [-],
n Manning's hydraulic roughness [s/m$^{1/3}$].

$$\mathrm{n} = v_q - \frac{5}{3} \cdot q^{\frac{2}{3}} \cdot S^{\frac{1}{2}} \tag{3}$$

where
n roughness coefficient according to Manning-Strickler [s/m$^{1/3}$],
S slope gradient [-],
q runoff rate [m^3/(s m)].

Rainfall simulator and experimental site

In order to generate an artificial rainfall with a constant rate of intensity, an Eijkelkamp small rainfall simulator was used in the study (Fig. 1). The experiment was performed in a laboratory at the Faculty of Civil Engi-

neering, Slovak University of Technology in Bratislava. The simulated rainfall system is not restricted by nature, i.e., the rainfall and its duration can be adjusted. Several researchers have conducted various runoff and erosion experiments using this system.
The rainfall simulators can be used to study:

- characteristics of soil infiltration,
- erosion and surface runoff,
- relative protection for different stages of vegetation growth,
- relative erodibility.

The simulators of rainfall events started to be used in the 1940s (Wilm, 1942; Meyer and McCune, 1958, in Zachar, 1982). Their development reflected progress in technology and hydrological processes, including an understanding of the infiltration processes.
The advantages of the Eijkelkamp rainfall simulator are the possibility of repeating artificial rain with a set intensity, length of precipitation, adjustable slope of the area investigated, portability and constant rainfall, and easily portable and mobile water sources. The disadvantages can be seen in the limited length of the precipitation (volume of reservoir) and in limiting the size of the area that can be used to perform the experimental simulation. With regard to the study presented, four laboratory experiments with 12 minutes of intermittent rainfall were simulated. The main differences between the rainfalls used lie in the initial soil moisture.
The area from which the soil samples were taken and analysed is located in the urban district of Turá Lúka, which is a part of the town of Myjava and is located in the northern part of the Myjava Hills. A small experimental catchment is located approximately in the middle of the cadastral area of Tura Lúka. This small catchment is endangered by water erosion, especially an eroded gully, due to the size of the catchment. Based on Novák's classification (Novák and Hlaváčiková, 2017), the geology of the area is characterised by a flysch massif, and the dominant soil types are cambisols and rendzina. The climate is characterized as mildly humid and warm with mild winters and an average annual precipitation of 650 to 700 mm. The total area of the catchment is 29 hectares, and the total size (length) of the eroded gully is approximately 300 meters (Hlavčová et. al, 2019). The predominant purpose of the catchment is based on agricultural production with a system of crop rotation. This catchment is a part of a research area managed by the Department of Land and Water Resources Management, Faculty of Civil Engineering, Slovak University of Technology, since 2015 within the 7RP RECARE European project.

Description of laboratory measurements

The soil sample was adjusted by loosening the soil before each rainfall simulation, which consisted of 12 minutes of intermittent rain. The basic characteristics of the selected artificial rainfall events are shown in Table 1.
Because of the limitations of the rainfall simulator (the storage of the reservoirs is only 2.3 litres of water), the rainfall simulations had to be interrupted. After the interruptions, the surface runoff´s volume, sediment weight, and soil moisture were measured.

Fig. 1. Rainfall simulator and laboratory experiment.

Table 1. The laboratory rainfall simulation experiment (plot area =0.0625 m^2)

Experiment No. (12-minutes artificial rainfall with the interruptions)	Slope [º]	Initial soil moisture [%]	Rainfall intensity [mm/min]	Surface runoff volume [l]	Sediment volume [g]
1	10.8	23.7	5.3	3.4	62.6
2	10.8	6	5.3	2.45	73.7
3	9.7	29	5.3	5.4	158.7
4	8	13.2	4.9	3.6	39.5

**Total time artificial rainfall is 42 minutes with the interruptions*

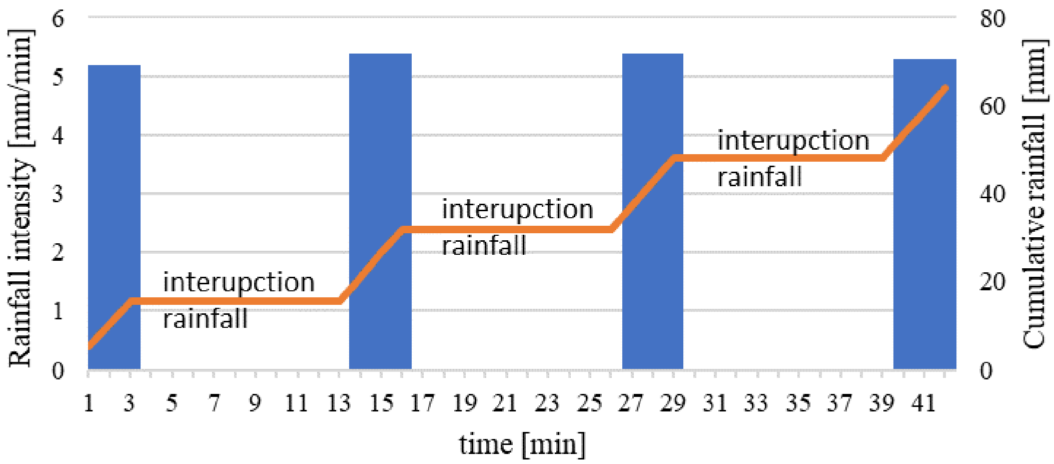

Fig. 2. Scheme of laboratory experiment – 42 minutes of artificial rainfall events (4 x 3 minutes, with 10-minute interruptions).

Methodology and input parameters

The experiment consisted of laboratory measurements of the surface runoff and sediment volume on small experimental plots using a rainfall simulator. In the first step, it was necessary to upscale the small area of the simulator to the scale of the Erosion-2D model (a limited scale) by the regression between the various slope lengths and relevant simulations of the surface runoff´s volume on the slope lengths of 1, 4 and 8 meters. In the second step, the upscaling was used to compare the results of the surface runoff of the model and the surface runoff of the experimental measurements. The flow chart of the experiment is shown in Fig. 3.
Table 2 comprises the ranges of the input parameters that are available in the parameter catalogue for the Erosion 2D and 3D model users. The choice of those parameters depends on the type of soil, cultivation method, and vegetation phase.
At the beginning, the tabular values that are recommended by the catalogue of parameters for the Erosion-2D model (Table 3), were used. In the next step, the changes in the parameters that have a significant impact on the results modelled (erosion resistance, hydraulic roughness, and the skin factor) were performed. In the process of parameterization, the parameters were manually changed (gradually to the entire recommended range), and the sensitivity of the model was monitored together with the process of parametrization.
These input data were specified based on the results of the erosion measurements from the laboratory experiments. The process of the parameterization was done for each intermittent rainfall event separately.
The parameter calibrations were performed:

- for the surface runoff,
- for the surface runoff and sediment,
- for the volume of the sediments.

In this study, the output parameters were primarily searched for the weight of the sediment, which determines the rate of erosion. The calibration of the parameters selected, i.e., erosion resistance, hydraulic roughness, and the skin factor, were chosen because of their influence on the erosion process. The intensity of

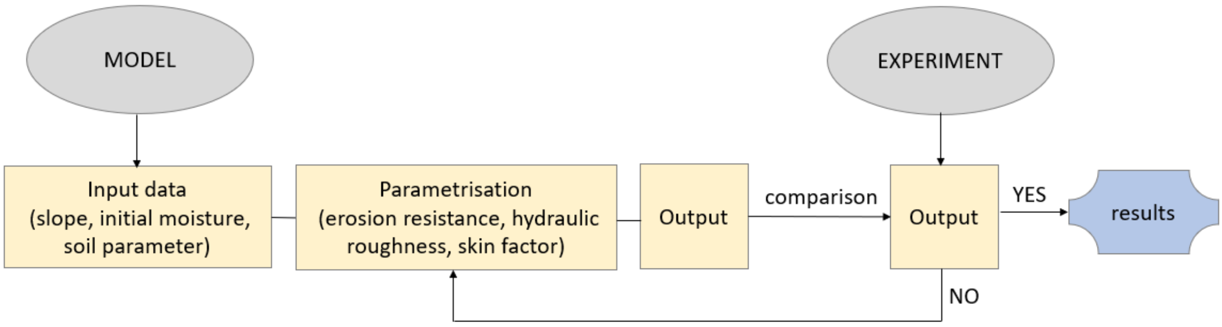

Fig. 3. Scheme of the experiment, consisting of laboratory measurements and hydrological modelling.

Table 2. Range input data of the Erosion-2D model for all the types of soil and types of cultivation method

Bulk density [kg/m^3]	Organic matter [%]	Erosion resistance [kg.m.s^{-2}]	Manning roughness [s.m$^{-1/3}$]	Skin factor [-]	Initial soil moisture [%]	Cover [%]
920–1960	0.8–1.9	0.00005–0.01	0.006–0.900	0.02–60	6–60	0–100

Table 3. Input data of the model Erosion-2D

Bulk density [kg/m^3]	Organic matter [%]	Erosion resistance [kg.m.s^{-2}]	Manning roughness [s.m$^{-1/3}$]	Canopy cover [%]	Skin factor [-]	Clay [%]	Silt [%]	Sand [%]
1800	1.15	0.0008	0.015	0	1	10	36	48

the erosion is the most prominent feature and is not directly measurable. During the process of parametrization it was found that the skin factor has the greatest impact on the formation and volume of surface runoff. The skin factor is also considered as a correcting factor since it is a parameter used to adjust and optimize the infiltration process and minimize the model errors as well.

Results and discussion

In the study, four extreme rainfall events with interruptions were analysed. The simulation was performed in the laboratory as a priority to ensure the same conditions. The following elements were significant:

- surface condition (without vegetation, the same tillage management),
- artificial rain (concept, rainfall intensity, duration of rain),
- slope ratios.

There was a significant and fundamental change in the initial soil moisture, which ranged from 6 to 29% (Table 1). Based on the results, it is obvious that the Erosion-2D model does not respond to very low initial soil moisture at the set intensity and duration of the rain. In the second experiment, where the initial soil moisture was 6%, no outputs from the model were obtained. For this reason, only 3 laboratory measurements were further analyzed.

In the following table (Table 4), the results of the erosion parameters obtained during the individual simulations of the parameters calibrated are displayed. The results presented the following schemes: A) original parameter settings, B) calibration of Manning’s roughness and changing the skin factor parameter, C) skin factor 1, without any correction and calibration of Manning’s roughness and erosion resistance.

The results show that the parameters were chosen in a suitable setting. The aim was to find and analyse the influence of the parameters and their sensitivity with respect to the initial soil moisture and the slope of the relief as well. All the parameters selected (Manning's roughness, the erosion resistance, and the skin factor) affect the erosion process, and their variability is extensive. In the next step, the results achieved were analysed by creating an arithmetical average of the parameters from the results for variants B and C.

Set up parameters:

- setup group 1 (Erosion resistance 0.0008 [kg.m.s^{-2}], Roughness 0.0151 [s.m$^{-1/3}$], skin factor 19),
- setup group 2 (Erosion resistance 0.000916 [kg m s^{-2}], Roughness 0.0248 [s.m$^{-1/3}$], skin factor 1).

A graphic representation of the model results for the groups of parameters is shown in Figure 4.

The results point to further possible improvement of the erosion parameters, where the size of the slope, the initial soil moisture, and the intensity of the rain should be taken into account. The largest volume of sediments from the measurements was confirmed in the third experiment, where the initial humidity was high. In comparison with the first experiment, where the intensity of the rain was the same, but the slope was lower by 1 degree, the volume of sediments was 50% less. For a better analysis, statistical evaluation, and subsequent parameterization of the model, a larger number of experiments is required.

Table 4. Summary from the rainfall simulation – Erosion-2D (plot area = 1 m^2), 12-minute artificial rainfall with interruptions (4 individual rainfalls)

Experiment No.	Scheme	Initial soil moisture [%]	Erosion resistance [kg m s^{-2}]	Manning roughness [s m$^{-1/3}$]	Skin factor [-]	Sediment Volume [kg/m]	Laboratory - sediment Volume [kg/m]
1	A)	23.7	0.0008	0.015	1	2.00	1.01
	B)	23.7	0.0008	0.016	16	1.01	
	C)	23.7	0.0015	0.0165	1	1.01	
3	A)	29.3	0.0008	0.015	1	2.28	2.54
	B)	29.3	0.0008	0.0055	40	2.57	
	C)	29.3	0.0004	0.04	1	2.55	
4	A)	13.2	0.0008	0.015	1	0.76	0.63
	B)	13.2	0.0008	0.024	0.8	0.64	
	C)	13.2	0.00085	0.018	1	0.64	

* Bulk density 1800 [kg/m^3]. organic matter 1.15 [%]. cover [%]

Table 5. Summary from the rainfall simulation – Erosion-2D (plot area = 1 m^2), 12-minute artificial rainfall with interruptions (variants of 4 individual rainfalls)

Exp. No.	Variant (single rainfall)	Total time [min]	Initial soil moisture [%]	Setup group 1 Sediment Volume [kg/m]	Setup group 2 Sediment Volume [kg/m]	Laboratory Sediment Volume [kg/m]
1	1 – 4	12	23.7	1.02	1.32	1.01
	1 – 3	9	23.7	0.76	0.95	0.51
	1 – 2	6	23.7	0.28	0.58	0.13
3	1 – 4	12	29.3	1.74	1.47	2.54
	1 – 3	9	29.3	1.68	1.09	1.83
	1 – 2	6	29.3	0.76	0.71	1.16
4	1 – 4	12	13.2	0.00	0.48	0.63
	1 – 3	9	13.2	0.00	0.28	0.46
	1 – 2	6	13.2	0.00	0.11	0.19

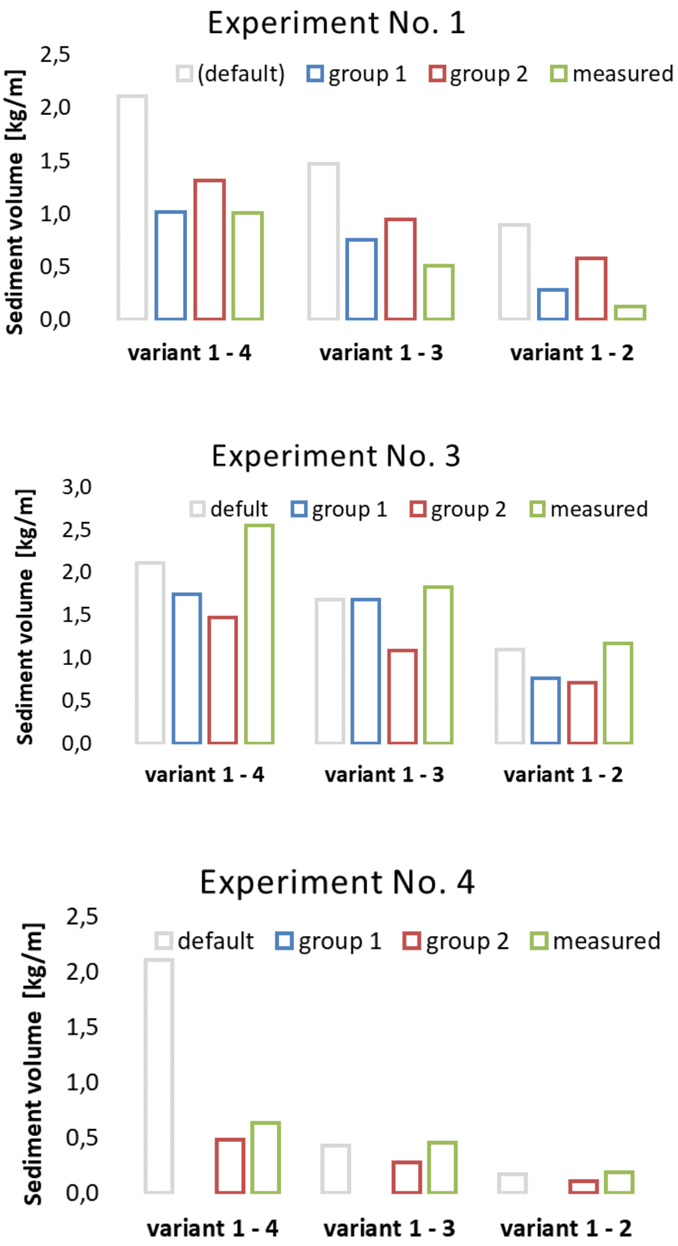

Fig. 4. The sediment volume of the Erosion-2D model and rainfall simulator.

Conclusion

In practice, various physical or empirical erosion models are applied for analysing and determining the intensity of soil erosion processes. In order to estimate the soil loss by water, physically-based erosion models require specific parameters describing the decisive processes involved (the infiltration of rainfall, surface runoff, degradation of the soil). The parametrization of such models represents a necessary and significant part of any scientific work.

In this study, the parameters of the Erosion-2D model, i.e., the skin factor, erosion resistance, and hydraulic roughness, were adjusted (set up) by comparing the modelled volumes of the soil sediment with the measured data on the experimental plots. The results from the laboratory experiments show that outputs from the rainfall simulations can be reproduced successfully and that based on those outputs, the process of determining a model´s parameters can be successfully performed. The disadvantage is seen in the area of the small simulator. The experimental results of the small-scale simulator are susceptible to measurement and model errors. It is necessary to work with a larger number of measurements and analyse the results. In conclusion, it is possible to state that the model overestimates the amount of sediment on higher slopes, which can be modified by a higher degree of roughness.

The skin factor has the greatest influence on the outputs in the Erosion-2D / Erosion-3D model. Further research will be focused on calibration of the skin factor together with the soil roughness for different initial conditions, including the slope elements, intensity of precipitation, and management practices.

Acknowledgement

This work was supported by the Slovak Research and Development Agency under Contract No. APVV-19-0340 and APVV-18-0347, the VEGA Grant Agency No. 1/0632/19. The authors thank the agencies for their research support.

References

Aksoy, H., Unal, N. E., Cokgor, S., Gedikli, A., Yoon, J., Koca, K., Inci, S. B., Eris, E. (2012): "A rainfall simulator for laboratory-scale assessment of rainfall-runoff-sediment transport processes over a two-dimensional flum," Catena, vol. 98, 63–72, 2012.

Boiffin, J. (1984): Structural degradation of the soil surface by the action of rainfall. Paris, Inst. Natl. d'Agronomie ParisGrignon, 1984.

Bramorski, I., Maria, I. C., Silua, R. L., Crestana, S. (2012): Relations between soil surface roughness, tortuosity, tillage treatments, rainfall intensity and soil and water losses from a Red Yellow Latosol. Revista Brasileira de Ciência do Solo. 36, 1291–1297.

Clarke, M. A., Walsh, R. P. D. (2007): "A portable rainfall simulator for field assessment of splash and slopewash in remote locations," Earth Surface Processes and Landforms, vol. 32, pp. 2052–2069. 2007.

Currence, H. D., Lovely, W. G. (1970): The analysis of soil surface roughness. Trans. ASAE 13:710–714, 1970.

Govers, G., Takken, I., Helming, K. (2000): Soil roughness and overland ûow. Agronomie 20:131–146, 2000.

Green, W. H., Ampt, G. A. (1911): Studies on soil physics. I: The flow of air and water through soils. J. Agr. Sci. 4, 1–24.

Hlavčová, K., Danáčová, M., Kohnová, S., Szolgay, J., Valent, P., Výleta, R., 2019. Estimating the effectiveness of crop management on reducing flood risk and sediment transport on hilly agricultural land – A Myjava case study, Slovakia, CATENA, 172, pp. 678–690.

Honek, D., Németová, Z., Kohnová, S., Šulc Michalková, M. (2020): The sensitivity analyses of soil parameters and their impact on runoff-erosion processes: the application of Erosion-3D model in small Slovak catchment. Pollack Periodica, 2020, No. 15, Vol. 1, p. 53–64.

Kamphorst, E. C., Jetten, V., Guérif, J., Pitkänen, J., Iversen, B. V., Douglas, J. T., Paz, A. (2000): Predicting depressional storage from soil surface roughness. Soil Sci. Soc. Am. J., 64:1749–1758, 2000.

Michael, A., Schmidt, J., Schmidt W. A. (1996): EROSION 2D/3D, Parameter Catalog Application (2D), Technische Universität Bergakademie Freiberg. 169.

Novák, V., Hlaváčiková, H. (2017): Hydrológia pôdy, Vydavateľstvo: VEDA, ISBN: 978-80-224-1529-3

Römkens, M., Helming, K., Prasad, S. (2002): Soil erosion under different rainfall intensities, surface roughness, and soil water regimes. CATENA. 46. 103–123. 10.1016/S0341-8162(01)00161-8.

Thomsen, L., Baartman, J., Barneveld, R., Starkloff, T., Stolte, J. (2015): Soil surface roughness: comparing old and new measuring methods and application in a soil erosion model. SOIL Discussions. 1. 399–410. 10.5194/soild-1-981–2014.

Vázquez, E., José Garcia, M., Paz-González, A. (2005): Characterizing anisotropy and heterogeneity of soil surface microtopography using fractal models. Ecological Modelling. 182. 337–353. 10.1016/j.ecolmodel.2004.04.012.

Werner, M. (2006): Erosion-3D User manual, Ver. 3.1.1. GEOGNOSTICS a. g., Berlin. 69.

Zachar, D. (1982): Soil Erosion, Developments in soil science 10, Elsevier scientific publishing company.

Bc. Matúš Tomaščík
Ing. Zuzana Németová, PhD.
doc. Ing. Michaela Danáčová, PhD. (*corresponding author, e-mail: michaela.danacova@stuba.sk)
Department of Land and Water Resources Management
Faculty of Civil Engineering, the Slovak University of Technology in Bratislava
Radlinského 11
810 05 Bratislava
Slovak Republic

DOI: 10.31577/ahs-2021-0022.01.0009

ACTA HYDROLOGICA SLOVACA

Volume 22, No. 1, 2021, 78 – 87

ASSESMENT OF SELECTED EMPIRICAL FORMULAS FOR COMPUTATION OF SATURATED HYDRAULIC CONDUCTIVITY

Renáta Dulovičová*, Yvetta Velísková, Radoslav Schügerl

This paper deals with the comparison of empirical formulas used for computation of saturated hydraulic conductivity values K_d. The disturbed samples of bed silts were obtained from the Komárňanský channel at the Žitný ostrov (ŽO), Slovakia. The bed silts were extracted from three different vertical parts of silt - top, middle and bottom part of silt layer in each selected cross-section profile of the Komárňanský channel. Because the samples are disturbed only the empirical formulas based on the grain size analyses were used. The measurements of silting and the extraction of bed silt samples were carried out in 2019. These measurements were used for calculation of saturated hydraulic conductivity values K_d. In the previous study we calculated the values of saturated hydraulic conductivity for disturbed samples K_d according to Bayer – Schweiger; Špaček I and Špaček II empirical formulas. In this current paper we used other empirical formulas based on the grain size analyses. We selected Hazen I.; Bayer; USBR and Orechova formulas which were in the past used in the software Geofil. These valid values K_d reached from 2.00 x10^{-10} to 9.07 x 10^{-06} m s^{-1}. We used the number of valid computed results (count) of K_d to determine the formula´s ability to give results meeting the validity requirements. The recommended formula for calculation of K_d of bed silts in Komárňanský channel based on this criterium is Hazen I., which range is 1.16 x 10^{-8} to 7.25 x 10^{-06} m s^{-1}.

KEY WORDS: bed silts, disturbed samples, grain size analysis, saturated hydraulic conductivity

Introduction

The bed silt permeability impacts water flow between surface water in the channel and surrounding groundwater in the scope of their interaction at this area. The permeability of bed silts is expressed by value of their saturated hydraulic conductivity. Therefore, it is important to obtain the values of saturated hydraulic conductivity. Engineering practice often requires the investigation of ground water movement, volumes in storage and computation of the amount of infiltrated water into or from the aquifer. Hydraulic engineers, hydrologists and hydrogeologists have been studying this topic for decades with a variety of conclusions. Thus, we focus on using a simple and useful method for quantifying hydraulic conductivity. Our approach includes the assessment of results obtained from selected empirical formulas.

A number of empirical formulas for saturated hydraulic conductivity determination are being used in engineering practice. Most of the ground water textbooks reference formulas of institutions and scholars such as Hazen, Beyer, Sauerbrei, Kozeny, USBR, Pavchich, Schlichter, Terzaghi, Kruger, Zunker, Zamarin, Boonstra and de Ridder, Špaček, Palagin, Schweiger, Carman-Kozeny, Seelheim, Orechová, Zieschang and others (Dulovičová and Velisková, 2005, user manual of commercial software GeoFil, Říha et al., 2018). Most of the empirical formulas are based on laboratory or field experiments. The structure of these formulas ranges from a simple function of grain size d_{10}, d_{15}, d_{17}, d_{20}, d_{50} or d_{60} to the most complex exponential equations with a number of other input data and parameters, which need to be computed through additional equations. However, many textbooks do not describe the exact conditions under which a formula was derived, nor the range of its application. Unfortunately, the values of saturated hydraulic conductivity documented in the literature do not always include the sizes of databases. Computed values exhibit a wide range of results which differ by factors of ten, hundred, thousands or more. Decisions about which formula can justify a result are often subjective. Thus, results might not always be in agreement with the values computed from formulas or values reported in the literature.

In the current literature research papers usually focus on a wide variety of saturated hydraulic conductivity related topics. Habtamu et al. (2019) evaluate saturated hydraulic conductivity with different land uses of disturbed and undisturbed soil, they developed an equation which replaces the time taking in-situ saturated hydraulic conductivity measurement. Duong et al. (2019) clarify the effects of soil hydraulic conductivity and rainfall intensity on riverbank stability using a GeoSlope analysis. Říha et al. (2018) present the verification of validity of various published porosity functions and empirical formulae with the use of the experimental data obtained from the glass beads. Wang et al. (2018) present an alternative model to predict soil hydraulic conductivities, in their study model testing with 24 soil data sets was successful in predicting conductivities over arrange of moistures. Ren and Santamarina, (2018) present an analysis of hydraulic conductivity of sediments as a function of void ratio. Hwang et al. (2017) compare saturated hydraulic conductivities of sandy soils to characterize properties of water retention. Ghanbarian et al. (2017) propose scale dependent pedotransfer functions to estimate saturated hydraulic conductivity more accurately than seven other frequently used models. (Gadi et al., 2017) studied spatial and temporal variation of hydraulic conductivity and vegetation growth in green infrastructures, using infiltrometer and a visual technique. Yusuf et al. (2016) studied hydraulic conductivity of compacted laterite, treated with iron ore tailings. Hussain and Nabi (2016) used seven empirical formulas to calculate hydraulic conductivity, based on grain size distribution of unconsolidated aquifer materials. Kutílek (1978) calculated the value of saturated hydraulic conductivity by empirical formulas coming out from grain size analysis. In this current paper we also used a way of several empirical formulas for saturated hydraulic conductivity determination for bed silts on Komárňanský channel.

Location and site description

Žitný ostrov (ŽO) is the area between two branches of the Danube River – Small Danube and Danube – Fig. 1 and it is a component of the Danube Lowland. This part was created by sediments transport from upper part of the Danube River (Čelková, 2014). This area formed as a flat plain with only small differences in altitude. Its average slope (about 0.25‰) was one of the reasons for building channel network here (Kováčová, 2017).

The longitudinal slopes of single channels of channel network are also very low. This fact had impact to production of bed silts on the channel bottom. The thickness and structure of bed silts influence mutual interaction between groundwater and water level in channel network (Baroková and Šoltész, 2014). As important characteristics influencing this interaction was determined the permeability of silts, expressed by saturated hydraulic conductivity value of silts. Komárňanský channel which is the subject of this study, is shown in Fig. 2. Komárňanský channel is a drainage subarea of Váh River drainage area.

At Fig. 3 is shown the view at Komárňanský channel.

Material and methods

Komárňanský channel is the largest one of three main channels of ŽO channel network. This channel was built in the late 19th century for drainage primary, now is used also for irrigation function. Komárňanský channel is supplemented from the Váh river over pumping station Komárno – Nová Osada and it connects with Chotárny channel through a manipulating objects northwest of the Okoč village. The last measured length of Komárňanský channel was about 28 km. The channel width was in range 10–29 m, the measurements of channel depth registered maximal values up to 2.7 m (according to located cross-section profiles). The values of saturated hydraulic conductivity in aquifers nearby this channel K_{fs} were 0.40–3.4 x 10^{-3} m s^{-1} (Mišigová, 1988).

The last measurements of silting of whole Komárňanský

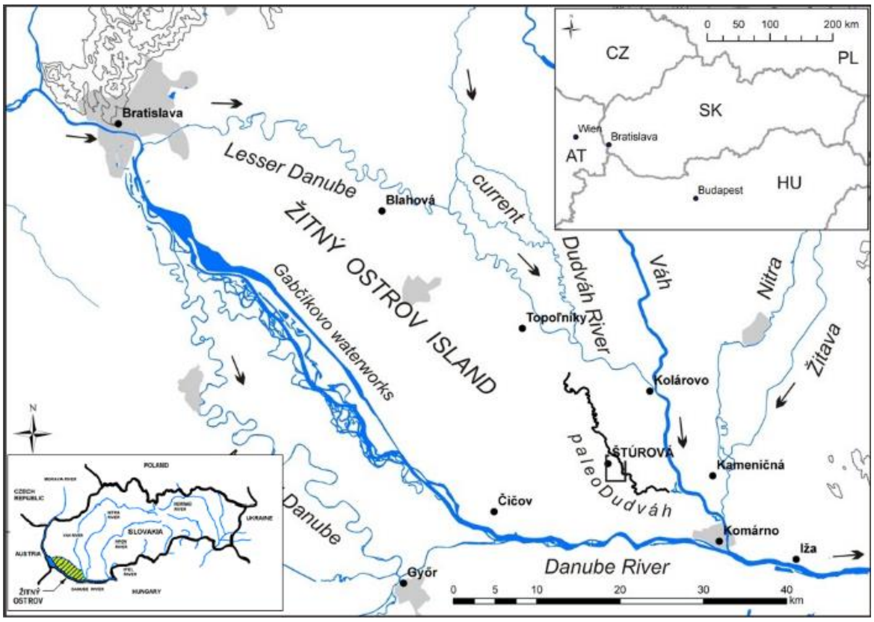

Fig. 1. Location of the ŽO area.

Fig. 2. Plan view of Komárňanský channel.

Fig. 3. View at Komárňanský channel.

channel were realized in 2019 from the displaceable inflatable boat by simple drill hole. The distance of cross-section profiles along the channel varied between 1.0–1.5 km. In all channel cross-section profiles there was measured the water depth and channel bed silt thickness with step 1.0–2.0 m along the channel width. The samples of channel bed silt were taken in these selected cross-section profiles where the largest channel bed silt thickness was noticed – in 8 cross-section profiles. Our oldest measurements of channel network silting up come from 1993. Fig. 4a) shows the state of silting at 15 rkm of Komárňanský channel in 1993, for comparison the Fig. 4b) shows the state of silting at the same 15 rkm of Komárňanský channel in 2019.

Fig. 5 illustrates the assummed silting dynamics during period 1993 to 2019. An example silting in rkm 15 has the decreasing tendency with time - highest in 1993, lowest in 2019. The following are the possible explanations: movement of the bed material, deposition of organic matter, erosion along the channel, maintenance of the channels just to mention a few. All these factors affect the thickness of the sediments. Comparison of the graphs of silting between 1993 and 2019 yields: 0.3 m thickness of silt in rkm 15 versus 0.6 m of silt in the same rkm 15. Hence the difference in silting is 0.3 m in 26 years, which represents on average 0.0115 m/year. Similar calculation can be done for any interval across the section.

Sediment sampling was conducted using the 04.23 Sediment Core Sampler, a rod operated type Beeker. This instrument collects the samples of sediments in 1 m long acrylic tube as shown in Fig. 6a, b. The silt sample was taken from each selected cross-section profile, then from each whole sample a part from top, middle and bottom layer was extracted and thus 24 samples of silts were obtained. Next, the granularity analyses for each disturbed sample were performed, which was a base for saturated hydraulic conductivity computation.

Determination of saturated hydraulic conductivity from granularity analysis

As it was mentioned above several empirical formulas for determination of hydraulic conductivity from granularity exist, but it is possible to apply only a few of them because their limited validity, which will be discussed below.

Therebefore we used for calculation of saturated hydraulic conductivity of bed silts K_d at Komárňanský channel the relationships by Beyer-Schweiger and Špaček (Špaček, 1987). In these relationships the value of saturated hydraulic conductivity K_d is function of d_{10} – particle diameter in 10% of soil mass and d_{60} – particle diameter in 60% of soil mass. Both these parameters were determined from granularity curves of all extracted

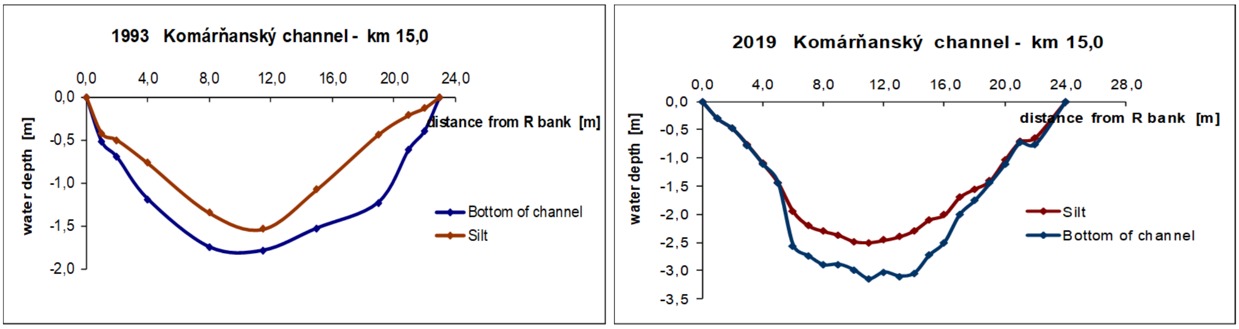

a) *b)*

Fig. 4. Comparison of Komárňanský channel silting at 15 rkm – the cross-section in 1993(a) and in 2019 (b).

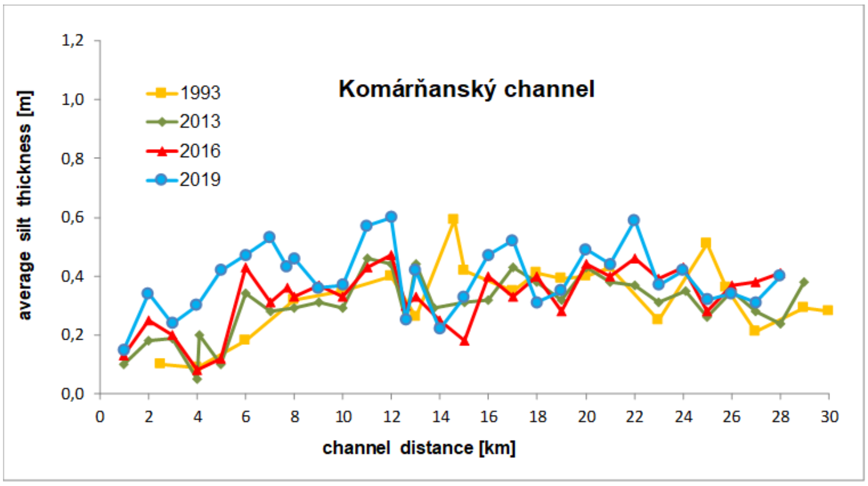

Fig. 5. Komárňanský channel silting during period 1993 to 2019.

a) *b)*

Fig. 6. Sediment sampling from boat (a), an acrylic tube with silt sample (b).

Table 1. **Saturated hydraulic conductivity values K_d based on measurements in 2019 – formulas by Bayer-Schweiger, Špaček I., Špaček II.**

Channel	Komárňanský			
Channel stationing [rkm]	***Silt layer***		***K_d [m s^{-1}]***	
		Bayer-Schweiger	***Špaček I.***	***Špaček II.***
2.0	top	-	5.33×10^{-07}	-
	middle	-	2.53×10^{-07}	-
	bottom	-	2.60×10^{-07}	-
7.0	top	-	4.10×10^{-07}	1.68×10^{-06}
	middle	-	-	2.92×10^{-05}
	bottom	-	-	2.45×10^{-05}
9.0	top	$2.56.10^{-08}$	5.00×10^{-07}	-
	middle	-	4.13×10^{-07}	-
	bottom	-	1.01×10^{-06}	-
12.0	top	-	8.07×10^{-07}	-
	middle	-	5.18×10^{-07}	-
	bottom	-	6.37×10^{-07}	-
20.0	top	-	1.19×10^{-06}	-
	middle	-	-	1.24×10^{-05}
	bottom	8.20×10^{-05}	-	1.98×10^{-04}
23.0	top	-	4.44×10^{-07}	-
	middle	-	7.35×10^{-07}	-
	bottom	-	5.70×10^{-07}	-
25.0	top	$5.04.10^{-08}$	6.94×10^{-07}	-
	middle	-	2.52×10^{-07}	-
	bottom	-	8.66×10^{-07}	-
28.0	top	-	2.40×10^{-07}	-
	middle	$1.09.10^{-08}$	3.34×10^{-07}	-
	bottom	-	5.06×10^{-07}	-

[-] symbol means that variables d_{10} and d_{60} are outside of validity range for application of Beyer-Schweiger and Špaček formulas

disturbed samples of Komárňanský channel bed silts. The equations of Bayer-Schweiger, Špaček I. and Špaček II. formulas and the calculation of saturated hydraulic conductivity values have been already cited in the paper published previously (Dulovičová, 2019). As was aforementioned these equations compute the saturated hydraulic conductivity as a function of d_{10} and $d_{60,}$ the conditions of validity depend on d_{10} and d_{60} as well. The valid values of saturated hydraulic conductivity from disturbed samples K_d along the Komárňanský channel according to Beyer-Schweiger, Špaček I. and Špaček II. formulas are summarized in Table 1. The source of the results is the previous publication (Dulovičová, et al., 2020).

We were interested to try using also other empirical formulas based on the grain size analyses. Our selection was following: 1. - the formula according to Hazen I.; 2. – formula according to Bayer; 3. – USBR formula and 4. – formula according to Orechova (all these formulas were in the past used in commercial software GeoFil (User's manual of software set GeoFil) and also were published in the past (e.g. Dulovičová and Velísková, 2005).

The Hazen I. formula, used for assessment of saturated hydraulic conductivity $K_{d\,H\,I.}$ [m s^{-1}], is:

1. Hazen I.
$$K_{dHI.} = \frac{116.(d_{10})^2}{100} \tag{1}$$

where ´
d_{10} – particle diameter in 10% of soil mass [cm];
condition of validity is: $d_{15} < 0.6$ [cm].

The Bayer formula $K_{d\,B}$ [m s^{-1}], has a form:

2. Bayer
$$K_{dB} = U^b.\mathrm{a}.(d_{10})^2 \tag{2}$$

$$U = \frac{d_{60}}{d_{10}}$$

where
d_{10} – particle diameter in 10% of soil mass [cm];
d_{60} – particle diameter in 60% of soil mass [cm];
a, b – constant factors – for consolidated soils a = 0.01; b = -0.23;
U – coefficient of uniformity;
conditions of validity are:
0.06 [cm]< d_{10} < 0.6 [cm] ∧ U < 20.

The USBR formula $K_{d\,USBR}$ [m s^{-1}], is:

3. USBR

$$K_{dUSBR} = \frac{0.36.(d_{20})^{2.3}}{100} \tag{3}$$

where
d_{20} – particle diameter in 20% of soil mass [mm]; condition of validity is: 0.01 [mm] < d_{20} < 2.0 [mm].

The Orechova formula $K_{d\,Or}$ [m s^{-1}], has a form:

4. Orechova

$$K_{dOr} = \frac{640.(d_{17})^2}{86400} \tag{4}$$

where
d_{17} – is particle diameter in 17% of soil mass [mm]; condition of validity is: $g_{0,063}$ [mm] < 35 %, it means that is valid for soils with fraction less than 0.063 mm content < 35 %.

The valid values of saturated hydraulic conductivity from disturbed samples of silts along the Komárňanský channel K_d according to these 4 formulas were calculated and summarized in Table 2.

Table 2. Saturated hydraulic conductivity values K_d based on measurements in 2019 – formulas by Hazen I., Bayer, USBR, Orechova

Channel	Komárňanský				
Channel stationing [rkm]	***Silt layer***	K_d [m s^{-1}]			
		Hazen I.	***Bayer***	***USBR***	***Orechova***
2.0	top	6.68x10^{-08}	-	5.67x10^{-09}	8.01x10^{-09}
	middle	1.21x10^{-08}	-	-	-
	bottom	1.16x10^{-08}	-	-	-
7.0	top	3.76x10^{-08}	-	1.15x10^{-09}	6.00x10^{-09}
	middle	7.25x10^{-06}	3.10x10^{-08}	3.98x10^{-08}	2.49x10^{-07}
	bottom	4.64x10^{-06}	1.87x10^{-08}	3.36x10^{-08}	1.85x10^{-07}
9.0	top	4.19x10^{-08}	2.00x10^{-10}	-	-
	middle	3.35x10^{-08}	-	-	-
	bottom	2.35x10^{-07}	-	4.84x10^{-09}	1.90x10^{-08}
12.0	top	1.59x10^{-07}	-	5.67x10^{-09}	2.27x10^{-08}
	middle	6.14x10^{-08}	-	1.15x10^{-09}	4.74x10^{-09}
	bottom	7.84x10^{-08}	-	-	-
20.0	top	3.51x10^{-07}	-	2.38x10^{-08}	4.63x10^{-08}
	middle	1.35x10^{-06}	4.92x10^{-09}	3.98x10^{-08}	1.85x10^{-07}
	bottom	-	6.43x10^{-07}	2.07x10^{-06}	9.07x10^{-06}
23.0	top	4.19x10^{-08}	-	-	-
	middle	1.34x10^{-07}	-	4.84x10^{-09}	2.27x10^{-08}
	bottom	7.84x10^{-08}	-	1.34x10^{-09}	7.41x10^{-09}
25.0	top	8.46x10^{-08}	3.92x10^{-10}	8.29x10^{-10}	-
	middle	1.16x10^{-08}	-	-	-
	bottom	1.86x10^{-07}	-	8.08x10^{-09}	2.96x10^{-08}
28.0	top	1.16x10^{-08}	-	-	-
	middle	1.81x10^{-08}	-	-	-
	bottom	5.61x10^{-08}	-	-	1.71x10^{-09}

[-] symbol means that variables d_{10}, d_{15}, d_{17}, d_{20} and d_{60} are outside of validity range for application of Hazen I., Beyer, USBR and Orechova formulas

Results and discussion

Sometime in the field it is not possible to extract undisturbed samples of bed silts or sediments. However, it is necessary to find out the rate of their permeability. One way is the determination of bed silt permeability using granularity analyses.

As mentioned above, according to publication (Dulovičová et al., 2020), the computation of saturated hydraulic conductivity uses the empirical formulas by Beyer-Schweiger, Špaček I. and Špaček II. As an input data were used the measurements from year 2019. These formulas are based on particle diameter d_{10} and d_{60}. These two variables control the validity of application (Šurda et al., 2013). The d_{10} and d_{60} were determined separately for top, middle and bottom layer of extracted samples along Komárňanský channel. The values of saturated hydraulic conductivity of disturbed samples extracted from top, middle and bottom layer of bed silt K_d according to Beyer-Schweiger and Špaček formulas are summarized in Table 1. We obtained 72 calculated values K_d, but only 29 of them were the valid values K_d due to the condition of the validity. These valid values K_d reached from 1.09 x 10^{-08} to 1.98 x 10^{-04} m s^{-1} (Dulovičová et al., 2020).

In this study we decided to use other formulas for calculation of saturated hydraulic conductivity K_d which are according to Hazen I., Bayer, USBR and Orechova. These formulas contain the variables d_{10}, d_{17}, d_{20} and d_{60}. Conditions of validity of these formulas are also function of d_{10}, d_{15}, d_{17}, d_{20} and d_{60}. The calculated values of saturated hydraulic conductivity K_d according to Hazen I., Bayer, USBR and Orechova formulas are summarised in Table 2. This computation produced 96 calculated values K_d, but only 57 of them were the valid values due to the condition of the validity. These values K_d reached from 2.00 x 10^{-10} to 9.07 x 10^{-06} m s^{-1}.

In the case of application Bayer-Schweiger formula we obtained only 4 valid K_d values: in rkm 9.0 and 25.0 were these values from top layer, in rkm 28.0 from middle layer and in rkm 20.0 from bottom layer of silt, they changed from 10^{-5} to 10^{-8}. Using by Špaček I. formula we obtained 20 valid K_d values: in rkm 2.0, 9.0, 12.0, 23.0, 25.0 and 28.0 from all three layers (top, middle and bottom), they varied from 10^{-6} to 10^{-7} m s^{-1} at which 10^{-7} predominated. In rkm 7.0 and 20.0 the valid values were obtained only from top layer of silt and their range was also from 10^{-6} to 10^{-7} m s^{-1}. Using by Špaček II. formula we obtained only 5 valid K_d values: in rkm 7.0 from all three layers, in rkm 20.0 from middle and bottom layer, these values varied from 10^{-4} to 10^{-5} m s^{-1}, with dominance 10^{-5}.

We used the count of valid results computed from each individual formula as a criterion for recommending the formula. As was mentioned above, for Bayer-Schweiger formula we received 4 results, for Špaček I. formula we received 20 results and for Špaček II. formula 5 results. Since the d_{10}, d_{60} meet requirement for validity in 20 cases by Špaček I. formula, we concluded the Špaček I. formula is the best fitting formula for calculation of saturated hydraulic conductivity of silts along the Komárňanský channel.

In the case of application of Hazen I., Bayer, USBR and Orechova formulas for calculation of saturated hydraulic conductivity values of bed silt K_d the results were following. Using by Hazen I. formula we obtained 23 valid K_d values: in rkm 2.0, 7.0, 9.0, 12.0, 23.0, 25.0 and 28.0 from all three layers, in rkm 20.0 only from top and middle layer. The values varied from 10^{-6} to 10^{-8} m s^{-1} at which 10^{-8} predominated. Using by Bayer formula we obtained only 6 valid K_d values: in rkm 7.0 and 20.0 from middle and bottom layer, in rkm 9.0 and 25.0 from top layer. The values varied from 10^{-7} to 10^{-10} m s^{-1}. Using by USBR formula we obtained 14 valid K_d values: in rkm 7.0 and 20.0 from all three layers, in rkm 2.0 from top layer, in rkm 9.0 from bottom layer, in rkm 12.0 from top and middle layer, in rkm 23. 0 from middle and bottom layer and in rkm 25.0 from top and bottom layer of silt. The range of these values was from 10^{-6} to 10^{-10} m s^{-1}at which 10^{-9} predominated. Using by Orechova formula we obtained also 14 valid K_d values: in rkm 7.0 and 20.0 from all three layers, in rkm 2.0 from top layer, in rkm 9.0 from bottom layer, in rkm 12.0 from top and middle layer, in rkm 23. 0 from middle and bottom layer, in rkm 25.0 and 28.0 from bottom layer of silt. The range of these values was from 10^{-6} to 10^{-9} m s^{-1}.

For illustration the Fig. 7a, b, c, d, e, f, g, h shows the graphical presentation of results K_d over the top, middle and bottom layer in 8 cross-section profiles along the Komárňanský channel, which were obtained by 4 different formulas (Hazen I., Bayer, USBR and Orechova).

As before, we used the count of valid results computed from each individual formula as a criterion for recommending the formula. As was mentioned above, for Hazen I. formula we received 23 results, for Bayer formula we received only 6 results, for USBR formula we received 14 results and for Orechova formula we received also 14 results. Since the d_{10}, d_{15}, d_{17}, d_{20} and d_{60} meet requirement for validity in 23 cases by Hazen I. formula, we concluded the Hazen I. formula is the best fitting formula for calculation of saturated hydraulic conductivity of silts along the Komárňanský channel.

Comparison of all 7 empirical formulas which were used for calculation of saturated hydraulic conductivity values of bed silts K_d shows that the most number of valid values was obtained by application of formula according Hazen I. (23 valid values of saturated hydraulic conductivity). We can say that in the case of using all introduced empirical formulas has shown the most suitable application of Hazen I. formula for calculation of saturated hydraulic conductivity of silts along the Komárňanský channel.

Fig. 8 represents the numbers (counts) of valid results from individual formulas. We used the number of valid computed results (counts) of K_d for quantitative evaluation of each formula. The Hazen I. formula was selected as it gave 23 valid K_d results from the total number of 24.

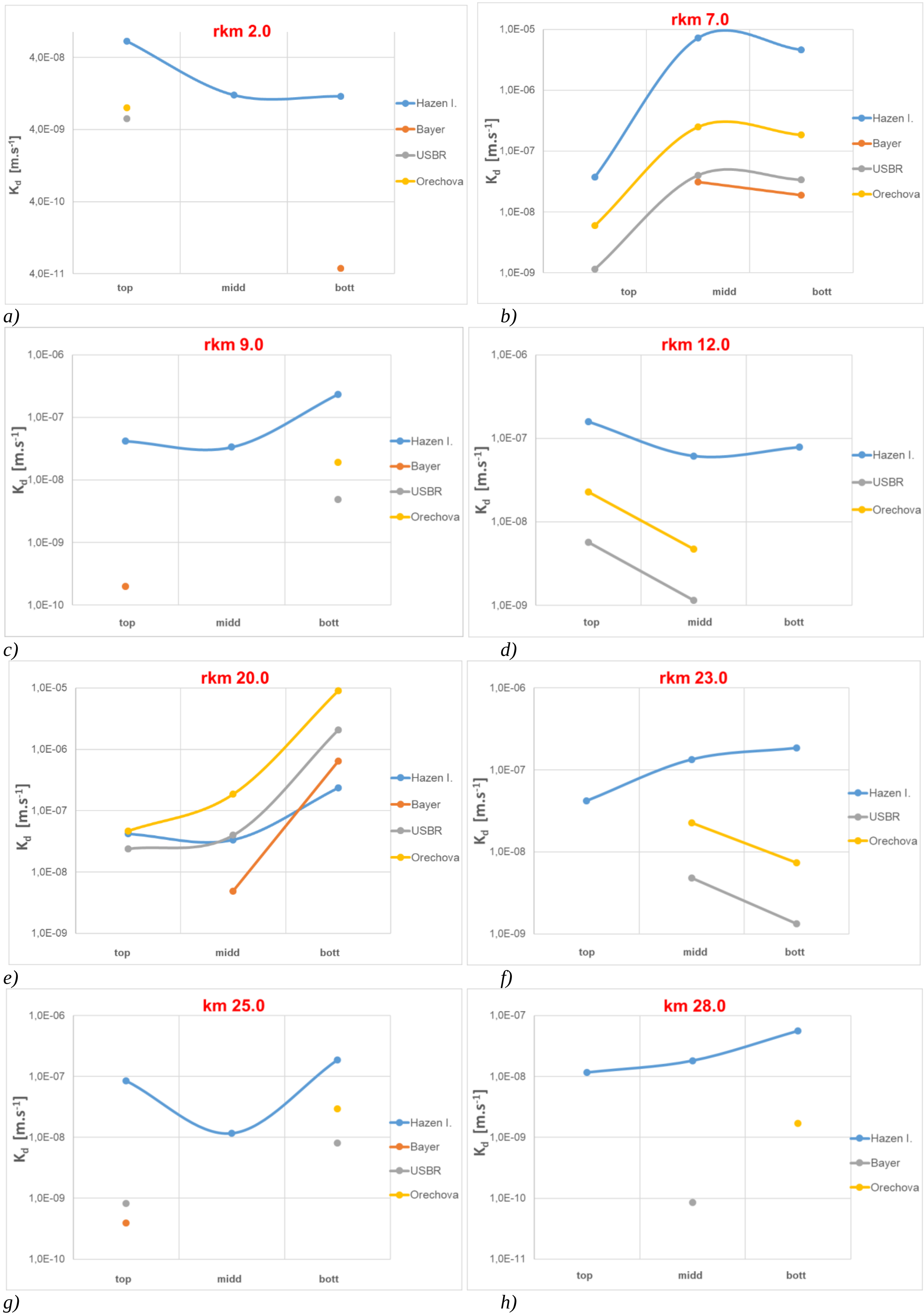

Fig. 7. The graphical illustration of K_d values from single parts of silt in selected cross-sections along Komárňanský channel: a) – km 2.0, b) – km 7.0, c) – km 9.0, d) – km 12.0, e) – km 20.0, f) – km 23.0, g) – km 25.0 and h) – km 28.0.

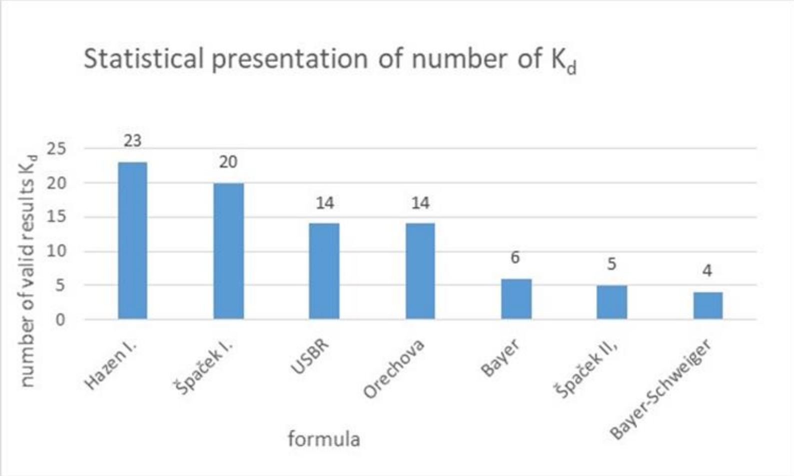

Fig. 8. The illustration of statistical evaluation of data range.

Conclusion

In this paper 7 empirical formulas were used for calculation of saturated hydraulic conductivity of bed silts along Komárňanský channel from 24 extracted silt samples. In the previous study (from year 2020) we used 3 formulas – according to Bayer –Schweiger, Špaček I. and Špaček II. The current study introduces 4 formulas – according to Hazen I., Bayer, USBR and Orechova. All 7 formulas are based on the granularity analyses, with the inputs d_{10}, d_{15}, d_{17}, d_{20} and d_{60}.

The resultant values are presented in Table 1 – the values calculated by Beyer-Schweiger and Špaček I., II. formulas and in Table 2 – the values calculated by Hazen I., Bayer, USBR and Orechova formula. The valid values of saturated hydraulic conductivity of bed silts according to Hazen I., Bayer, USBR and Orechova reached from 2.00 x 10^{-10} to 9.07 x 10^{-06} m s^{-1}. We used the number of valid computed results (count) of K_d to determine the formula´s ability to give results meeting the validity requirements. The recommended formula for calculation of saturated hydraulic conductivity of bed silts in Komárňanský channel for current study is Hazen I., due to the 23 computed valid results out of total number of results 24. The range of valid values is 1.16 x 10^{-8} to 7.25 x 10^{-06} m s^{-1}.

In the next level of our research is needful to compare these results with the values obtained from undisturbed samples of bed silts determined by the laboratory falling head method.

All obtained information about values of bed silts saturated hydraulic conductivity can be used for numerical simulation models and simultaneously they supplement insufficient information for future groundwater level regulation in surroundings of the Komárňanský channel or other channels at the ŽO area.

Acknowledgement

This work is support by the contract VEGA-02/0025/19.

References

Baroková, D., Šoltész, A. (2014): Analysis of surface and groundwater interaction in the Danube river branch system., SGEM Conference Proceedings, 14th SGEM Geo-Conference on Water Resources. Forest, Marine And Ocean Ecosystems, Vol. I., www.sgem.org, ISBN 978-619-7105-13-1/ ISSN 1314-2704, 51–58.

Čelková, A. (2014): The influence of groundwater on soil salinization in the alluvium in the left bank side of Danube river between Komárno and Štúrovo. Acta Hydrologica Slovaca, Vol. 15, No. 2, 413–423 (in Slovak)

Dulovičová, R., Velísková, Y. (2005): The saturated hydraulic conductivity of silts in the main canals of the Žitný Ostrov canal network (in Slovak). Acta Hydrologica Slovaca, Vol.6, No.2: 274–282. ISSN: 1335-6291

Dulovičová, R. (2019): Transformation of bed silts along lowland channel Gabčíkovo – Topoľníky and comparison of their saturated hydraulic conductivity values. Acta Hydrologica Slovaca, Vol. 20, No. 2, 151–159, DOI: 10.31577/ahs-2019-0020.02.0018

Dulovičová, R. Schügerl, R., Velísková, Y. (2020): Actual values of saturated hydraulic conductivity of channel bed silt and its distribution along Komárňanský channel. Acta Hydrologica Slovaca, Vol. 21, No. 1, 98–105, DOI: 10.31577/ahs-2020-0021.01.0012

Duong, T., T, Minh, D. D, and Yasuhara, K. (2019): Assessing the Effects of Rainfall Intensity and Hydraulic Conductivity on Riverbank Stability. MDPI Water Journal 2019, 11(4), 741: Available on https://doi.org/ 10.3390/w11040741, (website visited June 29, 2019)

Gadi, V. K., Tang, Y. R., Das, A., Monga, Ch., Garg, A., Berretta, Ch., Sahoo, L. (2017): Spatial and temporal variation of hydraulic conductivity and vegetation growth in green infrastructures using infiltrometer and visual technique. Catena, Vol. 155: 20–29. https://doi.org/ 10.1016/j.catena.2017.02.024

Ghanbarian, B., Taslimitehrani, V., Pachepsky, A. (2017): Accuracy of sample dimension-dependent pedotransfer functions in estimation of soil saturated hydraulic conductivity. Catena, Vol. 149, Part 1: 374–380. https://doi.org/10.1016/j.catena.2016.10.015

Habtamu, F. M., Tamene, M., Sinshaw, B. G. (2019): Evaluating Saturated Hydraulic Conductivity under

Different Land Use types, Gumara Watershed, Tana Sub-basin. Journal of Academia and Industrial Research (JAIR), Vol. 7, Issue 9: 124, ISSN: 2278-5213, (website visited June 29, 2019)

Hussain, F., Nabi, G. (2016): Empirical Formulae Evaluation for Hydraulic Conductivity Determination Based on Grain Size Analysis. Original Research Paper. Pyrex Journal of Research in Environmental Studies, Vol 3 (3): 026-032, Available on http://www.pyrex journals.org/pjres, (website visited February 17, 2018)

Hwang, H. T., Jeen, S. W., Suleiman, A. A., Lee, K. K. (2017): Comparison of Saturated Hydraulic Conductivity Estimated by Three Different Methods. Water – Open Access Journal, MDPI, 9, 942: 1–15. Available on http://creativecommons.org/licenses/by/4.0. doi:10.3390/w9120942, (website visited January 24, 2017)

Kováčová, V. (2017): Trends of nitrate ions content in Žitný Ostrov channel network. Acta Hydrologica Slovaca, Vol. 18, No. 1, 57–67 (in Slovak)

Kutílek, M. (1978): Vodohospodářská pedologie, Alfa Bratislava, SNTL 04-721-78, 296 p., (in Czech)

Mišigová, I. (1988): Methods of regional assessment of hydraulic properties of the rocks on the Žitný Ostrov. Report IHH SAS, (in Slovak)

Ren, X. W., Santamarina, J. C. (2018): The hydraulic conductivity of sediments: A pore size perspective. Technical note, Engineering Geology, Vol. 233: 48–54. https://doi.org/10.1016/j.enggeo.2017.11.022

Říha, J., Petrula, L., Hala, M., Alhasan, Z. (2018): Assessment of empirical formulae for determining the hydraulic conductivity of glass beads. J. Hydrol. Hydromech., 66, 3, 337–347 DOI: 10.2478/johh-2018-0021 337

Špaček, J. (1987): Determination of filtration coefficient from total grain-size curves. J. Meliorace, Vol. 23, No.1, 1–13 (in Czech)

Šurda, P., Štekauerová, V., Nagy, V. (2013): Variability of the saturated hydraulic conductivity of the individual soil types in the area of the Hron catchment. Nővénytermelés, Vol. 62, supplement, 323–326.

User's manual of software set GeoFil.

Wang, Y., Jin, M., Deng, Z. (2018): Alternative Model for Predicting Soil Hydraulic Conductivity Over the Complete Moisture Range. American Geophysical Union, Available on https://doi.org/10.1029/2018WR023037, (website visited June 29, 2019)

Yusuf, U. S., Slim, M. D., Uchechukwu, E. A. (2016): Hydraulic Conductivity of Compacted Laterite Treated with Iron Ore Tailings. Advances in Civil Engineering, Vol. 2016, Article ID 4275736, 8 pages, Available on http://dx.doi.org/10.1155/2016/4275736

Ing. Renáta Dulovičová (*corresponding author, e-mail: dulovicova@uh.savba.sk)
Ing. Yvetta Velísková, PhD.
Mgr. Radoslav Schügerl, PhD.
Institute of Hydrology SAS,
Dúbravská cesta 9,
841 04 Bratislava
Slovak Republic

DOI: 10.31577/ahs-2021-0022.01.0010

ACTA HYDROLOGICA SLOVACA

Volume 22, No. 1, 2021, 88 – 96

STABLE ISOTOPES OF OXYGEN AND HYDROGEN IN THE TAP WATER IN THE JALOVECKÝ CREEK VALLEY IN HYDROLOGICAL YEARS 2018–2020

Ladislav Holko*, Michal Danko, Patrik Sleziak

We present the results of probably the first monitoring of isotopic composition of tap waters in Slovakia. The isotopic composition ($\delta^{18}O$, $\delta^{2}H$) of the tap water in two municipalities in the Jalovecký Creek catchment in northern Slovakia documented their different sources. The tap water in the Liptovský Mikuláš town (part Ondrašová) is on average isotopically similar to the Váh River water while the tap water in the Jalovec village is similar to the Jalovecký Creek. The temporal variability of the isotopic composition of both tap waters shows the contribution of the isotopically lighter snowmelt water. The consistently high electrical conductivity of the tap water in Jalovec suggests that the water comes from the Mesozoic rocks. The ground water in the alluvium of the Jalovecký Creek sampled in a borehole in Jalovec was isotopically similar to local tap water in summer and isotopically heavier in other seasons. The streamflow mean transit times were about a half of those of the tap waters and the borehole ground water (about 2 years versus about 1 year, respectively).

KEY WORDS: stable isotopes of oxygen and hydrogen, tap water, mountain catchment, mean transit time

Introduction

Isotopes are atoms of the same element that differ in the number of neutrons in the nucleus. Because neutrons have a weight, the atoms containing more neutrons are heavier than the ones with less neutrons. Hydrogen and oxygen as the elements building the water molecule have three isotopes each, i. e. the ^{1}H, ^{2}H, ^{3}H (radioactive) and the ^{16}O, ^{17}O, ^{18}O, respectively. The lighter isotopes are much more abundant than the heavier ones. Excluding the radioactive isotope of ^{3}H (tritium, the isotope of hydrogen that has two neutrons in the nucleus), the natural waters are mixtures of nine combinations of the oxygen and hydrogen isotopes. Three of them are the most significant for hydrology – the most abundant $^{1}H_2{}^{16}O$, $^{1}H^{2}H^{16}O$ (abundance 310 ppm) and $^{1}H_2{}^{18}O$ (abundance 1990 ppm); e.g. Hoefs (1987). If unaffected by the geothermal processes, the isotopic composition of waters on the Earth changes only during the phase changes (evaporation, condensation) and by mixing of different waters. During water evaporation, lighter isotopes move to the vapour more easily than the heavier ones. Because this process is significantly affected by temperature, the water vapour in summer (or at low latitudes) contains more heavy isotopes than in winter (at high latitudes). During precipitation formation in clouds (condensation), heavier isotopes move to a condensate more easily than the lighter ones. Therefore, precipitation at the sea or in coastal areas (the first condensate) is isotopically heavier than that falling at a greater distance from the sea (ocean). Thus, evaporation and condensation create typical isotopic signatures of water that help trace the origin and movement of water in the hydrological cycle. A more detailed information about the concepts is provided e.g. in Kendall and McDonnell (1998) and Aggarwal et al. (2005). The concentrations of hydrogen and oxygen isotopes in water samples (*sample*) are expressed relatively as the δ- values (in ‰), representing the ratios of the heavy to light isotopes related to the same ratios in the international standard (*st*), e.g. in the case of oxygen:

$$\delta^{18}O_{sample} = \frac{(^{18}O/^{16}O)_{sample} - (^{18}O/^{16}O)_{st}}{(^{18}O/^{16}O)_{st}} \tag{1}$$

Plots of $\delta^{2}H$ against $\delta^{18}O$ (the dual isotope plots) are useful in identifying waters of different origin. The $\delta^{2}H$ - $\delta^{18}O$ relationship in precipitation (the input into the hydrological cycle of a catchment) determines the meteoric water line (Craig, 1961) along which usually most water samples plot. Groups of samples plotted at different positions represent waters of different origin (the reasons of different origin may not be explained solely by the isotopes). A number of examples can be found e.g. in Clark and Fritz (1997). Another application of the stable isotopes of hydrogen and oxygen in water utilizes the seasonal variability in the isotopic composition of precipitation (input) and runoff or ground water (output). Damping or time shift of the δ^2H or δ^{18}O in runoff with respect to precipitation allow calculation of the streamflow mean transit/residence time characterizing the time the water spent in a catchment (Zuber et al., 1986; McGuire and McDonnell, 2006; Kirchner, 2016a; 2016b). The third large group of the application of isotopes (perhaps the largest one) uses the two-component mixing model (Pinder and Jones, 1969) to calculate the components of catchment runoff hydrographs, ground water recharge, etc. (e.g. Stichler et al., 1986; Jasechko et al., 2014; Klaus and McDonnell, 2013; Kirchner, 2019).

Monitoring of the isotopic composition of tap water that has been increasingly reported for over a decade, can help in the management of water supply. Bowen et al. (2007) conducted a national-level monitoring of the tap water in the USA. While the intra-annual ranges of tap water isotopic composition were mostly relatively small (i. e. < 10‰ for δ^2H), the spatial variation was very large and similar to that of the isotopic composition of precipitation. Landwehr et al. (2014) concluded that the seasonal differences in the isotopic composition of tap waters in the USA were significant at many places. Zhao et al. (2017) constructed the TapWater Line for China. Good et al. (2014) identified probable situations of the nonlocal water use in the western U.S. by comparisons of the isotopic composition of tap waters and potential water resources within hydrological basins. The bi-annual series of samples from the Salt Lake Valley, USA (spring and autumn 2013 and 2014) allowed clustering of urban tap water into four groups (Jameel and Bowen, 2015). Jameel et al. (2016), using an extended data set (2013–2015) from the same area, found that mean tap water had a lower ^{2}H and ^{18}O concentrations than local precipitation, highlighting the importance of nearby montane winter precipitation as source water for the region. They identified a significant correlation between the water source and demographic parameters including population and income. A multi-year drought in California in 2012–2015 resulted in an increased need to understand the linkages between urban centers, water transport and usage and the impacts of climate change on water resources. Tipple et al. (2017) used stable isotopes of oxygen and hydrogen to improve the understanding of the complex water transport systems and varying municipality-scale management decisions in the San Francisco Bay Area. The isotopic composition of the tap water was consistent with the snowmelt from the Sierra Nevada Mountains, local precipitation, ground water and partially evaporated reservoir sources. They also estimated that about 6.6% of water in one reservoir system evaporated in 2015. Du et al. (2019) used samples of the tap water, precipitation and surface water in the urban area of Lanzhou, China, to construct the Local Tap Water Line and concluded that the isotopic composition of the tap water collected from one single sampling site can be considered as a representative for tap water isotopes in the area with a single tap water source. The tap water was isotopically different from local precipitation, but it was similar to that of the surface water. They concluded that the isotopic composition of tap water in Lanzhou can be used as a representative of isotopes in the surface water. De Wet et al. (2020) used the seasonal variation of δ^{18}O and δ^2H in tap water in South Africa to identify two tap water worlds – the municipalities that are supplied by seasonally invariant sources that have long residence periods, such as ground water, and those supplied by sources that vary seasonally in a manner consistent with evapo-concentration, such as surface water. Such a division of water sources allows for an efficient identification of municipalities that are dependent on highly variable or depleted surface water resources, which are more likely to be vulnerable to climate and demographic changes. Distributions of δ^{18}O and δ^2H in the tap water in France was recently analysed by Daux et al. (2021) to provide isoscapes useful in archaeology, forensics and evaluate whether the modelled data can be used as surrogates for the measured ones. The isotopic composition of the tap water reflected the effects of altitude and distance from the coast with small variations along the year.

To the best of our knowledge, the isotopic composition of tap waters in Slovakia has not yet been monitored and analysed. This article presents the results of a small study carried out in the foreland part of the Jalovecký Creek catchment, located in the Liptovská dolina valley in northern Slovakia. The temporal variability of δ^{18}O, δ^2H in the tap water at two sites based on a frequent sampling is compared with the isotopic composition of local precipitation, streams and ground water. The objectives of our work were to elucidate the origin of the tap waters and the ground water, investigate the temporal variability of their isotopic composition and estimate the mean transit times.

Material and methods

The tap water samples were collected once per week in hydrological years 2018–2020 at two sites. The first one is located in the Liptovský Mikuláš town (Ondrašová, elevation 570 m a.s.l.), the second one in the Jalovec village (696 m a.s.l.). The sampling started in November 2017 and June 2018, respectively. The tap water was allowed to flow for a few minutes before the sample was collected. Water temperature and electrical conductivity (EC) were measured by the handheld meter WTW. The tap water in Liptovský Mikuláš comes from several sources that include ground water from the Váh River alluvium and surface water of the Demänovka Creek from the Low Tatra Mountains. The tap water in Jalovec is supplied by the local spring from the Mesozoic rocks of the Western Tatra Mountains. Ground water samples were collected in Jalovec (at the same site as the tap water samples) from a borehole drilled in the alluvium of the Jalovecký Creek. The depth of the pump was 15 m and the samples were collected after at least of 10 minutes of pumping. Ground water temperature and conductivity were measured as well.

Isotopic composition of precipitation has been sampled at meteorological station in Liptovský Mikuláš (570 m a.s.l.). Monthly composite samples have been collected at the site for the isotopic analyses since November 1990 and the station is included in the WMO-IAEA network GNIP (Global Network of Isotopes in Precipitation). The isotopic composition of local streams has been sampled at three sites. Weekly samples have been collected from the Jalovecký Creek in Liptovský Mikuláš (570 m a.s.l.; catchment area to the sampling site is about 45 km^2). Monthly samples have been collected from the Jalovecký Creek also at the outlet of the mountain part of the catchment (820 m a.s.l., catchment area 22.2 km^2). Monthly samples have been collected also from the Váh River in Liptovský Mikuláš (catchment area about 1100 km^2). Water temperature and conductivity were measured during the sampling by the WTW device.

Isotopic composition of water samples ($\delta^{18}O$ and δ^2H) were measured at the Institute of Hydrology of the Slovak Academy of Sciences the by the off-axis integrated cavity output laser spectroscopy (Picarro L2130-i). Each sample was analysed at least two times with seven injections per vial (Holko, 2015). The results were referenced against the internal laboratory standards calibrated against the primary reference materials and reported as per mil (‰) relative to the Vienna Standard Mean Ocean Water. Typical precision, expressed as the 1-year variance of an internal control standard, was better than ±0.1‰ and ± 1.0‰ for $\delta^{18}O$ and δ^2H, respectively.

The differences in the isotopic composition, EC and water temperature were evaluated by the simple statistics, comparison of boxplots, dual plots of δ^2H against $\delta^{18}O$, and plots of temporal variability. An estimate of the mean transit time was done for the tap waters, ground water in the borehole and for the streams. Minima and maxima of $\delta^{18}O$ and δ^2H were used to provide the amplitude (one half of the difference between the minimum and maximum) and the mean transit time (MTT) was calculated according to formula:

$$\tau_r = \frac{\sqrt{\frac{1}{f^2} - 1}}{2\pi} \qquad (2)$$

where

τ_r – MTT in years,

f – ratio of the $\delta^{18}O$ and δ^2H amplitudes in the output (the tap water, the borehole and the streams, respectively) to the amplitude in precipitation (e.g. Herrmann and Stichler, 1981).

The MTT calculated by either isotope was expressed in month. The calculation assumes that the amplitude in precipitation measured in Liptovský Mikuláš was the same as the amplitude in the infiltration zones of all waters and that the tap water was not formed by mixing of water from several different sources (e. g. the alluvium and a spring).

Results and discussion

The basic statistical characteristics of $\delta^{18}O$, δ^2H, deuterium excess (calculated as d= δ^2H-8* $\delta^{18}O$), water temperature and electrical conductivity are given in Table 1. A significant difference in the mean isotopic composition of the tap waters in Liptovský Mikuláš and Jalovec confirms different water sources. The tap water in Liptovský Mikuláš is isotopically similar to the Váh River water while the tap water in Jalovec is isotopically significantly lighter (considering the analytical error) and similar to the Jalovecký Creek. The average isotopic composition of the Jalovecký Creek does not change much between the outlet of the mountain part of the catchment and the outlet of the entire catchment while the water temperature of the creek increases downstream with the altitude gradient of 0.6°C/100 m. For the comparison, the mean annual air temperatures (1988–2018) at 570 m a. s. l., 750 m a. s. l. and 1500 m a. s. l. (the mean elevation of the mountain part of the Jalovecký Creek catchment) are 7.3°C, 6.5°C and 3.0°C, respectively. The EC of the tap water in Jalovec is much higher than in Liptovský Mikuláš. We do not have the information about the tap water treatment before the supply, but the consistently greater electrical conductivity could be related to different origin of the tap waters (the Mesozoic spring for Jalovec and river alluvium for Liptovský Mikuláš, respectively).

The plot of the isotopic composition of all samples against the local meteoric water line (Fig. 1) allows a more detailed analysis of the links among the tap waters, streams and ground water in the borehole. The meteoric water line represents the precipitation falling in Liptovský Mikuláš, i. e. at a lower elevation than the elevation where the sampled waters infiltrate. A clear difference in the isotopic composition of the tap water in Liptovský Mikuláš and the similarity of the isotopic composition of the Jalovecký Creek at the outlet of the mountains and of the entire catchment (Liptovský Mikuláš) are documented by Figs. 1a and 1b, respectively. While many ground water samples collected in the borehole are different from the Jalovecký Creek water (slightly greater concentrations of heavy isotopes indicated partial contribution of local precipitation in addition to the isotopically lighter water sources), Fig. 1c shows that part of the tap water in Jalovec is isotopically identical with the ground water in the borehole. The temporal variability of isotopic composition of the samples (Fig. 2) reveals that the tap water and ground water in Jalovec are isotopically different in winter and spring (approximately between January and June). The faster decrease in the concentrations of heavy isotopes in the ground water sampled in the borehole during the snowmelt period compared to that of the tap water suggests a greater dynamics of the ground water turnover. On the other hand, the influence of the snowmelt water in the borehole is visible for a longer time than in the tap waters. A smaller decrease in $\delta^{18}O$ found in the tap water in Jalovec in spring 2020 (that is similar to the analytical accuracy) could suggest longer transit time compared to the tap water sampled in Liptovský Mikuláš. However, the data series from Jalovec are not complete in springs 2018 and 2019. The occurrence of the isotopically lighter

Table 1. **Statistical characteristics of the isotopic composition, water temperature and electrical conductivity of the samples; Stdev is the standard deviation, *Cv* is the coefficient of variation [%]; MTT is the mean transit time [months] calculated from the oxygen and deuterium, respectively**

Samples	Characteristic	Average	Min	Max	Stdev	*Cv* abs	MTT
L. Mikuláš precipitation	$\delta^{18}O$ [‰]	**-9.7**	-16.9	-4.4	3.4	35.1	-
L. Mikuláš tap		**-10.5**	-11.1	-10.1	0.2	1.9	24/30
Jalovec tap		**-11.2**	-11.5	-10.6	0.2	1.8	26/37
Jalovec borehole		**-10.8**	-11.2	-10.3	0.2	1.9	26/30
Jalovecký Creek mountains		**-11.3**	-12.4	-10.7	0.3	2.7	14/17
Jalovecký Creek L. Mikuláš		**-11.1**	-12.1	-9.8	0.3	2.7	10/12
Váh River L. Mikuláš		**-10.6**	-11.4	-9.8	0.4	3.8	15/17
L. Mikuláš prec.	$\delta^{2}H$ [‰]	**-69**	-128	-32	27	39.1	-
L. Mikuláš tap		**-71**	-74	-68	1	1.4	-
Jalovec tap		**-77**	-79	-74	1	1.3	-
Jalovec borehole		**-74**	-77	-71	1	1.4	-
Jalovecký Creek Mountains		**-76**	-84	-73	2	2.6	-
Jalovecký Creek L. Mikuláš		**-75**	-82	-67	2	2.7	-
Váh River L. Mikuláš		**-72**	-77	-66	3	4.2	-
L. Mikuláš prec.	d-excess [‰]	**8.8**	2	14.7	2.8	31.8	-
L. Mikuláš tap		**13.7**	11.9	14.9	0.5	3.6	-
Jalovec tap		**13**	11	13.6	0.5	3.8	-
Jalovec borehole		**12.4**	9.5	13.8	0.8	6.5	-
Jalovecký Creek Mountains		**14.2**	11.9	14.9	0.6	4.2	-
Jalovecký Creek L. Mikuláš		**13.4**	11	14.6	0.7	5.2	-
Váh River L. Mikuláš		**12.9**	11.3	14	0.6	4.7	-
L. Mikuláš tap	Water temperature	**11.1**	4.3	17.6	4.0	36.0	-
Jalovec tap	[°C]	**11.6**	3.7	16.9	4.1	35.3	-
Jalovec borehole		**9.3**	6.2	13.8	1.5	16.1	-
Jalovecký Creek Mountains		**5.7**	0	12.3	3.9	68.4	-
Jalovecký Creek L. Mikuláš		**7.3**	0	19.8	4.9	67.1	-
Váh River L. Mikuláš		**8.2**	0.4	17.7	5.3	64.6	-
L. Mikuláš tap	Water conductivity	**209**	111	465	44.8	21.4	-
Jalovec tap	[$\mu S\ cm^{-1}$]	**403**	376	419	11	2.7	-
Jalovec borehole		**136**	84	194	24	17.6	-
Jalovecký Creek Mountains		**43**	31	53	5	11.6	-
Jalovecký Creek L. Mikuláš		**139**	61	306	52	37.4	-
Váh River L. Mikuláš		**240**	130	376	60	25.0	-

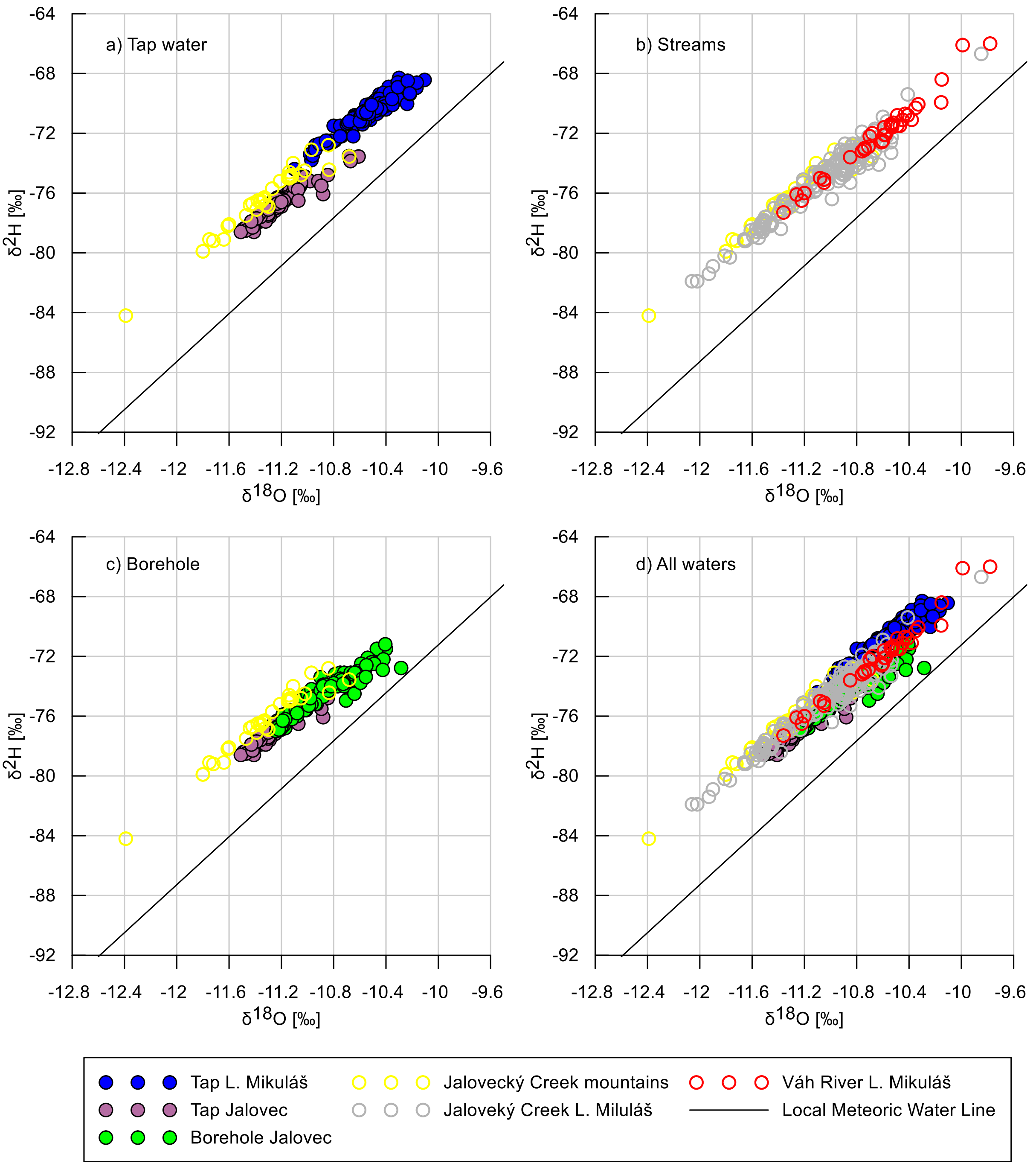

Fig. 1. The dual isotope plots for the sampled waters; a) different water sources of the tap waters, b) similarity in the isotopic composition of the Jalovecký Creek at the outlet of the mountains and at the entire catchment, c) partially overlapping isotopic composition of the borehole water and tap water in Jalovec, d) isotopic composition of all samples of the tap waters, stream waters and the borehole; the isotopic composition of the Jalovecký Creek mountains is shown in all panels to allow a better intercomparison of waters among the panels; the Local Meteoric Water line ($\delta^2H=8.02\delta^{18}O+9.0$) was constructed for the monthly composite data from precipitation station in Liptovský Mikuláš collected between November 2018 and October 2020 (hydrological years 2018–2020).

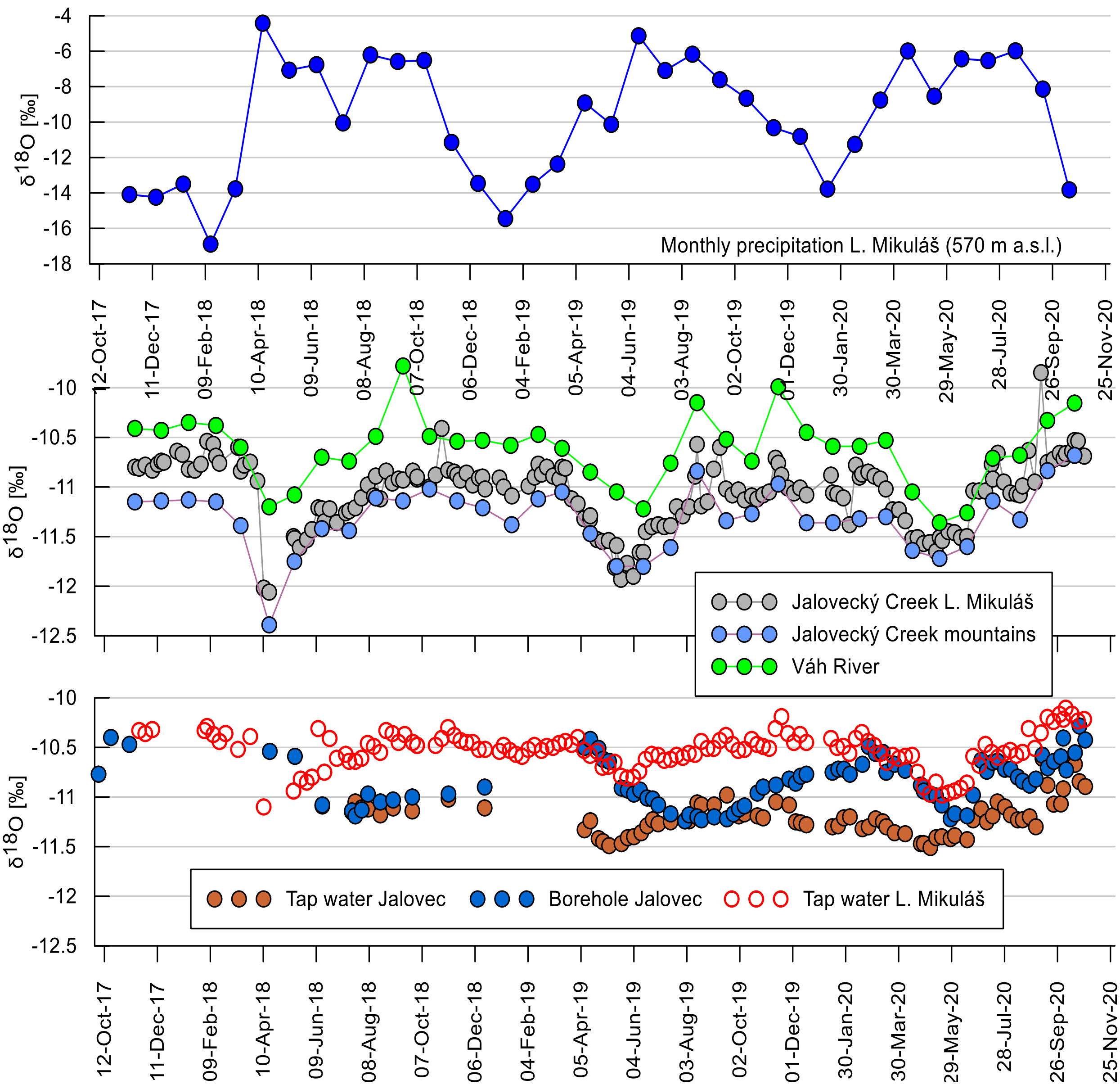

Fig. 2. Temporal variability of the isotopic composition of the samples between November 2017 and October 2020; note that the vertical axis in the uppermost panel has a different scale.

snowmelt water in the borehole is postponed compared to the Jalovecký Creek by about two months in springs 2018 and 2019, but only by two weeks in spring 2020 (Fig. 2). We cannot explain such a different behaviour among different years.

Interesting supplementary information is provided by the electrical conductivity and water temperature (Fig. 3). The EC shows a significant decrease during the snowmelt period, a small increase in the summer and the highest increase in winter before the beginning of the snowmelt in the Jalovecký Creek in Liptovský Mikuláš and in the Váh River.

The highest values occur in winter periods when the streamflow is presumably contributed by water from the longer storage (ground water). The EC variability in the Jalovecký Creek at the outlet of the mountains is much smaller (Table 1). Small temporal variability in EC was found also in the tap water in Jalovec (Fig. 3). The EC variability in the tap water in Liptovský Mikuláš was much higher and similar to that in the Jaloveký Creek

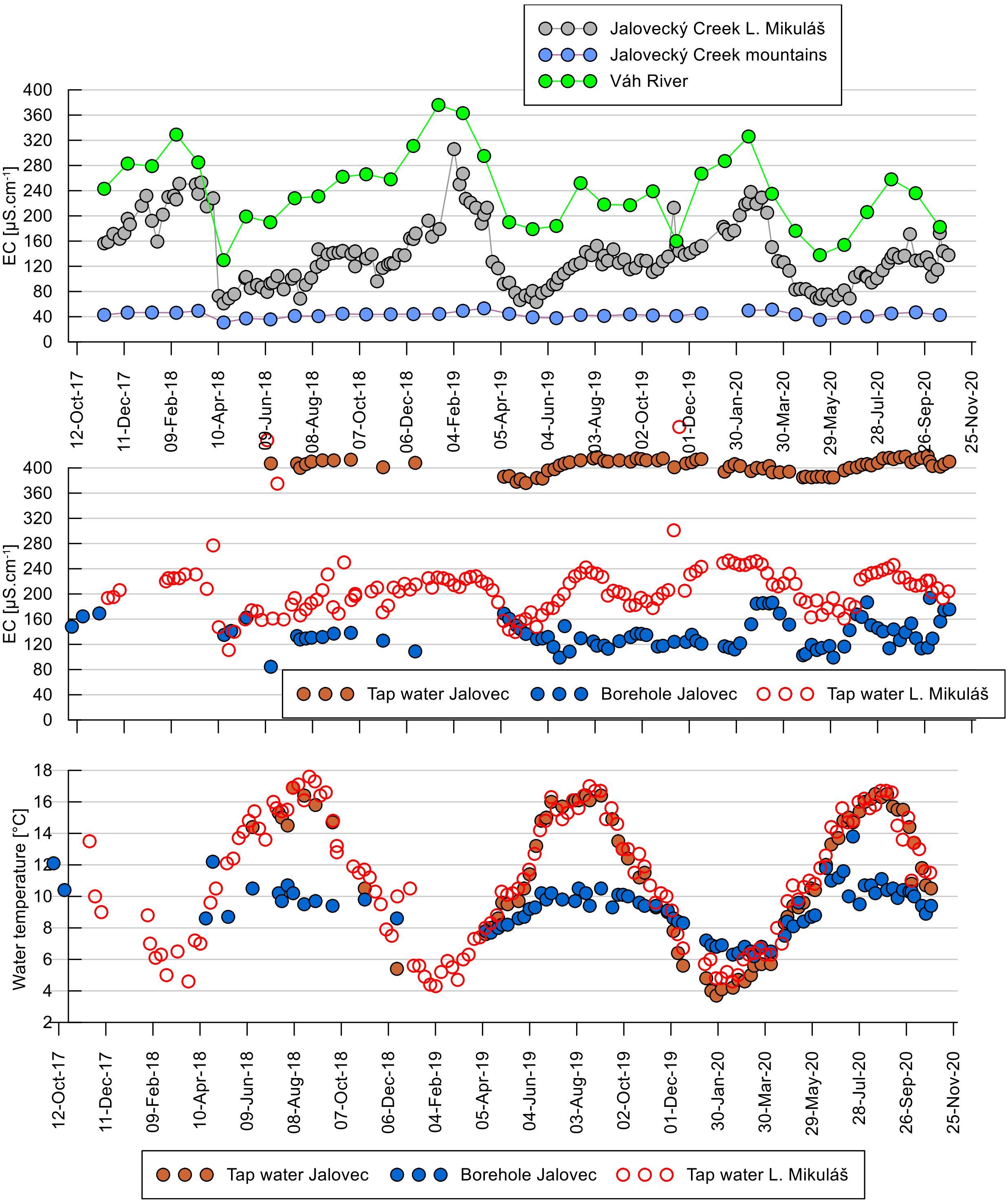

Fig. 3. Temporal variability of the electrical conductivity (EC) and water temperature between November 2017 and October 2020.

in Liptovský Mikuláš. Ground water in the borehole had a more stable EC in 2018 and 2019 (with winter maxima), but the EC time course became similar to that in the Jalovecký Creek in Liptovský Mikuláš since spring 2020.

Although there are gaps in the borehole data until April 2019, we can currently not explain why was the EC time course different in 2019 and 2020. The tap water temperature variability in Jalovec and Liptovský Mikuláš was similar while the ground water temperature had a much smaller amplitude (Fig. 3).

The mean transit times of the tap waters (assuming that the tap water did not originate by mixing of water from several different sources) and the ground water in the borehole are longer than those of the streams (about 2 years versus about 1 year). The differences in the MTT estimated from δ^{18}O and from δ^{2}H are quite great for the tap waters (particularly for Jalovec) while they are relatively similar for the streams (Table 1).

Conclusion

The results of our small study indicate that a more systematic monitoring of the isotopic composition of tap water at a larger area could provide a useful information also in Slovakia. While the basic relationships can be elucidated from the monthly data, the weekly sampling provides a more detailed information, especially about the influence of the snowmelt water.

Acknowledgement

Preparation of this article was supported by the grant from the Slovak Academy of Sciences (VEGA project No. 2/0065/19). We would also like to thank M. Rusina for the help with sampling.

References

Aggarwal, P. K., Gat, J. R., Froehlich, K. F. O. eds. (2005): Isotopes in the Water Cysle. Past, Present and Future of a Developing Science. Springer, Dordrecht., 381 pages.

Bowen, G., J., Ehleringer, J. R., Chesson, L. A., Stange, E., Cerling, T. (2007): Stable isotope ratios of tap water in the contiguous United States, Water Resour. Res., 43, W03419, doi:10.1029/2006WR005186.

Clark, I. D., Fritz, P. (1997): Environmental Isotopes in Hydrogeology. CRC Press. 352 pages.

Craig, H. (1961); Isotopic variations in meteoric waters. Science, vol. 133, 1702–1703.

De Wett, R. F., West, A. G., Harris, Ch. (2020): Seasonal variation in tap water δ2H and δ18O isotopes reveals two tap water worlds. Sci. Rep. 10:13544https://doi.org/ 10.1038/s41598-020-70317-2.

Daux, V., Minster, B., Cauquoin, A., Jossoud, O., Werner, M., Landais, A. (2021): Oxygen and hydrogen isotopic composition of tap waters in France. Geological Society, London, Special Publications, 507, https://doi.org/ 10.1144/SP507-2020-207.

Du, M., Zhang, M., Wang, S., Chen, F., Zhao, P., Zhou, S., Zhang, Y. (2019): Stable Isotope Ratios in Tap Water of a Riverside City in a Semi-Arid Climate: An Application to Water Source Determination. Water, 11, 1441; doi: 10.3390/w11071441

Good, S. P., Kennedy, C. D., Stalker, J. C., Chesson, L. A., Valenzuela, L. O., Beasley, M. M., Ehleringer, J. R., Bowen, G. J. (2014): Patterns of local and nonlocal water resource use across the western U.S. determined via stable isotope intercomparisons, Water Resour. Res., 50, doi: 10.1002/2014WR015884.

Herrmann, A., Stichler, W. (1981): Runoff modelling using environmental isotopes. Birmensdorf: Proceedings of IUFRO Workshop on Water and Nutrient Simulation Models, 41–58.

Hoefs, J. (1987): Stable Isotope Geochemistry. Springer, Berlin.

Holko L. (2015): Syringe life and memory effects in isotopic analyses performed by liquid water isotopic analysers – a case study for natural waters from central Europe. Isotopes in Environmental and Health Studies, DOI: 10.1080/10256016.2015.1090987

Jameel, M. Y., Bowen, G. (2015): Spatio-Temporal Variation in the Isotopic Composition of Tap Water in the Salt Lake Valley. https://digitalcommons.usu.edu/runoff/2015/2015 Posters/20/ accessed in March 2021.

Jameel, Y., Brewer, S., Good, S. P., Tipple, B. J., Ehleringer, J. R., Bowen, G. J. (2016): Tap water isotope ratios reflect urban water system structure and dynamics across a semiarid metropolitan area, Water Resour. Res., 52, 5891–5910, doi:10.1002/2016WR019104.

Jasechko, S., Birks, S. J., Gleeson, T., Wada, Y., Fawcett, P. J., Sharp, Z. D., McDonnell, J. J., Welker, J. M., (2014): The pronounced seasonality of global groundwater recharge. Water Resour. Res., 50, 8845–8867, DOI: 10.1002/2014WR015809.

Kendall. C., McDonnell, J. J., Eds. (1998): Isotope Tracers in catchment Hydrology, Elsevier, Amsterdam, 839 pages.

Kirchner, J. W. (2016a): Aggregation in environmental systems – Part 1: Seasonal tracer cycles quantify young water fractions, but not mean transit times in spatially heterogeneous catchments. Hydrol. Earth Syst. Sci., 20, 279–297.

Kirchner, J. W. (2016b): Aggregation in environmental systems – Part 2: Catchment mean transit times and young waterfractions under hydrologic nonstationarity. Hydrol. Earth Syst. Sci., 20, 299–328.

Kirchner, J. W. (2019): Quantifying new water fractions and transit time distributions using ensemble hydrograph separation. Theory and benchmark tests. Hydrol. Earth. Syst. Sci., 23, 343–349.

Klaus, J., McDonnell, J. J. (2013): Hydrograph separation using stable isotopes: Review and evaluation. Journal of Hydrology, 505, 47–64. https://doi.org/10.1016/j.jhydrol. 2013.09.006.

Landwehr, J. M., Coplen, T. B., Stewart, D. W. (2014): Spatial, seasonal, and source variability in the stable oxygen and hydrogen isotopic composition of tap waters throughout the USA. Hydrological Process. 28, 5382–5422.

McGuire, K. J., McDonnell. J. J. (2006): A review and evaluation of catchment transit time modeling. Journal of Hydrology, 330, 543–563.

Pinder, G. F., Jones, J. F. (1969): Determination of the ground-water component of peak discharge from the chemistry of total runoff. Water Resources Research 5 (2), 438–445. https://doi.org/10.1029/WR005i002p00438.

Stichler, W., Maloszewski, P., Moser, H., (1986): Modelling of river water infiltration using oxygen-18 data. Journal of

Hydrology, 83, 355–365. doi:10.1016/0022-1694(86) 90161-7

Tipple, B. J., Jameel, Y., Chau, T. H., Mancuso, Ch., J., Bowen, G., J., Dufour, A., Chesson, L., A., Ehleringer, J. R. (2017): Stable hydrogen and oxygen isotopes of tap water reveal structure of the San Francisco Bay Area's water system and adjustments during a major drought. Water Research, vol. 119, 212–224.

Zhao, S., Hu, H., Tian, F., Tie, Q., Wang, L., Liu, Y., Shi, Ch. (2017): Divergence of stable isotopes in tap water across China. Sci. Rep. 7, 43653; doi: 10.1038/srep43653.

Zuber, A. (1986): Review of existing mathematical models for interpretation of tracer data in hydrology. Proc. of an advisory group meeting on Mathematical Models for Interpretation of Tracer Data in Groundwater Hydrology, IAEA TEC-DOC-391, Vienna, 69-116.

RNDr. Ladislav Holko, CSc. (*corresponding author, e-mail: holko@uh.savba.sk)
Ing. Michal Danko, PhD.
Ing. et Ing. Patrik Sleziak, PhD.
Institute of Hydrology SAS
Dúbravská cesta 9
84104 Bratislava
Slovak Republic

DOI: 10.31577/ahs-2021-0022.01.0011

ACTA HYDROLOGICA SLOVACA

Volume 22, No. 1, 2021, 97 – 105

INFLUENCE OF SOIL TYPE ON STATISTICAL CHARACTERISTICS AND GRAPHICAL RESULTS INTERPRETATION OF THE WATER STORAGE DISTRIBUTION MONITORING ALONG THE VERTICAL OF THE SOIL PROFILE

Milan Gomboš*, Andrej Tall, Branislav Kandra, Dana Pavelková

The results of authors of submitted article are based on knowledge that soil retention capacity and soil water availability for plants is different in various soil types. Soil types are defined by texture. It is expected that different retention capacity of soil and different availability of soil water for plants is reflected in changes of moisture regime in space and time. Moisture regime monitoring results captures these changes. Changes can be statistically and graphically analysed and interpreted. The results gained from three localities of East Slovakian Lowland (ESL) of the year 2015 extreme drought period were selected for presentation. Examined localities differs by texture compound. Localities are representing the heaviest clay soils, lighter clay-loam-silty soils and the lightest loam soils. Soil volume humidity was monitored into the depth of 1.00 m by layers of 0.10 m. All samples were taken in the same day in examined localities. Descriptive statistics method was used for data processing. Graphical representation is processed in form of chronoizophlets, line and column graphs. Different monitoring results of volume moisture and water storage in different soil types are quantified in the article. Winter water refill of soil profile, soil water storage, vertical scatter of soil profile moisture volume, temporal and spatial moisture regime changes and availability of soil water for plant cover was analysed within this quantification. The results of analysis and interpretation of moisture regime in different soil environments are necessary for water management of the country and for the design of adaptive measures for the periods of soil drought.

KEY WORDS: monitoring, moisture regime, soil types, hydrolimits

Introduction

The retention capacity and potential of water in the soil affects the water regime of the landscape (Tall and Gomboš, 2013). Retention soil capacity and soil water availability for the crops is different in various soil types (Červeňanská et al., 2016; Červeňanská et al., 2018; Šoltész and Baroková, 2011; Constantin, 2016). Soil types are defined by texture. To assess the water storage available for plant cover, is conventionally use the following characteristic points of the moisture retention curve (soil-water content), wilting point (WP) representing the value of pF = 4.18, threshold point (TP) representing the value of pF = 3.3, field water capacity (FWC) representing the value of pF = 2.0 to 2.7. Wilting point is characterized by moisture at which the crops are insufficiently supplied by water and dies. Treshold point is characterized by moisture at which soil water starts to be unavailable for the plant cover. Biological activity of plants decreases and is oriented on survival. Soil moisture on FWC represents the moisture that stays in the soil after draining of gravity water.

These facts are also reflected in the results of moisture regime monitoring (Skalová et al., 2015). They are significant in statistical and graphical interpretation of results.

The aim of the paper is to show different monitoring results of individual soil types by statistical and graphical methods. The results of monitoring in three localities at the ESL in the extremely dry year of 2015 were selected for the differences presentation.

Methodology

Three localities in the East Slovakian Lowland (ESL) were selected (Fig. 1). Monitoring was carried out into the depth of 1.0 m by 0.1 m layers. The analysed monitoring results belongs into the warm (vegetation) half-year of April to September. Soil sampling was performed on the same day in all three localities. The vegetation period of 2015 was selected for the presentation of monitoring results. This is characterized by the smallest precipitation amount of the growing period from 1970 to 2018 (Fig. 2). Lack of precipitation caused the formation of soil drought. This was manifested by the drying of the vegetation cover (Fig. 3).

From the soil point of view, clay soils predominate in the Senné locality, clay-loam soils in Milhostov and loam soils in Somotor (Fig. 4). Soil moisture was determined by gravimetric method.

In the next step of the work, results were gained by descriptive statistics method and graphical methods in form of chronoizoplets, line and column graphs.

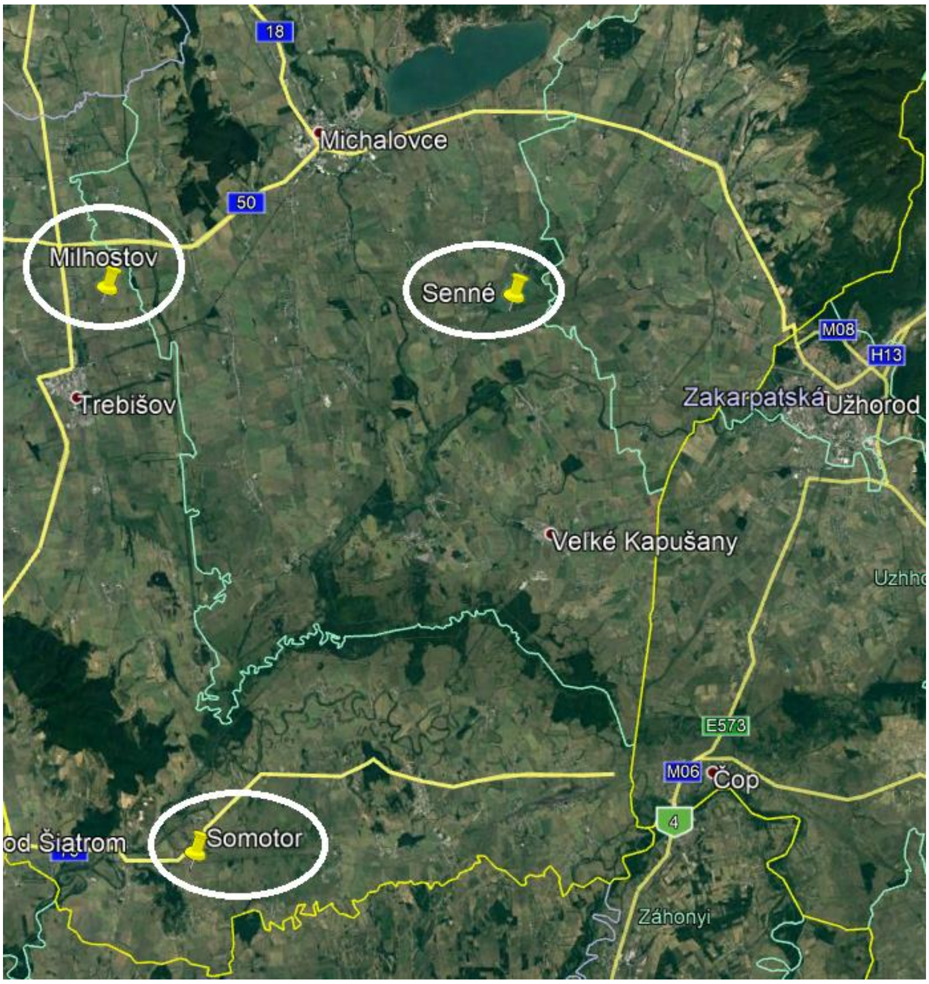

Fig. 1. Location of sampling sites.

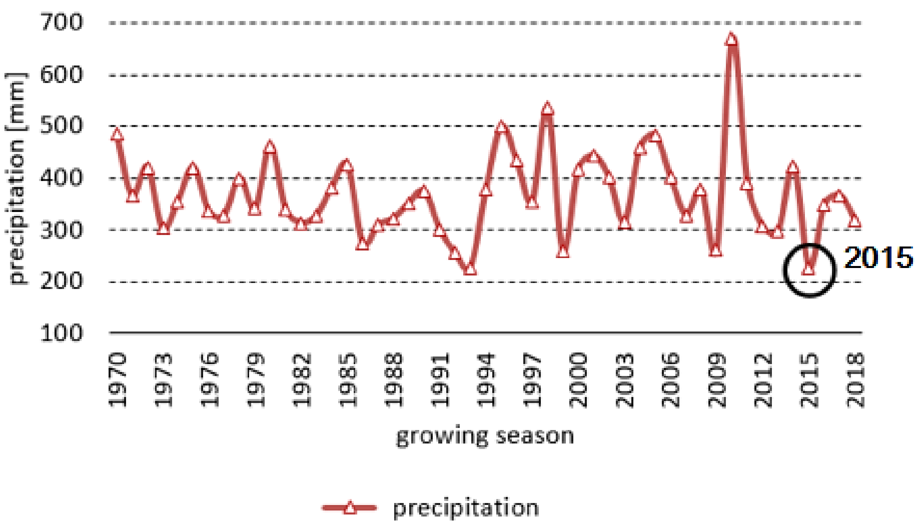

Fig. 2. Total precipitation of vegetation periods 1970–2018.

Fig. 3. *Soil drought manifestations on vegetation cover on the East Slovakian Lowland. The green belt is vegetation along the stream.*

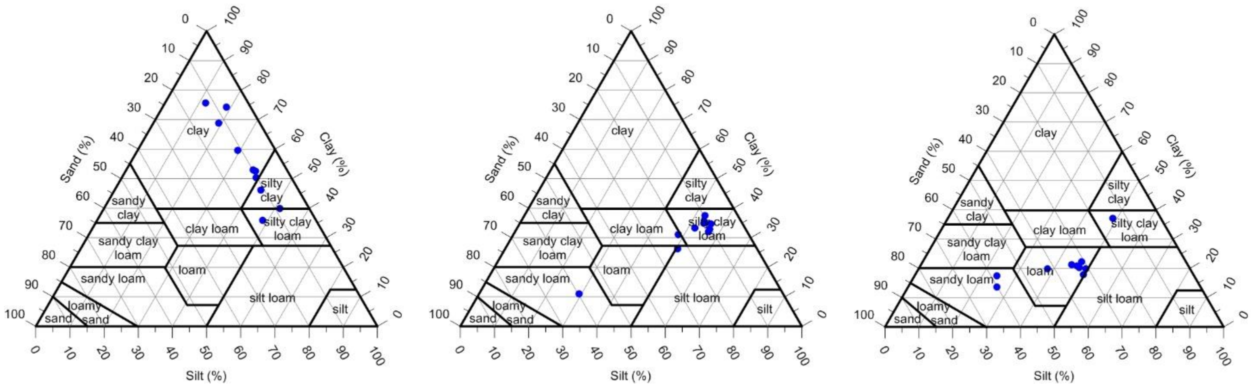

Senné **Milhostov** **Somotor**

Fig. 4. *Soil Identification Triangles by USDA.*

Results and discussion

It is necessary to state the average retention characteristics of sampling profiles into a depth of 1.00 m at the beginning of this chapter and are indicated in Table 1. From Table 1 results that feasible (available) water capacity (FWC–WP) is within the range 150–230 mm. Clay-e soil profile of Senné has the highest retention capacity. It is also the soil profile with the lowest water availability for the plant cover. The most available water for plants is in soil profile of Somotor. This profile has the lowest retention capacity. It is the lightest soil profile with a predominance of loam soils. There are also evident differences between WP, TP, FWC in individual localities.

Characteristics of descriptive statistics of water storage in individual profiles into a depth of 1.0 m are indicated in Table 2. The average value of the water storage in the lightest soil profile in Somotor is within the interval between WP and TP. It is just above TP in other two locations. The lighter the soil profile is, the greater is the variability of water storage. The statistical distribution of water storage is flatter than the normal distribution in all cases. The distribution steepness is higher than normal. The median is not the same as the average. The stated statistical shape characteristics also have a graphic form of expression, which is not mentioned in this article due to its extent.

Soil profile volumetric moisture measurements along the vertical of individual localities are indicated in Fig. 5. All measurements were executed on the same day during the same hydrometeorological conditions. The above figure aptly shows the variability of moisture over time and space in different soil environments. Envelope curves were constructed on the borders of the individual images. These indicates the variation range of the volume moisture along the vertical of the soil profile. A thick red line passes through the centre of the representation showing the average volume moisture values. From the figure results that envelope curves approach each other in the depth at heavy, clayey soil. This means that the variability of moisture decreases but the soil water content increases. Lighter soils are vertically uniformly dried in the whole examined profile. The rate of shift of moisture courses, their envelope curves and average values on the moisture axis is given by the soil hydro-physical properties.

Another effective graphical option for displaying monitoring results is shown in Fig. 6. There are indicated results of water storage monitoring in the soil into a depth of 1.0 m in the vegetation years around the year 2015 (range 2013–2020). There are also shown levels of hydro limits (threshold point, wilting point). This type of line display provides the information of the monitored water storage during the vegetal periods in relation to TP and WP. It is also possible to visually (also numerically) identify the replenishment of water storage during the winter using this representation. The process of soil drought formation begins in the following year in case of a low water storage refill during the previous winter half-year. From the above line courses results that the soil sensitivity to soil drought increases with the loss of clay particles in the soil profile. The moisture often drops below the wilting point in the lightest soil profile of Somotor.

Table 3 quantifies the increments of water storage in the examined profiles into a depth of 1 m. It is a numerical expression of the increments shown in Fig. 6. The results show that the largest winter soil water storage increase is in the clay soil profile of Senné. The variability of the winter increase of water storage with respect to the average (*cv* = *sd / avg*) is inversely

Table 1. Parameters of retention characteristics

Locality	Hydrolimits [mm]		
	WP	TP	FWC
Senné	320	480	520
Milhostov	230	310	420
Somotor	170	230	320

Table 2. Statistical characteristics of the water content of the soil in a depth of 1 m

Statistical characteristics	Locality		
	Senné	Milhostov	Somotor
Mean	489.9	349.7	184.7
Standard Error	9.3	12.6	15.8
Median	495.5	357.1	179.8
Standard Deviation	37.3	50.5	59.2
Sample Variance	1393.8	2547.2	3509.5
Kurtosis	-1.5	-1.2	-1.9
Skewness	-0.2	-0.3	-0.1
Range	108.4	159.8	146.6
Minimum	437.8	254.2	105.6
Maximum	546.2	414.0	252.2
Sum	7838.6	5595.2	2585.2
Count	16	16	14
Confidence Level (95.0%)	19.9	26.9	34.2

Table 3. Statistical characteristics of the water content of the soil in a depth of 1 m

Year	Localities								
	Senné			**Milhostov**			**Somotor**		
	vegetation period			vegetation period			vegetation period		
	end	start	increment	end	start	increment	end	start	increment
	[mm]			[mm]			[mm]		
2013	440.4	-	-	-	-	-	-	-	-
2014	491.4	539.5	99	311.0	-	-	244.4	-	-
2015	449.1	546.2	55	317.5	407.0	96	122.4	252.2	8
2016	457.4	565.4	116	339.2	415.8	98	158.6	246.2	124
2017	497.1	534.4	77	340.6	413.3	74	195.3	250.1	92
2018	404.7	550.6	54	325.7	415.4	75	118.0	259.9	65
2019	416	515.8	111	276.4	345.8	20	-	-	-
2020	460.5	552.1	136	325.0	380.4	104	-	-	-
avg	452.1	543.4	92.6	319.3	396.3	77.9	167.7	252.1	71.9
sd	32.4	15.7	31.7	21.7	28.1	31.0	53.0	5.8	49.1
cv	0.07	0.03	0.34	0.07	0.07	0.4	0.32	0.02	0.68

proportional to the content of clay particles. Another possible representation of these results is the column display in Fig. 7.

A very effective display method is the representation of monitored quantities using isolines (isolines, isoplets). An isoline is physically defined as a line along which has the selected scalar of physical quantity the same value. The name of the isoline depends on which quantity it displays. Isolines along which there is the same moisture in the soil profile at different times are called chronoisoplets. A picture of the temporal moisture development in the soil profile is obtained using the chronoisoplets. Fig. 8 shows the course of volume moisture in the examined profiles during the vegetation period of 2015 using this method. The individual moisture levels are also distinguished by colour in the picture. A different humidity regime in different soil environments is evident. The soil profile was dried to

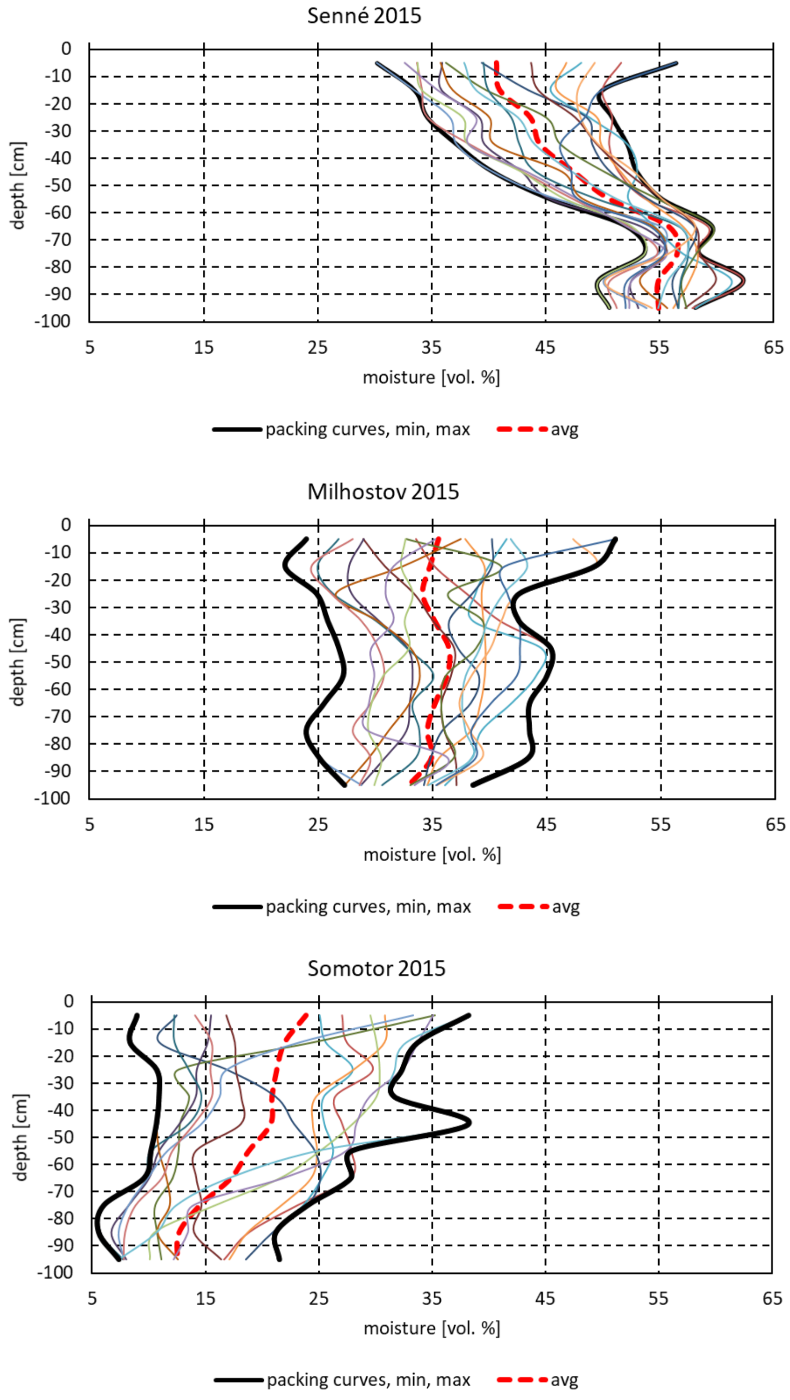

Fig. 5. The course of volumetric moisture along the soil profile vertical up to 1.0 m in 0.1 m layers.

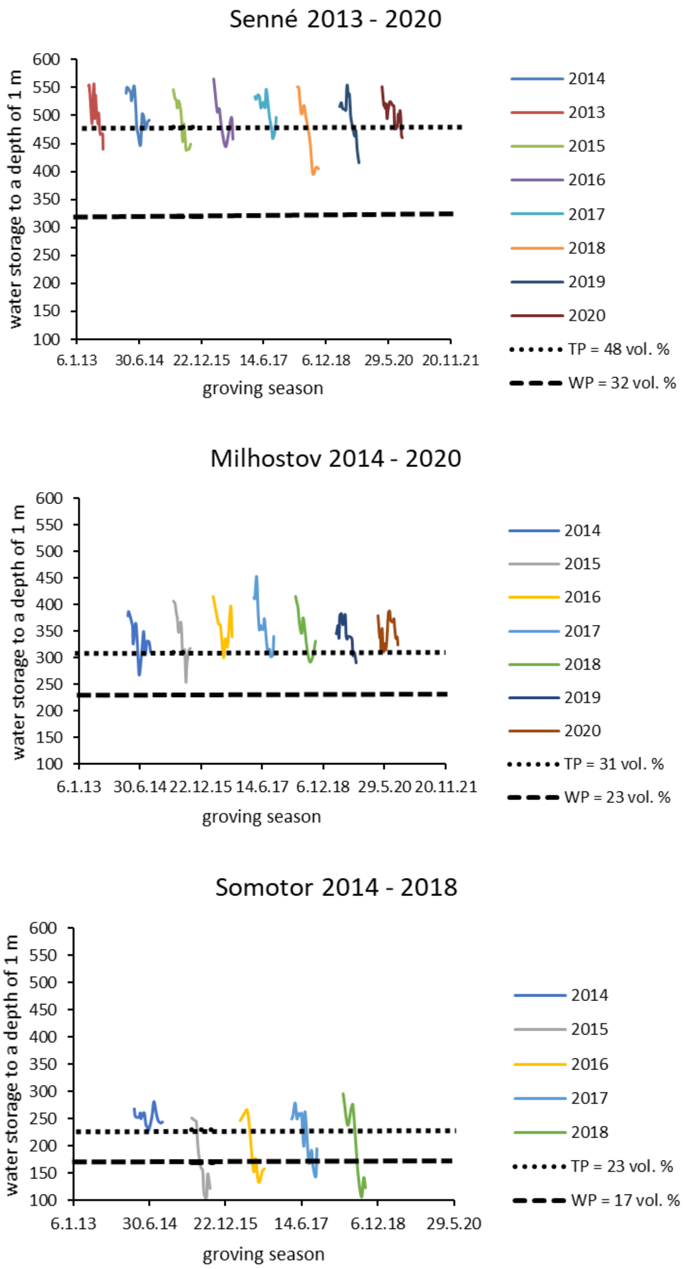

Fig. 6. *Results of water storage monitoring in the soil to a depth of up to 1.0 m during vegetal period.*

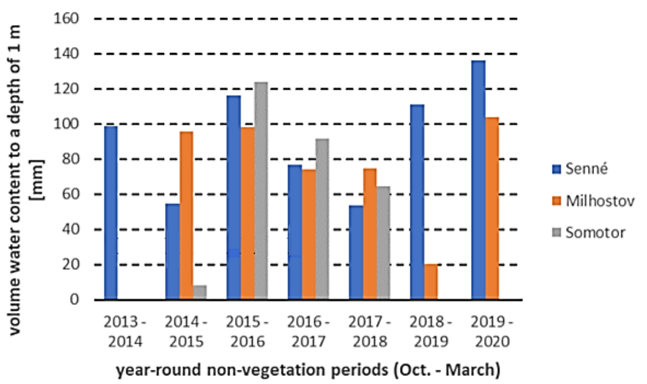

Fig. 7. *Graphical representation of water storage refill in the examined soil profiles during the winter half-year.*

a depth of 0.60 m in Senné locality. Overdrying was throughout the entire profile in the other two localities. Precipitation affected only the upper soil horizons in the Somotor locality.
The information value of listed representation is increased if the limits of moisture intervals between the chronoisoplets are given by the hydrolimits. This also gives an idea of the water availability for the plant cover. Chronoisoplets are determined by FWC, TP and WP hydrolimits in Fig. 9. It is clear from the above representations that the upper soil horizons were in the moisture state between TP and WP in the Senné locality.
These soil horizons reached a depth of max. 0.60 m. The entire monitored soil profile was dried to a moisture level between TP and WP to the depth of 1.00 m in the locality of Milhostov in August. In the Somotor

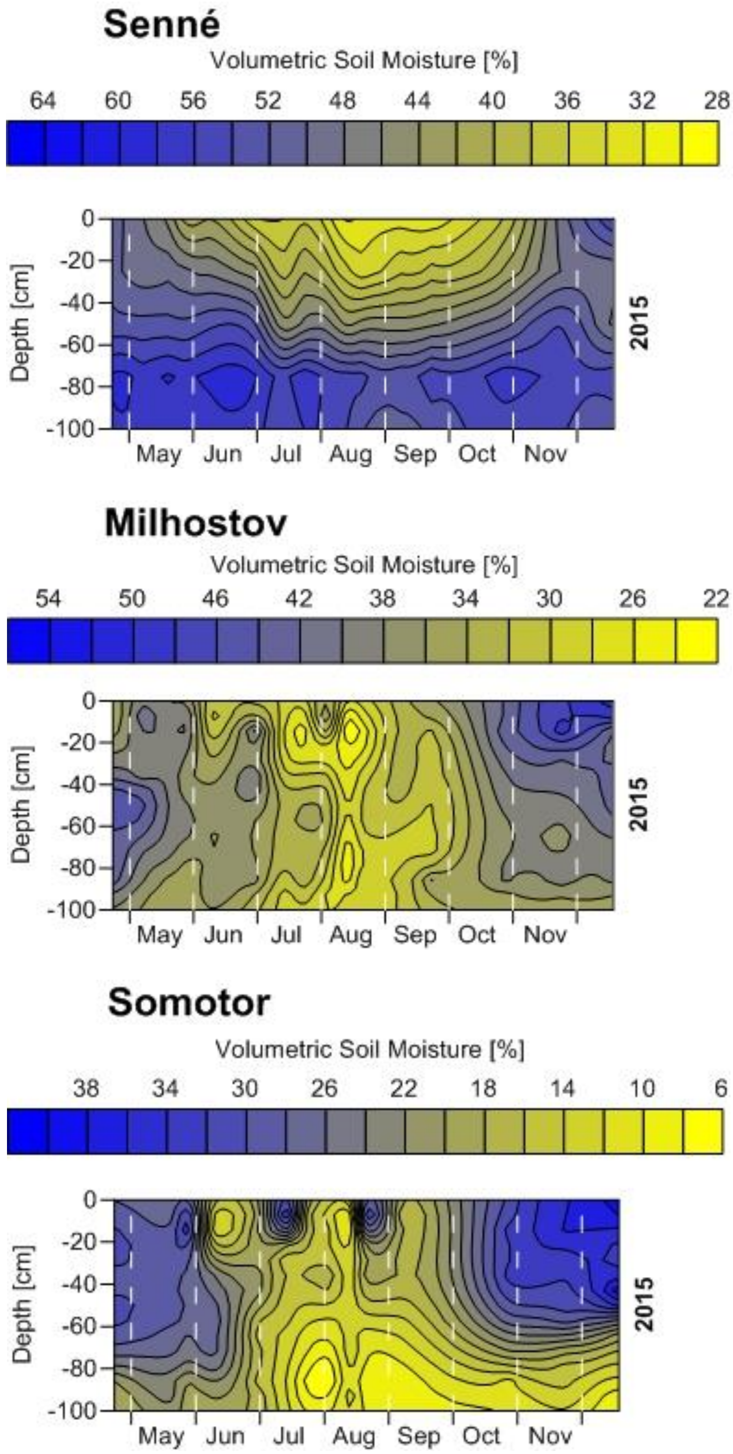

Fig. 8. Moisture isolines course of investigated profiles (chronoisoplets).

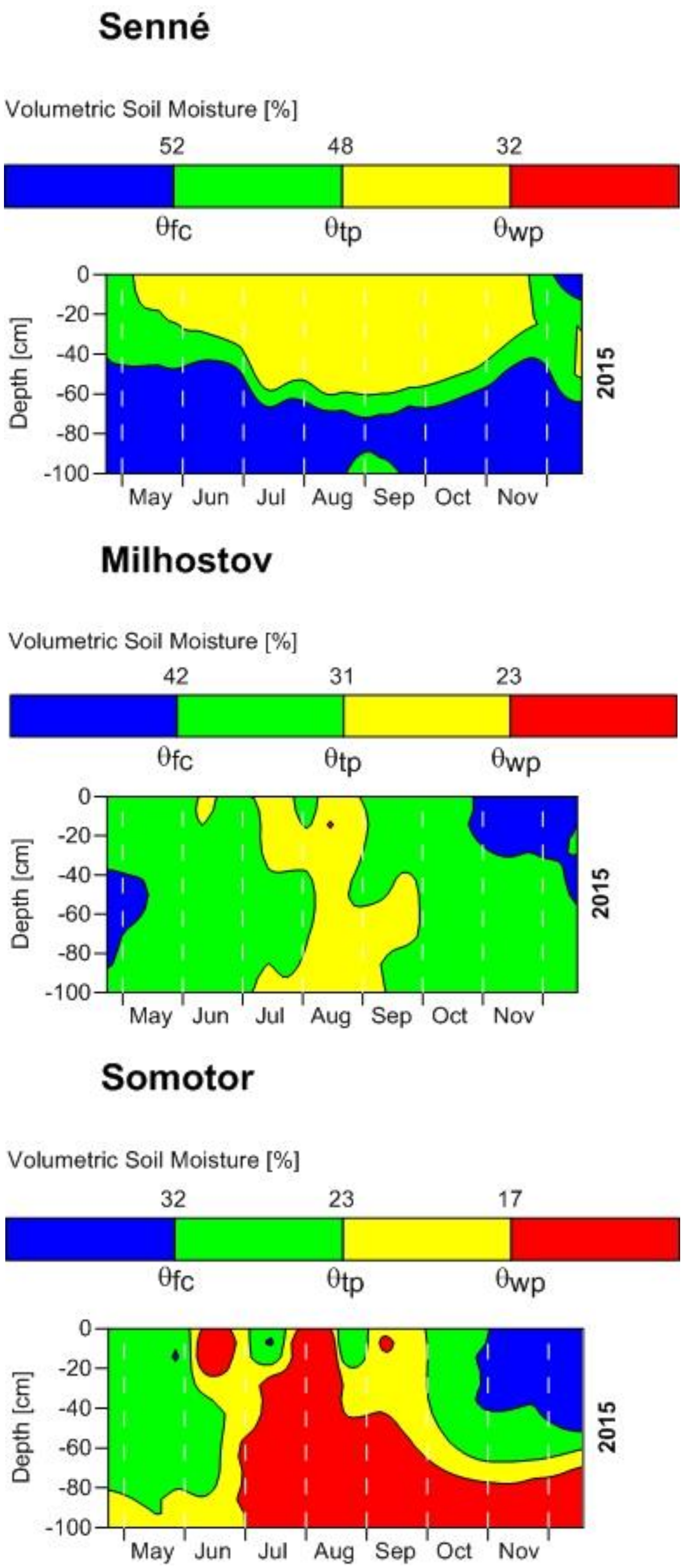

Fig. 9. Chronoisoplets of the investigated profiles qualified by hydrolimits.

locality at the end of July and in the middle of August, the entire soil profile was in a moisture state below the wilting point. The vegetation fall without irrigation in this locality.

Conclusion

The different results of the volumetric moisture monitoring and water supply to a depth of 1.00 m in different soil types was quantified in the article. The results of monitoring in three localities at ESL in the extremely dry year of 2015 were selected for the presentation of differences. The heaviest soils with the highest content of clay particles were in the Senné locality, lighter in the Milhostov locality and the lightest in the Somotor.

The results of monitoring confirmed that the lighter the soil profile is, the greater variability of water storage occurs. The statistical distribution of water storage in the soil was flatter than normal distribution and the steepness larger than normal distribution in all cases. Lighter soils are vertically uniformly dried along the entire examined profile. A significant shift of moisture courses, their envelope curves and average values on the moisture axis was identified numerically and graphically along the vertical of the soil profile. The increment of the clay component in the texture shifts the moisture course to higher values.

The results show that the largest winter increase of soil water storage is in the clay soil profile of Senné (92.6 mm), the smallest in the locality of Somotor (71.9 mm). The variability of winter soil water storage increase with respect to the average ($cv = sd / avg$) is inversely proportional to the content of clay particles (Senné, 34%; Somotor 68%). A graphical analysis showing the chronoisoplet was developed. Analysis proved that the drying of the soil profile manifested itself to a depth of 0.60 m in the Senné locality. In the localities of Milhostov and Somotor, it was in the entire examined profile into a depth of 1.00 m. In order to determine the availability of water for the plant cover in time and space, chronoisoplets were determined with FWC, TP and WP hydrolimits.

The results showed that the upper soil horizons were in the moisture state between TP and WP into a depth of max. 0.60 m the Senné locality. The entire monitored soil profile was dried to a moisture level between TP and WP to a depth of 1.00 m in the locality of Milhostov during August. In the Somotor locality at the end of July and in the middle of August, the entire soil profile was in a moisture state below the wilting point. In other words, the vegetation without irrigation in the said locality has dried up.

The results can be used in country water management designs and designs for adaptation measures to eliminate soil drought.

Acknowledgement

The authors would like to thank for the kind support of the project VEGA 2/0044/20.

References

Červeňanská, M., Baroková, D., Šoltész, A. (2016): Modeling the groundwater level changes in an area of water resources operations. In *Pollack Periodica*. Vol. 11, no. 3, 2016, 83–92. ISSN 1788-1994 DOI: 10.1556/606.2016.11.3.8.

Červeňanská, M., Janík, A., Baroková, D. (2018): Infiltration experiments: Realization and evaluation. In *Pollack Periodica*. Vol. 13, No. 1 (2018), 137–144. ISSN 1788-1994, DOI: 10.1556/606.2018.13.1.12.

Skalová, J., Kotorová, D., Igaz, D., Gomboš, M., Nováková, K. (2015): Regionalizácia pedotransferových funkcií vlhkostných retenčných kriviek pôd Slovenska [Regionaliation of the soil water retention curves of Slovakia using pedotransfer functions]. Bratislava: Slovenská technická univerzita v Bratislave, 2015. 143. ISBN 978-80-227-4455-3 (in Slovak)

Šoltész, A., Baroková, D. (2011): Impact of landscape and water management in Slovak part of the Medzibodrožie region on groundwater level regime. In Journal of Landscape Management. 2011, vol. 2, no. 2, 41–45.

Tall, A., Gomboš, M. (2013): Rajonizácia oblasti na VSN podľa potenciálu objemových zmien pôd. In Acta Hydrologica Slovaca, 2013, vol. 14, no. 1, 66–74. ISSN 1335-6291.

Constantin, A. (2016): Hydraulic Simulation of Water Distribution Network in Rural Area – First Stage in Water Infrastructure Improvement. In 16th GeoConference on Water Resources, Forest, Marine and Ocean Ecosystems : International Multidisciplinary Scientific GeoConferences SGEM2016 : Conference Proceedings, Volume I, Albena, Bulgaria, 30 June – 6 Jul 2016. p. 415–422.

Ing. Milan Gomboš, CSc. (*corresponding author, e-mail: gombos@uh.savba.sk)
RNDr. Andrej Tall, PhD.
Ing. Branislav Kandra, PhD.
Ing. Dana Pavelková, PhD.
Institute of Hydrology SAS
Dúbravská cesta 9
841 04 Bratislava
Slovak Republic

DOI: 10.31577/ahs-2021-0022.01.0012

ACTA HYDROLOGICA SLOVACA

Volume 22, No. 1, 2021, 106 – 112

MOISTURE CHANGES IN THE ORGANIC HORIZON OF THE FOREST SOIL UNDER DIFFERENT TREE SPECIES

Anton Zvala*, Peter Šurda, Justína Vitková

The course of soil moisture in the organic horizon of the forest soil depends mainly on the distribution of atmospheric precipitation and the air temperature during the year. The hydrological significance of the organic horizon of forest soil lies in the rainfall water retention and transfer of water to the lower (mineral) part of forest soil profile. Forest soil with a well developed organic horizon has a higher ability to retain soil moisture than the mineral component of forest soil. The effect of the forest type on the interception capacity is related to the leaf shape.

The primary aim of this paper was to analyse and statistically evaluate the changes of soil moisture in the organic horizons under the different tree species (oak, sycamore maple and beech). The evaluation of soil water storage (SWS) in examined organic horizons during the selected dry and wet period was another aim of paper. The soil moisture was measured with frequency domain reflectometry sensors every 10 days in the period from 29.6.2018 to 15.1.2020. The mean value of soil moisture measured in organic horizon under the oak was 13.44%, under sycamore maple 16.08% and under the beech 19.64%. The SWS in the examined organic horizons was determined for the selected dry (29.6.2018–30.8.2018) and wet period (14.3.2019–31.5.2019). The statistically significant difference was found between SWS in the organic horizon under the beech and other two examined organic horizons only during wet period.

KEY WORDS: moisture changes, organic horizon of forest soil, measurement of soil moisture, vegetation

Introduction

Soil moisture regime is influenced by a number of factors and has a specific dynamics and periodicity during the year (Ištoňa and Pavlenda, 2011). The course of soil moisture depends mainly on the distribution of atmospheric precipitation and the air temperature during the year (Rushton et al., 2006). The soils in the lowlands and hills regularly dry up in the summer and autumn, but there have been many extremely dry years, especially in the last few decades (Van den Hurk et al., 2008). In the dry season, the volumetric soil moisture values are generally low, so the range of the standard deviation is low for drought (Lee et al., 2014). In contrast, the higher variability expressed by the standard deviation of the average volume moisture is in the wet period (Famiglietti et al., 1998; Western and Grayson, 1998). Persistent change in climatic conditions is also reflected in changes of soil water storage, so it is necessary to monitor soil moisture (Robinson et al., 2012). The shortage and uneven distribution of precipitation, which has recently occurred in most of Slovakia, will affect the availability of forest soil water for plants, health and the production of forest trees from the lowlands to mountainous locations. Lowlands and hilly locations will be most endangered by the lack of moisture (Škvarenina et al., 2006; Tužínsky, 2004).

Organic horizon (O-horizon) of forest soil profile is dominated by organic material, consisting of undecomposed or partially decomposed litter, such as leaves, needles, twigs, moss, and lichens, which has accumulated on the surface. O-horizons are not saturated with water for prolonged periods. The mineral fraction of such material is only a small percentage of the volume of the material and generally is much less than half of the weight. (Soil Survey Staff., 1996).

The largest and most important changes in the soil moisture of the forest organic horizons occur during the growing season due to vegetation (Leathers et al., 2000). The hydrological significance of the organic horizon of forest soil is in the distribution of precipitation, which is not captured on forest vegetation and falls on the soil surface. After infiltration of precipitated water into the organic horizon, it is either retained or percolate deeper to the mineral component of the forest soil profile lying below the organic horizon (Kavvadias et al., 2001). Forest soil with a well developed organic horizon has a higher ability to retain soil moisture (Zvala et al., 2018; Xing et al., 2018) than the mineral component of forest soil. A thick layer of forest organic horizon reduces evaporation from the surface and soil moisture at greater depths is less responsive to short-term variability in environmental factors (Dickinson et al., 1991; Western et al., 2002; Wang et al., 2009). The moisture of the organic soil horizon has an impact on the decomposition of organic matter and the formation rate of the organic horizon (Cheng et al., 2018, Couteaux et al., 1995).

Litter layer as an upper part of forest soil organic horizon is an important buffer between the soil and atmospheric precipitation (Acharya et al., 2017; Dunkerley, 2015; Van Stan et al., 2017). Rainwater interception is one of the most important hydrological functions of the forest litter layer. The effect of the forest type on the interception capacity is related to the leaf shape (Li et al., 2013; Sato et al., 2004). Generally, leaf litter with a larger leaf area index attained a higher storage capacity than that with a smaller leaf area index. Li et al., 2021 found that also leaf distribution pattern notably impact leaf litter interception capacity, which is similar to leaf shape and slope impacts. Bulcock and Jewitt (2012) found that the leaf shape in the litter layer was an important factor influencing the interception rate of litter. Sato et al. (2004) noted that litter drainage not only flowed along the bottom of the litter layer but also produced lateral drainage during rainfall, which may be an important factor influencing the water conservation capacity of the litter layer and may also be affected by the leaf shape, forest floor slope, and leaf distribution.

Our hypothesis was that increased interception of litter, containing the leaves with specific leaf shape, may influence the infiltration process into the organic horizon and thus also influence the soil water storage in O-horizon. The primary aim of this paper was to analyze and statistically evaluate the changes of soil moisture in organic horizons under tree species (beech, sycamore maple and oak) with different shape of leaves. The evaluation of soil water storage (SWS) in examined organic horizons in selected dry and wet period was another aim of paper.

Material and methods

Study area

The research was conducted at Železná studnička locality (48° 11' 21" N`; 17° 04' 55" E) in Bratislava. The study area is part of the Bratislava Forest Park, located at the end of Mlynská dolina valley, belonging to the Malé Karpaty Mountains. The Vydrica stream flows through the central part of study area. The Vydrica valley has a hilly terrain with a height difference of about 250 meters.

Geologically, the area is formed by granitoid rocks, limestones, shales, phyllites and amphibolites (Atlas of the landscape of the Slovak Republic, 2002). The altitude of study area is 228 m above sea level. The soil cover is made up of Eutric Cambisols to Dystric Cambisols, associated with Leptosols and with Stagnic Cambisols, from medium heavy to lighter textured and stony weathering products of non-carbonate rocks (Atlas of the landscape of the Slovak Republic, 2002). The loess clays and sand walls occur locally as part of the slope system.

The average annual temperature of the area is 8–9°C and the average rainfall is in the range of 600–700 mm (Lapin et al., 2002).

The study area is dominated by species of the Carpathian foothills with the occurrence of lowland thermophilic species. According to the Catalog of Habitats of Slovakia (Stanová and Valachovič, 2002) following habitats occurs within the study area: beech and fir-beech flower forests, acidophilic beech forests, Carpathian oak-hornbeam forests, xeric and acidophilic oak forests, ash-alder floodplain forests and linden-maple forests. Forest covers about 98% of the study area, the remaining areas are permanent grasslands, water areas, reservoirs and built-up areas. (ENPRO, 2014).

Three measurement points (MP) of soil moisture (Fig. 1.)

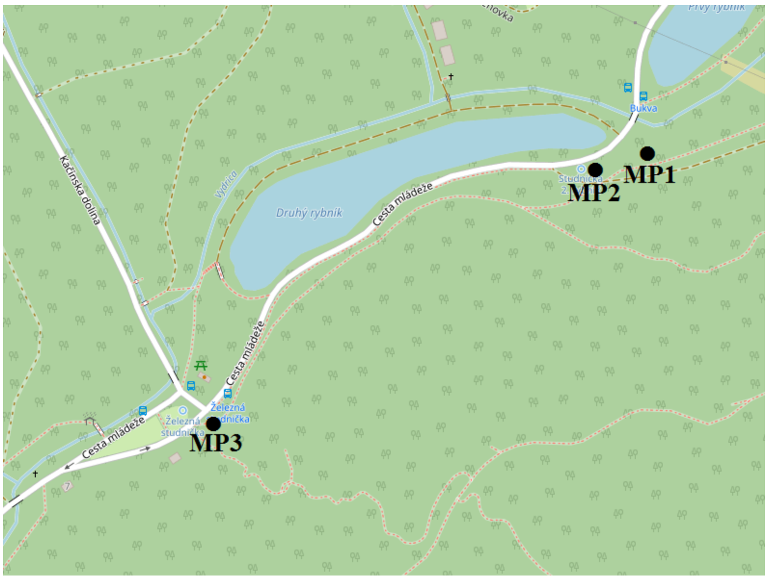

Fig. 1. Location of measurement point MP1, MP2 and MP3 (black points and designation) at study area Železná studnička in Bratislava, Slovakia.

were chosen within the study area to capture the variability of the O-horizons. MP 1 represents the O-horizon under the oak; MP 2 includes the O-horizon under the sycamore maple and MP 3 very deep O-horizon under the beech. All measurement points were on slope with the average depth of the O-horizon of about 10 cm. The mineral horizon is located at a depth of 100 cm from the forest soil surface.

Meteorological data (monthly air temperature, 10 day precipitation totals) for the time period of θ_v monitoring, measured by SHMU at the nearest weather station Bratislava – Koliba are presented at Fig. 2.

Properties of leaves

The more or less decomposed organic material – litter, from which the O-horizon is mostly formed, contains leaves from different tree species with different shape and size.

Oak at MP 1 (*Quercus robur)* has grooved leaves with 4–7 roundish lobes, which reach a maximum of half of the leaf. The upper leaf surface is dark green; the underside of the leaf is blue-greenish. The leaves are 7x3 cm in size (Table 1) and deeply and irregularly lobed, with a short stalk (2–7mm) (Eaton et al., 2016; The Plant List, 2010).

The leaves of sycamore maple at MP 2 (*Acer pseudoplatanus* L.) have long, reddish colored stems, which are usually five-lobed, with the front three lobes are about the same size. The underside of the sycamore maple leaf is gray-green in color, while the top is dark green. The leaf position of this tree is opposite. The leaves turn intense in autumn, from gold-yellow to red. The size depends on the age, but may reach 18x26 cm (Table 1) (Pasta et al., 2016).

The elliptical-shaped leaves of the beech at MP 3 (*Fagus sylvatica* L.) are alternate and petiolate and entire or with a slightly crenate margin, 5–10 cm long and 3–7 cm broad (Table 1), with 6–7 veins on each side of the leaf. The buds are long and slender, 15–30 mm long and 2–3 mm thick (The Plant List, 2010).

Field measurement of soil moisture

Volumetric soil moisture content, θ_v, is the volume of water per unit volume of soil. This is a dimensionless parameter, expressed either as a percentage (% vol), or a ratio [m^3 m^{-3}]. The soil water storage, *SWS*, represents the quantitative amount of water present in the soil with a specific thickness of the soil layer. It is expressed in mm (or cm) as the height of the water layer on an area of 1 m^2 for a soil layer of a given thickness.

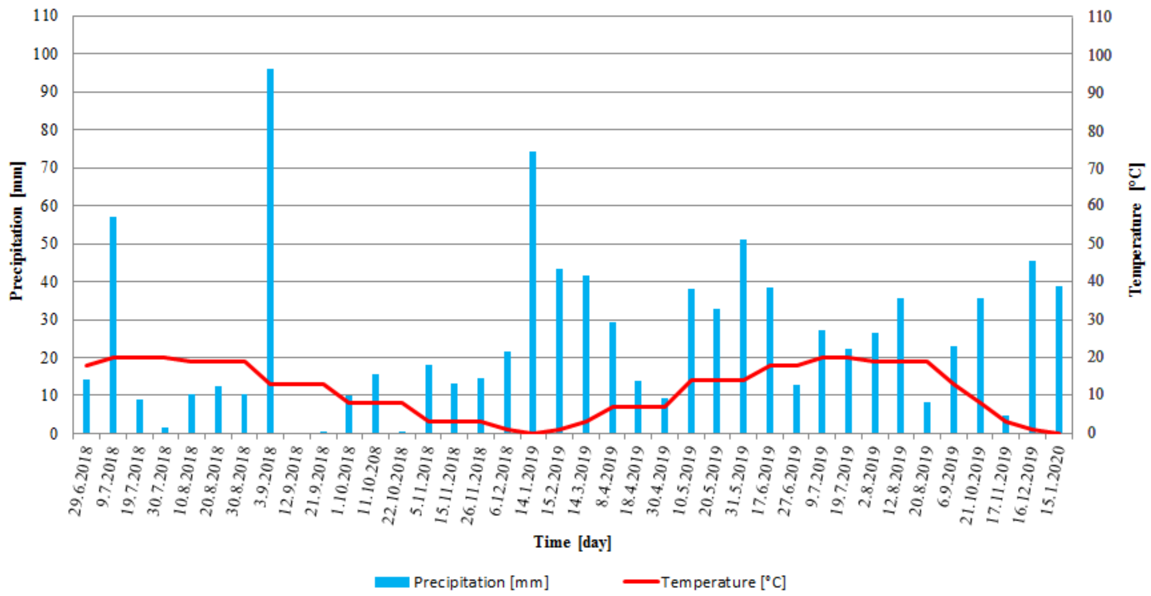

Fig. 2. The daily precipitation totals and the average monthly air temperature for locality Železná studnička, Bratislava for a time period of θv monitoring (29.6.2018–15.1.2020) (SHMU, 2020).

Table 1. Maximal leaf size of trees at MP1 (oak), MP2 (sycamore maple) and MP3 (beech)

Plant	Maximal size of leaf [cm]
oak (*Quercus robur)*	7x3
sycamore maple (*Acer pseudoplatanus* L.)	26x18
beech (*Fagus sylvatica* L.)	10x7

θv was measured with the sensor ThetaProbe ML2x-UM-1.21. ThetaProbe use the FDR method, which belongs to the indirect methods of θ_v measuring. This sensor measures directly the changes in the apparent relative permibility, which is converted into a DC voltage, virtually proportional to soil moisture content. The advantages of indirect methods are the non-destructiveness of the soil sample, the measurement results are immediately available, and the measurement can be performed repeatedly at the same place or stationary measurement with a computer controlled by a recorder of measured θ_v data. The Soil Moisture Meter type HH2 applies power to the sensor and measures the output signal voltage returned. The meter converts the mV reading into soil moisture units using a linearisation table and soil-specific parameters. Linearisation tables are pre-installed for sensors, along with soil parameters for the following soils: organic, mineral, peat mix, coir, mineral wool and Perlite (Eijkelkamp, 2021).
Measurements of soil moisture content were conducted every 10 days in the period from 29.6.2018 to 15.1.2020 on an area of about 4 m^2 at every MP.

Statistical analysis

Differences between the parameters estimated at different measurement points were evaluated using single factor ANOVA with Tukey's Honest Significant Difference (HSD) post-hoc test. The Tukey-Kramer method (also known as Tukey's HSD method) uses the Studentized Range distribution to compute the adjustment to the critical value. The Tukey-Kramer method achieves the exact alpha level (and simultaneous confidence level (1–α)) if the group sample sizes are equal and is conservative if the sample sizes are unequal. The statistical significance in the analysis was defined at $P<0.05$.

Results and discussion

Temporal changes in the moisture content of the deciduous forest organic horizon depend mainly on the distribution of atmospheric precipitation and on the air temperature during the year. Air temperature has here even greater effect than in mineral horizons, as organic material overheats faster and evaporation is more intense. The course of moisture at MP1, MP2 and MP3 was evaluated seasonally according to Fig. 3, 4 and 5. The highest values of moisture content were measured at all sites during spring season. At the start of summer, soil moisture decreases with the increasing air temperature. During the dry and hot summer season, soil moisture decreases to the lowest values. Soil moisture values are during summer reduced also by increased interception of trees and increased transpiration of vegetation. During the autumn, soil moisture values increased with the decrease of air temperature. The highest values of soil moisture during the monitoring period were measured during winter, as a consequence of the snow melting.
The mean values of soil moisture for the whole measurement period have, according Table 2, increasing trend in order MP1 (oak) < MP2 (maple) < MP3 (beech). Statistically significant difference is only between MP1 and MP3. The relationship between the different leaf size and soil moisture content was not confirmed in conditions of our study, as the mean value of soil moisture under the maple (tree with the largest leaves) is not significantly different from other two sites.
We found that the site MP1 (oak) differs most significantly from others. After more detailed analysis, we found that the lowest values of the SWS and soil

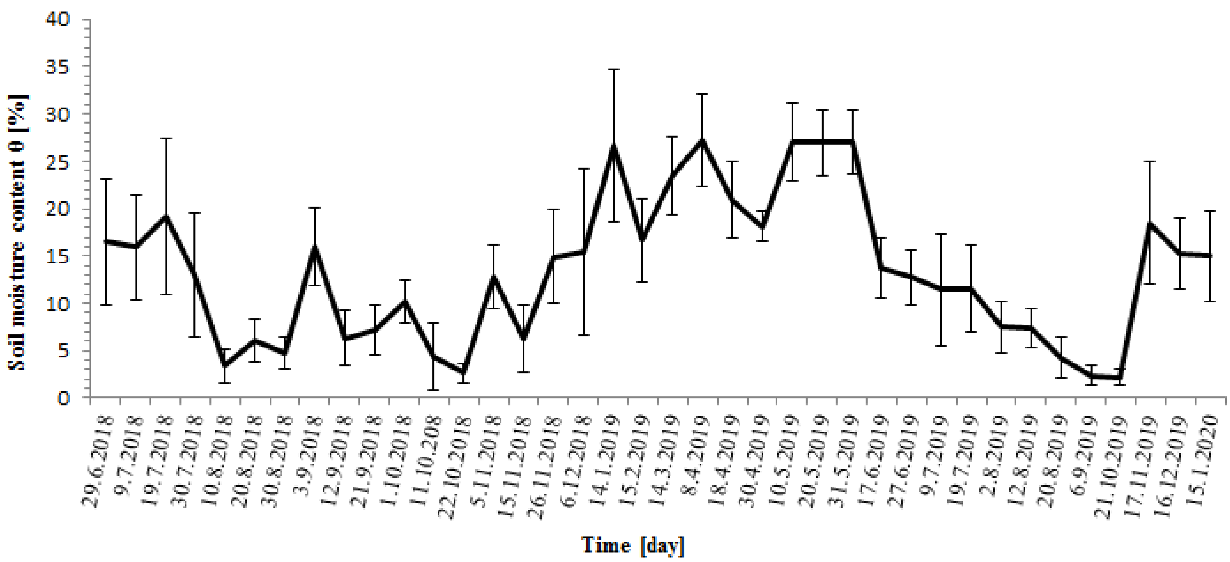

Fig. 3. Volumetric soil moisture content of the organic horizon under the oak with a standard deviation of measurement.

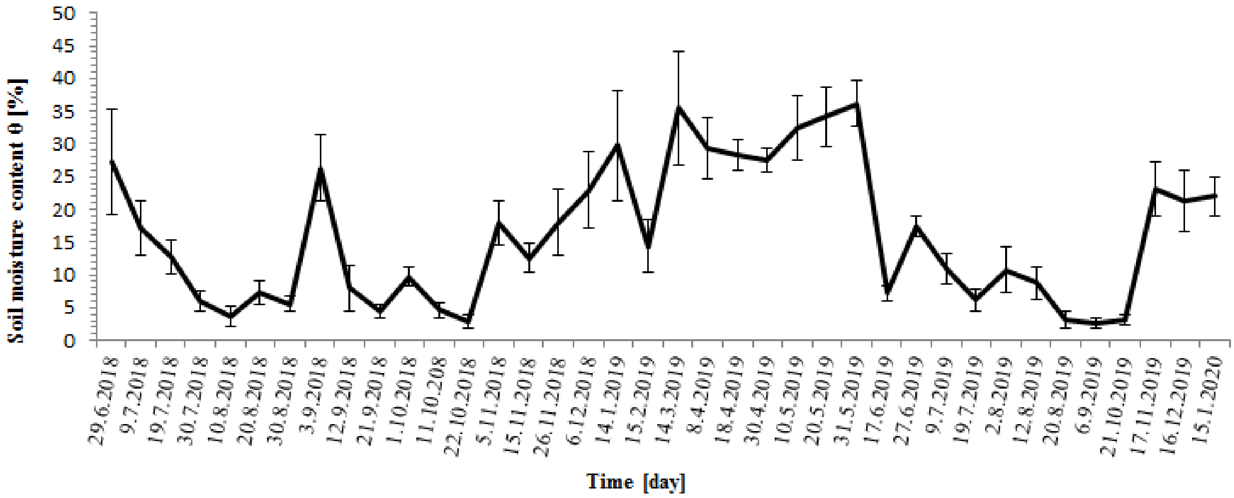

Fig. 4. Volumetric soil moisture content of the organic horizon under the sycamore maple with a standard deviation of measurement.

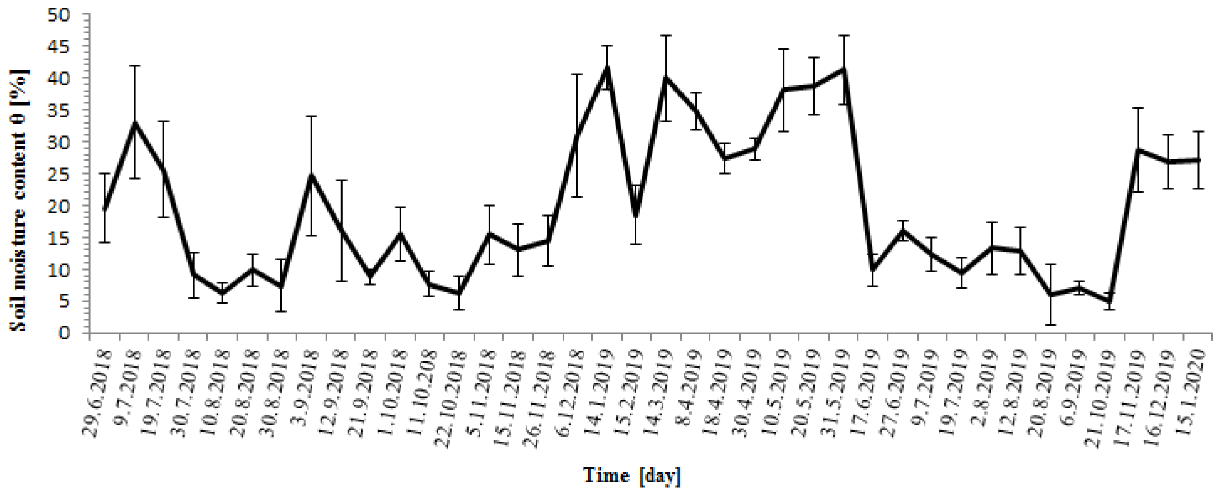

Fig. 5. Volumetric soil moisture content of the organic horizon under the beech with a standard deviation of measurement.

Table 2. Measured values of soil volumetric moisture, θ (±their standard deviation), θ_{min}– minimal value (lowest measured value of all measurements) of θ as the arithmetic mean of the 10 replicate measurements for maple, beech and oak, θ_{max}–maximal (highest measured value from all measurements) θ as the arithmetic mean of the 10 replicate measurements for maple, beech and oak, θ_{mean}–arithmetic mean of θ from every day of monitoring period, values of water storage in the organic horizon, W (±their standard deviation) during dry period 29.6.2018–30.8.2018 (W_{dry}) and during wet period 14.3.2019–31.5.2019 (W_{wet}); Arithmetic means with the same letter are not significantly different from each other (Tukey's HSD test, P>0.05)

Measuring point	θ_{min} [% vol.] (N=10)	θ_{max} [% vol.] (N=10)	θ_{mean} [% vol.] (N=38)	W_{dry} [mm] (N=7)	W_{wet} [mm] (N=7)
MP1 (oak)	2.21 ± 0.8^{a}	27.05 ± 4.11^{a}	13.44 ± 7.70^{a}	1.12 ± 0.64^{a}	2.44 ± 0.37^{a}
MP2 (maple)	2.61 ± 0.84^{a}	36.18 ± 3.57^{b}	$16.08 \pm 10.69^{a,b}$	1.14 ± 0.84^{a}	3.19 ± 0.35^{b}
MP3 (beech)	4.98 ± 1.21^{b}	41.6 ± 3.36^{c}	19.64 ± 11.61^{b}	1.58 ± 1.04^{a}	3.55 ± 0.55^{b}

moisture at MP1 may be related to the different mineral layer here, which is formed by fragments of weathering, accumulated at the foot of the slope. The layer of weathering fragments has better infiltration capacity, which may have effect on drainage of upper organic horizon. The properties of boundary layer between the mineral and organic horizon may have greater effect on SWS than the examined leaf size.

Conclusion

The soil moisture content during the period of measurement at sites MP1, MP2 and MP3 representing organic horizon formed from leaves of different trees (oak, sycamore maple and beech) has increasing trend during spring and autumn months and decreasing during summer. The group means of soil moisture content for whole measurement period increased in order: PM1<PM2<PM3. The statistically significant differences were found between MP1 and MP3. The relationship between the different leaf size and soil moisture content was not confirmed in conditions of our study. Group means of soil water storage (SWS) for whole period of measurement increased in the same order than the soil moisture content. Statistically significant difference between group means of SWS was determined only for the wet period between MP1 (oak) and other two measuring points. Statistically, the site MP3 (oak) differed mostly from other sites, which may be related with the different boundary layer between organic and mineral horizon.

Acknowledgement

This publication is the result of the project implementation the VEGA Grant Agency Issue 2/0096/19 Phytoindication of changes in soil hydrological regime.

References

Acharya, B. S., Stebler, E., Zou, C. B. (2017): Monitoring litter interception of rainfall using leaf wetness sensor under controlled and field conditions. Hydrological Processes, 31, 240–249. http://doi.org/10.1002/hyp.11047

Atlas of the landscape of the Slovak Republic, (2002): Bratislava: Ministry of the Environment of the Slovak Republic and Banská Bystrica: Slovak Environment Agency, 2002. 344. ISBN 80-88833-27-2.

Bulcock, H. H., Jewitt, G. P. W. (2012). Modelling canopy and litter interception in commercial forest plantations in South Africa using the variable storage gash model and idealised drying curves. Hydrology and Earth System Sciences, 16, 4693–4705. http://doi.org/10.5194/hessd-16-4693-2012

Couteaux, M. M., Bottner, P., Berg, B. (1995): Litter decomposition, climate and liter quality, Trends in Ecology & Evolution, Volume 10, Issue 2, 1995, 63–66, ISSN 0169-5347, https://doi.org/10.1016/S0169-5347 (00) 88978-8.

Dickinson, R. E., Henderson–Sellers, A., Rosenzweig, C., Sellers, P. J. (1991): Evapotranspiration models with canopy resistance for use in climate models. Agricultural and Forest Meteorology, 54, 373-388, doi: 10.1016/0168-923(91)90014-H.

Dunkerley, D. (2015): Percolation through leaf litter: What happens during rainfall events of varying intensity? Journal of Hydrology, 525, 737–746. http://doi.org/10.1016/j.jhydrol.2015.04.039

Eaton, E., Caudullo, G., Oliveira, S., de Rigo, D. (2016): Quercus robur and Quercus petraea in Europe: distribution, habitat, usage and threats. In: San-Miguel-Ayanz, J., de Rigo, D., Caudullo, G., Houston Durrant, T., Mauri, A. (Eds.), European Atlas of Forest Tree Species. Publ. Off. EU, Luxembourg.

Eijkelkamp, (2021): Manual soil moisture meter. Available online: https://en.eijkelkamp.com/products/field-measurement-equipment/soil-moisture-meter-hh2.html (accessed on 3 March 2021)

ENPRO Consult s.r.o., (2014): Available online: https://www.enviroportal.sk/sk/eia/detail/revitalizacia-sanatoria-zelezna-studnicka (accessed on 26 March 2021)

Famiglietti, J. S., Rudnicki, J. W., Rodell, M. (1998): Variability in surface moisture content along a hillslope transect: Rattlsnake Hill, Texas. J. Hydrol., 210, 259–281.

Cheng, C. X., Guo, K., Mao, Z. J., Sun, P. F., Ma, H. D., Wang, C. (2018): Effects of soil moisture on litter decomposition of three main tree species in Northeast China. Ying Yong Sheng Tai Xue Bao. 2018 Jul; 29 (7): 2251–2258. Chinese. doi: 10.13287/j.1001-9332.201807.030. PMID: 30039663.

Ištoňa, J., Pavlenda, P. (2011): Monitoring of water storage in forest soil on PMP Čifáre in the years 1999–2009, Forestry journal, 57(3), 178–186, ISSN 0323–1046.

Kavvadias, V. A., Alifragis, D., Tsiontsis, A., Brofas, G., Stamatelos, G. (2001): Litterfall, litter accumulation and litter decomposition rates in four forest ecosystems in northern Greece. Forest ecology and management 144: 113–127.

Lapin, M., Faško, P., Melo, M., Štastný, P., Tomlain, J. (2002): Climatic areas. In: Atlas of the landscape of the Slovak Republic, Bratislava: Ministry of the Environment of the Slovak Republic and Banská Bystrica: Slovak Environment Agency, 2002. 344. ISBN 80-88833-27-2.

Leathers, D. J., Grundstein, A. J., Ellis, A. W. (2000): Growing season moisture deficits across the northeastern United States, Climate Research, Vol. 14: 43–55, 2000.

Lee, L., Fitzgerald, J., Hewins, D. B., McCulley, R., Archer, S. R., Rahn, T., Throop, H. L. (2014): Soil moisture and soil-litter mixing effects on surface litter decomposition: A controlled environment assessment, Soil Biology and Biochemistry, Volume 72, 2014, 123–132, ISSN 0038-0717, https://doi.org/10.1016/j.soilbio.2014.01.027.

Li, K., Zhao, L., Hou, R., Fang, Q., Fan, CH. (2021): Effect of leaf distribution pattern on the interception storage capacity of leaf litter under simulated rainfall conditions. Hydrological processes, 35, 2, e14022, https://doi.org/10.1002/hyp.14022.

Li, X., Niu, J. Z., Xie, B. Y. (2013): Study on hydrological functions of litter layers in North China. Plos one, 8(7): e70328.

Pasta, S., de Rigo, D., Caudullo, G. (2016): Acer pseudoplatanus in Europe: distribution, habitat, usage and threats. In: San-MiguelAyanz, J., de Rigo, D., Caudullo, G., Houston Durrant, T., Mauri, A. (Eds.), European Atlas of Forest Tree Species. Publ. Off. EU, Luxembourg.

Robinson, J. L., Slater L. D., Schäfer, K. V. R. (2012): Evidence of spatial variability in hydraulic redistribution within an oak-pine forest from resistivity imaging. Journal of Hydrology. 430–431 (69–79).

10.1016/j.hydrol.2012.02.002
Rushton, K. R., Eilers, V. H. M., Carter, R. C. (2006): Improved Soil Moisture Balance Methodology for Recharge Estimation. Journal of Hydrology. 318. 379–399. 10.1016/j.jhydrol.2005.06.022.
Sato, Y., Kumagai, T., Kume, A., Otsuki, K., Ogawa, S. (2004). Experimental analysis of moisture dynamics of litter layers-the effects of rainfall conditions and leaf shapes. Hydrological Processes, 18, 3007–3018. https://doi.org/10.1002/hyp.5746
SHMU, (2020): Operational data from selected stations. Available online: http://www.shmu.sk/sk/?page=1&id=klimat_operativneudaje1&identif=11816&rok=2019&obdobie=1981-2010&sub=1 (accessed on 3 March 2021)
Soil Survey Staff., (1996): Keys to Soil Taxonomy. Seventh edition. United States Department of Agriculture, Washington D.C.
Stanová, V., Valachovič, M., (eds.) (2002): Catalog of Habitats of Slovakia. DAPHNE - Institute of Applied Ecology, Bratislava, 225.
Škvarenina, J., Kunca, V., Krízova, E., Tomlain, J. (2006): Impact of the climate change on the water balance of altitudional vegetation zones and changed critical loads in forest ecosystems in Slovakia. Forestry journal, 52(1–2), 49–59, ISSN 0323 – 1046.
The Plant List, (2013): Version 1.1. Available online: http://www.theplantlist.org/ (accessed on 26 March 2021).
Tužínsky, L. (2004): Water regime of forest soils. Zvolen. Technical university in Zvolen, 101.
Van den Hurk, B., Ettema, J., Viterbo, P. (2008): Analysis of Soil Moisture Changes in Europe during a Single Growing Season in a New ECMWF Soil Moisture Assimilation System, Journal of Hydrometeorology, Pages: 116–131 DOI: https://doi.org/10.1175/2007JHM848.1
Van Stan, J. T., Coenders-Gerrits, M., Dibble, M., Bogeholz, P., Norman, Z. (2017): Effects of phenology and meteorological disturbance on litter rainfall interception for a Pinus elliottii stand in the southeastern United States. Hydrological Processes, 31, 3719–3728. https://doi.org/10.1002/hyp.11292
Wang, C., Zuo, Q., Shi, J. (2009): Spatial and temporal characteristics of soil moisture in a field scale in arid areas of northwestern China. Chunese Academia of science, Peking, 5129–5133, doi:10.11821/dlxb201609003.
Western, A. W., Grayson, B. R. (1998): The Tarrawarra data set. Soil moisture patterns, soil characteriscs and hydrological flux measurements. Water Resour. Res., 10, 2765–2768.
Western, A. W., Grayson, B. R. B., Bloschl, G. (2002): Change in soil moisture: hydrological perspective. Annual Review of Earth and Planetary Scien., 30(2002), 149–180.
Xing, Z., Yan, D., Wang, D., Liu, S., Dong, G. (2018): Experimental analysis of the effect of forest litter cover on surface soil water dynamics under continuous rainless condition in North China, Kuwait J. Sci. 45 (2), 75–83, 2018
Zvala, A., Orfánus, T., Nagy, V. (2018): Water retention in organic forest floor soil horizons under spruce stand (Picea abies), In Acta Hydrologica Slovaca 19(1), 2018, 162–168, ISSN 1335–6291.

Mgr. Anton Zvala, PhD. (*corresponding author, e-mail: zvala@uh.savba.sk)
Ing. Peter Šurda, PhD.
Ing. Justína Vitková, PhD.
Institute of Hydrology SAS
Dúbravská cesta 9
841 04 Bratislava
Slovak Republic

DOI: 10.31577/ahs-2021-0022.01.0013

ACTA HYDROLOGICA SLOVACA

Volume 22, No. 1, 2021, 113 – 117

VIABILITY OF MAIZE (Zea mays L) SEEDS INFLUENCED BY WATER, TEMPERATURE, AND SALINITY STRESS

Noriza Khalid, Ákos Tarnawa, Zoltán Kende, Katalin M. Kassai, Márton Jolánkai*

The crops site provides a wide range of abiotic stresses to field crops. Successful protection against these impacts can be the use of adaptable cultivars. At the Crop Production Laboratory of the University of Hungarian Agricultural and Life Sciences, Gödöllő Hungary, maize Zea mays L genotypes of different geographic origin were exposed in an in vitro trial to various abiotic stress conditions (water supply representing poor and flooded state, temperature with suboptimal, optimal and high exposure, and saline and neutral environment). Samples of Hungarian and Malaysian hybrids were tested for viability, radicle and plumule growth under these conditions in four replications. The results obtained have proven that the various abiotic applications had altering effects on the germination performance of the seed samples studied.

KEY WORDS: water stress, temperature stress, salinity stress, viability, maize genotypes

Introduction

Germination of seeds is a biological process that is influenced by biotic and abiotic factors including water, oxygen, and temperature for sufficient viability. A combination of conducive environmental factors and various cellular processes will allow physiological and morphological changes within the seed which will result in activation of the embryo. Germination started as the seed absorbs water (seed imbibition), resulting expansion of the seed and elongation of the embryo. Favourable growing conditions will allow ATP regeneration hence, allowing activation of hormones and enzymes responsible for germination such as abscisic acid (ABA), gibberellins, ethylene, and auxin (IAA). Germination ends when the radicle has grown out of the seeds coating layers and with the protrusion of the coleoptile (Miransari and Smith, 2014).

There are studies reporting that temperature elevation can cause thermoinhibition on seeds germination. A study on Nigeria's main crops which include maize, rice and sorghum, shows the impact of increases in temperature on seed germination and seedling development. The germination rate decreases for seeds cultivated at a higher temperature. The high temperature also affects the root development of the seedlings. Furthermore, the temperature elevation also caused a significant reduction in the length of stem and leaf length reduction in various crops (Iloh et al., 2014).

Salinity of crop sites represent a profound problem for plant growth and development. High soil salinity level eventually creates soil conditions with physiological drought, simultaneously may causes ion toxicity, nutrient imbalance, and oxidative stress to the seed (Nayidu et al., 2012). According to Kaymakanova (2009), high salinity in soil solutions may result in high osmotic pressure that restricts the seed imbibition by preventing water absorption and entry into the seed. The inability to absorb water resulted by high salt concentration will also prevent the mobilisation of essential nutrients needed for germination. Besides that, a saline condition during the early growth stage also caused Na^+ and Cl^- toxicity to the embryo and young seedlings that result in stunted development of the plants (Khajeh-Hosseini et al., 2003; Kaymakanova, 2009). Salt stress caused by NaCl also decreases the content of essential hormones for germination, such as gibberellins while increasing the ABA levels (Atia et al., 2009).

Water availability is essential during germination for the seed imbibition process thus, no germination will occur in the absence of water. Nonetheless, excess water may cause waterlogged soil conditions, which will deprive the seeds from oxygen supply. Oxygen is utilised by imbibed seeds as the rapid respiratory metabolic process begins and carbon dioxide (CO_2) is released as a by-product. Prolonged flood during germination stage resulted by extreme weather conditions, for example torrential rain, or planting in an area with high water table, can threaten crops with low water-logged tolerance by restricting the respiratory activity essential for germination. In cereals seeds, starch stored in the endosperm of the seeds is converted to soluble sugars

such as sucrose during germination through combined actions of enzymes such as α-amylase, β-amylase, and α- glucosidase (Zhou et al., 2020).
It is common for one agricultural land to represent more than one abiotic stress at the same time. Water and temperature interactions often determine yield quantity and quality performance (Jolánkai et al., 2018). A combination of two or more abiotic stress will aggravate the impact of each stress and farmers may need to spend more input to remove or lessen the impacts. High temperature simultaneously with salt stress is a common condition, especially in semiarid and arid regions in the world (Shahid et al., 2017). High temperatures cause more detrimental effect on germination under salinity stress than germination in saline conditions under optimum temperatures. It was observed that the combination of these stresses reduced the germination rate, shoot length, and dry weight of wheat seedlings compared to the effect of one stress alone. The combined stresses also reduced the photosynthetic rate in the same crop due to a decline in pigmentation (Neelambari et al., 2018). In a physiology trial the high temperature may have increased the moisture evaporation causing salt content elevation by capillary movement and slowing down the activation of metabolic processes thus reducing the activity of different enzymes responsible for germination (Luan et al., 2014).
The aim of the study was to determine the impact of water availability, temperature variations and salinity on the viability of maize seeds. The hypothesis of the research focused on the possible stress tolerance abilities of maize hybrids of different geographic origin. Since maize (*Zea mays* L) crop have dispersed throughout the globe during the past half of a millennium spreading from tropical and subtropical grain belts via temperate zones up to polar regions nowadays, due to direct and indirect breeding and selection processes certain genotypes may have gained specific abilities for stress tolerance.

Material and methods

In a laboratory germination trial at the Crop Production Institute of the University of Agriculture and Life Sciences, Gödöllő, Hungary, maize *Zea mays* L genotypes of different geographic origin were exposed to various abiotic stress conditions (water supply representing poor and flooded state, temperature with suboptimal, optimal and high exposure, and saline and neutral environment).
The methods and the description of the trial were in accordance with general laboratory standards. Seed samples of Hungarian and Malaysian hybrids were tested for viability, radicle and plumule growth under these experimental conditions in four replications, run in a Memmer type climatic chamber.
During the germination trial three levels of temperature were applied: 10, 25 and 35ºC respectively. Water stress during the germination was applied in two variants – simulating a dry and a flooded state – using 5 ml and 30 ml water added to each petri dish. Testing salinity was observed in two variants: zero and 2% of NaCl solutions were applied.
The viability trials were run for 6 days after exposure, and after germination an additional 10 days were given for measuring shoot and root growth.
The results were obtained by recording germination followed by the daily measurement of radicle and plumule growth in mm. The results were evaluated by correlation and the level of significance was determined with *t* probe.

Results and discussion

According to the research hypothesis the following result has been obtained. The viability experiment has covered a wide range of abiotic stress factors in relation to the impact of temperature, water availability and salinity. Three levels of temperatures – 10, 25 and 35ºC – were applied during germination to test maize hybrids of different geographic origin. At 10ºC no maize hybrids germinated, at 25ºC both Hungarian and Malaysian hybrids produced their best germination performance, however at the highest 35ºC temperature the viability of Hungarian maize was very poor, but the Malaysian one, however with a reduced viability, still germinated over 50% (Fig. 1).
The development of plumules and radicles was in accordance with the germination figures. It is worth to state that at 35ºC neither hybrids developed roots, only shoots were detectable in this application.
Saline conditions during the germination period were strictly consequent. NaCl treated seed samples have produced diverse responses. The Hungarian maize hybrid did not germinate at all, while the Malaysian maize has shown a rather low, but consequent viability in an average of 47.5%. The shoot development of the germinating hybrid was poor, but the root development proved to be satisfactory (Fig. 2).
Water stress trials have shown consequent results (Fig. 3). Simulated dry conditions – 5 ml water – and flooded conditions – 35 ml water – resulted in diverse effects. Both maize hybrids performed better in dry conditions in comparison with the flooded version. However, the Malaysian hybrid proved to be more tolerant to both dry and moist conditions that the Hungarian hybrid. Concerning root and shoot development, Hungarian maize hybrid had a rather poor performance in both applications, while the Malaysian hybrid's phenological development was in accordance with the viability figures.
The last germination trial was focusing on the temperature x salinity interaction. The results of this observation are presented in Fig. 4. At 2% salt concentration combined with 35ºC temperature only 2.5% of the Hungarian maize hybrid seeds proved to be viable.
Figure 5 presents the data of the Malaysian hybrid that had an 52.5% viability record. The plumule and radicle development values were in accordance with these findings.

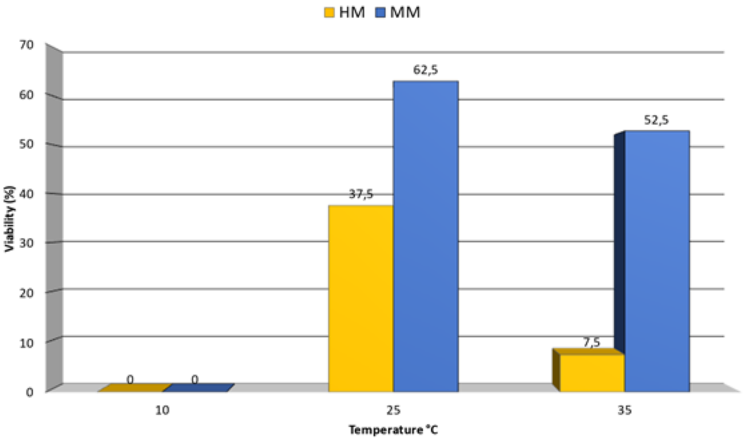

Fig. 1. Viability of seeds of maize hybrids at different temperatures.

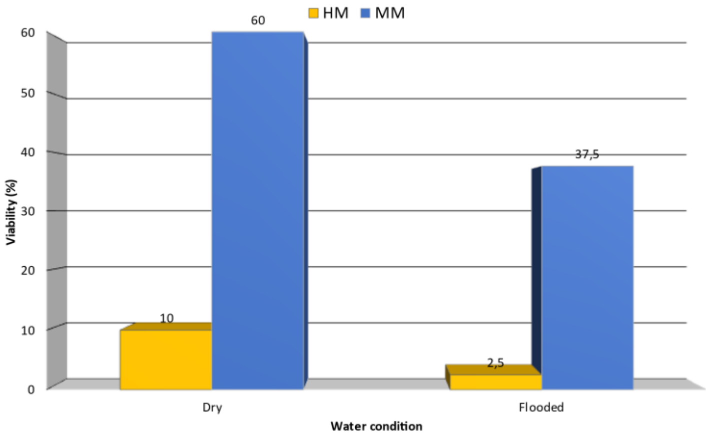

Fig. 2. Viability of seeds of maize hybrids at different NaCl levels.

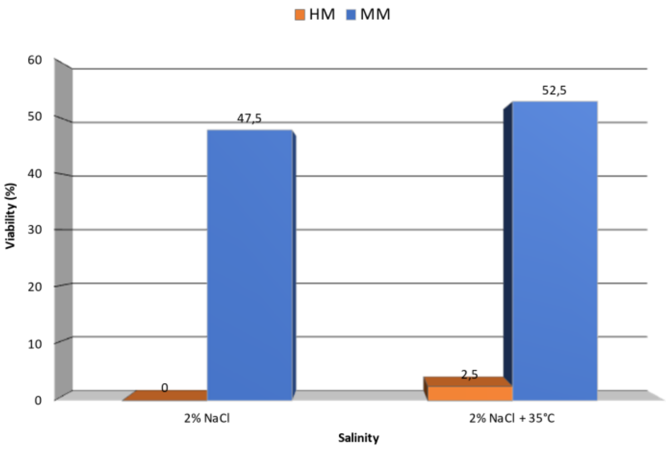

Fig. 3. Viability of seeds of maize hybrids at different water supply conditions.

Table 1 presents the correlation values of between the experimental figures. The correlation between the experimental variants was diverse. The strongest relations (0.99% significance) were found in the cases of hybrid x salinity, temperature x viability and plumule length x viability.

Strong correlations (0.95% significance) were obtained in the cases of water x radicle growth, salinity x viability and radicle growth x viability. The rest of the interrelations were not significant.

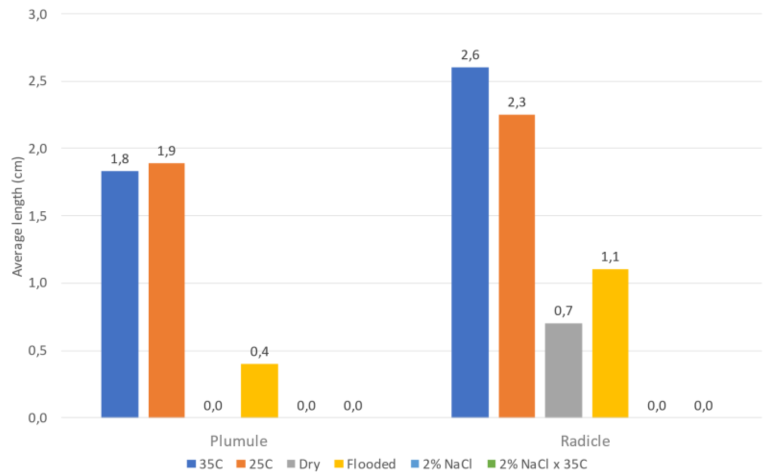

Fig. 4. Impact of various stress factors on the growth of plumules and radicles of the Hungarian maize hybrid.

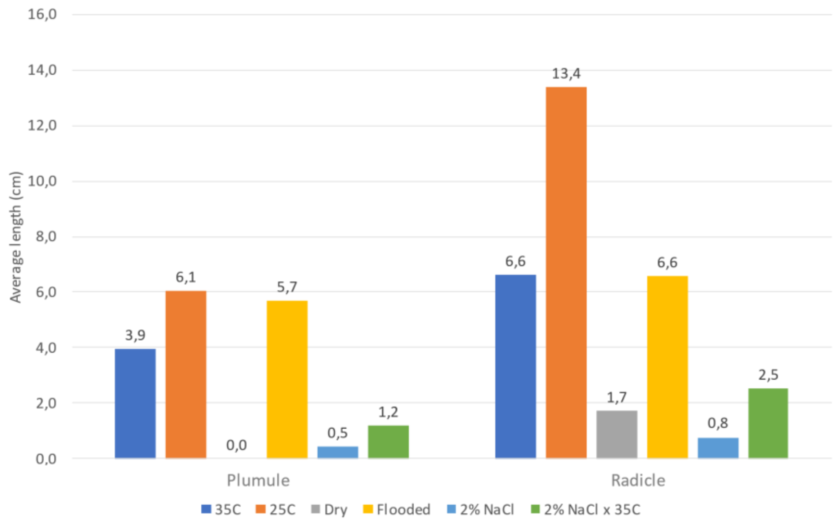

Fig. 5. Impact of various stress factors on the growth of plumules and radicles of the Malaysian maize hybrid.

Table 1. Correlation between experimental figures

r_{corr}	water	temperature	salinity	hybrid	viability	radicle	plumule
water	1						
temperature	na	1					
salinity	0.026	-0.057	1				
hybrid	na	na	-0.886**	1			
viability	-0.643	0.825**	-0.753*	0.534	1		
radicle	-0.689*	-0.467	-0.556	0.432	0.787*	1	
plumule	-0.742*	-0.511	-0.434	0.334	0.889**	0.723	1

* $LSD_{0.95}$
**$LSD_{0.99}$

Conclusion

In accordance with to the research hypothesis various results have been obtained. The viability experiment has covered a wide range of abiotic stress factors in relation with the impact of temperature, water availability and salinity.

The overall result of the experiments is the proof of the use of the appropriate plant variety in certain crop site conditions. It turned out that the Malaysian maize hybrid was much more adaptive to the extreme conditions represented by salinity, water stress and temperature stress. The conclusion of the research can be summarized that the crop site conditions are to be harmonized with the crop variety applied.

On the basis of this experiment further research should be done in favour of answering some questions that may emerge from some uncertain interactions like the behavioural patterns of radicle and plumule growth, the salinity x temperature interactions and finally the magnitude of viability. A broader screening of more varieties may provide a basis for novel statements in this field.

Acknowledgement

The authors of the article are indebted regarding the support received from NVKP and VKSZ funds of the Government of Hungary.

References

Atia, A., Debez A., Barhoumi Z., Smaoui A., Abdelly C. (2009): ABA, GA(3), and nitrate may control seed germination of Crithmum maritimum (Apiaceae) under saline conditions. Comptes rendus biologies, 332(8), 704–710.

Iloh, A., Omatta, G., Ogbadu, G. H., Onyenekwe, P. C. (2014): Effects of elevated temperature on seed germination and seedling growth on three cereal crops in Nigeria. Scientific research and essays, 9(18), 806–813.

Jolánkai, M., Kassai, M. K., Tarnawa, Á., Pósa, B., Birkás, M. (2018): Impact of precipitation and temperature on the grain and protein yield of wheat (Triticum aestivum L) varieties. Időjárás. 122. 1. 31–40.

Kaymakanova, M. (2009): Effect of salinity on germination and seed physiology in bean (Phaseolus vulgaris L.). Biotechnology and Biotechnological Equipment, Volume 23, 326–329.

Khajeh-Hosseini, M., Powell, A., Bingham, I. (2003): The interaction between salinity stress and seed vigour during germination of soyabean seeds. Seed Science and Technology, 31(3), 715–725.

Luan, Z., Xiao, M., Zhou, W., Zhang, H., Tian, Y., Wu, Y., Guan, B., Song, Y. (2014): Effects of Salinity, Temperature, and Polyethylene Glycol on the Seed Germination of Sunflower (Helianthus annuus L.). The Scientific World Journal, Volume 2014, 1–9.

Miransari, M., Smith, D. (2014): Plant hormones and seed germination. Environmental and Experimental Botany, Volume 99, 110–121.

Nayidu, N., Bollina, V., Kagale, S. (2012): Oilseed Crop Productivity Under Salt Stress. In: P. Ahmad, M. M. Azooz & M. N. V. Prasad, eds. Ecophysiology and Responses of Plants under Salt Stress. New York: Springer, 249–265.

Neelambari, Singh, A. K., Kumar, S. (2018): Effect of Individual and Combined Salinity and High Temperature Stress during Germination Stage of Different Wheat (Triticum aestivum L.) Genotypes. International Journal of Current Microbiology and Applied Sciences, 7(7), 1723–1730.

Shahid, S., Hadipour, S., Wang, X., Shourav, S. A., Minhas, A., Ismail, T. (2017): Impacts and adaptation to climate change in Malaysian real estate. International Journal of Climate Change Strategies and Management, 9(1), 87–103.

Zhou, W., Chen, F., Meng, Y., Chandrasekaran, U., Luo, X., Yang, W., Shu, K. (2020): Plant waterlogging/flooding stress responses: From seed germination to maturation, Plant Physiology and Biochemistry, Vol. 148, 228–236.

Noriza Khalid, MSc
Ákos Tarnawa, PhD
Zoltán Kende, PhD
Katalin M. Kassai, PhD
Márton Jolánkai, DSc (*corresponding author, e-mail: jolankai.marton@szie.hu)
Hungarian University of Agriculture and Life Sciences
2100 Gödöllő
Hungary

DOI: 10.31577/ahs-2021-0022.01.0014

ACTA HYDROLOGICA SLOVACA

Volume 22, No. 1, 2021, 118 – 124

NITRATES TRANSPORT COMPARISON THROUGH TWO DIFFERENT SOIL PROFILES IN THE EASTERN SLOVAKIA LOWLAND LYSIMETRIC STATION

Lucia Balejčíková*, Andrej Tall, Branislav Kandra, Dana Pavelková

Nitrates belong to the major nutrient required for plant growth and they are generally very well soluble in water often used as fertilizers in agriculture. The higher values of nitrates concentration will occur in the case of large amounts use of fertilizer in intensive agriculture, pipe damage or damaged drainage near wells. The fertilization reduction could be one of this problem solution for health protection, environmental and economic reasons. In our study, the spectrophotometric determination of nitrates concentration in 5 times over-fertilized soil in lysimeters localized in the Eastern Slovakia Lowland showed nitrates leaching in the 40 cm layer of sandy soil, while in the silty-loam soil profile nitrates were not detected. The main goal of the experimental work was to show different nitrates leaching through two types of soil profile differing in hydraulic soil properties. Low retention capacity and high hydraulic conductivity of sandy soil (locality Poľany) were favourable for nitrate leaching in comparison with higher retention and conductivity of silty-loam soil (locality Vysoká nad Uhom) under relatively low precipitation events in the studied period from April 29th to May 28th 2019.

KEY WORDS: nitrates, spectrophotometry, lysimeter, precipitation

Introduction

With a population increase in the world and industrial development, the amount of harmful waste substances, which leak out to the surface and groundwater, grows. Drinking water represents only about 3% of the total amount of water on Earth with a decreasing tendency. Criteria for the quality of drinking water for human consumption are laid down by the applicable legislation in every country. Healthy drinking water is assessed and controlled by drinking water quality indicators and their limits. Billions of people have no drinking water available, especially in India, China or states in Africa. Slovakia (Fig. 1), the main object of our research activity, a small country located in the middle of Europe, belongs to countries with good quality and quantity of drinking water.

Groundwater represents the most important source of drinking water in Slovakia. The largest amount of groundwater is bound to the quaternary sediments of the Danube area with the most important water management area in Central Europe – the Rye Island. Groundwater monitoring probes and river basins observation network could be visible on the Slovak website www.shmu.sk. The Council Directive 91/676/EEC concerning the protection of waters against pollution caused by nitrates from agricultural sources (the Nitrates Directive) was accepted in 1991. Based on water quality protection across Europe nitrates use from agricultural sources has to prevent polluting ground and surface waters. The council directive contributed to promoting the use of good farming practices. Nevertheless, there are sources of water pollution, so it is necessary to search methods for water purification, decontamination and reasonably separate, reduce and remove harmful substances. Nitrates, used as soil fertilizers in agriculture, belong to the frequent substances that cause pollution of water (Bibi et al., 2016). The most commonly used nitrate fertilizers are calcium nitrates ($Ca(NO_3)_2$), potassium nitrates (KNO_3) or ammonium nitrates (NH_4NO_3) (Kant and Kafkafi, 2013). In the case of nitrogen fertilizers applications, incorrect use may often occur, with nitrates being able to reach groundwater or other water sources when overdosed (Bibi et al., 2016). Nitrates pose a threat to human health, especially for the sensitive organisms of infants, because higher concentrations (over 10 mg l^{-1}) can lead to methemoglobinaemia, i.e. to the inability of haemoglobin to transfer oxygen, leading to suffocation (Kim-Shapiro et al., 2005; Greer and Shannon, 2005; Knobeloch et al., 2000). Nitrates are converted into more toxic nitrite by the bacterial activity in the human body. Nitrates and nitrites are involved as precursors to the formation of highly active carcinogenic substances that increase the risk of gastrointestinal cancer diseases of the gastrointestinal system and bladder. The literature

Fig. 1. The map of Slovakia in the middle of Europe (marked yellow).

also mentions the relationship of nitrites to the incidence of tumour diseases of the lymphatic system (Bruning-Fann and Kaneene, 1993; Forman, 1989; Magee and Barnes, 1967; Bogovski and Bogovski, 1981; Mirvish, et al., 1987). For these reasons, it is necessary to monitor the concentration of nitrates in water sources, especially those intended for human consumption. In 1993 Pekárová and Miklánek studied spatial distribution and concentrations trend change of nitrate-based on trend analysis in five sub-basins of the Ondava River in the Slovakia basin for 25-years-time series 1968/69–1992/93. Important differences were found if nitrate concentrations derived from daily samples were compared to those estimated from regular monthly samplings of the hydrometeorological network (Pekárová and Miklánek, 1993). In 2002 an ecologic study of nitrate in municipal drinking water and cancer incidence in Trnava district, Slovakia was published. These ecologic data supported the hypothesis that there is a positive association between nitrate in drinking water and non-Hodgkin lymphoma and colorectal cancer (Gulis, et al., 2002). Variation of nitrates in runoff from mountain and rural areas was studied by Holko et al. in 2006. Water samples collected at the outlet of the mountain part had lower concentrations of nitrates than the samples collected downstream in the rural area. The differences were smaller during the summer. The highest concentrations of nitrates and the highest differences among the uninhabited and inhabited areas were observed at the time of snowmelt (Holko et al., 2006). The next study of irrigation effect on nitrates movement in soil and risk of subsoil contamination has shown that movements of nitrates in irrigated and non-irrigated fields differed significantly mainly during the early stages of the vegetation period. Applied irrigation was not the reason for nitrates penetration below the root zone under the soil (Nováková and Nágel, 2009). To facilitate the detection, determination and monitoring of nitrates, many strategies have been developed. Various techniques and their limitations have been summarized in several papers (Moorcroft et al., 2001; Moo et al., 2016; Wang et al., 2017; Ciulu et al., 2018). Spectroscopic methods are by far the most widely used for nitrates determination due to the excellent limits of detection obtained, rapidity, sensitivity and the simplicity of the protocols. Based on this, a spectrophotometric UV-VIS method was used for our investigations of nitrates concentration in small volumes of water collected from lysimeters localized in Petrovce nad Laborcom situated in the eastern part of Slovakia operated by the Institute of Hydrology Slovak Academy of Sciences – Research Base for Lowland Hydrology. Lysimeters represent very convenient tools for this study thanks to the possibility to obtain water samples, which flowed through the given soil. Also, actual evapotranspiration using the balance equation can be calculated (Matusek et al., 2017). The most frequently used grass fertilizer, containing highly effective water-soluble nitrates, was applied to fertilize selected soil monoliths in lysimeters. Transport processes depend on soil type, the size of soil microparticles in a porous environment, plant cover of soil, irrigation, precipitation or season. From these factors, we focused on the study of soil type, precipitation and evapotranspiration effect on nitrate movement through the soil profile. In this way, the main aim of the work was to determine the capacity of the soil with grassy cover in the given season at specific sampling time intervals to bind and consume applied nitrates for the vegetation growth needs. We have found, that increasing the nitrate sorption capacity of the soil has the potential to reduce nitrate leaching to groundwater.

Material and methods

Lysimeters description

Lysimeter station in Petrovce nad Laborcom (Umwelt-Geräte-Technik, GmbH., Germany) was built in 2014 and was put into full operation in spring 2015. The geographical position is 48°45´19´´N and 21°54´48´´E; 117 m a.s.l. The Station consists of five cylindrical weighable lysimeters and a meteorological station. The whole station is powered by solar panels. The specific surface area of each lysimeter is 1 m^2, the height is 2.5 m and the total mass is about 5000–5300 kg. Lysimeters are equipped with UMP (i.e. *Unit with Moisture Probe*) probes (for measuring volumetric moisture, temperature and electric conductivity of soil), tensiometers and suction probes (for water sampling). The sensitivity of the weighing system is 10 g. The vegetation cover is grass, maintained by mowing at 12 cm (Matusek et al., 2017). Soil monoliths (undisturbed soil blocks) represent five different types of soils from various locations in the region. Lysimeters no. 1 with silty-loam soil (locality Vysoká nad Uhom) and no. 3 with sandy soil (locality Poľany) were selected for our study of transport processes of nitrates in standard and overdosed fertilized soil. It should be noted that the groundwater level for lysimeter no. 3 is constant and maintained at the depth of 1 m under the soil surface and lysimeter no. 1 is equipped by free drainage.

Fertilization and sampling

Fertilization and sampling were performed at the lysimeter station of the Research Base for Lowland Hydrology Institute of Hydrology, Slovak Academy of Sciences, localized in Petrovce nad Laborcom in the Eastern Slovakia Lowland. Standard used fertilizer "Kristalon" (producer AGRO CS a.s. the Czech Republic, originating in the Netherlands), containing highly effective water-soluble nitrates was diluted in water to achieve the standard and overdosed concentration of nitrates and applied on selected soil placed in lysimeter no. 1 and 3 during the vegetation period from the beginning of April to the end of May 2019 with average temperature 10°C in April and 15.2°C in May. The water samples were collected to identify nitrates transport processes from 3 different depths (40, 100 and 160 cm). Before fertilization for the study of the solute movement, the non-fertilised water sample was taken as a starting solution.

Spectrophotometric determination of nitrates concentration

The Hach Lange DR6000 is the most advanced laboratory UV-VIS spectrophotometer for water quality testing. It offers high-speed spectral scanning. For the determination of NO_3^- concentration, we used the LCK-340 cuvette test from the Hach Lange Company for the concentration range of nitrates 22–155 mg l^{-1}. For lower concentrations of nitrates (1.0–60.0 mg l^{-1}) LCK-339 cuvette test was used. Both LCK tests are based on the reaction of NO_3^- anions with 2,6-dimethylphenol in an aqueous solution containing sulfuric and phosphoric acid. First, water sampled from lysimeters was pipetted slowly to cuvette according to the procedure outlined in the instruction manual for the given LCK test. Then, the cuvette was closed and inverted a few times until no more streaks can be seen. Measurement of absorbance ran one-time at automatically set wavelength ~ 370 nm and the final concentration was subtracted from the display. During the sampling from lysimeters, the direct concentration of nitrates and nitrites was also determined using a portable field spectrophotometer–pHotoFlex pH. Reaction cell test with the program no. 314 was applied for NO_3^- determination (concentration range 1–133 mg l^{-1}) and reagent test with the program no. 334 for NO_2^- (concentration range 0.007–0.985 mg l^{-1}) determination. Reaction tests contained a mixture of organic and inorganic compounds with chronotropic reagents, which changed the colour of the solution with intensity according to the nitrates concentration in the added sample.

Results and discussion

To determination the concentration of nitrates transported through the soil, we focused on taken of aqueous samples from lysimeters (no. 1 and 3) with two different soil type monoliths localized in Petrovce nad Laborcom in the Eastern Slovakia Lowland. These lysimeters were chosen for our experiment thanks to the suitable water afflux and built-in suction probes to collect water. As a first step, the standard amount (recommended by the producer) of commercially used grass fertilizer was weighed and dissolved in water. The precise concentration of NO_3^- anions was determined by the LCK 340 test with the final value of 200.5 mg l^{-1}. Before fertilization, initial water samples were taken from three different depths (40, 100 and 160 cm) with final values below the detection limit of the LCK 339 test. This means that during the selected period there was no detected residual amount of nitrates from the nitrogen cycle in the soil or from the precipitation. After standard fertilization, the next four spectrophotometric measurements were realized on samples taken in daily intervals at the beginning of April, but the NO_3^- concentrations did not exceed the lowest detection limit of the LCK test for determination of NO_3^- concentration despite the occurrence of rain, which is supposed to accelerate the movement of nitrates into the lower soil layers. Most probably the whole amount of added NO_3^- anions in the form of fertilizer was up-taken by grass for growth needs in started vegetation period (Fig. 2).

Therefore, we added approx. 5 times the recommended fertilizer amount to achieve the transport of nitrates to the lower layers of the soil. The final concentration of NO_3^- anions in the dissolved aqueous solution of fertilizer was 1120 mg l^{-1}. Before the second fertilization of soil in lysimeter no. 1 and 3, initial water samples were taken from three different depths (40, 100 and 160 cm) with final values below the detection limit of the nitrate test. An increase in concentration detected using portable

Fig. 2. The photography of grass cover on lysimeters localized in Petrovce nad Laborcom in the Eastern Slovakia Lowland at the beginning of the vegetation period (3th April 2019).

field pHotoFlex pH device and laboratory LCK test was observed from the second day after fertilization only at the depth 40 cm in the lysimeter no. 3 containing sandy soil monolith (Fig. 3). Nitrates were not detected in the greater depth, i.e. did not achieve the groundwater level, which is 1 m under the surface of lysimeter no. 3. The observed difference between the determination of NO_3^- concentration using pHotoFlex pH and LCK tests in the graph (Fig. 3) can be related most probably by the difference between chemical principles of methods (various reagents, interference). At depths 100 and 160 cm in lysimeter no. 3 and in all depths of lysimeter no. 1, the NO_3^- concentration did not exceed the lowest detection limit of the used method. Because the grass cover and the meteorological conditions were the same for both lysimeters, it should be highlighted that the better sorption capacity of lysimeter no. 1 was caused by the different soil type. The silty-loam soil profile is characterized by a finer texture compared to the sandy soil profile, which results in much lower hydraulic conductivity values. The finer soil texture and hence the higher proportion of the silt and clay fractions in the silty-loam soil results in an incomparably higher specific surface area. We assume, that both, the lower hydraulic conductivity and higher specific surface of the soil profile in lysimeter no. 1, are responsible for its lower content and slower-moving of nitrates. Due to the fact, that precipitation, irrigation and evapotranspiration measured with an hourly step of a lysimeter no. 3 belong to factors affecting the nitrates concentration, we added these factors into the graph (Fig. 3). We can conclude, that heavy irrigation (contained fertilizer) together with significant precipitation during the first days of our experiment caused rapid movement of NO_3^- to the lower depth of the soil (Fig. 3).

In general, applied fertilizer, containing NO_3^- anions, undergoes various processes before becoming available for plants within the natural nitrogen cycle in the soil. Besides the most important grass uptake, we taking into account the binding of NO_3^- anions to soil particles, immobilization and mineralization in the soil organic matter, leaching to lower soil depths and transformation to NO_2^- anions. The excess of NO_2^- anions is measurable before its chemical transformation. Similarly, as nitrates, nitrites can also negatively affect human health when exceeding the limit set by the applicable legislation, i.e 0.5 mg l^{-1} in the European Union and for infants 0.1 mg l^{-1}. For this reason, we determined also the possible presence of NO_2^- anions using a portable field spectrophotometer – pHotoFlex pH (Fig. 4).

For depths 100 and 160 cm in lysimeter no. 3 and in all depths of lysimeter no. 1, the NO_2^- concentration did not exceed the lowest detection limit 0.007 mg l^{-1} of the used method. Fig. 4 represents results from determination NO_2^- concentration from 40 cm depth of lysimeter no. 3. We observed an increase of NO_2^- concentration at the end of the experiment only, but recommended limits were not exceeded. Fig. 5 represents the photography of the grass cover after the experiment as visible evidence that the grass cover was not "burned" by excessive fertilization.

It should be noted that irrigation, grass cover and meteorological conditions (precipitation, global radiation, wind speed, air temperature) were the same for both lysimeters. The main difference should come from the various components of soil monoliths, hydraulic conductivity and specific surface of soil particles. A low retention capacity and a high hydraulic conductivity of sandy soil may be favourable for nitrate leaching in comparison with higher retention and conductivity of silty-loam soil. Therefore our findings at the experimental site indicate a low ability of nitrates movement to the groundwater during the vegetation period after fertilization of silty-loam soil. An increased risk of nitrates movement below the soil root zone can be expected for increased fertilizers doses during winter periods when soil is wet, and after heavy rains, if fertilization is performed in the early spring times. Plant cover can eliminate this risk nevertheless the deep penetration of nitrates during the vegetation period depends highly on precipitations. For generalization, it is necessary to continue with monitoring studies of water balance.

The basic hydrophysical characteristics of the studied object used for nitrates transport were collected in the latest study within Research Base for Lowland Hydrology work and monitoring. Here similarly under the same meteorological conditions for both soil types, water balance components in 2018 differ due to variations in soil profiles. Measurements using

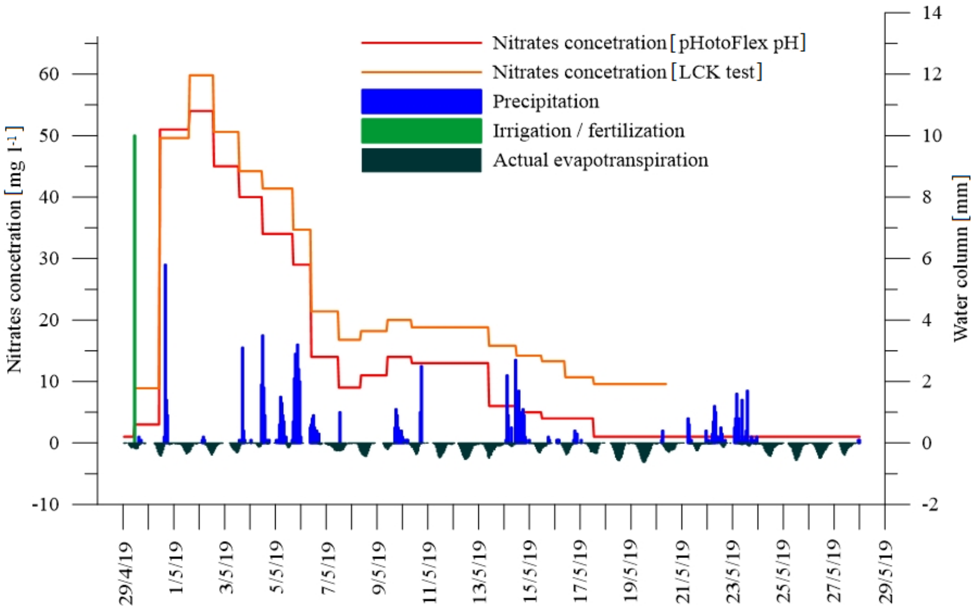

Fig. 3. The time course of nitrates concentration determined by portable field pHotoFlex pH device (red course) and LCK laboratory test (orange course) from lysimeter no. 3 in the 40 cm depth. Blue columns represent precipitation, green column illustrated water content after initiated irrigation/fertilization and dark green columns actual evapotranspiration.

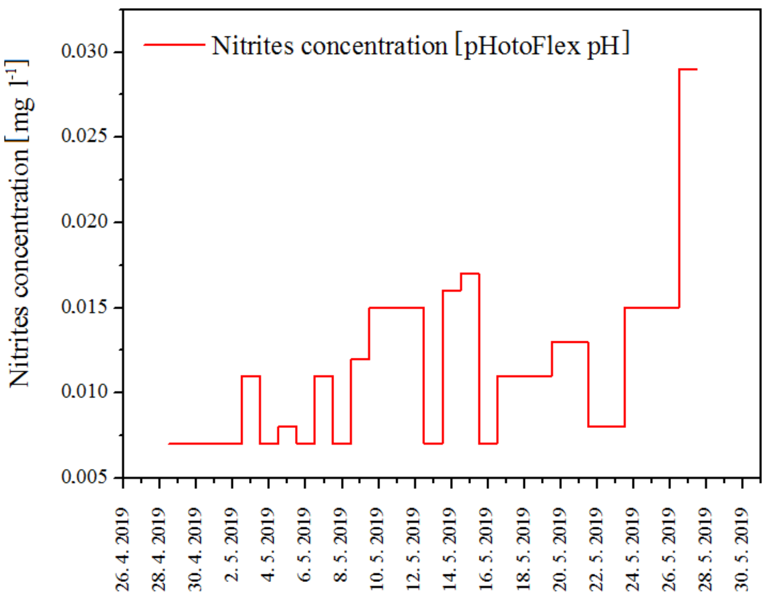

Fig. 4. The time course of nitrites concentration determined by portable filed pHotoFlex pH.

Fig. 5. The photography of grass cover on lysimeters localized in Petrovce nad Laborcom in the Eastern Slovakia Lowland at the end of experiment (27th May 2019).

hydrometer measurement method for particle-size analysis up to 1 m depth has shown the followed soil hydrometer measurement method for particle-size analysis up to 1 m depth has shown the followed soil profile composed of sandy loam surface, deeper horizons of loamy sand continued by pure sand from Poľany source. Soil collected from Vysoká nad Uhom locality was relatively homogeneous and consists of silt loam. Soil water retention curves, obtained by pressure plate extractor, confirmed greater heterogeneity of sandy soil (Poľany) compared to the profile from Vysoká nad Uhom. Saturated hydraulic conductivities were: 12, 430 and 470 cm day^{-1} for the Poľany soil profile and 10, 35 and 32 cm day^{-1} for the soil profile from Vysoká nad Uhom. The volumetric moisture content in the studied the year 2018 in the soil profile from locality Vysoká nad Uhom reached the level of the field capacity and in the soil profile from locality Poľany, field capacity was even exceeded (Tall and Pavelková, 2020).

In this work, we have demonstrated that the nitrates movement should be affected by the type, size and composition of the soil particles, which have absorbed and leached nitrates differently. We take into account that some difference can come from various transformation processes of nitrates in the natural nitrogen cycle in selected soil monoliths (bacterial metabolism). Except for bacteria use of nitrates in metabolic processes, chemical soil composition could affect nitrates content in the soil environment. One of the essential elements for plant growth is iron. Muradova and co-workers showed that Fe^0 can reduce nitrates thanks to redox potential. They indicated the pH value can be a helpful factor in nitrates reduction (Muradova et al., 2016). This investigation could partially explain the small detected nitrates amounts in sandy soil (in 40 cm depth) and non-detectable nitrates amounts in silty-loam profile (in all depths). Thus, nitrates remaining in relatively dry soils could be exposed to other redox-active iron compounds or other reactive components. Unfortunately, our experiment cannot distinguish loss of nitrates during the chemical transformation from the contribution of the nitrates movement and leaching. From the major observation, we have point on, that the 5 times higher nitrates concentration, as recommended fertilization, did not cause the nitrates to leach into the groundwater in the selected soils under specific meteorological conditions probably as the effect of good sorption capacity in both soils. With this experiment, we would like to point out that with a further increase in the concentration of added nitrates by over-fertilization, groundwater can be contaminated in combination with rich precipitation. Lysimeters are a suitable tool for studying the transport processes of various other ions, electrolytes, nutrients, substances, heavy metals, radionuclides, drugs, etc., which can reach and contaminate the groundwater source. Similar studies are necessary to determine the maximum limit concentration of substances that enter the soil while not reaching groundwater levels. The study of transport processes using lysimeters can also inspire the development of separation technology to prevent the leaching of harmful substances into groundwater.

Conclusion

The investigation of the nitrates movements through the soil monoliths was performed at the lysimeter station of the Hydrological Research Base, Institute of Hydrology, Slovak Academy of Sciences, localized in Petrovce nad Laborcom in the Eastern Slovakia Lowland. By simply spectroscopic measuring the nitrate concentration we have shown in our work that soil monoliths varying in type, size and grain composition of soil particles affect the nitrates movement differently. The main reason is associated with hydraulic conductivity and specific surface of soil particles. Our results suggest that the natural precipitation and irrigation exhibit a low risk of nitrates penetration to the groundwater during the vegetation period under standard and overdosed fertilization. It was shown a significant nitrate content decrease during the vegetation period probably due to the nitrates uptake by grass and good sorption capacity of the soil. These findings are valid for the soils with the hydraulic properties closely resembling those at the experimental site. We suggest that lysimeters represent a suitable model tool for the study of transport processes not only nitrates and nitrites useful mainly in agriculture but also other nutrients or vice-versa pollutants important for environmental research.

Acknowledgement

This work was supported by the VEGA Grant Agency project No. 2/0044/20.

References

Bibi, S., Saifullah, Naeem, A., Dahlawi, S. (2016): Environmental Impacts of Nitrogen Use in Agriculture, Nitrate Leaching and Mitigation Strategies. In: Hakeem K., Akhtar J., Sabir M. (eds) Soil Science: Agricultural and Environmental Prospectives. Springer, Cham 131–157. Online ISBN978-3-319-34451-5.

Bogovski, P., Bogovski, S. (1981): Animal species in which N-nitroso compounds induce cancer. International Journal of Cancer, vol. 27, 471–474.

Bruning-Fann, C. S., Kaneene, J. B. (1993): The effects of nitrate, nitrite and N-nitroso compounds on human health: A review. Veterinary and Human Toxicology, vol. 35, 521–538.

Ciulu, M., Ollivier, N., Demelas, C., Boudenne, J.-L., Coulomb, B., Théraulaz, F., Robert-Peillard, F. (2018): A highly-sensitive microplate fluorimetric method for the high-throughput determination of nitrate ion in aqueous compost extracts. Microchemical J., vol. 138, 424–429.

Forman, D. (1989): Are nitrates a significant risk factor in human cancer? Cancer Surveys, vol. 8, 443–458.

Greer, F. R., Shannon, M. (2005): Infant methemoglobinemia: the role of dietary nitrate in food and water. Pediatrics, vol. 116, 784–786.

Gulis, G., Czompolyova, M., Cerhan, J. R. (2002): An Ecologic Study of Nitrate in Municipal Drinking Water and Cancer Incidence in Trnava District, Slovakia. Environmental Research Section A, vol. 88, 182–187.

Holko, L., Kostka, Z., Lichner, Ľ., Píš, V. (2006): Variation of nitrates in runoff from mountain and rural areas. Biologia, vol. 61, S270–S274.

Kant, S., Kafkafi, U. (2013): Fertigation. Reference Module in Earth Systems and Environmental Sciences, Elsevier. ISBN 9780124095489

Kim-Shapiro, D. B., Gladwin, M. T., Patel, R. P., Hogg, N. (2005): The reaction between nitrite and hemoglobin: the role of nitrite in hemoglobin-mediated hypoxic vasodilation. Journal of Inorganic Biochemistry, vol. 99, 237–246.

Knobeloch, L., Salna, B., Hogan, A., Postle, J., Anderson, H. (2000): Blue babies and nitrate-contaminated well water. Environmental Health Perspectives, vol. 108, 675–678.

Magee, P. N., Barnes, J. M. (1967): Carcinogenic nitroso compounds. Advances in Cancer Research, vol. 10, 163–246.

Matusek, I., Reth, S., Heerdt, C., Hrckova, K., Gubis, J., Tall, A. (2017): Review of lysimeter stations in Slovakia. 17. Gumpensteiner Lysimetertagung, 209–212, ISBN: 978-3-902849-45-8.

Mirvish, S. S., Weisenburger, D. D., Salmasi, S. P. A., Kaplan, P. (1987): Carcinogenicity of 1-(2-Hydroxyethyl)-1-nitrosourea and 3-Nitroso-2-oxazolidinone Administered in Drinking Water to Male MRC-Wistar Rats: Induction of Bone, Hematopoietic, Intestinal, and Liver Tumors. JNCI: Journal of the National Cancer Institute, vol. 78, 387–393.

Moo, Y.C., Matjafri, M.Z., Lim, H.S., Tan, C.H. (2016): New development of optical fibre sensor for determination of nitrateand nitrite in water. Optik, vol. 127, 1312–1319.

Moorcroft, M. J., Davis, J., Compton, R. G. (2001): Detection and determination of nitrate and nitrite: a review. Talanta, vol. 54, 785–803.

Muradova, G. G., Gadjieva, S. R., Palma, L. D., Vilardi, G. (2016): Nitrates Removal by Bimetallic Nanoparticles in Water. Chemical Engineering Transactions, vol. 47, 205–210.

Nováková, K., Nágel, D. (2009): The Influence of Irrigation on Nitrates Movement in Soil and Risk of Subsoil Contamination. Soil and Water Research, vol. 4, S131–S136.

Pekárová, P., Miklánek, P. (1993) Spatial distribution and trend change of nitrate in Slovakia during 1968-1993. Acta Geologica Hispanica, vol. 28, 55–63.

Tall, A., Pavelková, D. (2020): Results of water balance measurements in a sandy and silty-loam soil profile using lysimeters. In Journal of Water and Land Development, vol. 45, 179–184.

Wang, Q.-H., Yu, L.-J., Liu, Y., Lin, L., Lu, R.-g., Zhu, J.-p., He, L., Lu, Z.-L. (2017): Methods for the detection and determination of nitrite and nitrate: A review. Talanta, vol. 165, 709–720.

RNDr. Lucia Balejčíková, PhD. (*corresponding author, e-mail: balejcikova@uh.savba.sk)
RNDr. Andrej Tall, PhD.
Ing. Branislav Kandra, PhD.
Ing. Dana Pavelková, PhD.
Institute of Hydrology
Slovak Academy of Sciences
Dúbravská cesta 9
841 04 Bratislava
Slovak Republic

DOI: 10.31577/ahs-2021-0022.01.0015

ACTA HYDROLOGICA SLOVACA

Volume 22, No. 1, 2021, 125 – 131

ESTIMATION OF NITRATE DISPERSION–DIFFUSION COEFFICIENTS IN AGRICULTURAL SOIL PROFILE

Viera Kováčová*

Nitrate nitrogen (N) is a water-soluble and mobile form of N that is highly susceptible to leaching. Nitrogen leaching requires water movement and N present in the soil solution. The quantitative expression for N leaching includes two factors, the volume of leachate and the N concentration. Controlling nitrogen leaching presents a major challenge for nitrogen managing. Nitrogen managing strategies regarding rate and time of N applications must be developed for the specific soils, hydrology, and crop-tillage systems of individual fields.

The diffusion-dispersion coefficient accounts for the various transport-controlled processes which include dispersion (mixing) and diffusion transport of the ions in concert with the liquid movement in the pores of the soil. Experiments studying transport of nitrate ions were conducted by soil column leaching tests in four soil columns separately. The dispersion-diffusion coefficients D_i were estimated.

KEY WORDS: water quality, nitrate ions, transport parameters, dispersion-diffusion coefficients

Introduction

Nitrogen is a crucial input in agricultural production, but it puts environmental pressure on soil and water contamination. To identify the likely factors influencing nitrogen contamination is one of the most important assignments. It was found out, that increased agricultural activity leads on average to higher nitrate contamination. Nitrogen naturally occurs in an oxidated, reduced and elementary form (gas N_2). Common forms of inorganic nitrogen comprise nitrates NO_3^-, nitrites NO_2^-, ammonium NH_4^+ and cyanides CN^-. Nitrogen in the form of amino acids is an essential component of organic matter. Groundwater is polluted by nitrogen compounds from household waste waters, animal wastes, but chiefly fertilizers. Nitrates mostly occur in natural waters as simple NO_3^- ions, rarely forming complexes. Nitrate content in natural waters varies depending on the vegetation season. Additionally, environmental factors such as precipitation and temperature play an important role. Nitrate leaching from agricultural land is usually considered a non-point source pollution problem, making the specific polluter hard to identify. Consequently, indicators that establish the functional relationship between pollution and agricultural activity in the context of site characteristics are necessary to allow effective policy regulation. Many studies in the literature have developed management options for protecting groundwater quality from nitrate contamination, (Curtin et al., 1994; Džatko, 2004; Kováčová and Velísková, 2013; Wick et al., 2012; Yong et al., 1992).

Input of inorganic N as a fertilizer is considered essential in modern agriculture in order to satisfy a growing world population. Nitrate (NO_3^-) is the one of the principal N forms taken up by plants. As such, inorganic N is widely used in agriculture and numerous studies have suggested that leaching of NO_3^- following high input rates of chemical fertilizer and due to mineralization of organic N already present in the soils can cause degradation of surface and groundwater quality. The ability of soil to adsorb anions can reduce NO_3^- leaching to the deeper horizons and maximilize the NO_3^- available for plant nutrition and can thus play a fundamental role in enhancing soil nutrition in some regions, where NO_3^- availability is often a limiting factor. Previous studies have reported the sorption of NO_3^- by soils. However, NO_3^- mobility in soils is mainly controlled by a number of soil properties including iron and aluminium oxide concentrations, organic matter content, pH of soil solutions and soil texture and clay mineralogy. Authors reported that NO_3^- sorption was directly related to NO_3^- concentration in the soil solution, (Hamdi et al., 2013; Hanes, 1999, Grattoni et al., 1993; Kanwar et al., 1980).

Agricultural activities are probably the most significant anthropogenic sources of nitrate contamination in groundwater. Nevertheless, when nitrogen-rich fertilizer application exceeds the plant demand and the denitrification capacity of the soil, nitrogen can leach to groundwater usually in the form of nitrate which is highly mobile with little sorption. Characterization of nitrogen sources and identification of areas with heavy nitrogen loadings from point and non-point sources is important for land use planners, environmental regulators, and is essential for developing fate and transport models. Once such high-risk areas have been identified, preventive measures can be implemented to minimize the risk of nitrate leaching to groundwater. Accurate quantification of nitrate leaching to groundwater is difficult due to the complex interaction between land use practices, on-ground nitrogen loading, groundwater recharge, soil nitrogen dynamics, and soil characteristics, (Almasri and Kaluarachchi, 2007; Lee et. al., 1991; Lee and Jose, 2005). Almasri and Kaluarachchi (2007) modeled nitrate contamination of groundwater in agricultural watersheds. They present and implements a framework for modeling the impact of land use practices and protection alternatives on nitrate pollution of groundwater in agricultural watersheds to estimate nitrate leaching to groundwater.

A theoretical analysis of the movement of nitrogen compounds in an unsaturated soil with zero-order denitrification is presented in many studies. Analytical solutions of equations describing miscible displacement for steady-flow conditions and uniform water contents are known for many boundary conditions (de Smedt and Wierenga, 1978; Kaledhonkar et al., 2001; van Genuchten and Alves, 1982; Yong et al., 1992).

The mathematical description of groundwater flow, contaminant transport and diffusion through porous media, can be found in many textbooks and monographs devoted to the development of the governing relationship and solution of the relationship subject to various initial and boundary conditions. However, that as good as the mathematical models are, and as efficient as the appropriate numerical models for solution of the complex field problems are, the quality of the inputs used, and the accuracy in representation of the physical, chemical and biological interactions with the transporting fluid and contaminants still remain as part of the essential requirements in the success of the analytical and predictive capability of the models. In the absence of proper inputs, the models will continue to render results that remain suspect.

Nitrogen (N) is a critical nutrient needed by all plants for growth. Nitrates (NO_3^-) are the one of the principal N forms taken up by plants. Numerous studies have suggested that leaching of NO_3^-following high input rates of chemical fertilizer and due to mineralization of organic N already present in the soils can cause degradation of surface and groundwater quality (Almasri and Kaluarachchi, 2007; Kováčová, 2017; Siman and Velísková, 2020).

Material and methods

The movement of one or several solutes in a natural soils involves many complicated phenomena. Estimation of adsorption, transport and transformation nitrogen compounds parameters is need for modeling the movement in an unsaturated soil. The concentration vs. time curve (elution curve) contains most of the information on the interaction between the solute and the soil.

A theoretical analysis of the movement of nitrogen compounds in unsaturated soil with zero-order denitrification is presented in many studies. Analytical solutions of equations describing miscible displacement for steady-flow conditions and uniform water contents are known for many boundary conditions.

The differential equation in the one-dimensional form used for consideration of advective-dispersive transport assume isothermal conditions, difference, no-volume change conditions is written (van Genuchten and Alves, 1982; Yong et al., 1992).

For one-dimensional flow the hydrodynamic dispersion equation for a noninteracting solute were described (van Genuchten and Wierenga, 1986):

$$\frac{\partial(\theta c)}{\partial t} = \frac{\partial}{\partial x}\left[D\,\frac{\partial(\theta c)}{\partial x}\right] - \frac{\partial\,(qc)}{\partial x} \tag{1}$$

where:
c – solute mass per unit volume of solute. [ML^{-3}],
D – diffusion-dispersion coefficient [L^2T^{-1}],
θ – volumetric water content [L^3L^{-3}],
q – Darcian Flux of the soil water [LT^{-1}],
t – time [T],
x – distance [x].

Equation (2) describing transport of water and chemicals in porous media, including sorption and microbial transformation terms is (Bolt, 1979; de Smedt and Wierenga, 1978; van Genuchten and Alves, 1982; Yong et al., 1992):

$$\frac{\partial c}{\partial t} = D\,\frac{\partial^2 c}{\partial x^2} - v\,\frac{\partial c}{\partial x} - \frac{\rho}{\theta}\frac{\partial S}{\partial t} \pm \Phi \tag{2}$$

where:
$\delta S / \delta t$ – represent sorption term [$MM^{-1}T^{-1}$],
Φ – represent kinetic change of chemicals [MT^{-1}],
v – average pore-water velocity [LT^{-1}].

The governing differential equation in the one-dimensional form used for consideration of advective-dispersive transport assume isothermal conditions, absence of significant density difference, no-volume change conditions, without transformations for *i*-ion can be written:

$$\frac{\partial c_i}{\partial t} = D_i\frac{\partial^2 c_i}{\partial x^2} - v_i\frac{\partial c_i}{\partial x} - \frac{\rho}{\theta}\frac{\partial S_i}{\partial t} \tag{3}$$

where:
D_i – diffusion-dispersion coefficient [L^2T^{-1}],
ρ – dry mass density [ML^{-3}],
v_i – average pore-water velocity [LT^{-1}],
S – adsorbed amount of ion [MM^{-1}].

The diffusion-dispersion coefficient accounts for the various transport-controlled processes which include dispersion (mixing) and diffusion transport of the ions in concert with the liquid movement in the pores of the soil. Parameter R (retardation factor) can be used to estimate the number of pore volumes of flow required to achieved breakthrough.

Another way of approaching the problem of modelling of contaminant transport in unsaturated soils is to conduct laboratory leaching column tests using unsaturated soil samples representative of the field situation.

If we substitute sorption item the transport equation will be in form:

$$R_i \frac{\partial c_i}{\partial t} = D_i \frac{\partial^2 c_i}{\partial x^2} - v_i \frac{\partial c_i}{\partial x} \tag{4}$$

where:

R_i – retardation factor.

Attributes of some ions (nitrate, chloride) can be used for estimation parameters D_i and v_i in the transport equation for non-reactive compound, when retardation factor $R \approx 1$ and for steady-state unsaturated liqiud miscible flow

$$\frac{\partial c_i}{\partial t} = D_i \frac{\partial^2 c_i}{\partial x^2} - v_i \frac{\partial c_i}{\partial x} \tag{5}$$

For characterization of the soil solute flow with defined ion composition except the v_i – average pore-vater velocity the values of dispersion-diffusion coefficient must be known. This parameter can be estimated by many ways. According to Gupta and Greenkorn (1974) is used for estimation D_i equation:

$$D_i = \frac{v_i . x}{4\pi \left(\frac{\partial c_i}{\partial \beta} \right)^2_{\beta=1}} \tag{6}$$

where:

β – pore volume,

$\beta = v_i . t/x$.

Lai and Jurinak (1972) used relation:

$$D_i = \frac{v_i . x}{4\pi V_0^2 S_0^2} \tag{7}$$

where:

V_o – cumulative eluate volume for concentration value $ci / (co)i = 0.5$

S_o – direction breakthrough curve in $c_i / (co)_i = 0.5$.

Description of area of interest

The studied soil samples were taken away from the Žitný ostrov area (Slovakia). The Žitný ostrov is one of the most productive agricultural areas of Slovakia, situated on the Danube Lowland. Under its surface is the richest water reservoir of Slovakia. For this reason, it is very important to deal with quantity and quality of water resources in this region. In terms of geomorphology, this territory can be characterised as a young riverside plain with a very low denivellisation of the surface with an overall inclination from north-west to south-east. The territory is break up in transversal as well as in longitudinal directions into different geomorphological areas. In the sense of transversal division, we recognise the upper, the middle and the lower parts of the Žitný ostrov. We distinguish the Pleistocene core, late Holocene aggradation dikes (walls) and early Holocene depressions. The early Holocene depressions are characterised by a relatively high groundwater table. In terms of climatic situations, the Žitný ostrov belongs to a very warm and very dry agroclimatic area with mild winter. In terms of hydrological conditions, the Quaternary formation of sandy gravels created conditions for accumulation of groundwaters (Čurlík and Šefčík, 1999; Koczka Bara et al., 2014).

Anthropogenic activities realized in river basins may result in a deterioration of water quality with detrimental effects on the ecosystems. Nitrate leaching from agricultural land is usually considered a non-point source pollution problem, making the specific polluter hard to identify (Čelková, 2014; Dulovičová et al., 2020; Wick et al., 2012).

Experiments studying transport of nitrate ions were conducted by soil column leaching tests in four soil columns separately. Defined geometry of the soil columns (radius r=0.03 m, cross-section area $2.826.10^{-3}$ m^2, length h=0.3 m) and unsaturated, steady state flow of liquid phase was used. The columns were filled up by the soil continuously. Soil samples were mechanically adapt (dried, crushed and 2 mm size sieved) and chemically (wash by LiCl) prepare. Laboratory experiments were conducted for three pore velocity: $v_1=3.5.10^{-6}$ m s^{-1}, $v_2=5.8.10^{-7}$ m.s^{-1}, $v_3 = 8.3.10^{-8}$ m.s^{-1} and four initial ion concentrations: c_o=100, 200, 300, 500 mg.l^{-1}. Volumetric water content of the soil, determined gravimetric, take values in range 0.32–0.38 cm^{-3} cm^{-3}. Dry mass density values were in range 1.32–1.40 g cm^{-3}. The columns were washed by defined volume V=500 cm^3. The time changes of nitrogen ion concentrations were observed. Nitrates were determined by spectrophotometer DR 2800 fy Hach Lange. The experiments were conducted in pH 6.5 and t=25°C conditions.

Results and discussion

Measured values were graphically plotted as function $c_i / (c_i)_o = f(t)$. The dispersion-diffusion coefficients D_i were estimated from the equation suggested by Lai and Jurinak (1972). For laboratory experiments were used soil samples from locality Okoličná na Ostrove (Calcarohaplic Phaeozem), characterful for Žitný ostrov. The soil texture, physical and chemical properties were determined and are presented in Table 1–3.

This locality was irrigated from Komárňanský channel water with high nitrate concentration level. In study Kováčová, (2020) surface water quality data collected from monitoring sites of Žitný ostrov channel network during the years from 1987 to 2019 were analyzed. The analysis allowed to identify long-term trends of the water quality.
The channel network at the Žitný Ostrov area was built up for drainage and also to provide irrigation water. Komárňanský channel is one of three main channels of this network: Komárňanský channel – is the P1M water body type (partial river-basin Váh, code SKV0226). For the evaluation the water quality we went out from the data obtained on Institute of Hydrology SAS during the 1987–2019.
The quantity of nitrates was evaluated according to Direction of SR government no.269/2010 for establishing requirements for obtaining the good water conditions, resp. previously valid norm STN 75 7221. Measurements for the Komárňanský channel show that the permitted values were exceeded sporadically in some months in the years 1987–2019.
The dependences $c/co = f(t)$ (breakthrough curves) were plotted and the values of $(c/co)_{max}$, $t(c/co)_{max}$ were obtain (Fig. 1).
The diffusion-dispersion coefficients for nitrate were estimated (Table 4). The concentration profiles were estimated and was investigated the influence of the flow electrolyte velocity on the change of nitrates ions concentration in the soil columns at defined conditions. From measuring values it follows that included with decreasing the flow velocity and increasing the initial concentration, the dispersion-diffusion coefficient is decreasing. The coefficients are compareble with results of other studies of the same soil structure, (Čelková, 2014; Hanes, 1999).

Table 1. Soil texture (grain composition)

locality	Soil unit	Sample depth [m]	Sand [%] >0.25 [mm]	Sand [%] 0.25-0.05 [mm]	Silt [%] 0.05-0.01 [mm]	Silt [%] 0.01-0.001 [mm]	Clay [%] <0.001 [mm]
Okoličná na Ostrove	Calcaro-haplic Phaeozem	0.1 – 0.3	7	18	38	37	15.6
		0.4 – 0.7	7	16	42	35	16.1
		0.7 – 1.0	11	19	41	29	14.3

Table 2. Physical properties

locality	Sample depth	ρ_s	ρ_d	P	θ_{FC}	θ_{PDA}	θ_{WP}	AC
	[m]	[g cm^{-3}]	[g cm^{-3}]	[%]	pF 2.3	pF 3.4	pF 4.2	[%]
Okoličná na Ostrove	0.1 – 0.3	2.70	1.62	40	34.1	21.5	15.4	10.8
	0.4 – 0.7	2.72	1.47	45.9	33.8	19.8	16.6	7.9
	0.7 – 1.0	2.73	1.54	43.5	29.6	17.3	15.3	5.6

ρ_s/ρ_d – particle/bulk density, P – tot. porosity, θ_{FC} – field cap., θ_{PDA} – point of dec. avail., θ_{WP} – wilting point, AC – min. air capacity

Table 3. Chemical attributes

locality	Depth	pH		$CaCO_3$	C_{ox}	Humus	EC	ESP
	[m]	H_2O	KCl	[%]	[%]	[%]	[mS m^{-1}]	[%]
Okoličná na Ostrove	0.1 – 0.3	7.9	7.6	29	1.8	3.5	95	3.15
	0.4 – 0.7	8.2	7.8	32	1.9	3.7	82	2.75
	0.7 – 1.0	8.4	7.9	30	1.2	2.8	113	2.51

$CaCO_3$ – cont. of carbonates, Cox – organic carbon, EC – electrical conductivity, ESP – exchangeable sodium percentage

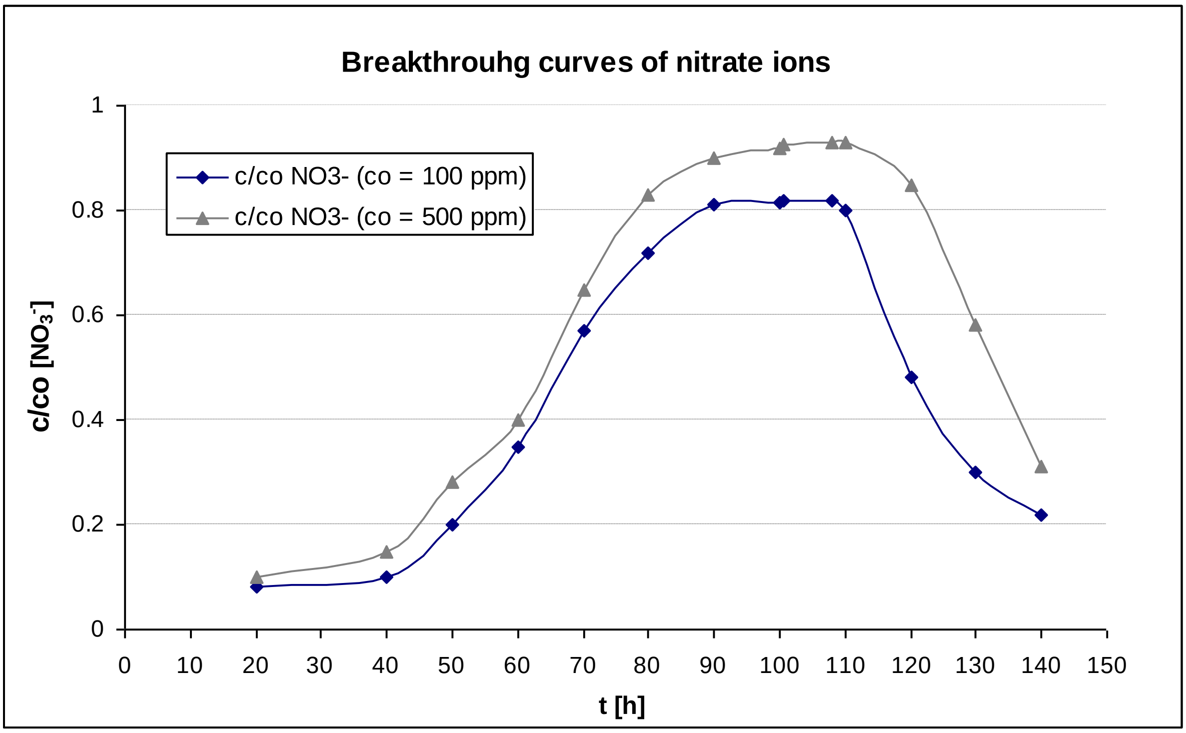

Fig. 1. Measured breakthrough curves for NO_3^- ions stemming from a pulse of NO_3^- (100 and 500 mg l^{-1}) leached through the short soil column at 25°C (pore velocity v_1=3.5.10^{-6} m s^{-1}).

Table 4. Dynamic parameters of the columns

c_o mg l^{-1} NO_3^-	100	200	300	500
θ [cm^3 cm^{-3}]	0.32	0.35	0.33	0.35
ρ [g cm^{-3}]	1.32	1.38	1.40	1.35
		v_1=3.5x10^{-6} m s^{-1}		
$(c/co)_{max}$	0.82	0.85	0.88	0.93
$t_{(c/co)max}$ [h]	100.5	102.3	105.0	108.3
D [m^2 s^{-1}]	2.1x10^{-9}	2.3x10^{-9}	1.2x10^{-9}	9.9x10^{-9}
		v_2=5.8x10^{-7} m s^{-1}		
$(c/co)_{max}$	0.85	0.87	0.92	0.95
$t_{(c/co)max}$ [h]	140.3	143.2	145.2	148.4
D [m^2 s^{-1}]	3.7x10^{-10}	4.6x10^{-10}	3.2x10^{-10}	2.5x10^{-10}
		v_3=8.3x10^{-8} m s^{-1}		
$(c/co)_{max}$	0.85	0.90	0.94	0.95
$t_{(c/co)max}$ [h]	210.0	218.5	225.0	230.5
D [m^2 s^{-1}]	5.2x10^{-11}	7.2x10^{-11}	9.1x10^{-11}	1.1x10^{-12}

θ – volumetric water content, ρ – dry mass density, v_1, v_2, v_3 – average pore water velocity, D – dispersion-diffusion coefficient

Conclusion

Many practices result in non-point source pollution of groundwater and the effects of these practices accumulate over time. These sources include fertilizer and manure applications, dissolved nitrogen in precipitation, irrigation flows, and dry atmospheric deposition.
The resulting process of the nitrates migration may be characterized with the solution of partial processes of the dispersion type, adsorption type, transformations type etc. Estimation of transport, adsorption and transformation nitrogen compounds parameters is need for modelling the movement in an unsaturated soil.
In this paper the main role was directed on the behaviour out the nitrate ions in dynamical conditions of the electrolyte flow. The concentration profiles were estimated and was investigated the influence of the flow electrolyte velocity on the change of nitrates ions concentration in the soil columns at defined conditions. The quantitative parameters of the transport equation were investigated.
The experiments studying transport of nitrogen ions were conducted by soil column leaching tests for unsaturated steady-state flow, defined geometry of the soil columns, defined volumetric water content, dry mass density. Measured values were depicted as a function *c/(c)o=f(t)*. The experiments were conducted for various average pore velocities $v_1=3.5x10^{-6}$ m s^{-1}, $v_2=8x10^{-7}$ m s^{-1}, $v^3=8.3x10^{-8}$ m s^{-1} and four initial ion concentrations: c_o=100, 200, 300, 500 mg l^{-1}. By interpreting of *c/co=f(t)* dependences (breakthrough curves) the significant values of $(c/co)_{max}$ and $t(c/co)_{max}$ for nitrogen ions were obtained and the dispersion-diffusion coefficients D_i were estimated. The transport parameters were obtained for soil, representative for Žitný ostrov as the input values for mathematical modelling of the movement of nitrogen compounds in this region.
From measuring values it follows that included with decreasing the flow velocity the dispersion-diffusion coefficient is decreasing.

Acknowledgement

This contribution was supported by project VEGA 2/0025/19 and project VEGA 1/0085/20.

References

Almasri, M. N., Kaluarachchi, J. J. (2007): Modeling nitrate contamination of groundwater in agricultural watersheds. J. of Hydrology, 343, 215–229. DOI: http://dx.doi.org/10.1016/j.jhydrol.2007.06.016

Bolt, G. H., (1979): Soil chemistry. B. Physico-chemical models. Amsterdam, Elsevier.

Curtin, D., Steppuhn, H., Selles, F. (1994): Structural stability of Chernozemic soils as affected by exchangeable sodium and electrolyte concentration. Can. J. Soil Sci., 74, 157–164.

Čelková, A. (2014): Analysis of reactive solute transport experiments in soil profile. In Növénytermelés, 2014, vol.63, supplement, 169–172. DOI:http://dx.doi.org/10.1007/3-540-26746-8_13

Čurlík, J., Šefčík, P. (1999): Geochemical atlas of the Slovak republic : Part V – Soils, Soil Sci. and Conservation Research Institute, Bratislava.

de Smedt, F., Wierenga, P. J. (1978): Solute Transport Through Soil With Nonuniform Water Content. Soil Sci. Soc. Am. J., vol.42, 873-879. DOI: http://dx.doi.org/10.2136/sssaj1978.03615995004200010002x

Dulovičová, R., Schűgerl, R., Velísková, Y. (2020): Actual values of saturated hydraulic conductivity of channel bed silt and its distribution along Komárňanský channel. Acta Hydrologica Slovaca, Vol. 21, No. 1, 2020, 98–105, doi: 10.31577/a(hs-2020-0021.01.0012

Džatko, M. (2004): Land use and soil anthropization. Soil Anthropization VIII – Proceedings of International Conference, Soil Science and Conservation Research Institute, Bratislava, 132.

Grattoni, C. A., Dawe, R. A., Bidner, M. S. (1993): On the simultaneous determination of dispersion and nonlinear adsorption parameters from displacement tests by using numerical models and optimalisation techniques. Advances ins Water Resour., 16, 127–135. DOI: http://dx.doi.org/10.1016/0309-1708(93)90003-x

Gupta, S. P., Greenkorn, R. A. (1974): Determination of dispersion and non-linear adsorption parameters for flow in porous media. Water Resour. Res., 10, 839–846. DOI: http://dx.doi.org/10.1029/wr010i004p00839

Hamdi, W., Gamaoun, F., Pelster, D.E., Seffen, M. (2013): Nitrate Sorption in an Agricultural Soil Profile. Applied and Environmental Soil Science, Vol. 2013, http://dx.doi.org/10.1155/2013/597824.

Hanes, J. (1999): Analysis of sorption attributes of soils. Soil Sci. and Conservation Research Institute, Bratislava, 138.

Kaledhonkar, M. J., Tyagi, N. K., van der Zee (2001): Solute transport modelling in soil for irrigation field experiments with alkali water. Agricultural Water Management, 51, 2, 153–171. DOI: http://dx.doi.org/10.1016/s0378-3774(01)00100-7

Kanwar, R. S., Baker, J. L., Johnson, H. P., Kirkham, D. (1980): Nitrate Movement with Zero-order Denitrifiction in a Soil Profile. Soil Sci. Soc. Am. J., vol.44, 898–902. DOI: http://dx.doi.org/10.2136/sssaj1980.03615995004400050003x

Koczka Bara, M., Velísková, Y., Dulovičová, R., Schügerl, R. (2014): Influence of surface water level fluctuation and riverbed sediment deposits on groundwater regime. Journal of Hydrology and Hydromechanics, vol. 62, no. 3, 177–185. DOI: http://dx.doi.org/10.2478/johh-2014-0030

Kováčová, V., Velísková, Y., (2013): Evaluation of surface water qualitative parameters in Žitný ostrov area from the nitrogen compounds position. Acta Hydrologica Slovaca, 14, 1, 133–142.

Kováčová, V. (2017): Trendy vývoja obsahu dusičnanov v kanálovej sieti Žitného ostrova [Trends of nitrate ions content in Žitný ostrov channel network]. In Acta Hydrologica Slovaca, 2017, roč. 18, č. 1, p. 57–67. ISSN 1335-6291.

Kováčová, V. (2020): Assessment of surface water eutrophication at Žitný ostrov region. Acta Hydrologica Slovaca, Vol. 21, No. 1, 2020, 65–73, doi: 10.31577/ahs-2020-0021.01.0008

Lai, S. H., Jurinak, J. J. (1972): Cation adsorption in one dimensioanl flow through soils, WRK, 8, 99–102.

Lee, K. H., Jose, S. (2005): Nitrate leaching in cottonwood and loblolly pine biomass plantations along a nitrogen fertilization gradient. Agriculture, Ecosystems and Environment, 105, 615–623.

Lee, Y. W., Dahab, M. F., Bogardi, I. (1991): Nitrate risk management under uncertainty. Journal of Water Resources Planning and Management, 118, 2, 151– 65.

Siman, C., Velísková, Y. (2020): Impact of different proportion of agricultural land in river catchments on nitrogen surface streams pollution. Acta Hydrologica Slovaca, Vol. 21, No. 1, 2020, 56–64, doi: 10.31577/ahs-2020-0021.01.0007

van Genuchten, M. Th., Alves, W. J. (1982): Analytical solutions of the one-dimensional convestive-dispersive solute transport equation. U.S. Department of Agriculture, Technical Bull. 1661, 151. DOI: http://dx.doi.org/10.1016/0012-8252(83)90054-5

van Genuchten, M. Th., Wierenga, P. J. (1986): Solute Dispersion Coefficients and Retardation Factors. Am. Soc. of Agronomy – Soil Sc. Soc. of America, Methods of soil Analysis. Part I. Physical and Mineralogical Methods, Madison, USA, 1025–1054. DOI: http://dx.doi.org/ 10.2136/sssabookser5.1.2ed.c44

Wick K., Heumesser Ch., Schmid E. (2012): Groundwater nitrate contamination: Factors and indicators. Journal of Enviromental Management (111), 178–186. DOI:

Yong, R. N., Mohamed, A. M. O., Warkentin, B. P. (1992): Principles of Contaminant Transport in Soils, Elsevier Science Publishers B.V, 327. DOI: http://dx.doi.org/ 10.1201/b17405-11

Ing. Viera Kováčová (*corresponding author, e-mail: kovacova@uh.savba.sk)
Institute of Hydrology SAS
Dúbravská cesta 9
84104 Bratislava
Slovak Republic

DOI: 10.31577/ahs-2021-0022.01.0016

ACTA HYDROLOGICA SLOVACA

Volume 22, No. 1, 2021, 132 – 138

INFLUENCE OF ELECTROLYTE CONCENTRATION, SODIUM ADSORPTION RATIO AND CATION COMBINATIONS ON RELATIVE SATURATED HYDRAULIC CONDUCTIVITY OF SALINE SOIL

Anežka Čelková*, Anton Zvala

Soil hydraulic conductivity (*K*) is an important parameter in the transport of water and salts in the soils. This study was performed to determine the influence of water quality parameters flowing through the soil on the relative saturated hydraulic conductivity (*rKs*) of salt affected soil. Its aim was to examine the effect of electrolyte concentration at different SAR (sodium adsorption ratio) values of Na–Ca and Na–Mg leaching solutions on changes in *rKs* of saline soil. The experiments were conducted under laboratory conditions in packed soil columns with saline soil from the Jatov locality, Slovakia. The leaching solutions at SAR values of 5, 10, 20, 30, 40 and at the concentrations of Na–Ca and Na– Mg binary electrolytes of 20, 40, 60, 100 and 120 mmol l^{-1} were used. The concentration and composition of the water flowing through the soil showed a significant influence on relative saturated hydraulic conductivity of the soil used in the experiments. The results of the measurements indicated a decrease in *rKs* by gradually decreasing the electrolyte concentration and with increasing SAR values of the percolating electrolytes of both cationic pair Na–Ca and Na–Mg. The laboratory experiments also showed that the values of *rKs* of the soil measured with Na–Ca solutions were higher than those measured with Na–Mg solutions.

KEY WORDS: electrolyte concentration, sodium adsorption ratio, calcium, sodium and magnesium cation, relative saturated hydraulic conductivity, saline soil

Introduction

Soil salinity and sodicity are serious environmental hazards that can limit agricultural production and cause destructive soil degradation. These problems are especially high in arid and semiarid areas, where the poor quality water is often used for irrigation. The substances dissolved in irrigation water in different ways affect the soil properties (physical, chemical, microbiological), the growth and development of plants. The degree of their influence depends on salts concentration, method of irrigation, amount of irrigation water and on irrigated land (Richards (ed.), 1954; Ayers and Westcot, 1985).

The adverse effect of poor quality irrigation water on the physical properties of the soil is associated with the accumulation of dispersive cations such as sodium and potassium in the soil solution, which affect soil physical properties. The high concentration of Na^+ in irrigation water can result in chemical instability of the soil, degradation of soil structure, clogging of pores, infiltration problems and reduction of the soil hydraulic conductivity (*K*), due to exchange and equilibrium processes between the soil soluble and solid phases (Rhoades et al., 1992). Ca^{2+} and Mg^{2+} cations can reduce the negative effect of Na^+ on the soil structure. Generally, the beneficial cation effects on soil stability and hydraulic properties relate to the type of exchangeable cations in the following order $Ca^{2+} > Mg^{2+} > K^+ > Na^+$ (Rengasamy and Marchuk, 2011; Quirk and Schofield, 1955). Due to the dominance of sodium salts in many sources of irrigation water, sodium-related parameters such as exchangeable sodium percentage (ESP) of soils and sodium adsorption ratio (SAR) of irrigation water have been commonly used to study the effects of sodium in irrigation water on soil structural stability (Rengasamy, 2018; Shainberg and Letey, 1984; Shainberg and Shalheved, 1984). SAR of the irrigation water is used as a measure of the risk of sodicity/alkalinity of irrigation water. According to Richards (ed.), (1954) and Rhoades et al., (1992), at SAR values higher than 6 to 9, irrigation water can be expected to cause problems in soils containing clay-type swellable minerals.

Hydraulic conductivity is a key parameter for research involving water and salts movement in the soil and can be affected by pore size and distribution of soil particles, mineralogical composition and concentration and composition of the water flowing through the soil. The studies by Jayawardane et al., (2011); Chinchmalatpure et al., (2014); Menezes et al., (2014); Suarez et al., (1984); Rengasamy and Marchuk (2011),

indicated the combined effect of percolating water quality and soil properties on saturated hydraulic conductivity (*Ks*). In soils with different structure, the changes in *Ks* in leaching with solutions of different concentration and ion composition were observed. They found out, that *Ks* was significantly affected by SAR, different concentrations and ratios of exchangeable cations (Ca^{2+}, Mg^{2+}, Na^+, and K^+), pH and total electrolyte concentration of soil solution, ESP as well as by the cations and anions of the soils. Hydraulic conductivity of the soil is strongly dependent on soil structure, which can be degraded during wetting and leaching. The results of studies by Frenkel et al., (1978); Shainberg et al., (1981) and Ben-Hur et al., (2009) showed that plugging of pores by dispersed clay particles is a major cause of reduced Ks for surface soils irrigated with sodic waters. Shainberg et al., (1981) examined the changes in *Ks* and clay dispersivity as a function of concentration and SAR of percolating solutions. They found, that both the *Ks* and clay dispersivity of the soil mixture were very sensitive to the level of exchangeable Na^+ and to the salt concentration of percolating solution.
The aim of this study was to determine how the sodium adsorption ratio and the different concentration of Na–Ca and Na–Mg leaching electrolytes affect the relative saturated hydraulic conductivity of saline soil from Jatov locality – Slovakia.

Material and methods

The laboratory experiments were performed on disturbed saline soil samples from the Jatov locality (48°7′58″ N latitude 18°01′41″ E longitude) from the topsoil horizon (0–30 cm). The Jatov locality is located on the Danube plain, in the middle of southwestern Slovakia and is one of the driest and warmest areas in Slovakia. The annual average air temperature is 9°C–10°C and the average annual rainfall are 500–600 mm. The physical and chemical characteristics of soil sample used for the experiments are given in Table 1 and Table 2. These parameters were determined by using the standard methods according to Hraško et al., (1962); Richards (ed.), (1954); Gupta et al., (1985); Sotáková, (1988); Valla et al., (1983). Soil chemical parameters were obtained by analysis of saturated soil extract (Table 1) and by analysis of soil water extract (1:5) (Table 2).
The soil was air dried, crushed and passed through a 2 mm sieve. This was then mixed thoroughly and the subsamples were used to fill the plexiglass soil columns (4 cm diameter and 20 cm long) to a bulk density of 1.3 g cm^3. The soil column was placed in a vertical position. Its outlet end was closed with a perforated plexiglass plate and a filter paper (to prevent the escape of soil particles) and a plexiglass plug with valves. The column was wetted slowly from bottom of the column with solution at the highest electrolyte concentration and the highest SAR value.
To study the effect of electrolyte concentration at different SAR values and at different cation combinations of Na–Ca and Na–Mg in percolating binary electrolytes on *rKs* of the soil, 60 combined electrolytes were prepared. The desired levels of concentrations and SAR of the experimental solutions were obtained by mixing the chemical compounds $NaCl+CaCl_2.2H_2O$ in the first case and by mixing the $NaCl+MgCl_2.6H_2O$ chemical compounds in the second case. The leaching solutions with SAR values of 5, 10, 20, 30 and 40 were prepared in concentrations of 20, 40, 60, 100 and 120 mmol l^{-1} of both Na–Ca and Na–Mg solutions. The SAR values for Na–Ca cationic pair were calculated by using the equation (1) and the SAR values for Na–Mg cationic pair were calculated by using the equation (2) (Richards (ed.), 1954):

$$SAR = Na^+/(\sqrt{(Ca^{2+}/2)}) \tag{1}$$

where
SAR – sodium adsorption ratio [-],
Na^+, Ca^{2+} – the cation concentration [mmol l^{-1}].

$$SAR = Na^+/(\sqrt{(Mg^{2+}/2)}) \tag{2}$$

where
SAR – sodium adsorption ratio [-],
Na^+, Mg^{2+} – the cation concentration [mmol l^{-1}].

All solutions were prepared at an equilibrated pH values of 8. The ratio of the cation concentrations of c_{Na+}/c_{Ca2+} and c_{Na+}/c_{Mg2+} in all Na–Ca and Na–Mg leaching solutions which were used in the experiments, are given in Table 3 and Table 4.
The soil column was initially saturated with Na–Ca salt solution at the highest electrolyte concentration and SAR 40 by capillary tension from the bottom of the column. Subsequently, the same solution was applied to the top

Table 1. Physicochemical characteristics of soil sample (Jatov)

Grain size distribution [%]					Org. C	pH	EC	CEC	ESP	SAR
0.001 [mm]	0.001–0.01 [mm]	0.01–0.05 [mm]	0.05–0.25 [mm]	0.25–2.0 [mm]	[%]	[-]	[mS m^{-1}]	[mmol kg^{-1}]	[-]	[-]
23.7	15.4	32.7	25.4	2.8	1.25	8.5	273	434	12.9	32

CEC – cation exchange capacity
ESP – exchange sodium percentage
EC – specific electrical conductivity
SAR – sodium adsorption ratio

of the column to measure the saturated hydraulic conductivity at a constant hydraulic head of 2.0 cm. When the Ks of the soil column of the effluent had stabilized, the sequentially lower concentration solution with the same SAR was applied. This process continued with the solutions with gradually lower concentrations until the final solution with the lowest concentration. The experiment was then repeated sequentially with Na–Ca solutions at SAR values of 30, 20, 10 and 5 using the experimental procedure described above for the electrolyte at SAR 40. For any given SAR, the same soil column was used to measure Ks at progressively lower electrolyte concentrations using the same approach as in the related studies (Jayawardane et al., 2011; Aram et al., 2019). The leachate solutions were collected from each column at time intervals to calculate Ks. After reaching hydraulic equilibrium, as indicated by the output rate, the saturated hydraulic conductivity was calculated (Klute and Dirkson, 1986). For each binary electrolyte, the equilibrium hydraulic conductivity value was taken as the hydraulic conductivity measured at the end of each leaching cycle when the flow rate reached approximately steady state. The values of Ks were calculated at sequential time intervals (t) using Darcy's law (3):

$$Ks = VL/AHt \qquad (3)$$

where
V – volume of solution at steady state [cm^3],
L – length of the soil column [cm],
A – cross-sectional area of the soil column [cm^2],
H – hydraulic head difference [cm],
t – time interval [h].

The saturated hydraulic conductivity of the soil column obtained by using the greatest electrolyte concentration and the corresponding SAR value was taken as the initial hydraulic conductivity Ks_0. Subsequently, the columns were gradually leached with solutions of the same SAR, but with a reduced electrolyte concentration. The obtained hydraulic conductivity was marked as Ks_i.

Table 2. Chemical composition of soil water extract (1:5)

Na^+ [mmol kg^{-1}]	K^+ [mmol kg^{-1}]	Ca^{2+} [mmol kg^{-1}]	Mg^{2+} [mmol kg^{-1}]	SO_4^{2-} [mmol kg^{-1}]	Cl^- [mmol kg^{-1}]	HCO_3^- [mmol kg^{-1}]
23.5	0.89	0.79	0.32	1.25	0.79	24.4

Table 3. The ratio of the cation concentrations in Na–Ca binary electrolyte

c [mmol l^{-1}]	c_{Na+}/c_{Ca2+}				
	SAR 5	**SAR 10**	**SAR 20**	**SAR 30**	**SAR 40**
20	0.67	1.88	6.29	13.40	23.81
40	0.42	1.10	3.35	7.02	12.02
60	0.33	0.82	2.39	4.83	8.19
80	0.28	0.67	1.87	3.72	6.25
100	0.24	0.57	1.56	3.24	5.10
120	0.21	0.50	1.35	2.62	4.33

c – the concentration of Na–Ca binary electrolyte
c_{Na+}/c_{Ca2+} – the ratio of cation concentrations in the Na–Ca electrolyte

Table 4. The ratio of the cation concentrations in Na–Mg binary electrolyte

c [mmol l^{-1}]	$c_{Na+}/_{Mg2+}$				
	SAR 5	**SAR 10**	**SAR 20**	**SAR 30**	**SAR 40**
20	1.11	3.12	10.37	22.11	39.29
40	0.69	1.81	5.53	11.57	19.83
60	0.54	1.36	3.94	7.97	13.52
80	0.45	1.10	3.08	6.15	10.32
100	0.40	0.94	2.58	5.35	8.41
120	0.35	0.84	2.24	4.33	7.14

c – the concentration of Na–Mg binary electrolyte
c_{Na+}/c_{Mg2+} – the ratio of cation concentrations in the Na–Mg electrolyte

The changes in hydraulic conductivity between treatments were represented as a relative saturated hydraulic conductivity (*rKs*) to provide a hydraulic conductivity reduction from the initial Ks_0. The values of soil *rKs* was calculated according to the equation (4):

$$rKs = Ks_i/Ks_0 \qquad (4)$$

where

rKs – relative saturated hydraulic conductivity of the soil [-],

Ks_0 – initial saturated hydraulic conductivity of the soil [cm h^{-1}],

Ks_i – saturated hydraulic conductivity of the soil leached by the following solution i [cm h^{-1}].

Using the methodology described above for Na–Ca solutions, the experiments to measure the soil Ks were then repeated with Na–Mg solutions, substituting calcium chloride for magnesium chloride in preparing the leaching solutions with the corresponding SAR value. At the end of each experiment, the soil *rKs* values were calculated for all leaching electrolyte concentrations with corresponding SAR values for both solutions Na–Ca and Na–Mg.

Results and discussion

By laboratory experiments on a disturbed soil sample from the surface layer (0–30 cm) of the soil from the Jatov locality a changes in relative saturated hydraulic conductivity of the soil leached with Na–Ca and Na–Mg solutions with different concentrations and different SAR were observed. The measured results showed that the concentration, SAR and cation combinations of the electrolyte flowing through the studied saline soil have a significant effect on *rKs* of the soil. The values of *rKs* increased with increasing electrolyte concentration at all SAR for both cationic pair Na–Ca and Na–Mg. With increasing SAR of percolating electrolyte, the values of soil *rKs* decreased. A graphical representation of the dependence of soil *rKs* on the concentration and SAR of both leaching solutions Na–Ca and Na–Mg is shown in Fig. 1 and Fig. 2.

When comparing the *rKs* values determined in leaching with Na–Ca solutions at SAR value of 5 and at a concentrations of 20, 40, 60, 80, 100 mmol l^{-1}, with the rKs values determined in leaching with Na–Ca solutions at SAR 10, 20, 30, 40 and at a corresponding concentrations, a reduction in *rKs* of the soil was found. The highest reduction in *rKs*, up to 67.3%, was found when the leaching solution at a concentration of 40 mmol l^{-1} and SAR 40 was used. Percentage reduction in *rKs* values determined in leaching with Na–Ca solutions at SAR 10, 20, 30, 40, compared to *rKs* values determined in leaching with SAR 5 solutions is shown in Table 5.

The course of soil *rKs* dependence on electrolyte concentration and SAR for Na–Mg cationic pair was similar as in the first case when Na–Ca solutions were

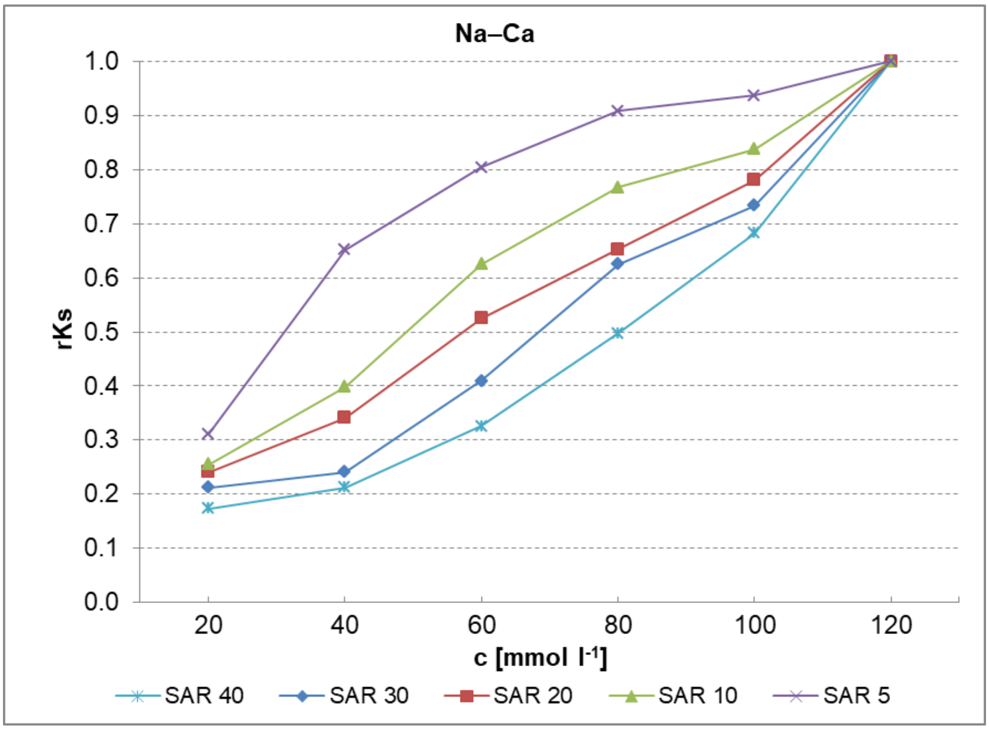

Fig. 1. The relative saturated hydraulic conductivity (rKs) of the soil versus concentration of Na–Ca binary electrolyte at a sodium adsorption ratio (SAR) of 5, 10 20, 30 and 40.

used in leaching (Fig. 2). The soil *rKs* increased with increasing electrolyte concentration at all SAR values. With increasing of SAR of percolating electrolyte, the values of *rKs* decreased. Percentage reduction in *rKs* values determined in leaching with Na–Mg solutions at SAR 10, 20, 30, 40 compared to *rKs* values determined in leaching with solution at SAR 5 at a corresponding concentrations, is shown in Table 6. The highest percentage reduction in *rKs*, up to 66.8%, was found in leaching with Na–Mg solution at a concentration of 40 mmol l^{-1} and SAR 40.

When comparing the results of soil *rKs* measurements, when the binary electrolyte NaCl + $CaCl_2.2H_2O$ in the first case, and the binary electrolyte NaCl + $MgCl_2.6H_2O$ in the second case, were used in leaching, a decrease in soil *rKs* values was found for Na–Mg cationic pair compared to Na–Ca cationic pair. Percentage reduction in *rKs* values by using Na–Mg electrolytes for leaching at a concentration of 20–100 mmol l^{-1} and at SAR of 5, 10, 20, 30 and 40, compared to Na–Ca leaching electrolytes at the same concentrations and SAR is shown in Table 7. The lowest reduction in *rKs* values of 1.67% was found in leaching with electrolyte with a concentration of 100 mmol l^{-1} and SAR 10. The highest reduction in *rKs* values of 32.75% was found when the electrolyte with a concentration of 20 mmol l^{-1} and SAR 40 was used in leaching.

The measurements showed that *rKs* of the soil increased with increasing of the concentration of both solutions Na–Ca and Na–Mg at all SAR values (5, 10, 20, 30 and 40) and decreased with increasing of SAR. These results are confirmed by several previous works by Jayawardane

Table 5. Percentage reduction in *rKs* values for Na–Ca electrolytes

c [mmol l^{-1}]	Reduction in *rKs* [%]			
	SAR 10	SAR 20	SAR 30	SAR 40
20	18.2	22.7	31.7	45.1
40	38.9	47.6	63.0	67.3
60	22.2	34.7	48.7	59.3
80	15.5	28.0	30.8	43.7
100	10.5	16.6	21.6	27.3

rKs – relative saturated hydraulic conductivity
c – the concentration of Na–Ca binary electrolyte

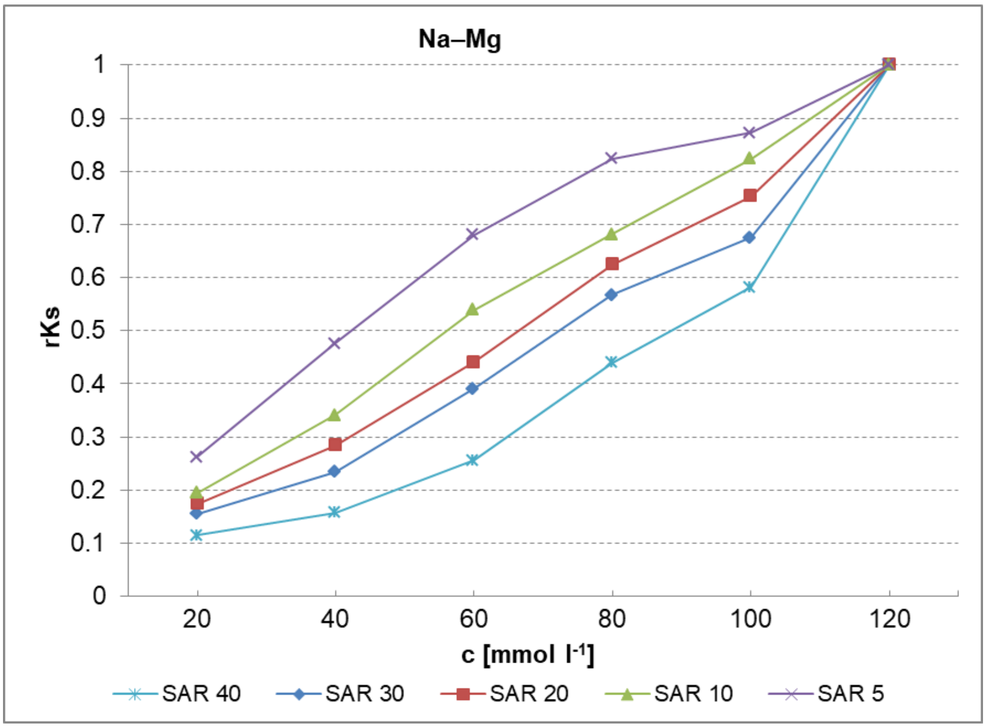

Fig. 2. The relative saturated hydraulic conductivity (rKs) of the soil versus concentration of Na–Mg binary electrolyte at a sodium adsorption ratio (SAR) of 5, 10 20, 30 and 40.

Table 6. Percentage reduction in *rKs* values for Na–Mg electrolytes

c [mg l^{-1}]	Reduction in *rKs* [%]			
	SAR 10	SAR 20	SAR 30	SAR 40
20	25.8	33.8	40.6	56.2
40	28.3	40.3	50.8	66.8
60	20.8	35.3	42.5	62.4
80	17.21	24.1	31.1	48.9
100	5.6	13.7	22.6	33.3

rKs – relative saturated hydraulic conductivity
c – the concentration of Na–Mg binary electrolyte

Table 7. Percentage reduction in *rKs* values by using Na–Mg electrolytes compared to Na–Ca electrolytes

c [mmol l^{-1}]	Reduction in *rKs* [%]				
	SAR 5	SAR 10	SAR 20	SAR 30	SAR 40
20	15.71	23.53	27.80	26.76	32.75
40	26.99	14.32	16.72	2.90	25.82
60	15.30	13.76	16.19	5.10	21.71
80	9.25	11.08	4.29	9.55	13.89
100	6.83	1.67	3.59	8.04	14.54

rKs – relative saturated hydraulic conductivity
c – the concentration of Na–Ca resp. Na–Mg binary electrolyte

et al., (2011); Chinchmalatpure et al., (2014); Menezes et al., (2014); Dikinya et al., (2007). The reduction in *rKs* was related to the ratio of the cation concentrations of c_{Na+}/c_{Ca2+} and c_{Na+}/c_{Mg2+} in all Na–Ca and Na–Mg leaching solutions used at the experiments (Table 3 and Table 4). The higher was this ratio, the higher was the reduction in soil *rKs*. The reduction in the Ks may be attributed to swelling and dispersion of the soil clays caused by Na^+ ions. At an electrolyte concentration of 20 mmol l^{-1} and SAR 40, the most unfavorable ratio of c_{Na+}/c_{Ca2+} and c_{Na+}/c_{Mg2+} in the electrolytes was found. With increasing electrolyte concentration, this ratio decreased, the adverse effect of sodium on the soil structure was reduced, as a result of which the *rKs* of the soil increased. At higher concentrations, the Ca^{2+} and Mg^{2+} cations can counteract the dispersive nature of Na^+ and thus reduce the dispersive effects on the soil structure. With increasing SAR of the electrolyte, the ratio of c_{Na+}/c_{Ca2+} and c_{Na+}/c_{Mg2+} in the leaching electrolytes increased, the adverse effect of sodium on the soil structure increased, causing a decrease in *rKs* of the soil. Laboratory experiments also showed that *rKs* measured with Na–Ca solutions were higher than those measured with Na–Mg solutions. The effect of magnesium is different from that of calcium because they have different affinities for adsorption on the exchange complex. The flocculation effect of Ca^{2+} is higher than that of Mg^{2+} which is not as efficient in flocculating clay as Ca^{2+} and under specific conditions can have a dispersive effect. Na–Mg soils were found to give rise to more dispersed clay and lower hydraulic conductivity than Na–Ca soils (Rengasamy and Marchuk, 2011; Rengasamy et al., 2016; Shainberg and Letey, 1984).

The concentration, SAR and combination of cations of the electrolyte flowing through the soil greatly affect its permeability. When selecting water for irrigation, it is therefore important to monitor not only its total ion concentration but also the ratio of the exchangeable cations (Na^+, K^+, Mg^{2+} and Ca^{2+}), which significantly affect the structure of the soil and thus its hydraulic conductivity.

Conclusion

The changes in the relative saturated hydraulic conductivity of saline soil as a function of concentration, SAR and cation combinations of percolation solutions were measured. The results obtained from laboratory experiments indicated an increase in soil *rKs* with decreasing SAR values and with increasing concentration of both leaching solutions Na–Ca and Na–Mg. The greatest impact on *rKs* of the soil has sodium, the excessive amount of which causes dispersion of clay soil particles and thus reduces its permeability. At higher concentrations of leaching solutions, the Ca^{2+} and Mg^{2+} cations have the effect of reducing the dispersive effects of sodium. Results also revealed that *rKs* of the soil measured with Na–Ca solutions was higher than those measured with Na–Mg solutions. Mg^{2+} cations have a different affinity for adsorption on the exchange

complex than Ca^{2+} and are not as effective at clay flocculation as Ca^{2+}.
In further experiments aimed at studying the effect of concentration and SAR of leaching solutions on *Ks* of saline soil, it will be appropriate to use more soil types with different clay content and different ESP of the soil.

Acknowledgement

This work was supported by the Slovak Scientific Grant Agency VEGA Project VEGA 2/0096/19.

References

Aram, A., Biggs, A. J. W., Šimůnek, J., Bennett, J. McL. (2019): A pH-Based Pedotransfer Function for Scaling Saturated Hydraulic Conductivity Reduction: Improved Estimation of Hydraulic Dynamics in HYDRUS. Vadose Zone Journal, vol. 18, no. 1, 13. Available online: https://escholarship.org/uc/item/7mt7t8jd

Ayers, R. S., Westcot, D. W. (1985): Water quality for agriculture. FAO Irrigation and Drainage Paper 29, Rev. 1. FAO, Rome. Available online: http://www.fao.org/3/T0234E/T0234E00.htm

Ben-Hur, M., Yolcu, G., Uysal, H., Lado, M., Paz, A. (2009): Soil structure changes: aggregate size and soil texture effects on hydraulic conductivity under different saline and sodic conditions. Australian Journal of Soil Research, 47, 688–696.

Dikinya, O., Hinz, C., Aylmore, G. (2007): Influence of sodium adsorption ratio on sodium and calcium break-through curves and hydraulic conductivity in soil columns. Australian Journal of Soil Research, vol. 45, no. 8, 586–597.

Frenkel, H., Goertzen, J. O., Rhoades, J. D. (1978): Effects of Clay Type and Content, Exchangeable Sodium Percentage, and Electrolyte Concentration on Clay Dispersion and Soil Hydraulic Conductivity. Soil sci. Soc. Am. J., vol. 42, 32–39.

Gupta, R.K, Singh, C.P., Abrol, I.P. (1985): Determining cation exchange capacity and exchangeable sodium in alkali soils. Soil Science, vol. 139, 326–331.

Hraško, J., Červenka, L., Facek, Y., Komár, J., Němeček, J., Pospíšil, F., Sirový, V. (1962): Rozbory pôd. Bratislava, SVPL.

Chinchmalatpure, A. R., Bardharr, G., Nayak, A. K., Rao, G. G., Chaudhari S. K., Sharma, D. K. (2014): Effect of Sodium Adsorption Ratio with Different Electrolyte Concentrations on Saturated Hydraulic Conductivity of Selected Salt Affected Soils of Gujarat. Journal of the Indian Society of Soil Science, vol. 62, no.1, 1–8.

Jayawardane, N. S., Christen, E. W., Arienzo, M., Quayle, W. C. (2011): Evaluation of the effects of cation combinations on soil hydraulic conductivity. Soil Research, vol. 49, 56–64.

Klute, A., Dirkson, C. (1986): Hydraulic conductivity and diffusivity: Laboratory methods. In Methods of Soil Analysis, Part 1. (Klute, A., ed.). American Society of Agronomy, Madison, WI, USA.

Menezes, H. R., Almeida, B. G., Almeida, C. D. G. C., Bennett, J. M., Silva, E. M., Freire, M. B. G. S. (2014): Use of threshold electrolyte concentration analysis to determine salinity and sodicity limit of irrigation water. R. Bras. Eng. Agric. Ambiental, vol. 18, 53–58.

Rengasamy, P. (2018): Irrigation Water Quality and Soil Structural Stability: A Perspective with Some New Insights. Agronomy, vol. 8, no. 5, 72. Available online: https://doi.org/10.3390/agronomy8050072

Rengasamy, P., Marchuk, A. (2011): Cation ratio of soil structural stability (CROSS). Soil Research, 2011, vol. 49, 280–285.

Rengasamy, P., Tavakkoli, E., Mcdonald, G. K. (2016): Exchangeable cations and clay dispersion: net dispersive charge, a new concept for dispersive soil. British Society of Soil Science. European Journal of Soil Science. Available online: https://onlinelibrary.wiley.com/doi/abs/10.1111/ejss.12369

Richards, L. A., (ed.) (1954): Diagnosis and improvement of saline and alkali soils. U.S. Salinity Laborat. Staff, USDA, Washington, D.C., Agriculture Handbook No. 60, 160.

Rhoades, J. D., Kandiah, A., Mashali, A. M. (1992): The use of saline waters for crop production. FAO irrigation and drainage paper 48, Food and agriculture organization of the United Nations Rome, 1992. Available online: http://www.fao.org/docrep/T0667E/T0667E00.htm

Quirk, J. P, Schofield, R. K. (1955): The effect of electrolyte concentration on soil permeability. Journal of Soil Science, vol. 6, 163–178.

Shainberg, I., Letey, J., (1984): Response of Soils to Sodic and Saline Conditions. HILGARDIA, Journal of Agricultural Science, California, vol. 52, no. 2, 57.

Shainberg, I., Shalheved, J. (ed.) (1984): Soil salinity under Irrigation. Processes and management. Ecological Studies 51. Springer –Verlag Berlin Heidelberg, 350.

Shainberg, I., Rhoades, J. D., Praither, R. J. (1981): Effect of Low Electrolyte Concentration on Clay Dispersion and Hydraulic Conductivity of a Sodic Soil. Soil Sci. Soc. Am. J., vol. 45, 263–277.

Sotáková, S. (1988): Návody na cvičenie z geológie a pôdoznalectva. Príroda, Bratislava.

Suarez, D. L., Rhoades, J. D., Lavado, R., Grieve, C. M. (1984). Effect of pH on saturated hydraulic conductivity and soil dispersion. Soil Sci Soc. Am. J., vol. 48, 0–55.

Valla, M., Kozák, J., Drbal, J. (1983): Cvičení z půdoznalství II, SPN, Praha, 280.

Ing. Anežka Čelková (*corresponding author, e-mail: celkova@uh.savba.sk)
Mgr. Anton Zvala, PhD.
Institute of Hydrology SAS
Dúbravská cesta 9
84104 Bratislava
Slovak Republic

DOI: 10.31577/ahs-2021-0022.01.0017

ACTA HYDROLOGICA SLOVACA

Volume 22, No. 1, 2021, 139 – 146

COMPARISON OF THE SOLUTE (NITRATES) TRANSPORT THROUGH TWO TYPES OF SOIL PROFILES USING 1-D HYDRUS SOFTWARE

Lucia Balejčíková*

Nitrates, used especially in agricultural activities, are still a widespread risk for human health when exceeding recommended limits in various water drinking sources. Leaching of nitrates from soil to groundwater depends on various factors (as soil properties, the size of soil particles, the ability of specific soil components and plant to absorb water and nitrates, meteorological conditions). The main goal of the presented work was to show nitrates leaching through different soil types. Different solute transport processes and solute distribution in the soil profile were demonstrated using HYDRUS-1D model simulation. This mathematical computation research could contribute to the set-up of suitable fertilizers concentration applied in agriculture on the soil surface with defined hydraulic properties. This method represents the economically advantageous and simple first step before fertilizers application. Particularly, the main idea of such theoretical simulations is a timely environmental measures implementation against groundwater contamination.

KEY WORDS: soil profile, hydraulic properties, solute transport, mathematical simulation

Introduction

Nitrates are naturally occurring ions featured in the natural nitrogen cycle. Within fertilizers, composition creates support for crop growth in agriculture, which produce the main sources for human nutrition. Together with human consumption rate and growth, increased fertilization irrigation with domestic wastewater and changes in land-use patterns caused widespread pollution of drinking water sources by nitrates. Mobile ions easily pass through the soils and reach the aquifer (Balejčíková et al., 2020). This serious environmental problem still exists in many parts of the world. The main risk areas include South America, most European countries, the Eastern part of Africa, India and Australia (Zhou, 2015). In Slovakia, the situation with nitrates level is stabilized thanks to applied legislation, although there increased concentrations were measured by monitoring (Balejčíková et al., 2020). Fig. 1 shows a map of Slovakia with risk regions from 2019.

The main problem is associated with nitrates limits in relationship with organism and water sources used for drinking purposes. Higher-level over 50 mg l^{-1} and over 10 mg l^{-1} for infants (recommended by WHO and included in EU countries legislative) are linked with methaemoglobinaemia, the blue-baby syndrome development leading often to death (Greer and Shannon, 2005), and with the possible formation of n-nitroso compounds, potential carcinogens in the digestive tract. The precise mechanism is unknown, probably the most important role plays the interaction between haemoglobin and various enzymes and nitrosamines (Gushgari and Halden, 2018). Also, the recent study aimed at the finding of the reason for patients mortality infected by the SARS-CoV-2 virus observed higher concentrations of nitrates post-mortal occurring (Lorentea et al., *in press*). This finding even more emphasizes the reasons for dealing with nitrates hydrological research. For nitrates to remove or concentration decreasing to acceptable health levels it is necessary to develop a suitable method for drinking water treatment (e.g. chemical reduction, reverse osmosis, electrodialysis, ion exchange, biological reduction, nanomagnetic separation or nanofiltration) (Kapoor and Viraraghavan, 1997; Soares, 2000; Shrimali and Singh, 2001; Bhatnagar and Sillanpää, 2011; Archna et al., 2012; Anand et al., 2018; Madhura et al., 2019;). When we take into account costs used for any separation technique applying, still it is advantageous to eliminate and economically manipulate with fertilization. Set-up of the initial concentration of nitrates in fertilizers applied on some soil surface is related to pre-determination of hydro-pedological and physico-chemical characteristics of the specific soil type, presence of cracks, denitrification bacteria, plant cover type, phenology and meteorological conditions. Fertilizer manufacturer takes into account surface and does not list all factors affecting transport processes of nitrates in the soil. Climate change

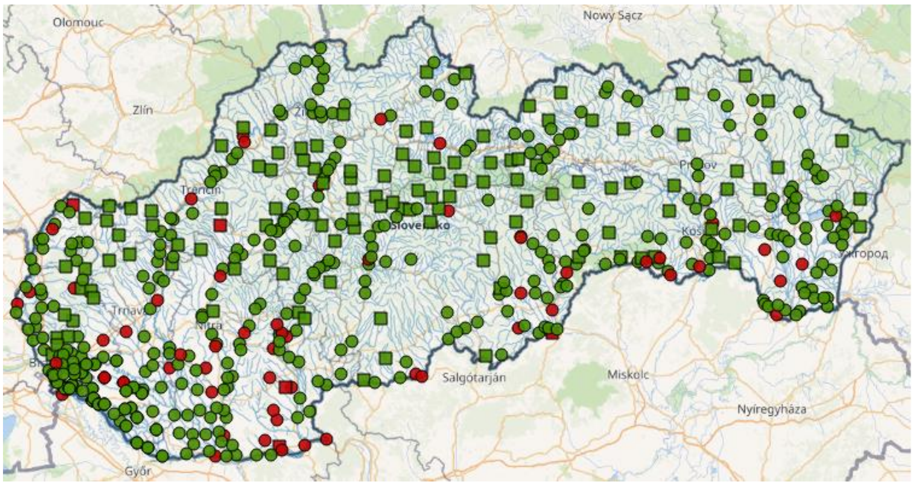

Fig. 1. The map of Slovakia with red marked points represented nitrates concentration over 50 mg l^{-1} from monitoring data of 2019 (the figure taken from a public source of www.shmu.sk).

affects the hydrological cycle, groundwater levels, resources and transport processes of various substances. Precise consequences of climate variations on the nitrate leaching to groundwater are not yet well enough understood (Stuart et al., 2011). The impacts of these changes are still difficult to predict, so it is necessary to deal with monitoring studies and the development of model scenarios to understand the impact of all factors on nitrate transport and leaching. The main goal of the study is the application of HYDRUS-1D software on 2 types of soil profile, occurring in the East Slovak Lowland. Numerical simulation using HYDRUS software allows to model the transport, distribution and leaching of water and dissolved nitrates. Theoretical calculation could be eventually compared with field data from the experiment and help to find all factors contributing to transport processes.

Methods

HYDRUS-1D computation

The HYDRUS-1D program was based on the one-dimensional Richards equation to simulate water and solute movement in variably saturated media, and the equation was solved by numerical method (Šimůnek et al., 2005). Richards equation (1) describes the basic water movement:

$$\frac{\partial\theta(h,t)}{\partial t} = \frac{\partial}{\partial z}\left[K(h)\left(\frac{\partial h}{\partial z}+1\right)\right] \tag{1}$$

where
h – soil water pressure head [l],
θ – volumetric water content [$cm^3\ cm^{-3}$],
t – time [days, d],
z – vertical coordinate [cm] with the origin at the soil surface (positive upward),
$K(h)$ – unsaturated hydraulic conductivity [$cm\ d^{-1}$].

The one-dimensional Hydrus-1D computer program (Šimůnek et al., 2008) was selected to simulate nitrates movement through the soil profile in the vertical direction. The Hydrus-1D program numerically solves the Richards equation for saturated and unsaturated water flow and the convection-dispersion equations for heat and solute transport. The governing one-dimensional solute flow equation for a partially saturated porous medium is described using the modified form (2) of the Richards equation:

$$\frac{\partial(\theta.C)}{\partial t} = \frac{\partial}{\partial z}\left[\theta.D\left(\frac{\partial C}{\partial z}\right)\right] - \frac{\partial(q.C)}{\partial z} + S_C \tag{2}$$

Initial and boundary condition are:

$C = C_0(z)$ *at* $-100 \le z \le 0,\ t=0,$
$\frac{\partial C}{\partial z} = 0, at\ z = -100, t>0,$

where
C – NO_3-N concentration in the soil solution [$mg\ l^{-1}$],
D – effective dispersion coefficient of the soil matrix [$cm^2\ d^{-1}$],
S_c – sink term that includes mineralization, microbial immobilization and denitrification:
$S_c = S \times C_r + k_{min} - k_{im} \times C - k_{den} \times C,$

where
S – plant water uptake [$cm\ d^{-1}$],
C_r – outflow nitrogen concentration that is a function of soil nitrogen concentration (C) and maximum root nitrogen uptake coefficient (C_{RM}),
k_{min} – mineralization rate constant [$\mu g\ cm^{-3}\ d^{-1}$],
k_{im} – microbial immobilization rate constant [d^{-1}],
k_{den} – denitrification rate constant [d^{-1}].

The boundary conditions (3) in the case of nitrogen application treatments are:

$$-\theta . D \left(\frac{\partial C}{\partial z}\right) + q . C = q_0 . C_0(t), at z = 0, t > 0 \quad (3)$$

where
$C_0(t)$ – nitrogen application rate at different times.

The equation for advection-dispersion (4), which describes the solute transport in a variably saturated soil is:

$$\frac{\partial \rho S}{\partial t} + \frac{\partial \theta C}{\partial t} = \frac{\partial}{\partial z}\left\{\theta . D \frac{\partial C}{\partial z}\right\} - q \frac{\partial C}{\partial z} \quad (4)$$

where
ρ – bulk soil density [g cm^{-3}],
C and S – solute concentrations in the liquid [g cm^{-3}] and solis [g g^{-1}] phases
$S = K_d C$ with K_d [cm^3 g^{-1}] is the partition coefficient,
z – spatial coordinate,
D – dispersion coefficient [cm^2 d^{-1}],
q – volumetric flux density [cm d^{-1}] (Kanzari et al., 2018).

Results and discussion

This study was aimed at numerical simulation of NO_3^- application in the situation of the early stage of the vegetation period when water and solute root uptake are minimized and thus neglected. The main goal of this computation was to highlight the difference in the vertical transport of NO_3^- through two various soil profiles. The representative comparative texture consisting of silty-loam and sandy soil was selected due to their occurrence in the East Slovak Lowland. The vertical depth of soil was chosen according to the height of monoliths in the lysimetric station in Petrovce nad Laborcom, Slovakia (Matusek et al., 2017). Precise soil texture was not obtained from field measurements, therefore this numerical computation was based on the theoretical general data. The selected difference in soil types allows using HYDRUS-1D to show significant changes in aqueous solute transport when we neglect other factors as nitrogen mineralization, (de)nitrification, salts and water uptake by root and meteorological conditions in the early stages of the vegetation period. Firstly, the main input used parameters of the HYDRUS-1D model were collected in Table 1.
In the Table 1, θ_r [cm^3 cm^{-3}] is saturated water content, θ_s [cm^3 cm^{-3}] is residual water content, α [cm^{-1}] and n are empirical parameters, K_s [cm d^{-1}] is saturated hydraulic conductivity, L is tortuosity parameter in the conductivity function, D [cm^2 d^{-1}] is dispersion coefficient, K_d [cm^3 g^{-1}] is distribution coefficient and ρ is bulk density of specific soil type [g cm^{-3}]. The main difference

Table 1. Parameter used at HYDRUS-1D numerical simulation

Soil texture		Silty-loam soil	Sandy soil
Parameter	**Units**	**Values**	
Depth	[cm]	250	250
Number of layers	[-]	1	1
Simulation time	[days (d)]	30	30
Time steps	[-]	daily	daily
Hydraulic properties			
θ_r	[cm^3 cm^{-3}]	0.067	0.045
θ_s	[cm^3 cm^{-3}]	0.45	0.43
α	[cm^{-1}]	0.02	0.145
n	[-]	1.41	2.68
K_s	[cm d^{-1}]	10.8	712.8
L	[-]	0.5	0.5
Boundary conditions			
Water flow			
Upper boundary condition		Constant pressure head	
Lower boundary condition		Free drainage	
Solute transport			
Upper boundary condition		Concentration flux BC	
Lower boundary condition		Zero concentration gradient	
Solute transfer properties			
Layer	[cm]	0–250	0–250
D	[cm^{2}d^{-1}]	55	55
K_d	[cm^3 g^{-1}]	0.7	0.7
ρ	[g cm^{-3}]	1.33	1.7

between silty-loam and sandy soil comes from their different hydraulic properties, related to the structure of the porous system with different geometry, size and connectivity. The relationship between pressure head, h, and water content, θ, for silty loam (Fig. 2a) and sandy soil (Fig. 2b) shows the main effect of soil texture described by parameters in Table 1. Saturation in Fig. 2b is achieved at air-entry pressure.

The ability of soil to pass water through pore space can be demonstrated as a dependence of hydraulic capacity versus pressure head (Fig. 3a, b). Maximum capacity for sandy soil indicates the maximum amount of infiltration moisture in the soil subsurface illustrated in Fig. 3b.

The most important hydrogeological parameter, hydraulic conductivity, is affected by both soil and fluid properties and characterizes the ability of water and solute transport through characteristic soil profile due to hydraulic gradient. It depends on the soil pore geometry as well as the fluid viscosity and density. The hydraulic conductivity for a given soil for example becomes lower when the fluid is more viscous than water. Saturation in our case was achieved for sandy soil at air-entry (h) value (Fig. 4b) in contrast to silty-loam profile (Fig. 4a). The main affecting parameter, in this case, is soil density associated with the soil texture.

Fig. 5 shows soil moisture (theta) at 40, 100 and 160 cm depth of layers within horizons below the ground surface divided according to the layout of lysimeter monoliths located in the East Slovak Lowland. 1-D profile with the hydraulic properties of silty-loam (Fig. 5a) and sandy soil (Fig. 5b) as a function of time shows the soil moisture (theta) response in a shorter time for sandy soil (Fig. 5b). Fig. 6 represents wetting profiles soil moisture (theta) distributions in depth. Different wetting profiles are related to variations in soil textures and thus fitting parameters for simulation applied on both soil types. Wetting front is achieved easier in the sandy soil profile (Fig. 6b). It should be noticed, that the wetting front

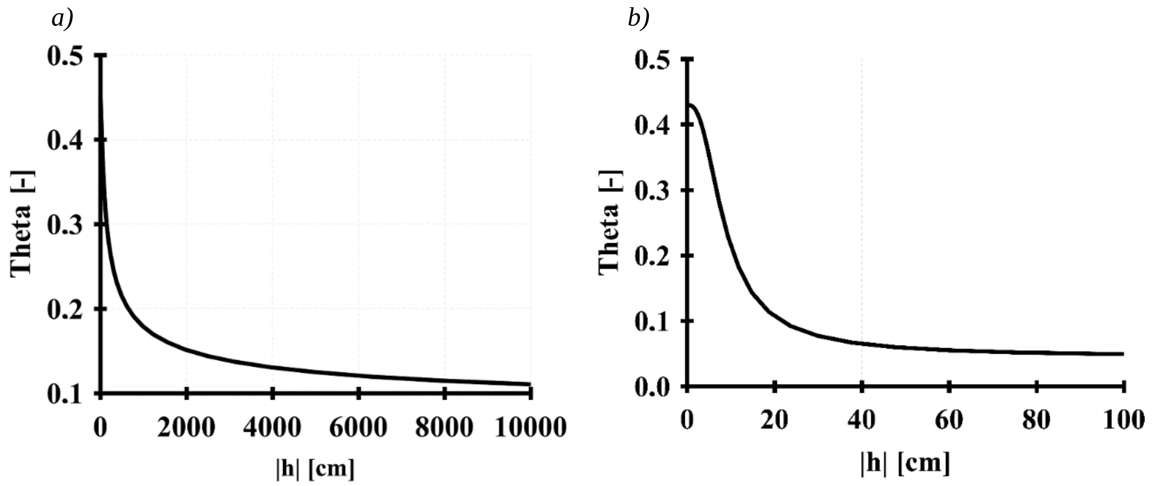

Fig. 2. Simulated pressure head versus water content for a) silty-loam and b) sandy soil profile.

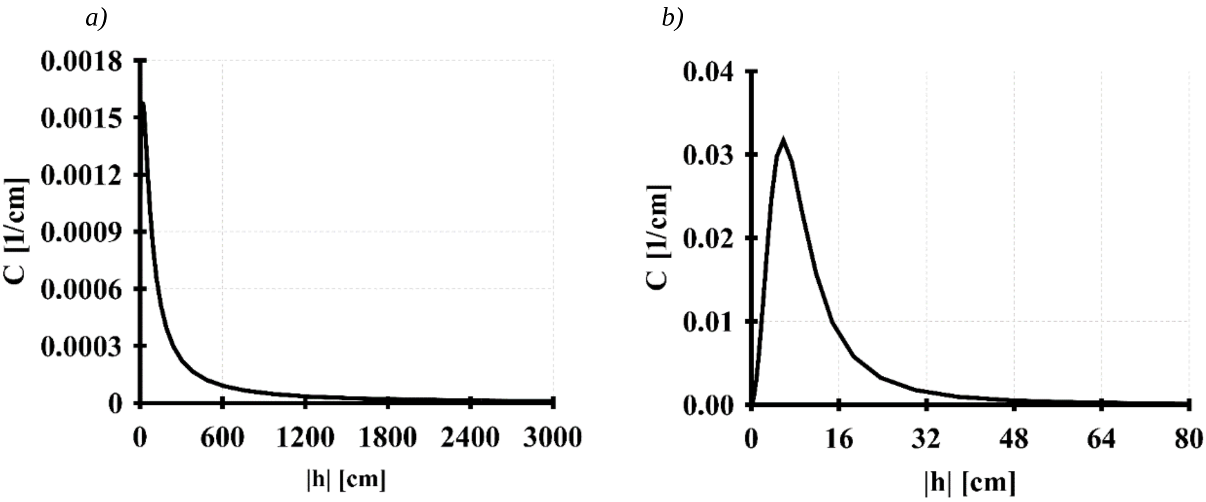

Fig. 3. Simulated pressure head versus hydraulic capacity for a) silty-loam and b) sandy soil profile.

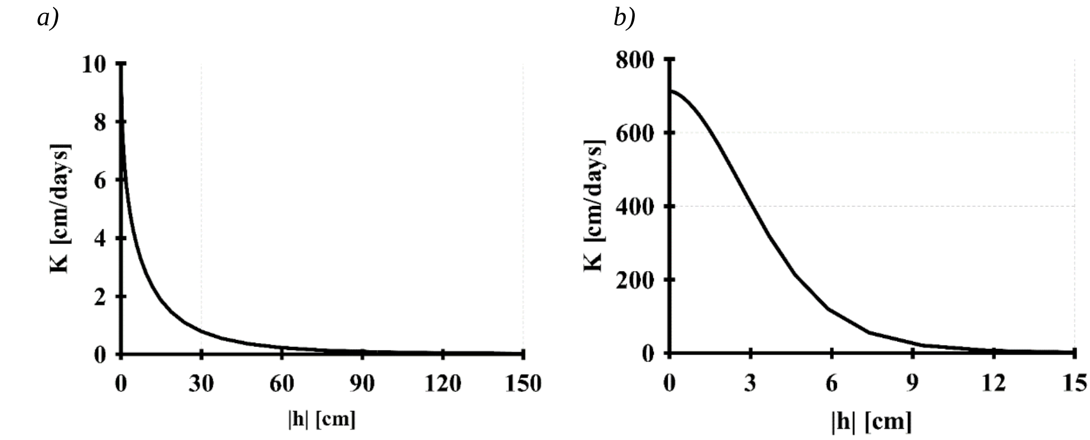

Fig. 4. *Simulated pressure head versus hydraulic conductivity for a) silty-loam and b) sandy soil profile.*

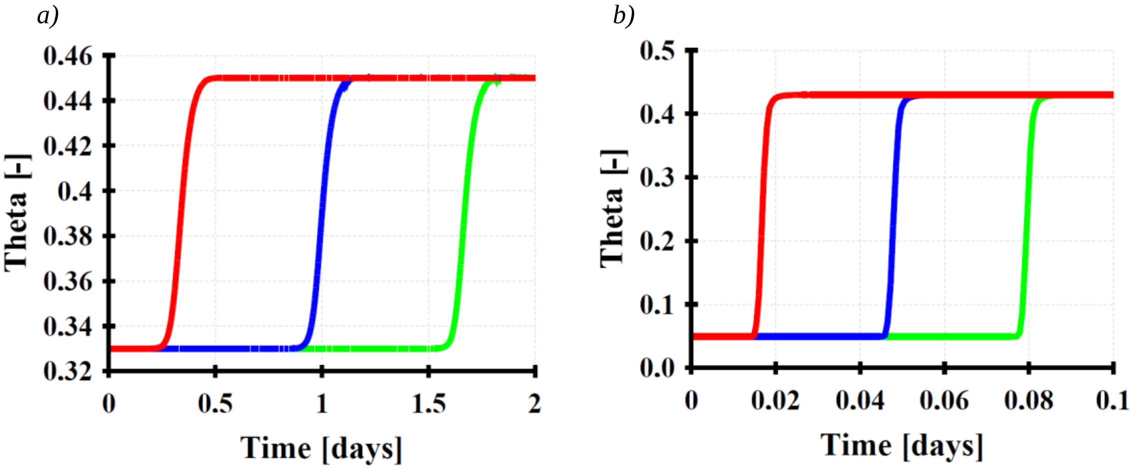

Fig. 5. *Soil moisture (theta) simulation in time for a) silty-loam and b) sandy soil profile.*

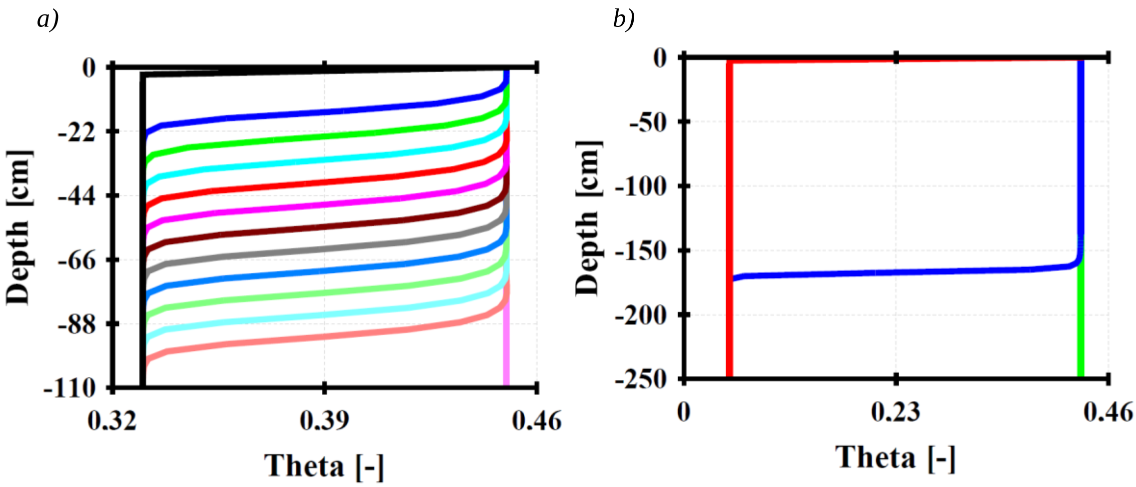

Fig. 6. *Depths versus soil moisture (theta) simulation for a) silty-loam and b) sandy soil profile.*

for a sandy profile is very sharp (Fig. 6b) in comparison with the smoother wetting front for a silty-loam profile (Fig. 6a.) associated with finer-textured soil having relatively lower *n* and *α* values requiring coarser discretization. After water infiltration into the dry soil profile, water tends to approach the saturated water content. The wetting front changes from its initial low value to a value near saturation in a small distance (silty-loam soil – Fig. 6a) and high distance (sandy soil – Fig. 6b). The rate at which the wet front process with depth of wetting is about 8 times greater in the sandy soil profile.

Fig. 7 was constructed after concentrations set-up of applied solute (nitrates) according to the standard NO_3^- concentration (*i.e.* solute concentration = 0.003 mmol cm^{-3}) on the different soil profiles. This concentration is recommended by the user manual of "Kristalon" grass fertilizer (producer AGRO CS a.s. the Czech Republic, originating in the Netherlands). The rate of solute transport throughout the sandy soil profile achieve a constant maximum concentration of 0.003 within ~ 1 day for all three observation points (40, 100 and 160 cm) in comparison with the silty-loam profile. The solute is transported about 50 times faster in the first layer (40 cm) for sandy soil than in the silty-loam soil profile. In the two next layers, the rate increased more than 100 times in the sandy soil against silty-loam soil.

Fig. 8 represents the similar 50 times increasing solute transport rate in the case of sandy soil in contrast to silty loam after 5 times higher solute initiation concentration (*i.e.* 0.016 mmol cm^{-3}) for the first layer (40 cm). Solute (nitrates) flow shows the symmetrical shape,

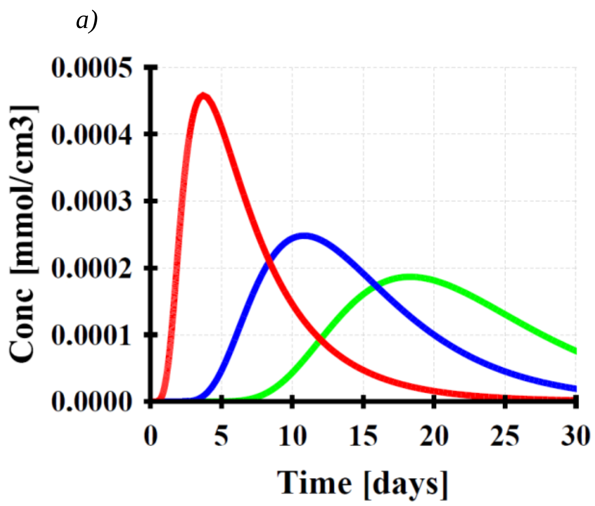

Fig. 7. Solute concentration simulation in time for a) silty-loam and b) sandy soil profile.

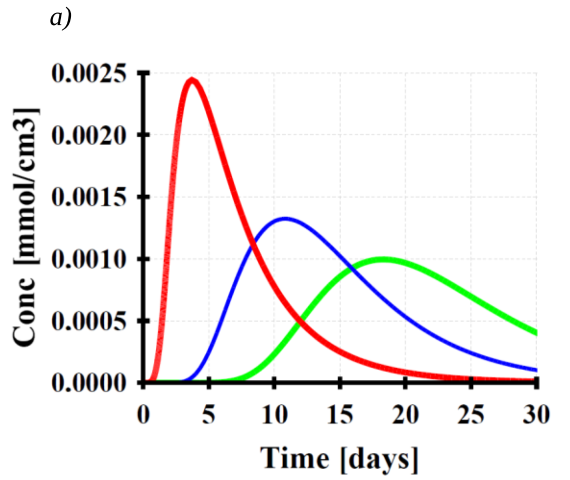

Fig. 8. Solute concentration simulation in time for a) silty-loam and b) sandy soil profile.

demonstrating equilibrium behaviour in sandy loam soil column divided into 3 depth (observation points): 40, 100 and 160 cm (Fig. 8b).

Our numerical 1-D simulation demonstrates a significant difference in water and solute vertical flow through two different soil profiles. Silty-loam soil texture has better retention capacity in comparison with sandy soil.

Illustrations exported from 1-D HYDRUS numerical simulation could contribute to the economically and environmentally fertilizers application by the inclusion of soil type into the instructions for use of the fertilizer. Our results could be supported by the field experiments performed in a lysimetric station after summarization of all input specific parameters. Lysimeter monoliths could be the suitable experimental tool for the study of transport processes by applying fertilizers, nutrients, pesticides, colloids, pathogens or nanoparticles at the soil surface in real-time and real conditions and then by numerical computation predict especially the rate of contamination to the ensuring necessary measures for health and life protection. This simulation was aimed at soil fertilization in the early stage of the vegetation period when we neglect root water and nutrients up-take for plant growth. This article indirectly points to the fact, that during the vegetation period greater retention of water and solute in the case of fine soil texture (silty-loam) could lead to increasing of solute concentration, which plants are not able to take up together with water against the concentration gradient. The result is slower growth followed by wilting. Fertility will decrease. Faster leaching of nitrates through sandy soils creates another problem. Except for contamination of water sources provided for drinking, nitrates flow through drainage water to the rivers could cause algal overgrowth and eutrophication.

Conclusion

The present simulation study demonstrated the high impact of soil hydraulic properties on water and solute (nitrates) transport. We have shown about 50 times solute flow rate increasing for sandy soil compared to silty-loam in the first 40 cm layer of the soil profile. Nitrates move more than 100 times faster in the deeper layers 100 and 160 cm in sandy soil in contrast to silty-loam. This research aimed at numerical simulation of water and solute transport could be a suitable, quick and strong tool for the management of water and fertilization in agriculture to the protection of the health and life of the population. The study suggests reconsidering modification of the "instructions for use" of a given fertilizer distributed on the world market suitable for a given type of soil profile in a specific locality of the world. Reduction of economic and crop losses in advance could be high motivation. Another reason for using computation modelling is to estimate the rate of spread of a pollutant in the soil profile in the case of large-scale accident or industrial accident event and to take the necessary measures, warn people, stop the distribution of water resources for domestic use, water purification, and animal protection). Preventive measures should be identified and these need to be derived through interdisciplinary including collaboration between regulators, the farming community, government departments and scientists.

Acknowledgement

The work was supported by the project VEGA Grant Agency No. 2/0044/20.

References

Anand, A., Unnikrishnan, B., Mao, J.-Y., Lin, H.-J., Huang, C.-C. (2018): Graphene-based nanofiltration membranes for improving salt rejection, water flux and antifouling–A review. Desalination, vol. 429, 119–133.

Archna, Sharma, S. K., Sobti, R. C. (2012): Nitrate Removal from Ground Water: A Review. E-J Chem, vol. 9, no. 4, 1667–1675.

Balejčíková, L.; Tall, A.; Kandra, B.; Pavelková, D. (2020): Relationship of nitrates and nitrites in the water environment with humans and their activity. Acta Hydrologica Slovaca, 2020, vol. 21, 74–81.

Bhatnagar, A., Sillanpää, M. (2011): A review of emerging adsorbents for nitrate removal from water. Chemical Engineering Journal, vol. 168, 493–504.

Greer, F. R., Shannon, M. (2005): Infant methemoglobinemia: the role of dietary nitrate in food and water. Pediatrics, vol. 116, 784–786.

Gushgari, A. J, Halden, R. U. (2018): Critical review of major sources of human exposure to N-nitrosamines. Chemosphere, vol. 210, 1124–1136.

Kanzari, S., Nouna, B. B., Mariem, S. B., Rezig, M. (2018): Hydrus-1D model calibration and validation in various field conditions for simulating water flow and salts transport in a semi-arid region of Tunisia. Sustainable Environment Research vol. 28, 350–356.

Kapoor, A., Viraraghavan, T. (1997): Nitrate Removal From Drinking Water—Review. Journal of Environmental Engineering, vol. 123, 371–380.

Lorentea, L., Gómez-Bernal, F., Martín, M. M., Navarro-Gonzálvez, J. A., Argueso, M., Perez, A., Ramos-Gómez, L., Solé-Violán, J., Marcos y Ramos, J. A., Ojeda, N., Jiménez, A.: Working Group on COVID-19 Canary ICU. (2021): High serum nitrates levels in non-survivor COVID-19 patients. Medicina Intensiva, Available online 10 November 2020, In Press, Corrected Proof.

Madhura, L., Singh, S., Kanchi, S., Sabela, M., Bisetty, K., Inamuddin (2019): Nanotechnology-based water quality management for wastewater Treatment. Environmental Chemistry Letters, vol. 17, 65–121.

Matusek, I., Reth, S., Heerdt, C., Hrckova, K., Gubis, J., Tall, A. (2017): Review of lysimeter stations in Slovakia. 17. Gumpensteiner Lysimetertagung, 209–212, ISBN: 978-3-902849-45-8.

Shrimali, M., Singh, K. (2001): New methods of nitrate removal from water. Environmental Pollution, vol. 112, 351–359.

Soares, M. (2000): Biological Denitrification of Groundwater. Water, Air, & Soil Pollution, vol. 123, 183–193.

Stuart, M. E., Gooddy, D. C., Bloomfield, J. P., Williams, A. T. (2011): A review of the impact of climate change on future nitrate concentrations in groundwater of the UK. Science of the Total Environment, vol. 409, 2859–2873.

Šimůnek, J., van Genuchten, M. Th., Šejna, M. (2005): The HYDRUS-1D Software Package For Simulating The One-Dimensional Movement of Water, Heat and Multiple Solutes in Variably-saturated Media, Version 3.0. Department of Environmental Sciences, University of California Riverside, Riverside, California, USA.
Šimůnek, J., van Genuchten, M.T., Šejna, M. (2008): Development and applications of the Hydrus and STANMOD software packages, and related codes. Vadose Zone Journal, vol. 7, 587–600.
Zhou, Z. (2015): A Global Assessment of Nitrate Contamination in Groundwater. Internship report.

RNDr. Lucia Balejčíková, PhD. (*corresponding author, e-mail: balejcikova@uh.savba.sk)
Institute of Hydrology SAS
Dúbravská cesta 9
841 04 Bratislava
Slovak Republic

DOI: 10.31577/ahs-2021-0022.01.0018

ACTA HYDROLOGICA SLOVACA

Volume 22, No. 1, 2021, 147 – 155

MATHEMATICAL MODELING OF SOIL EROSION PROCESSES USING A PHYSICALLY-BASED AND EMPIRICAL MODELS: CASE STUDY OF SLOVAKIA AND CENTRAL POLAND

Zuzana Németová*, Silvia Kohnová

The article is focused on mathematical modelling of the soil erosion processes on the selected areas within the Slovak Republic and Poland. The study includes the validation of the models used based on the actual measurements. The intensity of the soil erosion processes was calculated using the physically-based EROSION-3D model and the empirical USLE-SDR model. The simulations were done based on continuous rainfall events and a long-term simulation. The results modelled were confronted with the actual measurements in both areas investigated. Since a model's validation and calibration as well as a relevant interpretation of the results obtained are the hardest and most challenging parts of any research, it is necessary to constantly enhance the techniques and methods of the calibration and validation of models, thereby deepening the knowledge of individual models. The results show the process has to be performed before the application of the models used together with the advantages and disadvantages of the physically-based and empirical models used, including a comparison and validation of the models applied.

KEY WORDS: mathematical model, validation, calibration, erosion, extreme rainfall event, physically-based model

Introduction

A basic and fundamental definition of soil erosion is a process involving the detachment, transport, and accumulation of soil materials from any part of the Earth's surface. Since soil erosion occupies the most serious position among the individual degradation processes, it plays an irreplaceable role in scientific research (Rawat et al., 2011; Markantonis et al., 2012). Soil is one of the fundamental elements that provide resources for human food supplies; therefore, the significance of soil erosion research lies in an understanding of soil erosion processes over large areas of the Earth (Wainwright et al, 2003).

Since soil erosion research by the Soil Erosion Service of the US Department of Agriculture began around in 1930 (Bennet, 1933), a large number of soil erosion and sediment transport models have been developed, but choosing a suitable model that fits the needs of individual users is still a complicated and problematic task. The models are a useful tool to simulate nature, but they suffer from a range of problems, such as overestimation due to the uncertain results of the models or difficulties in obtaining input data (Hajigholizadeh and Hector, 2018). It is important to note that the modelling of nature is always constrained by many differences in the sense of spatial and temporal variability, spatial heterogeneity, the transport media, and the high instability of the input data (Jakeman et al., 1999). Nature is and always will be beyond us.

The most influential factors that impact water erosion are the climate, topography, soil structure, vegetation, anthropogenic activities, and management systems used (Kuznetsov et al., 1998). All of these factors can influence various elements of sediment and erosion processes along with deposition as well. It is assumed that the major triggers of splash and sheet erosion are rainfall intensity and the runoff rate (Wei et al., 2009). These two factors can be very powerful together with the human activities in catchments. Inappropriate anthropogenic activities that cause changes in the magnitude and nature of the material inputs to estuaries can also involve erosion with consequences for populations and ecosystems (Iglesias et al., 2019).

The degree of sedimentation in a catchment is heterogeneous in space and over time, depending on the land use, soil type, topography, any slopes, vegetation cover, and the climate (Marttila and Klöve, 2010).

The estimation of erosion and sediment processes can be modelled by different kinds of models, i.e., empirical models, physically-based models or conceptual models. The selection of the methods used depends on the size of the study area, the objectives of the research, the available input data or the possible validation and calibration of the models (García-Ruiz et al., 2015). The selection of a model is a very important step, but the possibility of validating and calibrating it to the specific catchment conditions is a necessary part of the overall success of the modelling. There are several methods established for the validation of the models used, e.g., the bathymetric measurement of sediment deposited in a reservoir has been presented as a suitable method for assessing the volume of eroded material in a research area.

The modelling of the amount of sediments is a useful approach for quantifying the historical impact of agriculture on soil erosion and sediment yields, as well as a good method for calibrating and testing the erosion models in contrast to the actual measurements (Boyle et al., 2011).

The aim of this study is the application of physically-based and empirically-based erosion models in two different countries, i.e., the Slovak Republic and Poland, together with a comparison of the models with the actual measured data in both research areas investigated.

Material and methods

The subchapter describes the methods used and the areas under research. Because two different countries were investigated, the chapter is divided into two main parts. The first contains a description of the Svacenicky Creek research area in Slovakia, and the second describes the investigation site of the Zagożdżonka catchment in Poland.

Svacenický Jarok research area (Slovak Republic)

The area investigated is located in the western part of Slovakia (Fig. 1) in the area of the Myjava Uplands. The whole catchment area is prone to intensive erosion processes and quick runoff responses, which are the results of a massive 600-year transformation from a natural to an agricultural landscape (Fig. 1a). The current composition of the land use is as follows: arable land covers 66% of the area, while forests occupy 9%, grasslands 9%, water bodies 7%, gardens 6%, buildings 2%, and shrubs 1% of the catchment. The Svacenický stream passes through the area as a right-hand tributary of the Myjava River. The creek flows into a small water reservoir (polder) in the lower part. The town of Myjava has been impacted by frequent floods in the past (Stankoviansky, 2003; Dotterweich et al., 2013), and the construction of the polder was necessary in order to ensure flood protection in terms of the reduction of flood flows.

Parameters input and field terrain survey of the Svacenicky Jarok

For the modelling of the soil water erosion, physically-based EROSION-3D model was used. In the case of the model's inputs, the rainfall data, relief parameters, and soil input characteristics were needed. The rainfall data were obtained at the Myjava meteorological station during the period evaluated (Figs. 4 and 5). Information about the soil was obtained during the field measurements. The relief parameters are represented by a digital elevation model (Fig. 1b). A long-term simulation was performed with the EROSION-3D model based on continuous rainfall events. The results from the model were compared with the bathymetric measurements in order to perform the validation of the physically-based EROSION-3D model. More information about the bathymetric measurements can be found in Németová et al. (2020), Honek et al. (2020).

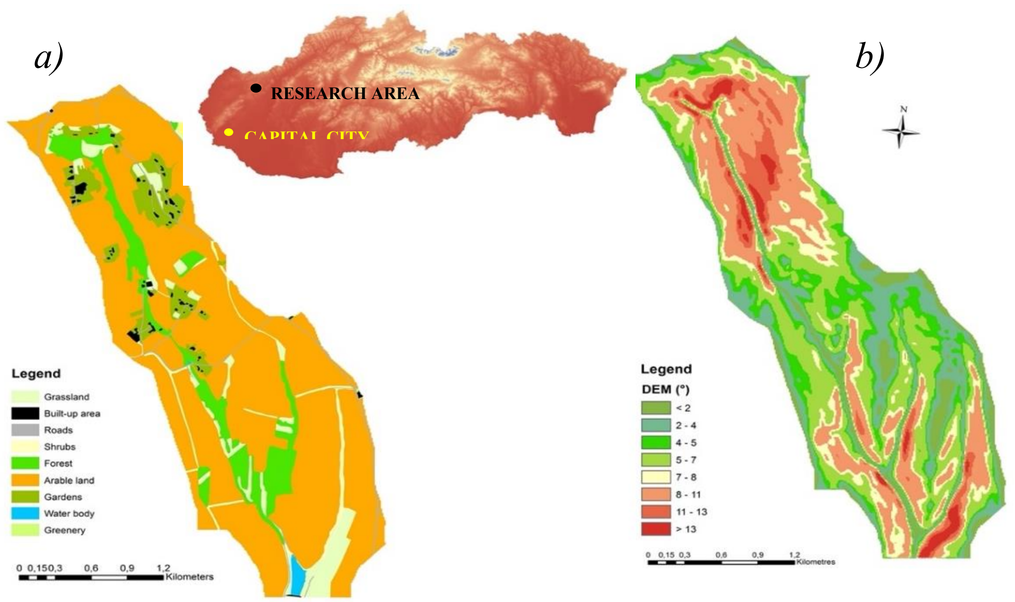

Fig. 1. Localization of the Svacenicky Jarok, Slovak Republic research area; a) Land use, b) Digital elevation model.

The measurement of a terrain represents a necessary step in order to determine the adequate soil input parameters and therefore ensure the relevant outputs. A field survey and soil sampling in the Svacenicky Jarok were carried out in the summer of 2018 in cooperation with Masaryk University in Brno. The measurement of the terrain was performed not only with the aim of taking and evaluating the soil samples, but also to enable interchanges with local experts in order to identify the crops cultivated in the period from 2012 to 2018. Laboratory analyses were conducted for the selected soil input parameters in the laboratory of the Slovak University of Technology in Bratislava and Masaryk University in Brno. An example of the results analysed is shown in Table 1.

Sensitivity analyses of the soil input parameters

Sensitivity analyses represent a useful element of the evaluation of every model. The analyses include the process of changing the input values with the identification of the impact of these changes on the final results. The goal of the sensitivity analyses consists of knowledge of the quantification and identification of a model's inputs and outputs as well as an understanding of the model's relationships. The analyses should be done before the application of every model in order to see how the parameters input influence the individual outputs. Here, the soil input parameters were increased and decreased by about 10% in comparison with the reference (initial) state. The sensitivity analyses were performed in previous studies; for more information, see Honek et al. (2020) or Németová et al. (2020).

Methodology of creating a connection between the plots and a map of the land use

It was necessary to connect the individual plots (LPIS parcels; LPSI – agricultural areas with stable natural or artificial boundaries) with the current land use according to the direct years (2012–2018) and therefore ensure the association between the plots and the land use maps regarding the individual years (Table 2). A new land-use map was created for each year, where the particular areas were divided into parcels according to the LPIS. The arable land does not represent one homogenous unit but is composed of different elements formed by defined LPIS plots with the cultivated crops for the years 2012–2018. This means that each area, i.e., parcel, has its own ID (in GIS), which corresponds to the specific crop (Fig. 2, Table 2). The dominant crops for the selected years together with the amount of precipitation are shown in the Table 3.

Zagożdżonka (Poland) research area

The second research area (Zagożdżonka catchment) is located in central Poland, approximately 100 km south of the capital city of Warsaw in the Mazovia Lowlands (Fig. 6). The catchment is characterized by a lowland disposition and topography typical of this part of Poland. Agricultural production is dominant, with arable land covering 48% of the area. The forests cover 39% of the catchment, and the pastures occupy the remaining 13%. The localization of the catchment is shown in Fig. 6.

Table 1. **Results of the terrain measurements and laboratory analyses (bulk density and organic carbon content)**

Designation of the soil sample	AMSL [m]	N [°]	E [°]	Weight before drying [g]	Bulk density reduced [g cm^{-3}]	Organic carbon content [%]
1	310	48°45'17"	17°33'4"	220.9	1.1121	9.5
2	310	48°45'14"	17°33'4"	230.7	1.2599	12.5
3	310	48°45'10"	17°33'2"	258.6	1.4828	11.8
4	310	48°45'10"	17°32'58"	239.5	1.2707	8.8
5	310	48°45'16"	17°32'58"	245.5	1.408	9.4
6	360	48°45'33"	17°32'37"	215.5	1.07	9.2
7	340	48°45'34"	17°32'39"	208.5	1.1605	10.7
8	330	48°45'35"	17°32'40"	194.7	1.0315	15.1
9	420	48°46'52"	17°31'30"	198.9	1.0965	12.1
10	410	48°46'52"	17°31'32"	188.0	1.0109	12.8
11	370	48°46'53"	17°31'34"	238.9	1.4657	10.9
12	410	48°47'3"	17°31'30"	235.4	1.0588	10.1
13	410	48°47'3"	17°31'30"	208.5	0.8895	9.7
14	420	48°47'13"	17°31'25"	228.3	1.334	8.6
15	430	48°47'14"	17°31'29"	183.9	1.0475	7.4
16	450	48°47'17"	17°31'34"	174.7	0.9818	6.9

Staw Górny water reservoir

The Staw Górny water reservoir was constructed in 1976 in order to provide water for a local chemical factory. The total area of the reservoir is 14 hectares; the original volume of the reservoir was 252,000 m^3 at a water level of 146.70 m.a.s.l. After 10 years (1986), the water level increased about 42 centimetres. Because of intensive erosion activity in the Zagożdżonka catchment, sedimentation represents a major problem to be dealt with. Several measurements of the water level were performed; i.e., the first measurements of the water reservoir were taken in 1979–1980 based on the Range Line method (Banasik and Mordziński, 1982) and then from 1991–2003 (Banasik et al., 2005). The last survey was performed based on the hydrographic system in 2009 (Banasik et al., 2001; Banasik, et al., 1995).

Input parameters (Zagożdżonka research area)

The simulations were conducted using the physically-based EROSION-3D model and USLE-SDR empirical model. The USLE-SDR empirical model represents a suitable approach for determining the amounts of sediment in the areas under consideration. The results from both models used were contrasted with the terrain measurements of the sediments in the Staw Górny reservoir. All the input parameters required for the models (the EROSION-3D and USLE-SDR models) were provided by the University of Warsaw under the COST program (CA 16209). The EROSION-3D model requires three input parameters (relief characteristic in the form of digital elevation model, soil input parameters and rainfall data. The equation of empirical model USLE-SDR consists of three components (sediment removal ratio, annual soil loss per unit area and catchment area) and the parameters were estimated for the Zagożdżonka catchament using topographic maps, soil and land maps in the previous studies (Banasik et al., 1995; Banasik et al., 2005). A summary of the rainfall events used in the EROSION-3D model is displayed in Fig. 7.

Results and discussion

Comparison of the results modelled with the actual measurements, Svacenicky Jarok, Slovak Republic

The validation of the EROSION-3D model was performed on a continuous series of precipitation

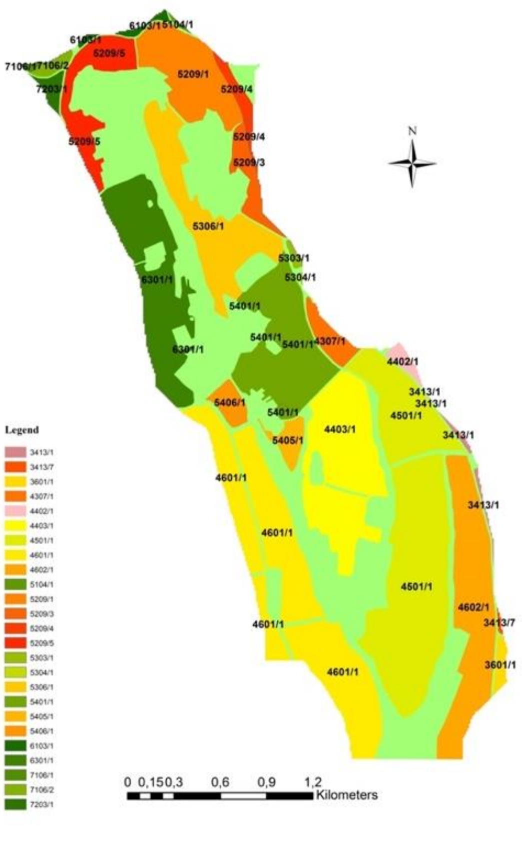

Fig. 2. Land Parcel Identification System (LPIS), Svacenicky Jarok, Slovak Republic = agricultural areas with stable natural or artificial boundaries.

Table 2. Identification of the crops according to the individual parcels

Parcel number	2012	2013	2014
3413/1	sorghum	lantern	sorghum
3413/7	wheat	barley	beet
3601/1	wheat	barley	beet
4307/1	sorghum	alfalfa	sorghum
4402/1	sorghum	alfalfa	sorghum
4403/1	beet	wheat	rye
4501/1	wheat	wheat	rye
4602/1	wheat	barley	beet
5104/1	corn	wheat	corn
5209/1	corn	wheat	corn
5209/3	corn	wheat	corn
5209/4	corn	wheat	corn
5209/5	alfalfa	alfalfa	corn
5303/1	sorghum	alfalfa	sorghum
5304/1	sorghum	alfalfa	sorghum
5306/1	sorghum	wheat	wheat
5401/1	beet	wheat	wheat
5405/1	corn	wheat	corn
5406/1	corn	wheat	corn
5601/1	corn	wheat	rye
6103/1	alfalfa	alfalfa	alfalfa
7106/1	alfalfa	alfalfa	alfalfa
7106/2	alfalfa	alfalfa	alfalfa
7203/1	alfalfa	alfalfa	alfalfa

measured at the Myjava meteorological station and on the basis of bathymetric measurements of sediments in the Svacenicky Creek polder. In the case of the rainfall events used, one-minute events were selected, which are considered to be erosively effective (Renard et al., 1997). For each precipitation event, a specific set of soil characteristic parameters was defined that corresponded to the date of the occurrence of the precipitation. The final results of the modelling with the EROSION-3D model are displayed in Fig. 8. The results reflect the two periods evaluated, i.e., 2013 (Fig. 8a) and 2014 (Fig. 8b). Fig. 8a represents the year 2013 with the land use composition shown in Fig. 3a. The predominant part of the area represents winter wheat, which is generally considered to be a protective crop. The intensity of the sediments and erosion processes are distributed throughout the whole territory (with more influence on the right part) in comparison with scenario B, where the most intensive impact of the soil erosion processes is related to the arable land represented by corn and rye (Fig. 3b). In the case of the predicted amounts of sediments, the year 2013 (Fig. 8a) was closer to the measured amounts of sediment in comparison with the year 2014 (Fig. 8b). A higher amount of the sediments modelled was predicted in the year 2014, even though the land use structure is composed of rye. On the other hand, the most intensive processes were detected in the year 2014.

Comparison of the results modelled with the actual measurements, Zagożdżonka, Poland

The average amount of annual sedimentation in the Staw Górny reservoir is about 1080 m^3. When the EROSION-3D and USLE-SDR models were compared, the empirical USLE-SDR model approached the sediments measured in the reservoir. In this case, the EROSION-3D model predicted a 45% lower amount of sediment than was actually measured but offered a satisfactory tool for the identification of the local places endangered by soil water erosion (Fig. 9). The amount of sediments determined by the EROSION-3D model was lower because the EROSION-3D model does not take bottom sediments into account, whereas the amount of sediments quantified by the USLE-SDR model considers bottom sediments as well. The summary of results (modelled and measured) are included in the Table 4. Because of the lowland character of the catchment and because no significant rainfall events occurred, there were no intensive erosion processes. The analyses were done in cooperation with the University of Warsaw under the COST program (CA 16209).

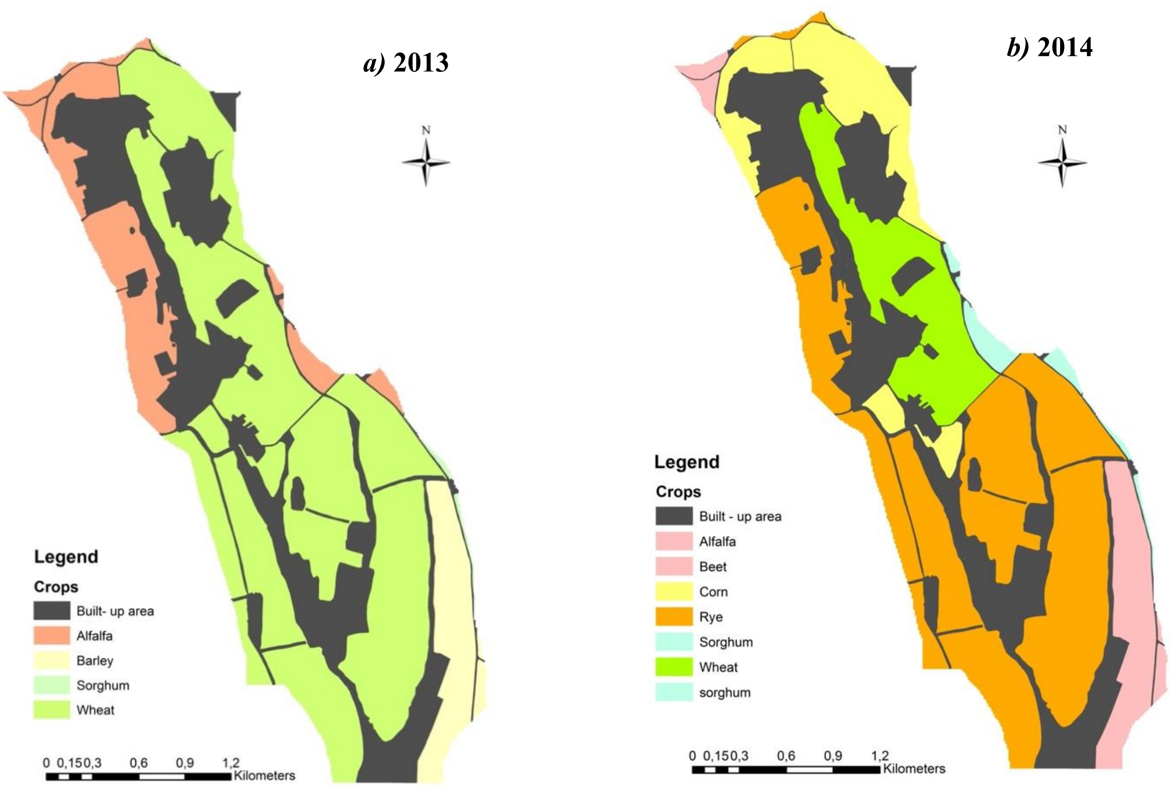

Fig. 3. a) Land-use composition structure, 2013, Svacenicky Creek, Slovakia, b) Land-use composition structure, 2014, Svacenicky Creek, Slovakia.

Table 3. **A summary of the rainfall events and dominant crops during the period selected (2013, 2014)**

Year	**Rainfall amount** [mm]	**Predominnat crop (>50% of area)**
2013	471.1	Winter wheat (Triticum aestivum)
2014	558.28	Rye seed (Secale cereale)

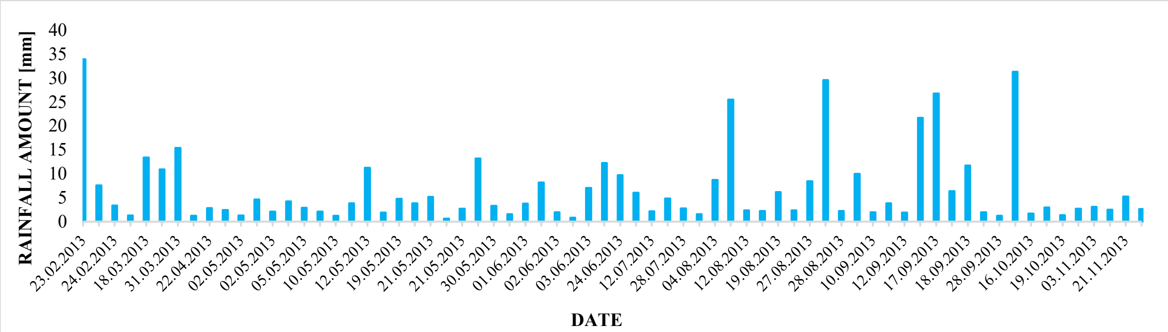

Fig. 4. The amount of rainfall events during the period analysed (February 2013–November 2013).

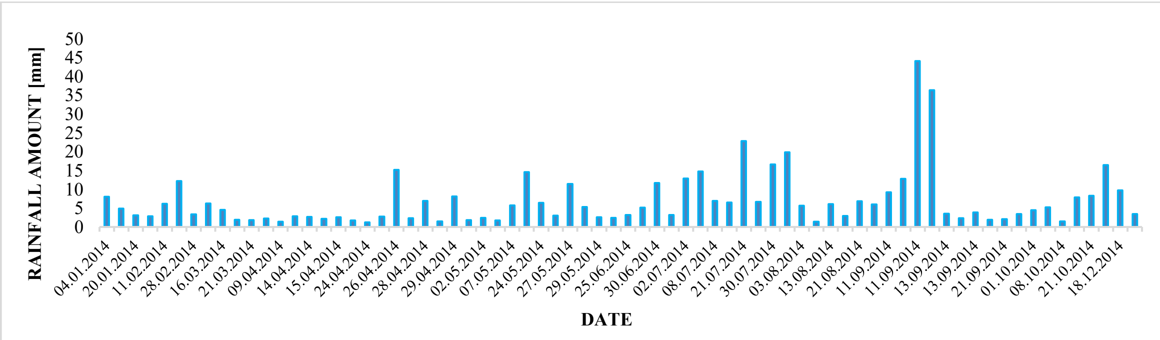

Fig. 5. The amount of rainfall events during the period analysed (January 2014–December 2014).

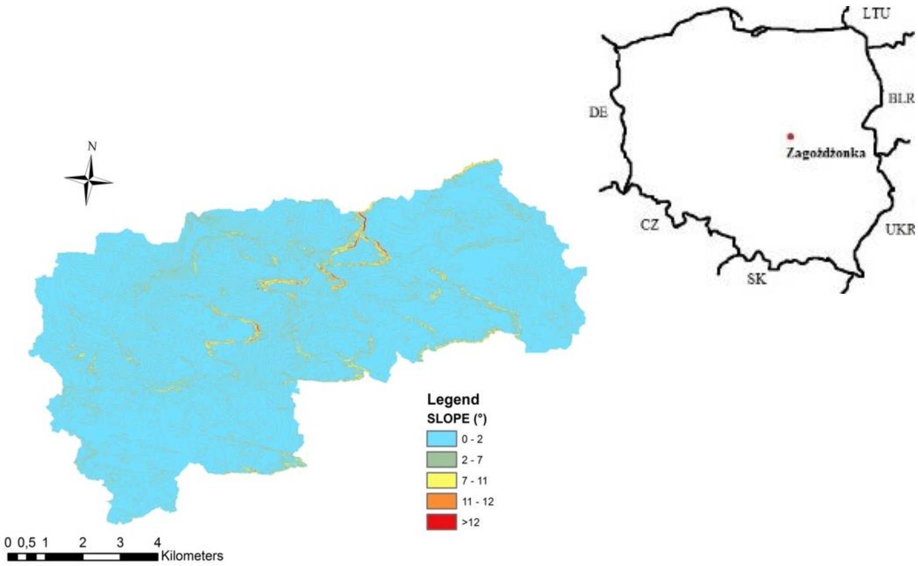

Fig. 6. Localization of the Zagożdżonka research area with a representation of the slopes.

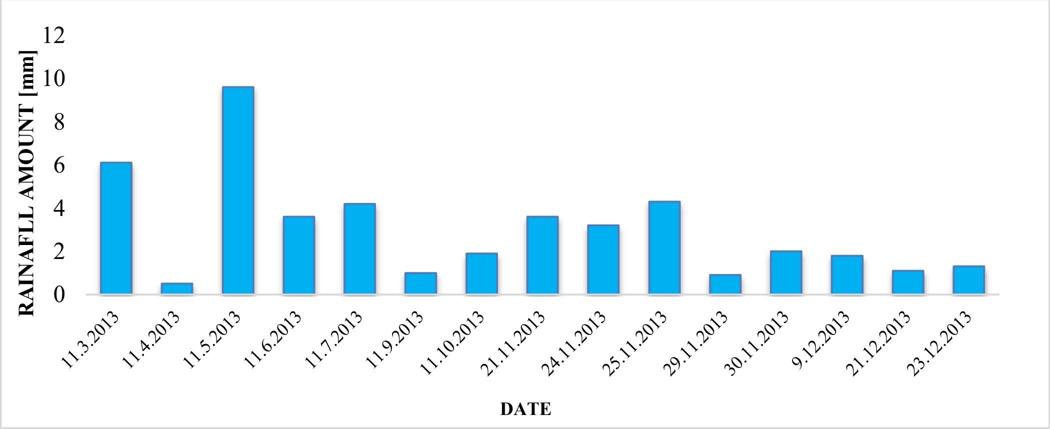

Fig. 7. *The amount of rainfall events during the period analysed (November 2013–December 2013).*

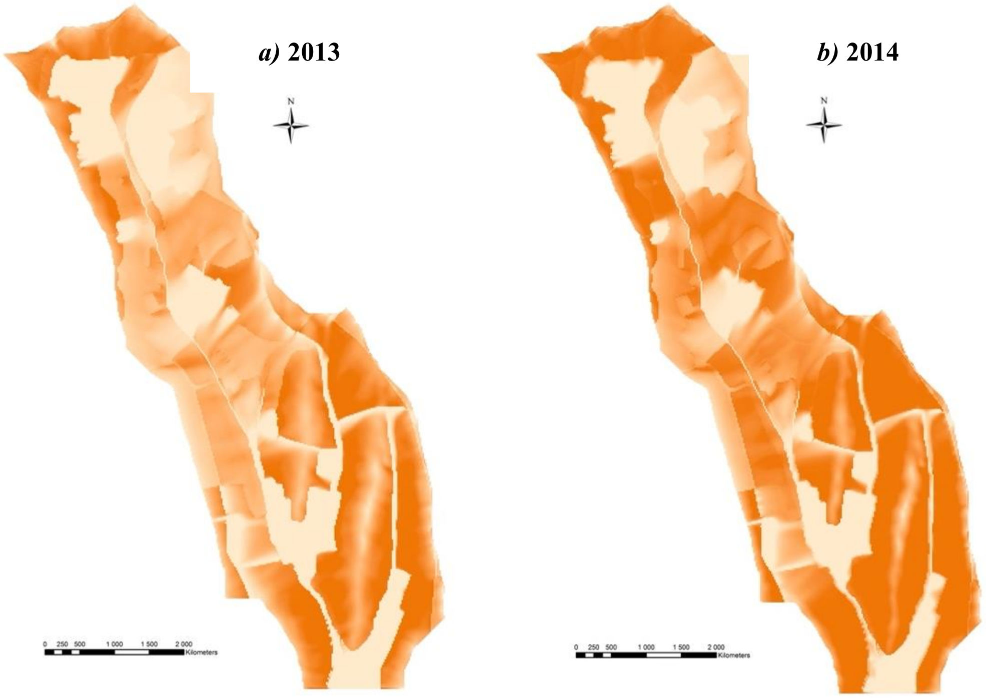

Fig. 8. *The modelled results (EROSION-3D model), Svacenicky Jarok: a) 2013, b) 2014.*

Table 4. **Comparison of measured and modelled sediments (USLE-SDR, Staw Górny Reservoir, EROSION-3D model)**

Methods for the determination of sediments	Amount of sediments [m^3]
Measurement in the reservoir Staw Górny	1080
USLE-SDR	708
EROSION-3D model	486

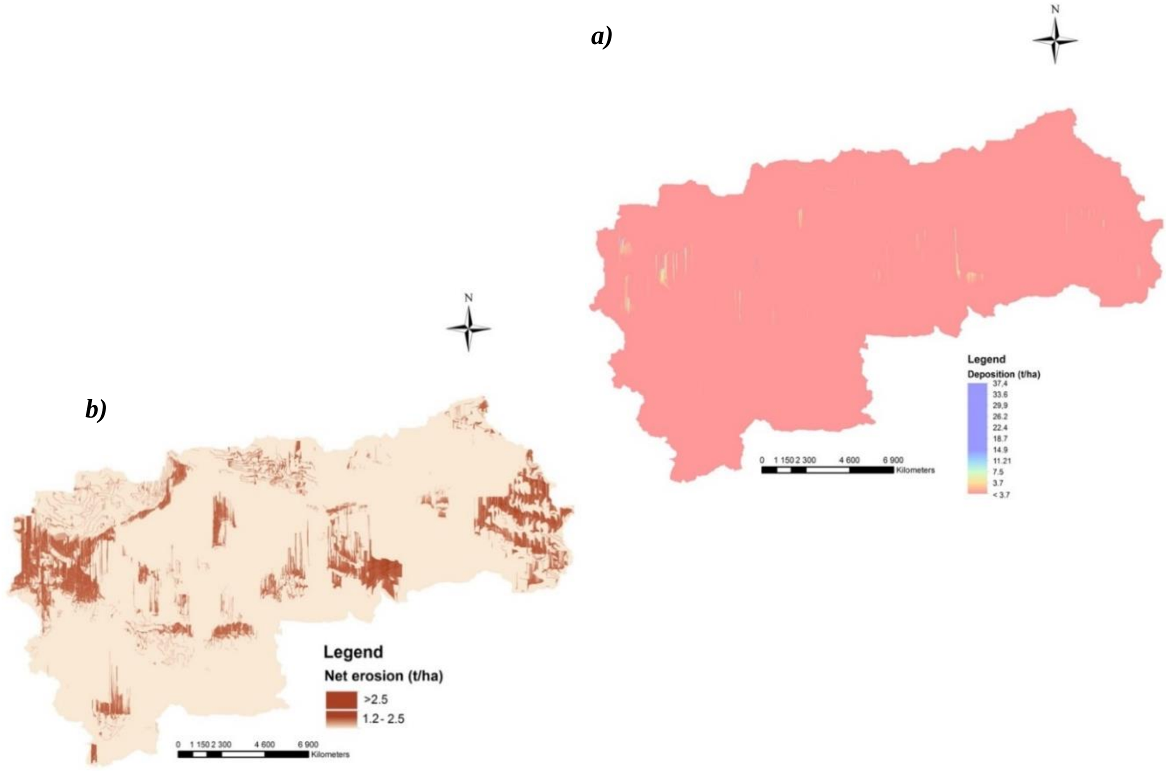

Fig. 9. The amount of deposition (a) and the net erosion (b) during the period evaluated (November 2013–December 2013).

Conclusion

The paper deals with the application and validation of mathematical models used to evaluate the intensity of erosion-transport processes in the Slovak Republic and Poland. The physically-based EROSION-3D model and the empirical USLE-SDR model were used to determine the intensity of the soil erosion and sediment processes. The data modelled were compared with the actual measured data from a bathymetric survey (Slovakia) and from measurements of a water reservoir (Poland).
A large number of mathematical models are available nowadays, but their validation and an appropriate interpretation of the results obtained remain a problem in general. Within the paper, the validation of the models was performed on the basis of the actual measurement of the amount of sediments and on the basis of a continuous series of precipitation events. In the case of the first locality (Svacenický Jarok, Slovak Republic) the EROSION-3D model was validated based on the bathymetric measurement of the sediments in the Svacenický Jarok polder using an Autonomous Underwater Vehicle (AUV) in cooperation with the Institute of Hydrology of the Slovak Academy of Sciences. At the second research site (Zagożdżonka, Poland), the physically-based EROSION-3D model and the empirical USLE-SDR model were used to determine the amount of sediments, and the modelled results were compared with the measured amount of sediments in the Staw Górny reservoir.
Two modelling approaches were used in the study, i.e., a physically-based model and an empirical model; the advantages and disadvantages found within both models were noted. It is not possible to conclude which model can be considered more suitable or better because each of them has certain advantages and disadvantages. In both areas, the EROSION-3D model predicted a lower amount of sediments compared to the amount of sediments observed in the reservoirs. The USLE-SDR empirical model overestimated the impact of precipitation events in comparison with the EROSION-3D model. The advantage of USLE-SDR can be seen in the possibility of considering bottom sediments, while the EROSION-3D model does not include the bottom sediments in the model's calculations. A significant advantage of the EROSION-3D model lies in its ability to determine and analyse different management practices and thus simulate various scenarios of land use changes. Therefore, the practical use of the EROSION-3D model was determined to provide a satisfactory tool for evaluating and locating sites endangered by erosion-sediment processes.

Acknowledgement

This work was supported by the Slovak Research and Development Agency under Contract No. APVV-19-0340, the VEGA Grant Agency No. 1/0632/19 and 1/0782/21. The authors thank the agencies for their research support.

References

Banasik, K., Mordziński, S. (1982): Wyniki badan i prognoza zamulania malego zbiornika wodnego (Investigative results and prediction of small reservoir siltation). In: *Selected problems of hydraulic structures – designing and construction.* 1982, 62–77. Warsaw Agricultural University Press, Warsaw, Poland.

Banasik, K., Hejduk, L., Popek, Z. (2005): Sediments problems of small river catchments and reservoir in Poland. Publications of the Institute of Geophysics, *PAS*, Monograph, 2005, vol. 387, 179–207.

Banasik, K., Gorski, D., Mitchell, J. K. (2001): Rainfall erosivity for East and Central Poland. In: *Soil Erosion Research for the 21th Century*. 279–282.

Banasik, K., Skibiński, J., Górski, D. (1995): Methods of estimation of erosion and reservoir sedimentation). In: *Methodology of water resources management in a small river catchments*. Warsaw: Warsaw Agricultural University Press 1995.63–78, 136–143.

Bennet, H. H. (1933): A Plan for Erosion Control Under the Erosion Section of the Public Works Administration Corporation. File 1-275 Soil Erosion. Central Classified Files: Record Group 48. MD: National Archives and Records Administration 1933.

Boyle, J. F., Plater, A. J., Mayers, C., Turner, S. D., Stroud, R. W., Weber, J. E. (2011): Land use, soil erosion, and sediment yield at Pinto Lake, California: comparison of a simplified USLE model with the lake sediment record. Journal of Paleolimnology, vol. 45, 199–212.

Dotterweich, M., Stankoviansky, M., Minár, J., Koco, Š., Papčo, P. (2013): Human induced soil erosion and gully system development in the Late Holocene and future perspectives on landscape evolution: The Myjava Hill Land, Slovakia. *Geomorphology*, vol. 201, 227–245. ISSN: 0169-555X.

García-Ruiz, J. M., Beguería, S., Nadal-Romero, E., González-Hidalgo, J. C., Lana-Renault, N., Sanjuán, Y. (2015): A meta-analysis of soil erosion rates across the world. Geomorphology, vol. 239, 160–173.

Hajigholizadeh, M. M., Hector, A. F. (2018): Erosion and Sediment Transport Modelling in Shallow Waters: A Review on Approaches, Models and Applications. International Journal of Environmental Research and Public Health, vol. 15, no. 3, 518.

Honek, D., Németová, Z., Kohnová, S., Šulc Michalková, M. (2020): Sensitivity analysis of soil parameters and their impact on runoff-erosion processes. Pollack Periodica, vol. 15, no. 1, 53–64. ISSN 1788-1994. doi:10.1556/606.2020.15.1.6.

Iglesias, I., Avilez-Valente, P., Bio, A., Bastos, L. (2019): Modelling the Main Hydrodynamic Patterns in Shallow Water Estuaries: The Minho Case Study. Water, vol. 11, 1040; DOI: 10.3390/w11051040.

Jakeman, A. J., Green, T. R., Beavis, S. G., Zhang, L., Dietrich, C. R., Crapper, P. F. (1999): Modelling upland and instream erosion, sediment and phosphorus transport in a large catchment. Hydrological Processes, vol. 13, 745–752.

Kuznetsov, M. S., Gendugov, V. M., Khalilov, M. S., Ivanuta, A. (1998): An equation of soil detachment by flow. Soil Tillage Res, vol. 46, 97–102.

Markantonis, V., Meyer, V., Schwarze, R. (2012): Valuating the intangible effects of natural hazards – review and analysis of the costing methods. Natural Hazards and Earth System Sciences, vol. 12, 1633–1640. DOI: 10.5194/nhess-12-1633-2012.

Marttila, H., Klöve, B. (2010): Dynamics of erosion and suspended sediment transport from drained peatland forestry. Journal of Hydrology, vol. 388, 414–425. DOI: 10.1016/j.jhydrol.2010.05.026.

Németová, Z., Honek, D., Kohnová, S., Hlavčová, K., Šulc Michalková, M., Sočuvka, V., Velísková, Y. (2020): Validation of the EROSION-3D Model through Measured Bathymetric Sediments. Water, vol. 12, no. 4, 1082. https://doi.org/10.3390/w12041082.

Rawat, P. K., Tiwari, P. C., Pant, C. C., Sharama, A. K., Pant, P. D. (2011): Modelling of stream run-off and sediment output for erosion hazard assessment in Lesser Himalaya: need for sustainable land use plan using remote sensing and GIS: a case study. Natural Hazards, vol. 59, 1277–1297. DOI: 10.1007/s11069-011-9833-5.

Renard, K., Foster, G., Weesies, G., Mccool, D., Yoder, D. (1997): Predicting Soil Erosion by Water: a Guide to Conservation Plannin with Revised Universal Soil Loss Equation (RUSLE). USDA Agricultural Handbook, vol. 703, 404. ISBN 0-16-048938-5.

Stankoviansky, M. (2003): Historical evolution of permanent gullies in the Myjava Hill Land, Slovakia. Catena, vol. 51, no. 3–4, 223–239. ISSN: 0341-8162.

Wainwright, J., Parsons, A. J., Michaelides, K., Powell, D. M., Brazier, R. (2003): Linking Short- and Long-Term Soil— Erosion Modelling. In Long Term Hillslope and Fluvial System Modelling, 1st ed.; Lang A., Dikau R., Eds.; Springer: Berlin, Heidelberg, 2003; 37–51.

Wei, H., Nearing, M. A., Stone, J. J., Guertin, D. P., Spaeth, K. E., Pierson, F. B., Nichols, M. H., Moffet, C. A. (2009): A New Splash and Sheet Erosion Equation for Rangelands. Soil Science Society of America Journal, vol. 73, 1386–1392. DOI: 10.2136/sssaj2008.0061.

Ing. Zuzana Németová, PhD. (*corresponding author, e-mail: zuzana.nemetova@stuba.sk)
prof. Ing. Silvia Kohnová, PhD.
Slovak University of Technology
Radlinského 11
810 05 Bratislava
Slovak Republic

DOI: 10.31577/ahs-2021-0022.01.0019

ACTA HYDROLOGICA SLOVACA

Volume 22, No. 1, 2021, 156 – 163

FLOOD RISK ASSESSMENT AND FLOOD DAMAGE EVALUATION – THE REVIEW OF THE CASE STUDIES

Mária Šugareková*, Martina Zeleňáková

This article presents a brief overview of selected flood risk and flood damage assessment studies. The assessment on the Luvuvhu River focused on risk assessment based on hazard and vulnerability parameters. To these parameters was added another parameter, the exposure parameter in the assessment in the study of Sri Lanka. Hazard, vulnerability and exposure assessment were also performed on the Yangtze River in China, where the authors presented a proposal for a multi-index flood risk assessment concept. The output of these studies are flood risk maps for each indicator, as well as individual risk assessments in the given area. The next section is focused on the flood damage evaluation. The main tool for calculating flood damage in a study conducted in Beijing is flood risk. The calculation process focuses on the Integrated Flood Management (IFRM) method, which consists of risk identification, damage assessment and flood management to design flood protection measures. In flood management, the term vulnerability often occurs, which is a weakness or shortcoming that allows the hazard to be applied. Closely related to this concept is the sensitivity parameter, which can be used to estimate flood damage in the next case study in affected area in Netherland. The last of selected studies presents the application of the RESTful Application Program Interface (API) for the financial estimation of building damage. The API web service allows you to calculate flood damage to buildings without determining the flood risk.

KEY WORDS: flood, flood risk assessment, flood damage calculation, vulnerability, damage

Introduction

One of the most widespread natural disasters is floods, which also bring with them a certain level of risk. One of the most discussed topics is the protection of people and property against floods, as well as mitigating the negative impacts of floods on environmental components. An effective defence mechanism can be to prevent floods by building flood protection measures, or to be aware of the need for information on the causes and consequences of floods.

The degree of risk can be expressed in several ways and also at several levels. The flood risk assessment equation also includes a number of variables that vary depending on the assessed region or input data. However, the issue of flood risk is also focused on the assessment of flood damage that occurs in the event of a flood. The presented paper in the first part briefly describes several selected studies, which are based on flood risk assessment, the second part is devoted to flood damage and how to determine them. Selected studies provide an interesting view of the assessment, whether risks or damages, because, despite global differences, they have a common denominator.

Material and methods

Flood risk assessment

According to the generally accepted definition, risk can be expressed as a combination of the probability of damage occurring and its consequence. The risk is most often expressed by multiplying the value of the probability of the occurrence of a negative phenomenon P and the value of the severity of its consequence C (Zvijáková and Zeleňáková, 2015). A similar equation is used to express flood risk, but is supplemented by other relevant values.

Luvuvhu river catchment

A study carried out in South Africa (Ntanganedzeni and Nobert, 2020) focused on the analysis of flood frequencies and the assessment of flood risk in the Luvuvhu river basin, which covers an area of 4 826 km^2. The Luvuvhu River springs in the south-eastern slopes of the Soutpansberg mountain range and flows through the Kruger National Park. On the border between Mozambique and Zimbabwe, it flows into the Limpopo River. The northern border of the river Luvuvhu is formed by a dominant topographical element – the Soutpansberg mountain range. The highest and steepest slopes of this mountain range are located at

the top of the basin. The variable topography has a significant impact on the overall hydrological conditions in the river basin.
Based on the availability and distribution of data, 4 stations were selected in the river basin, where a vulnerability and hazard analysis were carried out. The main goal of the vulnerability analysis was to identify risk elements in the studied area. However, in terms of the scope of work, the study included only an analysis of spatial vulnerability. The vulnerability aspect was analyzed by determining the use of the area to be exposed to the flood and the total area flooded at the time of the flood. The vulnerability aspect has been identified for specific land uses.
To assess the flood risk, the authors of the study used the method of Gilard and Givone, which consists in combining the results of the hazard analysis and the vulnerability analysis. The combination is based on the existing relationship between flood hazard classes and vulnerability classes of land use in the area addressed. Flood hazard, the first aspect of flood risk, analyzes the determination of hydraulic parameters such as the extent of the flooded area or the depth of the flooding. This aspect suggests that a particular flooded area will be affected by a flood with the same hydraulic parameters, regardless of what the area (land) is used for. The vulnerability of land use as a second aspect points to the sensitivity of individual land use classes. This means that floods present a different level of risk depending on land use.
For the purposes of this study, the hazard was determined using an analysis of the frequency of floods, flooded areas and a map showing the hydraulic parameters of floods. Vulnerability was determined by analyzing the use of land exposed to floods.
The results of the study show that although a flood with the same hydraulic parameters will occur in the entire floodplain, the level of risk will not be the same in the entire study area, due to land use. For this reason, flood classes with a risk value were determined based on the flood depth analysis.

West province of Sri Lanka

In the study by Weerasinghe (Weerasinghe et. al., 2018), the exposure parameter was also assigned to the hazard and vulnerability parameter. The study presents the results of a qualitative assessment of flood risk based on the expression of the mentioned parameters.
Data on topography, precipitation intensity, land cover and geology were used to analyze the flood risk. Thematic maps, on the creation of which selected input parameters were used (flow accumulation, precipitation intensity, land use, slope, altitude, length of the drainage system) were generated using the GIS platform. Each selected parameter was assigned a weight rating according to the extent to which it contributes to the flood. The total value of the hazard is expressed as the sum of the products of individual parameters with their weight rating. The exposure analysis consisted of identifying the elements at risk of flooding. The elements were categorized into two groups – real estate and population. The elements were further quantified on the basis of the ratio between the total number (real estate and population) in the addressed area and the number of endangered elements in the area.
The authors of this study took into account 3 types of the vulenrability in the analysis: social vulnerability, economic vulnerability and housing vulnerability. The social vulnerability index was calculated on the basis of the claim that society's ability to cope with natural risks depends on the wealth factor. Although vulnerability (not only the territory) is influenced by many other factors, the authors of this study relied mainly on the financial possibilities of the population in the area. The indicator of social vulnerability was the age of the population, in this case gender was not taken into account. Each age group was assigned a weight score based on qualifications, as well as subjective perception. The total social vulnerability index was calculated in a standard way - the sum of the products of each age category with a weighted rating. The analysis of economic vulnerability consisted in dividing the population according to economic status into employed, unemployed and economically inactive (children and pensioners). The basic assumption for the evaluation was that unemployed and economically inactive people depend on employed people, and thus the expression of economic vulnerability is the ratio of the sum of unemployed and economically inactive population to the sum of employed population. The last vulnerability assessed was the vulnerability of housing. The indicator was the number of housing units with low resistance to hazards, on the basis of which housing units were divided into permanently inhabited, temporarily inhabited and uninhabited. According to the claim that temporarily inhabited and uninhabited units are often damaged by floods, housing vulnerability was quantified by the ratio of the sum of temporarily inhabited and uninhabited housing units to the sum of inhabited units.
The overall flood risk was finally determined by the product of hazard, exposure and vulnerability. In this case, the partial results were summed and fitted to the final equation.

Yangtze river catchment

A risk assessment procedure based on hazard, vulnerability and exposure parameters was also used in a case study on the Yangtze River in China (Zhang et. al., 2020). This river is one of the largest rivers in the world, with a catchment area of approximately 1.8 million km^2. The river springs in the north of the Tanggula Mountains and flows through 11 regional provinces. Its range is more than 6 300 km, and eventually flows into the East China Sea on the island of Chongming in Shanghai. As its other tributaries extend to other areas, the river eventually flows through 19 regional provinces and occupies approximately 18.75% of China's total area.
A study carried out on this river looked at the development of a multi-index concept (MIC) based on GIS modeling. The MIC consists of three layers – the object layer, which includes the Yangtze River; an index layer that includes hazard, vulnerability and

exposure parameters, and the last is an indicator layer that contains 13 flood risk indicators. These 13 indicators are divided between the index layer as follows: the hazard parameter contains an indicator of the cumulative average of precipitation in a maximum of 3 days. The vulnerability parameter includes data on absolute elevation between a point and the Yellow Sea level, relative elevation (difference between absolute heights of two points), runoff density (depending on the density of the river network in the area), surface runoff factor and surface coverage, financial returns, financial savings, health service levels and the monitoring and warning system. The last exposure parameter contains data on population density, GDP, degree of soil erosion and risk of soil contamination.

To assess the relative importance of flood risk indicators, the method of the AHP analytical hierarchy was subsequently used, which assigned a weight rating to each indicator. After normalization, the data were transferred to the GIS environment, from which flood risk maps for each indicator were subsequently generated.

Flood damage evaluation

Identification of flood risk in Beijing

Flood damage is also very closely linked to flood risk. In the study (Wang et. al. 2021), flood risk is the main element for calculating the damage caused by floods. The authors of the study come up with the IFRM (Integrated Flood Management) method, which includes the identification, assessment and management of flood risk with a focus on 3 objectives:

1. Identification of significant areas with a high flood risk through the use of flood risk identification.
2. Assessment of economic damage caused by floods in significant areas by means of flood risk assessment.
3. Use of flood risk management to select the best design measures to improve the capacity of the drainage system.

The first stage of the process begins with the identification of flood risk based on available flood data, flood risk maps and the definition of significant areas where there is a high probability of flood risk. Due to the extent of the results achieved, the proposed methodology is recommended to be implemented at the city level.

The flood risk assessment itself is described in the second stage, which includes the hazard analysis, the assessment of the underlying exposure element, the vulnerability analysis and the quantification of the data. The flood risk analysis contains information on the extent and intensity of the flood situation. While the extent is determined by the spatial flooding of the area, the intensity carries information about the depth of the flood. The expression of the supporting element of exposure means the identification of the element which contributes most to flood damage, especially to economic damage. The analysis of the exposure exposure element consists of the following steps:

- identification of the factors that have the greatest impact on the economic damage caused by floods,
- determination of the influence factor of the exposure element,
- obtaining the spatial distribution of the supporting element of the exposure.

Once the load-bearing element of the exposure is defined, a vulnerability analysis is performed to determine the damage depth curve. In this study, vulnerability include economic damage caused by floods, from which a curve is generated expressing the relationship between the depth of the flood and the economic damage (the so-called damage depth curve). This curve is also generated for each exposure carrier. As there are different types of buildings in the studied area, their economic value is also different. Said damage depth curve is therefore used to calculate the vulnerability of buildings in the addressed area. The quantification of flood damage is the result of all previous analyzes, and at the same time it carries with it the assumption that the amount of damage depends on the recurrence of floods.

Flood risk management belongs to the third stage of this methodology. In the understanding of this study, flood risk management involves the construction of design measures to achieve flood mitigation. The aim of this study was to select a design measure that will include the best possible engineering benefits to improve urban drainage systems. Engineering benefits in this case are defined as the ratio of flood mitigation to investment in measures.

The estimation of the expected potential flood damage

In flood management, the term vulnerability often occurs, which is a weakness or shortcoming that allows a hazard to be applied. Closely related to this concept is the sensitivity parameter, which can be used to estimate flood damage (de Moel, et al., 2012). In the case study, flood damage is defined by a combination of a failure model, a flood model and a damage model. These three models are implemented in the MC framework in order to determine the sensitivity of the model chain to different assumptions, and to assess the uncertainty regarding the resulting damage estimate.

The following data are required to assess the expected potential damage: information on hydraulic loads and the probability of their occurrence (shock wave with water level), a model simulating an increase in dam failure in the event of a collapse, a hydraulic model simulating an increase in flooding in the event of a dam collapse, and a damage model simulating flooding with damage estimation.

The analysis was carried out in the western part of the Netherlands, whose territory is prone to floods. In the studied area there are dams and low-lying polders, which are exposed to storm floods. This area is divided into 53 so-called dam circuits (the area surrounded by dams), which have a high level of flood protection. For the purposes of this study, circuit 14 was selected, which includes the 3 largest Dutch cities and the main airport. The flood situation in the study area can occur for several

reasons: the western part can be flooded by the North Sea, the inland area near Rotterdam is exposed to storms, and the southern part of the study area can be affected by floods from the Lek River and the Rhine River. In addition to dams, there are several polders in this area, some of which reach an elevation of up to 6.5 m above sea level.
The combination of the astrological tide with the increase in storms is considered to be an estimate of the volume of the shock wave and the height of the water level after the failure of one of the dams. An estimate of the volume of running water is also related to the dam failure, but the dam failure may depend on the water level on both sides of the dam and also on the material itself from which the dam is made. The water level difference is determined by raising the water level directly inside the damaged dam and subtracting from the water level on the other side of the dam.
To construct a flood height estimation model, a new approach has been proposed that directly calculates the value of the direct result of a regular two-dimensional flow, the maximum flood depth of an area, and a given specific volume. The mentioned new model approach was designed to simulate flooding in areas surrounded by dams and other protective structures. The second setting was to allow modeling of a large amount of flood estimation at different volumes.
The last link in the model chain was the damage estimate, for which two vulnerability parameters were proposed – the maximum risk value and the shape of the depth damage curve. Uncertainty estimates were derived from the available literature, which consists of a combination of several methodologies for estimating the damage depth curve and a factor estimating the magnitude of the uncertainty.

Flood damage calculation

The common parameter for estimating flood damage in the Canadian study (McGrath et. al., 2019) and in the study mentioned in the previous subchapter is the depth of the flood. Many studies deal mainly with flood risk, but it is also important to have data on flood damage. The present study presents the application of the RESTful Application Program Interface (API) for the financial estimation of building damage. The API web service allows you to calculate flood damage to buildings without determining the flood risk.
The API application programming language is Python Script, which contains a database of input parameters. Input parameters include information about buildings – classification of buildings according to occupancy (how many residential units are in the building), number of floors in the building, year of construction, existence and use of the basement and garage. The application offers the user the possibility to calculate the flood damage using the damage depth curve, if the depth of the flood is known. If this data is not available, the calculation is based only on the expected depth of the flood in the area (after substituting other necessary data). In the second case, the estimate of the depth of the flood is identified as a percentage.

Results and discussion

Flood risk assessment

Selected studies presented in this article assessed flood risk at various levels. The study carried out on the Luvuvhu River, unlike the others, contained only two parameters according to which the flood risk was assessed. However, the differences in the studies are not only in the number of evaluation parameters, but also in the method of flooding. In contrast to the flood risk on the Luvuvhu River and the Yangtze River, where river floods were taken into account, in the western province of Sri Lanka, an assessment of the flood risk caused by torrential rain floods was considered.
As the assessments were based on different input data and different indicators, these results cannot be unambiguously generalized. Therefore, the results of the studies are presented as separate subchapters.

Results of the flood risk analysis in the Luvuvhu river basin

The flood risk in this study was analyzed on the basis of hazard and vulnerability parameters. However, in terms of the scope of work, only spatial vulnerability was addressed. The authors of the study were based on data on land use, and on the consequences of flooding given types of land use. The result of the study is that even if the flood floods the whole area, the flood risk will not be the same in all places. Therefore, based on the flood depth analysis, the following classification was established:

- flood depth <2 m – low level of risk,
- flood depth 2–4 m – medium level of risk,
- flood depth 4–6 m – high level of risk,
- flood depth >6 m – very high level of risk.

In this case, the damage depends on the depth of the flood, regardless of the purpose of land use. The results of the study testify to the truth of this statement.

Results of the flood risk analysis in the western province of Sri Lanka

The authors of the study took into account the parameters of risk, vulnerability and exposure when analyzing the flood risk. The parameters of vulnerability were based on the state of the population in terms of social, economic, and in terms of housing. The exposure parameter was divided into asset and population exposure. The result of this study is flood risk maps that apply to each type of assessment parameter. These 3 maps are individually analyzed, the results relate to the area addressed. The flood risk value is determined on a rating scale from 1 to 5, where a value of 1 indicates a very low risk and a value of 5 indicates a very high risk. In the results of the analysis for the population, economic vulnerability appears to be a better indicator compared to social vulnerability. The results of this study serve to prepare for the planning of measures aimed at early warning of natural disasters, have an informative character for the population and also provide a basis for the allocation of funds to mitigate the consequences of natural disasters.

Results of the flood risk analysis in the Yangtze river catchment

In this study, too, the parameters of risk, vulnerability and exposure were included in the flood risk analysis. In this case, however, the authors proposed a multi-index concept, which consists of 3 layers, namely the object, index and indicator layer. The results of this study can be summarized as follows: the flood risk posed by the Yangtze River depends smoothly on precipitation. GDP indicators, the surface runoff and land cover factor, as well as the degree of soil erosion also play an important role. Separate risk values were also determined for each parameter. The risk of exposure has changed significantly over time, while the risk of vulnerability and exposure has changed relatively less over time. The main advantages of the proposed procedure include its comprehensive proposal for the selection of indicators for flood risk assessment, and the output of maps from the GIS environment.

Flood risk analysis

Above mentioned studies focused on the flood risk analysis in term of the available and data diversity. The common parameters of the analysis are hazard and vulenrability in all three selected cases, the parameter of exposure is added in Sri Lanka and Yangtze river catchment flood risk assessment. The results of the mentioned studies shows that there are similar input data, but the assessed parameters are different, so there are different results for each study city. Based on the flood risk analysis in the Yangtze river catchment, the flood risk assessment in Slovak condition will be prepared, considering parameters such as hazard, vulnerability and exposure. Table 1 represents a brief summary and comparison of mentioned flood risk assessment studies.
A big difference between case studies are in input data. While studies performed at Luvuvhu and Yangtze river consider especially hydraulic parameters, the study in Sri Lanka reflect social related data. MIC analysis mentioned in the Yangtze river study can be modified, and it is the most suitable for the further utilization. According to Yangtze river study, the further studies will be developed.

Results of identification of flood risk in Beijing

In the identification of flood risk, 20 high-risk areas were identified in the city of Beijing, one of which was defined as a significant area with a higher flood risk. By combining the parameters found in the second stage, the expected amounts of flood damage for different payback periods were calculated. According to the economic results of the flood damage obtained in the second stage, it is assumed that the drainage system should contribute to the reduction of the damage caused. Flood risk management was used to assess the engineering benefits of design measures. The proposed increase in the capacity of the drainage system has proved to be the most economical design measure in terms of the ratio of flood mitigation to investment in the design measure. The IFRM method in this study was used to identify the most risky area, calculate the economic losses caused by floods, identify the design measures with the best engineering advantage and support flood risk management in Beijing. However, the assessment was carried out only at the level of direct economic damage to buildings. In the subsequent use of this methodology, indirect damages, which include transport and electrical infrastructure as well as the sewerage and water supply system, should also be considered in the assessment.

The results of the estimation of the expected potential flood damage

In this study, damage estimation was performed according to the MC model with the implementation of model simulation. The area addressed was the western part of the Netherlands with selected areas that are prone to floods. To facilitate the process, a new approach has been developed to calculate inundation depths, as well as to model simulations requiring large amounts of input data.
The conclusion of the mentioned study was to perform several model estimates in each solved area with the percentage expression of uncertainties. Finally, the results of modeling in case the dams in the solved area were not damaged are also compared and the scenario when the dams were damaged was also considered, and based on these assumptions the model situations were simulated and subsequently compared with each other. The combination of uncertainty and sensitivity analyzes provided a better overview of which parameters are important in estimating damage.

The results of the flood damage calculation

The API application was designed primarily to facilitate access to information on possible flood damage, and was used in this study to assess flood damage in Gatineau and Fredericton. In both cases, the flood damage was estimated at several million USD, and at the same time was compared with the real flood damage, which was quantified during the floods in the period under review. The difference between real and projected flood damage is about 13%.

Flood damage analysis

Submitted flood damage case studies describes a different way to determine flood damage in the conditions of the study area. All three studies are specific, because of the approach to calculate or assumpt the flood damages. We can see the similarity in the input data, but as well as in the flood risk assessment above mentioned, the differences between input data and the results are also obvious. Table 2 represents a brief comparison of

Table 1. Summary and comparison flood risk assessment studies

Flood risk assessment				
		Luvuvhu river catchment	West province of Sri Lanka	Yangtze river catchment
Assessed parameters		hazard + vulnerability	hazard + vulnerability + exposure	
Input data	*hazard*	hydraulic parameters (depth of the flood, extent of the flooded area)	flow accumulation, precipitation intensity, land use, slope, altitude, length of the drainage system	cumulative average of precipitation in a maximum of 3 days
	vulnerability	flood exposed area	social vulnerability – age of the population economic vulnerability - employed, unemployed and economically inactive population housing vulnerability – permanently inhabited, temporarily inhabited and uninhabited	absolute and relative elevation, runoff density, surface runoff factor, surface coverage, financial returns, financial savings, health service levels, monitoring and warning system
	exposure	-	real estate, population	population density, GDP, degree of soil erosion, risk of soil contamination
Results		the damage depends on the depth of the flood, regardless of the purpose of land use	flood risk maps that are applied to the each type of assessed parameter	the flood risk depends smoothly on precipitation, GDP indicators, the surface runoff and land cover factor, as well as the degree of soil erosion also play an important role
Advantages		the results could be modified and used to the similar flood risk assessment with the same parameters	-	modified – the MIC analyse may be used at various level of input data and parameters
Disadvantages		contains only hazard and vulneability index	a few flood related parameters, analyzed are mostly social parameters (especially vulnerability and exposure index)	-

flood damage analysis.

All selected studies briefly described in Table 2 performed damage analysis on their own input data. The one common parameter is flood depth, from which the next steps follow. Study performed in Beijing could have a wider utilization because of the three stages of flood risk assessment. Economic damage can be extended by other damage asets (soil, infrastructure, people, etc). The API offers very simply flood damage analysis, especially for the citizens of the affected area. The study in Netherland is special, because of the considering the dam circuits.

Table 2. **Comparison of flood damage analysis**

Flood damage analysis		
Beijing	Western part of Netherland	Canada
flood depth		
considered flood risk		without considering flood risk
a curve is expressing the relationship between the depth of the flood and the economic damage	flood damage is defined by a combination of a failure model, a flood model and a damage model	the API offers the user the possibility to calculate the flood damage using the damage depth curve, if the depth of the flood is known
related only to type of the building	analysis performed under special conditions (dams)	consider only the know or expected flood depth
consists three extended stages (flood risk areas, economic damage, design measures)	consists of failure, flood and damage model	input parameters contains information about buildings and flood depth
wider utilization	analysis is performed and used under the special conditions (dams)	using only on the build flood damage assessment

Conclusion

Flood risk assessment and flood damage calculation can take place at different levels and on the basis of different available data. This article focuses on a brief overview of case studies that focus on the determination of flood risk, but also on the assessment of flood damage. Differences in the assessment and assessment of flood risk can be visible already in the selection of assessment parameters, but despite the same assessment parameters, the results will always be different. Hazard, vulnerability and exposure are abstract concepts to which each assessor can assign their own indicators on the basis of which their assessment will be made. However, the differences may not only be in the input indicators, but also in the scope of the evaluation. The flood risk can therefore be determined for the river basin, which covers an area of several thousand km^2, but also in an area smaller than the cadastral area of a small village. However, the definition of risk remains the same, the difference may be in its interpretation. The damage caused by floods is also very closely related to the flood risk. In the presented article, selected procedures for flood damage assessment are based on the identification of the risk in the endangered area. In each of the selected studies, the authors focused on a specific goal – flood damage, but each of them chose different parameters for their interpretation. The issue of flood damage is as important and extensive as the issue of flood risk. On the basis of this review contribution, it is possible to further direct future research with a focus on the aforementioned flood damage and risks with regard to the development of a methodology for flood damage assessment. Submitted paper serves as a theoretical base to the further research. The aim of the paper is to provide a brief review of the actual studies of flood risk assessment and flood damage calculation. By the combination of the above mentioned studies, the new approach to flood risk assessment and flood damage evaluation will be developed.

Acknowledgement

This work has been supported by the Slovak Research and Development Agency through the projects SK-PT-18-0008 and SL-PL-18-0033. This work has also been supported by the Ministry for Education of the Slovak Republic through project VEGA 1/0308/20 Mitigation of hydrological hazards – floods and droughts – by exploring extreme hydroclimatic phenomena in river basins.

References

de Moel, H., Asselman, N. E. M., Aerts, J. C. J. H. (2012): Uncertainty and sensitivity analysis of coatal flood damage estimates in the west of the Netherlands. Natural Hazards and Earth System Sciences, 1045–1058.

Weerasinghe, K. M., Gehrels, H., Arambepola, N. M. S. I., Vajja, H. P., Herath, J. M. K., Atapattu, K. B. (2018): Qualitative Flood Risk assessment for the Western

Province of Sri Lanka. Procedia Engineering vol. 212, 203–510.

McGrath, H., Kotsollaris, M., Stefanakis, E., Nastev, M. (2019): Flood damage calculations via a RESTful API. International Journal of Disaster Risk Reduction 35, 101071.

Ntanganedzeni B., Nobert, J. (2020): Flood risk assessment in Luvuvhu river, Limpopo province, South Africa. Physics and Chemistry of the Earth.

Wang, H., Zhou, J., Tang, Y., Liu, Z., Kang, A., Chen, B. (2021): Flood economic assessment of structural measure based on integrated flood risk management: A case study in Beijing. Journal of Environmental Management, 280, 111701.

Zhang, D., Shi, X., Xu, H., Jing, Q., Pan, X., Liu, T., Wang, H., Hou, H. (2020): A GIS-based spatial multi-index model for flood risk assessment in the Yangtze River Basin, China. Environmental Impact Assessment Review, vol. 83, 106397.

Zvijáková, L., Zeleňáková, M. (2015): Riziková analýza v procese posudzovania vplyvov objektov protipovodňovej ochrany na životné prostredie, Leges, Praha.

Ing. Mária Šugareková (*corresponding author, e-mail: maria.sugarekova@tuke.sk)
prof. Ing. Martina Zeleňáková, PhD.
Department of Environmental Engineering
Faculty of Civil Engineering
Technical University of Košice
Vysokoškolská 4
040 01 Košice
Slovak Republic